



**FABRÍCIO RAMOS SILVESTRE PEREIRA**

**CONECTOMA CEREBRAL: APLICAÇÕES DE IMAGEAMENTO  
POR RESSONÂNCIA MAGNÉTICA NUCLEAR EM  
NEUROCIÊNCIAS**

Campinas

Inverno de 2013





UNIVERSIDADE ESTADUAL DE CAMPINAS

FACULDADE DE CIÊNCIAS MÉDICAS

FABRÍCIO RAMOS SILVESTRE PEREIRA

CONECTOMA CEREBRAL: APLICAÇÕES DE IMAGEAMENTO POR  
RESSONÂNCIA MAGNÉTICA NUCLEAR EM NEUROCIÊNCIAS

**ORIENTADORA:** PROFA. DRA. GABRIELA CASTELLANO

Tese de doutorado apresentada ao programa de Pós-Graduação em Fisiopatologia Médica da Faculdade de Ciências Médicas da Universidade Estadual de Campinas para obtenção do título de Doutor em Ciências.

ESTE EXEMPLAR CORRESPONDE À VERSÃO FINAL  
DA TESE DEFENDIDA PELO ALUNO FABRÍCIO  
RAMOS SILVESTRE PEREIRA ORIENTADO PELA  
PROFA.DRA. GABRIELA CASTELLANO

---

Gabriela Castellano

Campinas

Inverno de 2013

Ficha catalográfica  
Universidade Estadual de Campinas  
Biblioteca da Faculdade de Ciências Médicas  
Maristella Soares dos Santos - CRB 8/8402

P414c Pereira, Fabricio Ramos Silvestre, 1975-  
Conectoma cerebral : aplicações de imageamento por ressonância magnética nuclear em neurociências / Fabricio Ramos Silvestre Pereira. – Campinas, SP : [s.n.], 2013.

Orientador: Gabriela Castellano.  
Tese (doutorado) – Universidade Estadual de Campinas, Faculdade de Ciências Médicas.

1. Neurociências. 2. Imageamento por ressonância magnetica nuclear. 3. Mapeamento de funções cerebrais. 4. Conectividade cerebral. 5. Conectoma. I. Castellano, Gabriela, 1970-. II. Universidade Estadual de Campinas. Faculdade de Ciências Médicas. III. Título.

Informações para Biblioteca Digital

**Título em outro idioma:** Brain connectome : applications of nuclear magnetic resonance imaging in neurosciences

**Palavras-chave em inglês:**

Neurosciences  
Magnetic resonance imaging  
Brain function mapping  
Brain connectivity  
Connectome

**Titulação:** Doutor em Ciências

**Banca examinadora:**

Gabriela Castellano [Orientador]  
Florindo Stella  
Renato Cabral Rezende  
Paulo Cesar Centoducatte  
Mauro Antonio Pires Dias da Silva

**Data de defesa:** 22-07-2013

**Programa de Pós-Graduação:** Fisiopatologia Médica

---

## BANCA EXAMINADORA DA DEFESA DE DOUTORADO

FABRÍCIO RAMOS SILVESTRE PEREIRA

---

Orientador (a) PROF(A). DR(A). GABRIELA CASTELLANO

---

### MEMBROS:

---

1. PROF(A). DR(A). GABRIELA CASTELLANO

2. PROF(A). DR(A). FLORINDO STELLA

3. PROF(A). DR(A). RENATO CABRAL REZENDE

4. PROF(A).DR(A). PAULO CESAR CENTODUCATTE

5. PROF(A).DR(A). MAURO ANTONIO PIRES DIAS DA SILVA

---

Programa de Pós-Graduação em Fisiopatologia Médica da Faculdade de Ciências Médicas da Universidade Estadual de Campinas

---

Data: 22 de julho de 2013

---



Dedico esta tese aos trabalhadores do MST e da Via  
Campesina. Pela coragem com que enfrentam a legislação  
em busca de justiça social.

*Quem me dera, ao menos uma vez,  
Que o mais simples fosse visto como o mais importante  
Renato Russo*



## Agradecimentos

*Quem me dera, ao menos uma vez,  
Ter de volta todo o ouro que entreguei  
A quem conseguiu me convencer  
Que era prova de amizade  
Se alguém levasse embora até o que eu não tinha.*

Neste trabalho desejo agradecer ao leitor que tomou essa brochura para se entreter. Seja pela curiosidade ou por interesse acadêmico, o fato é que agora tem acesso a um pouco de minha vida discente. Mas me parece insuficiente apresentá-la sem dar os devidos créditos aos muitos que permitiram que ela se materializasse.

Diferente da maioria dos trabalhos, meus agradecimentos (ainda que menores) também são direcionados a alguns adversários pois me permitiram, não sem sofrimento, entender que colegas podem se tornar inimigos quando interesses além da academia ficam expostos. Contudo, como relatei na dissertação de mestrado, publicado há pouco mais de dois anos, os agradecimentos mais fervorosos são dirigidos aos trabalhadores, que entendo ser os verdadeiros mantenedores dos aparatos de Estado (como as universidades públicas) apesar da hegemonia dos governantes desmerecerem esse crédito.

Meus agradecimento também são direcionados a meus tios Mário e Roseli, pois apesar de eu não os ter mencionado na publicação anterior, ambos figuraram entre os mais importantes personagens de minha formação discente e patrocinaram meu interesse pela linguagem, função humana que vim a trabalhar de relance nessa tese. Agradeço também a Ana Raquel, uma personagem nova em minha vida que mesmo sem fazer qualquer ação propositiva, fez-me ponderar sobre as opções em minha vida. Profundo agradecimento teço aos professor Geraldo pois foi ele que no momento mais difícil de minha carreira, acreditou em minhas potencialidades e em meus valores éticos. A ele se deve o posto que fora ocupado na mestrado pelo Professor Pélico, mentor e suporte para minhas ideias e produções.

Por fim, mas não menos importante, a meus pais que mais se orgulham dessa produção do eu próprio; às minhas saudosas avós que em sua humildade e simplicidade conseguiram esculpir as lições mais importantes dessa tese – a honestidade, ausente em diversos espaços da academia; à Gabriela, minha amiga, que foi convertida em orientadora, e ficou incumbida da árdua tarefa em me cobrar a apresentação desse trabalho apesar das inúmeras evasivas que eu sempre promovia. A ela devo mais que minha gratidão e desculpas, devo-lhe uma menção ilustre por ter-me aceitado como aluno em um momento difícil de minha formação e de minha vida pessoal. O fato deste trabalho de doutorado, um calhamaço com quase duas centenas de páginas, ter sido concluído em dois anos sem que eu tivesse qualquer bolsa institucional mas que contra as expectativas já produziu meia dúzia de artigos científicos em revistas indexadas (com elevado Fator de Impacto) e, inclusive, alguns já terem sido citados por outros pesquisadores internacionais é prova da competência que reconheço em minha orientadora.

Finalmente, quero agradecer à Fabiana, minha companheira de estrada há quase duas décadas. A pessoa solidária que me confortou nos momentos delicados vividos no último ano. Quem me trouxe sobriedade nos tempos de incertezas e que me apoia na nova e promissora etapa que se abre.

..

<b>RESUMO</b> .....	<b>xix</b>
<b>ABSTRACT</b> .....	<b>xxiii</b>
<b>INTRODUÇÃO</b> .....	<b>27</b>
<b>Conectividade Anatômica (acMRI)</b> .....	<b>32</b>
<b>Conectividade Funcional (fcMRI)</b> .....	<b>46</b>
<i>Homogeneidade regional ( ReHo – regional homogeneity )</i> .....	48
<i>Análise por componente independente ( ICA – independent component analysis )</i> .....	50
<i>Análise por clusterização temporal ( TCA – temporal clustering analysis )</i> .....	52
<b>Conectividade Efetiva (ecMRI)</b> .....	<b>55</b>
<i>Modelagem de equações estruturais ( SEM – structural equation modelling )</i> .....	57
<i>Modelagem causal dinâmica (DCM – Dinamic Causal Modelling)</i> .....	65
<b>OBJETIVOS</b> .....	<b>69</b>
<b>Objetivos Gerais:</b> .....	<b>70</b>
<b>Objetivos Específicos:</b> .....	<b>70</b>
<b>METODOLOGIA</b> .....	<b>71</b>
<b>Experimento 1 – Conectividade efetiva: SEM aplicado à plasticidade etária e codificação de palavras com conteúdos emocionais.</b> .....	<b>72</b>
<b>Experimento 2 – Conectividade efetiva: SEM aplicado a ELTM esquerdo com codificação de palavras neutras e abstratas</b> .....	<b>79</b>
<b>Experimento 3 – Modulação de conectividade efetiva por codificação de palavras neutras e abstratas</b> .....	<b>92</b>
<b>Experimento 4 – Análise de imageamento por tensor de difusão em pacientes idosos com e sem diagnóstico de depressão</b> .....	<b>96</b>

<b>Experimento 5 - Anormalidade em substância branca e cinzenta em pacientes com mutação do gene SPG11.</b> .....	<b>103</b>
<b>Experimento 6 - Alterações de substância branca em pacientes com doença de Alzheimer e transtorno cognitivo leve.</b> .....	<b>109</b>
<b>Experimento 7 - Alterações neuropsiquiátricas associados com danos de redes funcionais em pacientes com doença de Alzheimer e transtorno cognitivo leve.</b> .....	<b>120</b>
<b>Experimento 8 - Pasticidade cerebral em codificação de memória verbal e visual de pacientes com epilepsia medial temporal.</b> .....	<b>130</b>
<b>Experimento 9 - Redes neurais de pacientes obesos com disfunção hipotalâmica.</b> .....	<b>144</b>
<b>DISCUSSÃO</b> .....	<b>151</b>
<b>SEM aplicado à plasticidade etária e codificação verbal</b> .....	<b>155</b>
<b>SEM aplicado a ELTM esquerdo com codificação verbal</b> .....	<b>156</b>
<b>DCM aplicado a ELTM unilateral com codificação verbal</b> .....	<b>157</b>
<b>CONSIDERAÇÕES FINAIS</b> .....	<b>159</b>
<b>REFERÊNCIA BIBLIOGRÁFICA</b> .....	<b>163</b>



## *LISTA DE ABREVIATURAS*

---

<b>AAL</b>	Atlas anatômico automatizado / Automated Anatomical Labeling
<b>AD</b>	Difusividade Axial / Axial Diffusivity
<b>BDI</b>	Inventário de Depressão de Beck / Beck Depression Inventory
<b>BOLD</b>	Nível de oxigenação dependente / Blood Oxygenation Level Dependence
<b>CBF</b>	Fluxo sanguíneo cerebral / Cerebral Blood Flow
<b>CBV</b>	Volume sanguíneo cerebral / Cerebral Blood Bolume
<b>CMRO<sub>2</sub></b>	Taxa de metabolismo cerebral de oxigênio / Cerebral Metabolic Rate of Oxygen
<b>COUHES</b>	Comitê sobre uso de humanos como sujeitos experimentais / Committe on the Use of Humans as Experimental Subjects
<b>CT</b>	Tomografia Computadorizada / Computer Tomography
<b>DCM</b>	Modelagem Causal Dinâmica / Dinamic Causal Modelling
<b>dOHb</b>	Deoxi-hemoglobina / Deoxyhemoglobin
<b>Doppler</b>	Efeito Doppler
<b>DTI</b>	Imageamento por Tensor de Difusão / Diffusion Tensor Image
<b>DWI</b>	Imageamento ponderado por difusão / Diffusion-weithted image
<b>EEG</b>	Eletroencefalografia
<b>efMRI</b>	Conectividade Efetiva / Effective Connectivity
<b>ELT</b>	Epilepsia de Lobo Temporal
<b>ELTM</b>	Epilepsia de Lobo Temporal Mesial
<b>EPI</b>	Imagem Echo-Planar / Echo Planar Image
<b>F2</b>	Giro Frontal Médio
<b>F3-OPER</b>	Giro Frontal Inferior – porção opercular

<b>F3-TRIANG</b>	Giro Frontal Inferior – porção triangular
<b>FA</b>	Anisotropia Fracional / Fractional Anisotropy
<b>fcMRI</b>	Conectividade Funcional / Functional Connectivity
<b>fMRI</b>	Ressonância Magnética Funcional / Functional Magnetic Resonance Image
<b>FOV</b>	Campo de visão / Field of view
<b>HIP</b>	Hipocampo / Hippocampus
<b>ICA</b>	Análise por Componente Independente / Independent Component Analysis
<b>ICA</b>	Análise por Componente Independente / Independent Component Analysis
<b>MD</b>	Difusividade Média / Mean Diffusivity
<b>MEG</b>	Magnetoencefalografia
<b>MIT</b>	Instituto de Tecnologia de Massachusetts / Massachusetts Institute of Technology
<b>ML</b>	Máximo Verossímil / Maximun Likelihood
<b>MLE</b>	Estimativa de Máximo Verossímil / Maximun Likelihood Estimation
<b>MLF</b>	Função de Máximo Verossímil / Maximun Likelihood Function
<b>MNI</b>	Instituto Neurológico de Montreal / Montreal Neurologic Institute
<b>MRI</b>	Imageamento por Ressonância Magnética / Magnetic Resonance Image
<b>OHb</b>	Oxi-hemoglobina / Oxyhemoglobin
<b>PCA</b>	Análise por Componente Principal / Principal Component Analysis
<b>PDF</b>	Função de distribuição de probabilidade / Probabilistic distribution function
<b>PET</b>	Tomografia por emissão de pósitron / Positron Emission Tomography
<b>PHIP</b>	Parahipocampo / Parahippocampus
<b>PLS</b>	Quadrado Mínimo Parcial / Partial Least Square

<b>PPI</b>	Iteração Psico-fisiológica / Psico-Physiologic Interaction
<b>rCBF</b>	Taxa do fluxo sanguíneo cerebral / rate of Cerebral Blood Flow
<b>RD</b>	Difusividade Radial / Radial Diffusivity
<b>ReHo</b>	Homogeneidade Regional / Regional Homogeneity
<b>RM</b>	Ressonância Magnética
<b>SEM</b>	Modelagem por Equação Estrutural / Structural Equation Modelling
<b>SPECT</b>	Tomografia por emissão de fóton único / Single Photon Emission Computer Tomography
<b>SVD</b>	Decomposição em valor singular / Singular Value Decomposition
<b>TMS</b>	Estimulação Magnética Transcranial / Transcranial Magnetic Stimulation
<b>VBM</b>	Volumetria baseada em voxel / Voxel Based Morphometry

**Tabela 1:** Lista das estruturas seguímentadas automaticamente no FreeSurfer

**Tabela 2:** Lista de palavras e não-palavra utilizada na emulação de memória verbal

**Tabela 3:** Lista de figuras e “não-figura” utilizada na emulação de memória visual

**Tabela 4:** Parâmetros de conectividade funcional entre regiões frontais e temporais

- Figura 1:** Ilustração de imagens ponderadas por difusão em 6 direções.
- Figura 2:** Representação da difusão da molécula de água
- Figura 3:** Representação dos tensores de difusão
- Figura 4:** Espectro de índices de difusão (FA, MD e RD)
- Figura 5:** Exemplo de valores de índices de difusividade em regiões cerebrais
- Figura 6:** Visualização dos tratos cerebrais
- Figura 7:** Representação da definição de voxels “vizinhos”
- Figura 8:** Redes funcionais identificadas pelas técnicas de separação de componentes
- Figura 9:** Etapas de processamento da técnica de TCA
- Figura 10:** Grupos de codificação de palavras com conteúdo emocional
- Figura 11:** Ilustração de estruturas seguímentadas pelo Freesurfer.
- Figura 12:** Modelo anatômico: Hipocampos – Amígdalas (estático).
- Figura 13:** Parâmetros de conectividade: Modelo Hipocampos – Amígdalas.
- Figura 14:** Paradigma de codificação e evocação imediata: memória verbal
- Figura 15:** Paradigma de *resting state*
- Figura 16:** Paradigma de evocação tardia e reconhecimento: memória verbal
- Figura 17:** Paradigma de codificação e evocação imediata: memória visual
- Figura 18:** Paradigma de evocação tardia e reconhecimento: memória visual.
- Figura 19:** Modelo estrutural de ecMRI de regiões frontais e temporais (estático) .
- Figura 20:** Parâmetros de conectividade efetiva: controles vs pacientes ELTM esquerda
- Figura 21:** Modelo anatômico com modulação de conectividade efetiva (dinâmico)
- Figura 22:** Parâmetros de conectividade efetiva modulados pela codificação verbal

## **RESUMO**



O conectoma cerebral refere-se ao mapeamento dos circuitos neurais com os objetivos de 1) identificar regiões que dão suporte às atividades mentais e comportamentais, e 2) detectar alterações nesses circuitos que levam a distúrbios de ordem psiquiátrica e neurológica. Na prática, os estudos de conectoma cerebral consistem na integração de técnicas multimodais de imageamento como ressonância magnética (RM), eletroencefalograma (EEG) e magnetoencefalograma (MEG) com o intuito de estimar os tipos e os níveis de conexão entre regiões cerebrais remotas. Essa “conectividade” entre regiões cerebrais é geralmente classificada em três tipos: anatômica, funcional e efetiva.

No presente trabalho, as técnicas de conectividade, usando dados de MR, foram aplicadas na comparação de grupos saudáveis e patológicos.

Pela técnica de conectividade anatômica observou-se anomalias na substância branca de pacientes com mutação no gene SPG11. Essas anomalias foram detectadas através da redução da anisotropia fracional (FA) e aumento da difusividade média (MD), difusividade radial (RD) e difusividade axial (AD) em regiões subcorticais dos lobos temporal e frontal, bem como no giro do cíngulo, cuneus striatum, corpo caloso e tronco cerebral. Tais achados indicam que o dano neuronal é mais difuso do que indicava a literatura. Um segundo estudo de conectividade anatômica demonstrou que esses índices de difusividade não foram robustos para diferenciar idosos com e sem diagnóstico de depressão indicando a necessidade de avanços na formulação de novos índices com maior sensibilidade.

A técnica de conectividade funcional foi empregada em três estudos. No primeiro, observou-se que pacientes com epilepsia de lobo temporal medial unilateral apresentam redução da conectividade funcional durante a execução de tarefas de memória verbal e visual. Essa redução foi predominantemente ipsilateral à lesão e associada ao material-específico utilizado no teste de memória. No segundo estudo, verificou-se uma redução dos padrões de conectividade funcional hipotalâmica em sujeitos obesos e a sua parcial elevação após a

cirurgia bariátrica concomitantemente à redução de indicadores bioquímicos de inflamação. No terceiro estudo, observou-se que pacientes com doença de Alzheimer apresentaram elevação dos níveis de conectividade funcional na rede saliente (*Saliency Network*) e redução na rede de modo padrão (*Default-mode network*). Adicionalmente, verificou-se nos pacientes a correlação positiva da síndrome hiperativa com os níveis de conectividade funcional no cíngulo anterior e em áreas da ínsula direita. O conjunto desses resultados ilustra um possível significado clínico para futuro diagnóstico e tratamento da doença de Alzheimer.

Pela técnica de conectividade efetiva observou-se que em função do envelhecimento sadio há uma mudança dos parâmetros de conectividade durante a codificação de palavras com conteúdo emocional. A influência do hipocampo sobre a amígdala ipsilateral é reduzida nos sujeitos mais velhos enquanto a influência da amígdala direita sobre o hipocampo direito é elevada. Tais achados reforçam a tese da ininterrupta plasticidade etária e da dinâmica cerebral normal. Essa mesma técnica foi também empregada para demonstrar os diferentes padrões de influência entre os lobos frontal e temporal de pacientes com ELTM esquerda e sujeitos controle. Encontrou-se alteração nos padrões de conectividade efetiva dos pacientes, indicando que estes podem ser potenciais biomarcadores para a epilepsia.

## **ABSTRACT**



Connectome refers to the neural circuitry mapping aiming to identify brain regions that support mental and behavioral functions as well as to detect circuit changes that are linked to psychiatric or neurologic disorders. In practice, connectome studies link several neuroimaging approaches such as MRI, EEG and MEG by means of the estimation of connections among remote brain regions. This “connectivity” among brain regions is usually classified as anatomic, functional or effective.

In this work, the technique of connectivity, using MR data, was applied to compare healthy and pathological groups.

By means of the anatomical connectivity abnormalities in the white matter of patients with SPG11 mutation were observed. These abnormalities were expressed as the reduction of the levels of fractional anisotropy (FA) and the increase in mean (MD) and radial diffusivities (RD) in sub-cortical regions of temporal and frontal lobe as well as in cingulated gyrus, cuneus, striatum, corpus callosum and brainstem. These findings suggest that neuronal damage/dysfunction is more widespread than previously recognized in this condition. Another anatomical connectivity study showed that such indices of diffusivity were not robust to statistically differentiate between old subjects with and without depression. This lacking on finding differences between both groups indicates that new indices of diffusivity have to emerge in order to provide complementary information about brain subtle microstructures.

Functional connectivity was applied to three studies. In the first study, it was observed that patients with unilateral medial temporal lobe epilepsy presented lower levels of functional connectivity during visual or verbal memory tasks. Such reduction was ipsilateral to the side of the lesion and associated to the specific-material used in the memory task. In the second work, the levels of functional connectivity were reduced in hypothalamic regions of obese patients but a partial

reversibility of hypothalamic dysfunction was observed after bariatric surgery. In the third, patients with Alzheimer disease presented higher values of functional connectivity in the salience network and a reduction of connectivity values in the default-mode network. Also in these patients, significant correlations between the levels of hyperactivity syndrome and the salience network were observed in the anterior cingulate cortex and right insula areas. These results indicate the potential clinical significance of resting state alterations in future diagnosis and therapy of Alzheimer disease.

The effective connectivity approaches demonstrated that old and young subjects have significant differences when encoding words with emotional contents. The influence of the hippocampus on the ipsilateral amygdale was lower for older subjects whereas the influence of the right amygdale on the right hippocampus was increased for these subjects. These findings suggest that brain plasticity also happens as function of age. The same approach was used to estimate the influence from frontal to temporal lobes in patients with left MTLE compared to healthy subjects. The patterns of effective connectivity were changed in patients and may be potentially considered as biomarkers for epilepsy.

## **INTRODUÇÃO**



O estudo da dinâmica cerebral normal e patológica tem despertado interesse da humanidade há milhares de anos (Feldman and Goodrich, 1999, Minagar et al., 2003), contudo, foi no final do século passado que esses estudos ganharam impulso vigoroso graças ao advento de técnicas mais apuradas de imageamento cerebral. As técnicas como **MEG**, **EEG**, **MRI**, **CT**, **SPECT**, **Doppler**, **PET** entre outras, são algumas das modalidades capazes de apresentar sinais fisiológicos em forma de gráficos ou imagens. Cada técnica tem limitações, apesar de também possuir vantagens. O imageamento por ressonância magnética (**MRI**), em particular, congrega duas importantes vantagens: a possibilidade de imageamento estrutural com elevada resolução anatômica e a capacidade de detecção indireta da atividade cerebral.

Regiões cerebrais em atividade elevam o consumo metabólico e requisitam maior aporte de oxigênio no local (Paulson et al., 2010). Para isso, um complexo arranjo neuronal e vascular deve ser acionado para abastecer essas regiões. Mecanismos como o aumento de fluxo sanguíneo (Chaigneau et al., 2007), a dilatação de vasos (Glielmi et al., 2009), a elevação da extração de oxigênio pelos tecidos (Herman et al., 2009), entre outras respostas fisiológicas, representam apenas uma pequena parcela da intrincada, porém harmônica, dinâmica cerebral.

Durante a atividade neural e o excessivo aporte de oxigênio, a concentração venosa de oxi-hemoglobina (**OHb**) eleva-se. No entanto, em decorrência das propriedades diamagnéticas dessa molécula (Savicki et al., 1984, Pauling, 1977), a conformação magnética resultante no local não é alterada. Por outro lado, simultaneamente, a molécula de desoxi-hemoglobina (**dOHb**) tende a ficar mais diluída no interior do vaso, apesar de sua quantidade absoluta sofrer um pequeno aumento. neste caso, as propriedades paramagnéticas da **dOHb** (Pauling and Coryell,

1936, Zborowski et al., 2003) aumentam proporcionalmente sua participação na determinação da componente magnética resultante. Essa variação nas concentrações de ambos os estados moleculares da hemoglobina pode ser observada qualitativamente na **RM** (Ogawa et al., 1990), de forma que uma diminuição na concentração de dOHb resulta num aumento do sinal de RM.

Finda a atividade neuronal, a relação oxi/desoxi hemoglobina retorna aos padrões basais, restaurando a componente magnética associada com o este estado. Esse comportamento em conjunto é conhecido como fenômeno **BOLD** (Blood Oxygenation Level Dependent). Ele fornece indícios da dinâmica cerebral e tem sido largamente empregado para se inferir funções cerebrais (Engel et al., 1994, Greene et al., 2001, Abbott et al., 2010), uma vez que a atividade elétrica neuronal relaciona-se com o sinal **BOLD** (Logothetis et al., 2001).

O sinal hemodinâmico também pode ser utilizado para detectar regiões cerebrais funcionalmente conectadas. Determinadas áreas remotas apresentam sincronia nas flutuações do fluxo sanguíneo local. Estas flutuações hemodinâmicas, de baixas frequências e sincronizadas, foram observadas sem que o indivíduo realize alguma tarefa a ele sugerido. As informações oriundas do imageamento ao longo do tempo (**fMRI**), bem como sua análise espectral, carregam significados fisiológicos capazes de serem traduzidos em mapas estatísticos. No estudo de conectividade, esses mapas dizem respeito a possíveis interações funcionais entre regiões remotas (Cordes et al., 2001, Goelman, 2004, Kruger and Glover, 2001). Entretanto, as séries temporais que constituem as aquisições de **fMRI** são coletadas juntamente com ruídos de fundo. Os ruídos de baixas frequências sobrepostos ao sinal **BOLD** provocam distorções na observação do suposto fenômeno neural. Tais perturbações magnéticas juntamente com o sinais genuinamente biológicos expõem a polêmica sobre o tema.

Alguns estudos chegam a considerá-lo apenas um fenômeno elusivo (Fingelkurts and Kahkonen, 2005, Horwitz, 2003), destacando: a enorme variabilidade existente entre as distintas atividades cerebrais (Waldvogel et al., 2000), entre indivíduos (Della-Justina et al., 2008), e entre algoritmos de pós processamento da imagem (Friston et al., 1993b, Zhao et al., 2004), bem como a elevada capacidade plástica do cérebro para realizar conexões (Das and Gilbert, 1995, Hyde and Knudsen, 2002, Roder et al., 2002, Webster et al., 1995) e as diferentes escalas de tempos em que ocorre o fenômeno neural e a aquisição do dado é feita.

Assim como as propriedades funcionais do cérebro são inferidas *in vivo* pelo acoplamento da atividade neuronal com a flutuação magnética local, propriedades micro-estruturais dos tratos cerebrais são estimadas pela difusividade da molécula de água no tecido (Le Bihan et al., 1986). Os tratos cerebrais, constituídos pelos axônios dos neurônios, possuem características particulares devido à forma alongada. Graças a essa forma, as moléculas de água tendem a deslocar-se prioritariamente ao longo do eixo principal (difusividade axial) dos axônios, enquanto há uma maior limitação para deslocamento dessas moléculas nas direções perpendiculares a esses eixos (difusividade radial). A propriedade de difusão da água em uma direção prioritária é conhecida como anisotropia e pode ser estimada com imagens tensoriais revelando possíveis danos neuronais na micro-estrutura da substância branca.

### **Conectividade Anatômica (acMRI)**

Depreende-se por conectividade anatômica a detecção das vias físicas que interligam áreas cerebrais remotas. O conceito pressupõe a combinação inseparável com a conectividade funcional, dado que, o surgimento de novas conexões neurais, bem como a deleção de outras existentes, é mediado em grande parte pela própria atividade neural. As novas conexões anatômicas são estabelecidas levando-se em consideração: 1) os axônios e as sinapses que tomam parte na competição (deleção ou criação) da via; 2) definindo em qual tipo de competição (excitação ou inibição) as estruturas estarão envolvidas; e 3) regulamentando as normas (especialização ou generalização, convergente ou divergente, etc) seguida pela atividade eletrofisiológica (van Ooyen, 2001). Estudos pregressos (Ridge and Betz, 1984) em ratos demonstraram que neurônio de unidade neuro-motoras, após séries de estimulações crônicas, possuem maior vantagem competitiva que os neurônios não estimulados, reforçando a tese da indissociabilidade entre conectividade anatômica e funcional, entretanto não se tem estudos conclusivos em humanos.

As formas de imageamento utilizada para se estudar a conectividade anatômica são a técnica de imageamento por tensores de difusão (**DTI** – *Diffusion Tensor Image*) e a técnica conhecida como *Molecular Imaging*. Esta última utiliza traçadores biofármacos que interagem com as fibras neurais e as expõem sobre forma de imagem (Frost, 2003) e sua natureza pode ser radioativa, magnética ou metabólica, a primeira baseia-se em princípios de difusividade.

A **DTI** envolve a aquisição de imagens ponderadas por difusão (**DWI** – *Diffusion-Weighted Image*) que são sensibilizadas em vários gradientes, de diferentes direções, no mínimo de 6 para imagens em 3 dimensões (Chen and Hsu, 2005). Calcula-se a diagonalização do tensor de difusão em cada voxel, elegendo o autovetor

para representar a orientação local (Basser et al., 1994). Dado que a molécula de água no interior das fibras neurais tem uma orientação prioritária, que segue ao longo da fibra, a tratografia utiliza o princípio da anisotropia para estabelecer a conectividade anatômica.

Todo fluido possui a propriedade intrínseca de difusão  $D$ , que reflete a mobilidade das moléculas em um ambiente microscópico. As moléculas de água podem ser sensibilizadas pela técnica de **MRI** em intervalos de tempo que variam desde milissegundos até poucos segundos, e em deslocamentos que estendem-se de  $10^{-8}$  a  $10^{-4}$  metros. Essa distância é da mesma ordem que a dimensão da célula e, deste modo, a quantificação da constante **D** nos diferentes tecidos oferece informações sobre os mesmos.

A difusão da água *in vivo* é afetada pela dinâmica do transporte celular através de sub-compartimentos celulares ou por membranas impermeáveis, o que torna possível caracterizar os tecidos a partir do tempo de difusão, pois há, por exemplo, diferentes padrões de difusão entre as substâncias cinzenta e branca.

Cada molécula em uma amostra comporta-se independentemente. Colisões entre moléculas provocam deslocamentos randômicos, sem direções prioritárias, através do trecho conhecido como “caminho livre”. Dado um intervalo de tempo, é possível estimar a distância difundida, contudo, não é possível determinar as direções que a molécula percorreu. Apesar desse processo ser de caráter randômico, há mecanismos físicos que o dirigem. Em fluidos com diferentes concentrações, esta grandeza geralmente é utilizada para descrever tais processos, entretanto, em tecidos biológicos, a principal grandeza a ser considerada é a agitação térmica, geralmente expressa como a probabilidade (**P**) de se encontrar uma partícula em determinada posição (**R**) em um dado intervalo de tempo (**t**).

Em analogia à segunda lei da difusão de Fick, o mecanismo pode ser descrito por:

*Equação 1*

$$\frac{\partial P}{\partial t} = D \nabla^2 P$$

$D \equiv$  coeficiente de difusão

Para as situações em que o ambiente não oferece uma direção prioritária de deslocamento da molécula de água (isotropia), a solução da *Equação 1* assume a distribuição gaussiana em três dimensões equivalente a:

*Equação 2*

$$P_{(X,t)} = \frac{1}{\sqrt{D4\pi t}} \exp\left(\frac{-R^2}{4D t}\right)$$

$R \equiv$  Deslocamento espacial

O caminho médio livre pode ser calculado em termos da constante de difusão:

*Equação 3*

$$\langle R^2 \rangle = \int R^2 P_{(R,t)} dR = 6D t$$

$R \equiv$  Vetor distância percorrida pela molécula de água no tempo  $t$

O processo de difusão também pode ser modelado assumindo que as partículas escolhem caminhos randômicos feitos por  $n$  sucessivos deslocamentos de tamanhos  $\xi$  e em intervalos de tempo constantes  $\tau$  sobre o tempo total de:

*Equação 4*

$$t = n\tau$$

$\tau \equiv$  intervalo de tempo constante

Após cada deslocamento, há uma nova colisão e uma nova orientação randômica. Deste modo pode-se escrever o caminho médio livre por:

*Equação 5*

$$\langle R^2 \rangle = n\xi^2 = \frac{t\xi^2}{\tau}$$

$\xi \equiv$  tamanho do deslocamento

Combinando as *Equação 3* e *Equação 5*, tem-se o coeficiente de difusão obtido pelo comportamento do caminho médio livre. Esta equação, conhecida como equação de Einstein, é expressa por:

*Equação 6*

$$D = \frac{\xi^2}{6\tau}$$

$D \equiv$  coeficiente de difusão

Quando o ambiente oferecer diferentes propriedades de difusão, a depender da escolha de uma direção específica, o coeficiente de difusão deverá ser expresso em sua forma tensorial. Considerando que a probabilidade de deslocamento da molécula ainda possa ser estimada a partir da distribuição gaussiana, o tensor de difusão será caracterizado por:

*Equação 7*

$$D = \begin{pmatrix} D_{XX} & D_{XY} & D_{XZ} \\ D_{YX} & D_{YY} & D_{YZ} \\ D_{ZX} & D_{ZY} & D_{ZZ} \end{pmatrix}$$

$D \equiv$  coeficiente de difusão

Considerando constante cada elemento da matriz da *Equação 7*, pode-se aplicar a segunda lei de Fick para o caso anisotrópico.

*Equação 8*

$$\frac{\partial C}{\partial t} = \sum D_{ij} \frac{\partial^2 C}{\partial i \partial j}$$

$D \equiv$  coeficiente de difusão

No caso particular, em que as moléculas não possuam carga elétrica resultante, como as moléculas de água, a matriz do tensor de difusão é simétrico ( $D_{ij} = D_{ji}$ ), portanto,  $D$  pode ser completamente descrito por  $D_{xx}$ ,  $D_{yy}$ ,  $D_{zz}$ ,  $D_{xy}$ ,  $D_{xz}$  e  $D_{yz}$  que representam a difusividade em 6 direções, referenciadas no equipamento de ressonância magnética. A **Figura 1** ilustra o tensor de difusão  $D$  em um estudo de imageamento por tensor de difusão (DTI).

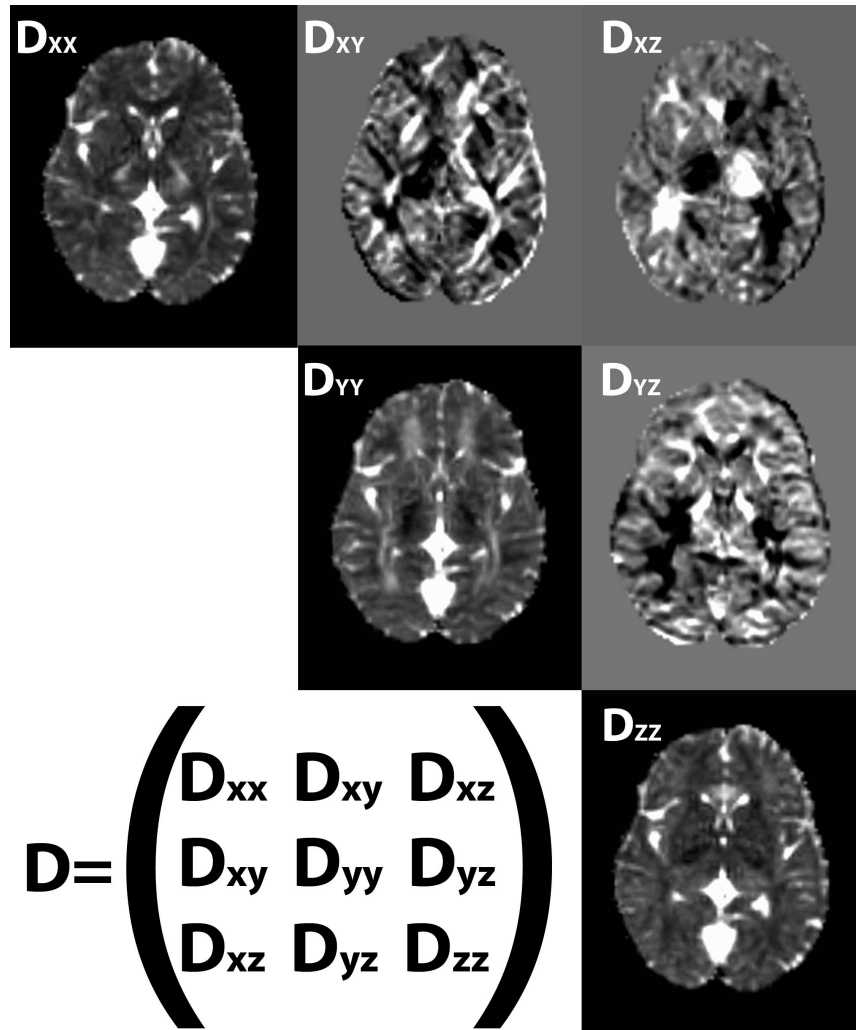


Figura 1: Tensor de difusão  $D$  estimado por imagens ponderadas por difusão que foram obtida por RM com gradiente em 32 direções.

Conhecida essas 6 diferentes componentes do tensor de difusão, é possível transformá-lo em outro tensor com elementos nulos excetuando-se a diagonal, pois esta representaria as propriedades intrínsecas da amostra, independentemente do sistema de coordenadas em que ela foi medida. A operação consiste em escolher um sistema de eixo que anula os elementos do tensor que não fazem parte da diagonal principal. Como resultado, um conjunto de autovalores ( $\lambda_1$ ,  $\lambda_2$  e  $\lambda_3$ ) e autovetores ( $\epsilon_1$ ,

$\epsilon_2$  e  $\epsilon_3$ ) do tensor  $\mathbf{D}$  é produzido. A representação geometricamente tradicional desse autovalores e autovetores é sob a forma de uma elipsóide em cujos eixos possuem tamanho identificados por  $(\lambda_1, \lambda_2$  e  $\lambda_3)$ . A **Figura 2** ilustra o caminho médio livre percorrido pela molécula de água no espaço anisotrópico (**Figura 2A**), a comparação qualitativa desse deslocamento nos meios isotrópico e anisotrópico (**Figuras 2B**) e a representação geométrica da elipsóide que quantifica os índices de anisotropia (**Figura 2C**).

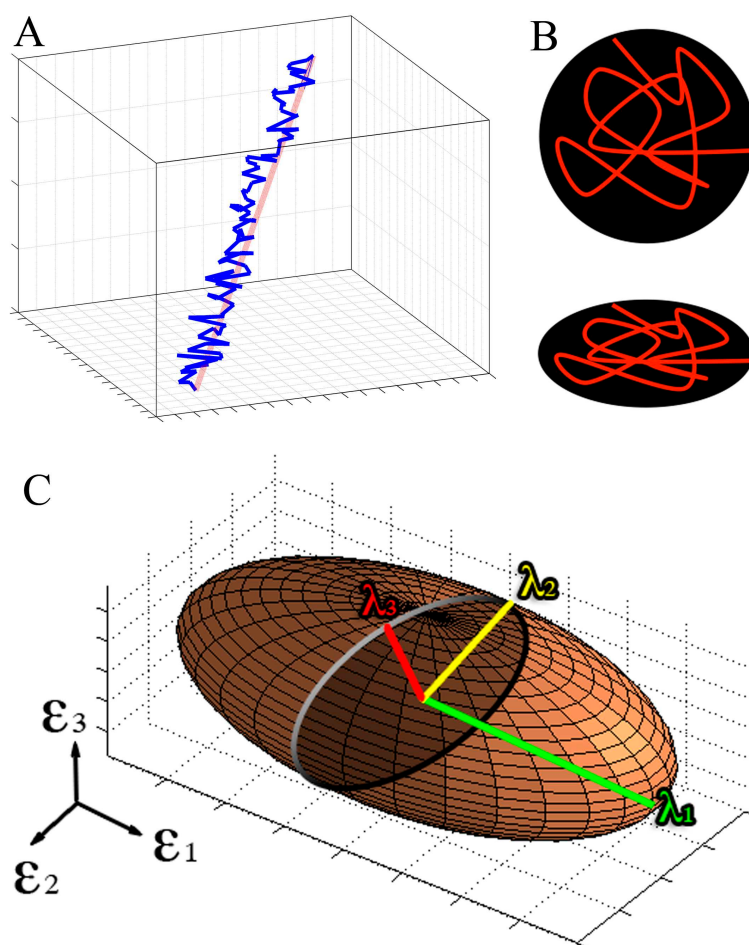


Figura 2: Representação da difusão da molécula de água. A) caminho médio livre (vermelho) e sucessivos trechos de choque (azul). B) Ilustração da difusão nos meios

isotrópico (primeiro) e anisotrópico (segundo). C) Representação geométrica e quantificação do índice de anisotropia.

A parametrização de uma elipsóide (como aquela descrita na **Figura 2C**) pode ser feita em relação aos autovalores encontrados na diagonalização da matriz D de acordo com a *Equação 9* abaixo.

*Equação 9*

$$P_{(\theta, \varphi)} = \begin{pmatrix} \lambda_3 \cos(\theta) \text{sen}(\varphi) \\ \lambda_2 \text{sen}(\theta) \text{sen}(\varphi) \\ \lambda_1 \text{sen}(\varphi) \end{pmatrix}$$

$\lambda_1, \lambda_2$  e  $\lambda_3 \equiv$  Autovalores

$\theta$  e  $\varphi \equiv$  ângulos sobre as superfícies da elipsóide

Deste modo, diferentes tensores de difusão produzem, em cada voxel da imagem, representações elipsoidais distintas. A **Figura 3** abaixo exemplifica a dependência geométrica para alguns valores de tensor de difusão.

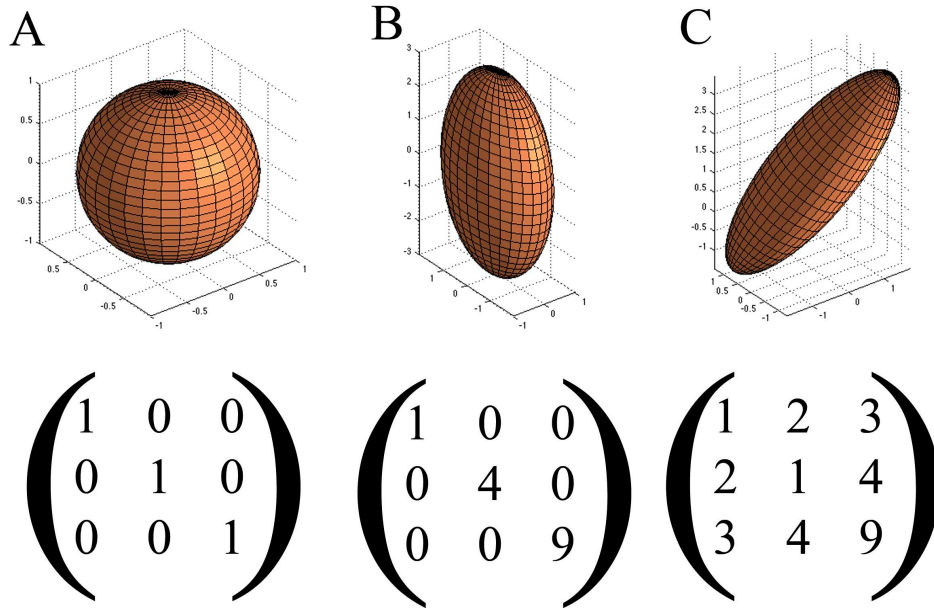


Figura 3: Representação de tensores de difusão. A) geometria isotrópica. B) geometria anisotrópica com grau de isotropia no plano horizontal. C) geometria anisotrópica.

Obs.: Os eixos ortogonais não são os eixos do ressonador, e estão orientados nas direções pósterio-anterior (x), látero-lateral (y) e ínfero-superior (z).

O grau de anisotropia é computado por índices relacionados aos autovalores. Diversos índices podem ser utilizados entretanto, os mais comuns são a anisotropia fracional (FA) definida na *Equação 10*, a difusividade média (MD) definida na *Equação 11* e a difusividade radial (RD) definida na *Equação 12*.

*Equação 10*

$$FA = \sqrt{\frac{1}{2} \left[ \frac{(\lambda_1 - \lambda_2)^2 + (\lambda_1 - \lambda_3)^2 + (\lambda_2 - \lambda_3)^2}{\lambda_1^2 + \lambda_2^2 + \lambda_3^2} \right]}$$

*FA*  $\equiv$  índice de anisotropia fracional

$\lambda_1, \lambda_2$  e  $\lambda_3$   $\equiv$  Autovalores

*Equação 11*

$$MD = \frac{\lambda_1 + \lambda_2 + \lambda_3}{3}$$

*MD*  $\equiv$  *índice de difusividade média*

$\lambda_1, \lambda_2$  e  $\lambda_3 \equiv$  *Autovalores*

*Equação 12*

$$RD = \frac{\lambda_2 + \lambda_3}{2}$$

*RD*  $\equiv$  *índice de difusividade radial*

$\lambda_2$  e  $\lambda_3 \equiv$  *Autovalores*

O índice FA possui valores adimensionais variando entre 0 e 1. O valor 0 (zero) é característico de geometrias completamente isotrópicas enquanto o valor 1 (um) representa geometrias completamente anisotrópicas. Os índices MD e RD têm valores adimensionais variando de 0 ao infinito e representam respectivamente a difusividade média em uma dada região e a difusividade perpendicular ao eixo de maior difusão. A **Figura 4** apresenta o espectro dos valores de FA e a respectiva representação geométrica.

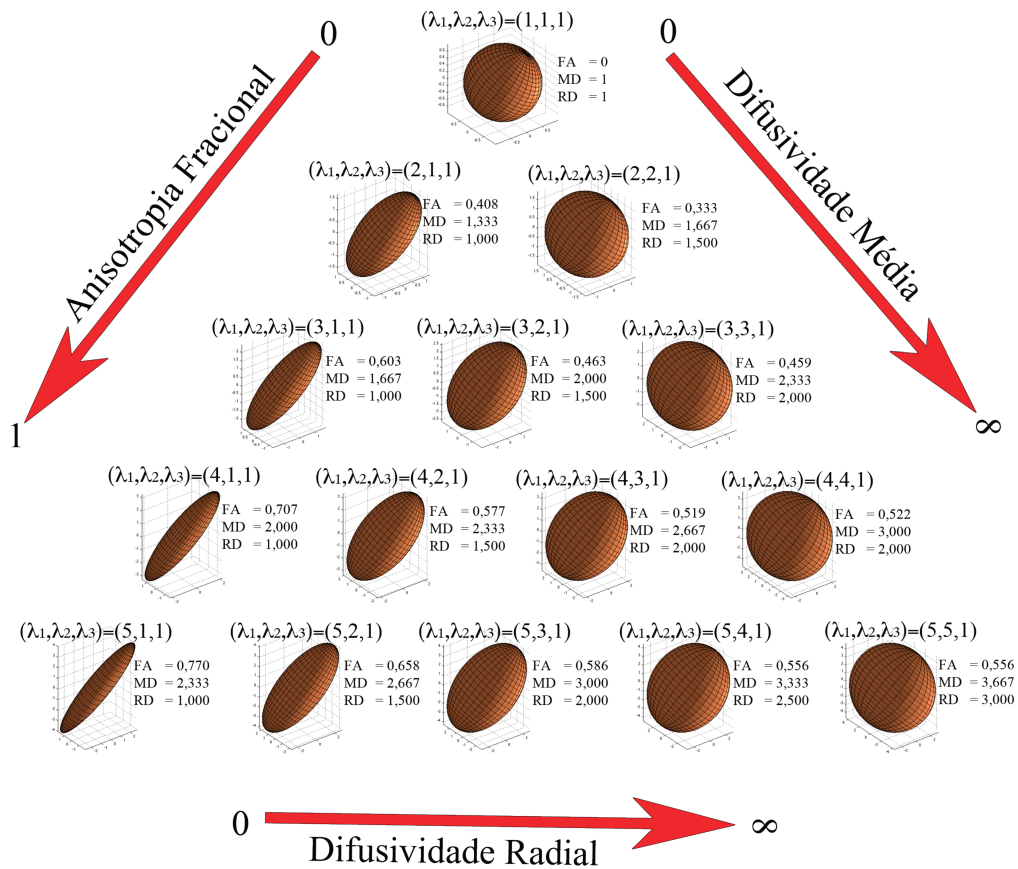


Figura 4: Espectro dos índices de anisotropia fracional (FA), difusividade média (MD) e difusividade radial (RD) ilustrando que a anisotropia cresce à medida em que um dos autovalores cresce em relação aos demais e que a difusividade aumenta quando os autovalores tendem a terem a mesma ordem de grandeza.

A aplicação do conceito de difusividade em estudos DTI revela quantitativamente padrões de difusividade da molécula de água em regiões específicas do cérebro. A **Figura 5** ilustra os padrões de difusividade (FA, MD e RD) em algumas regiões de interesse (ROI).

Radiação talâmica anterior

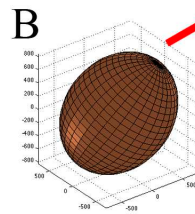
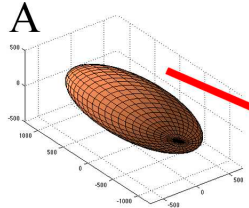
MNI = (27, 33, 16)

FA=0,5234

MD=796

RD=554

$$D = \begin{pmatrix} 772 & -107 & -16 \\ -107 & 867 & 31 \\ -16 & 31 & 753 \end{pmatrix}$$



Polo frontal

MNI = (36, 43, 16)

FA=0,1243

MD=775

RD=719

$$D = \begin{pmatrix} 766 & -27 & -61 \\ -27 & 728 & 47 \\ -61 & 47 & 831 \end{pmatrix}$$

Corpo caloso

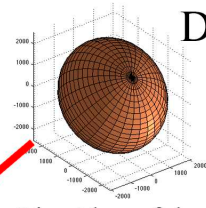
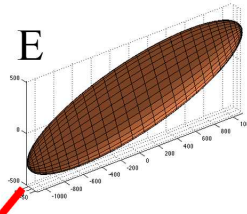
MNI = (-9, 27, 16)

FA=0,8144

MD=522

RD=214

$$D = \begin{pmatrix} 1078 & -26 & -202 \\ -26 & 69 & 145 \\ -202 & 145 & 421 \end{pmatrix}$$



Líquido cefalorraquidiano

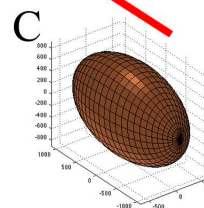
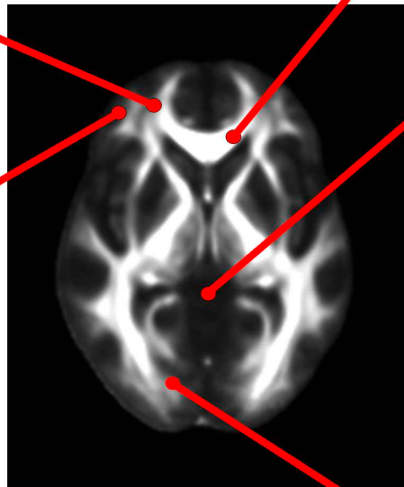
MNI = (0, -28, 13)

FA=0,1322

MD=2396

RD=2247

$$D = \begin{pmatrix} 2088 & 116 & 32 \\ 116 & 2542 & 126 \\ 32 & 126 & 2558 \end{pmatrix}$$



Forceps maior

MNI = (23, -80, 10)

FA=0,2714

MD=892

RD=785

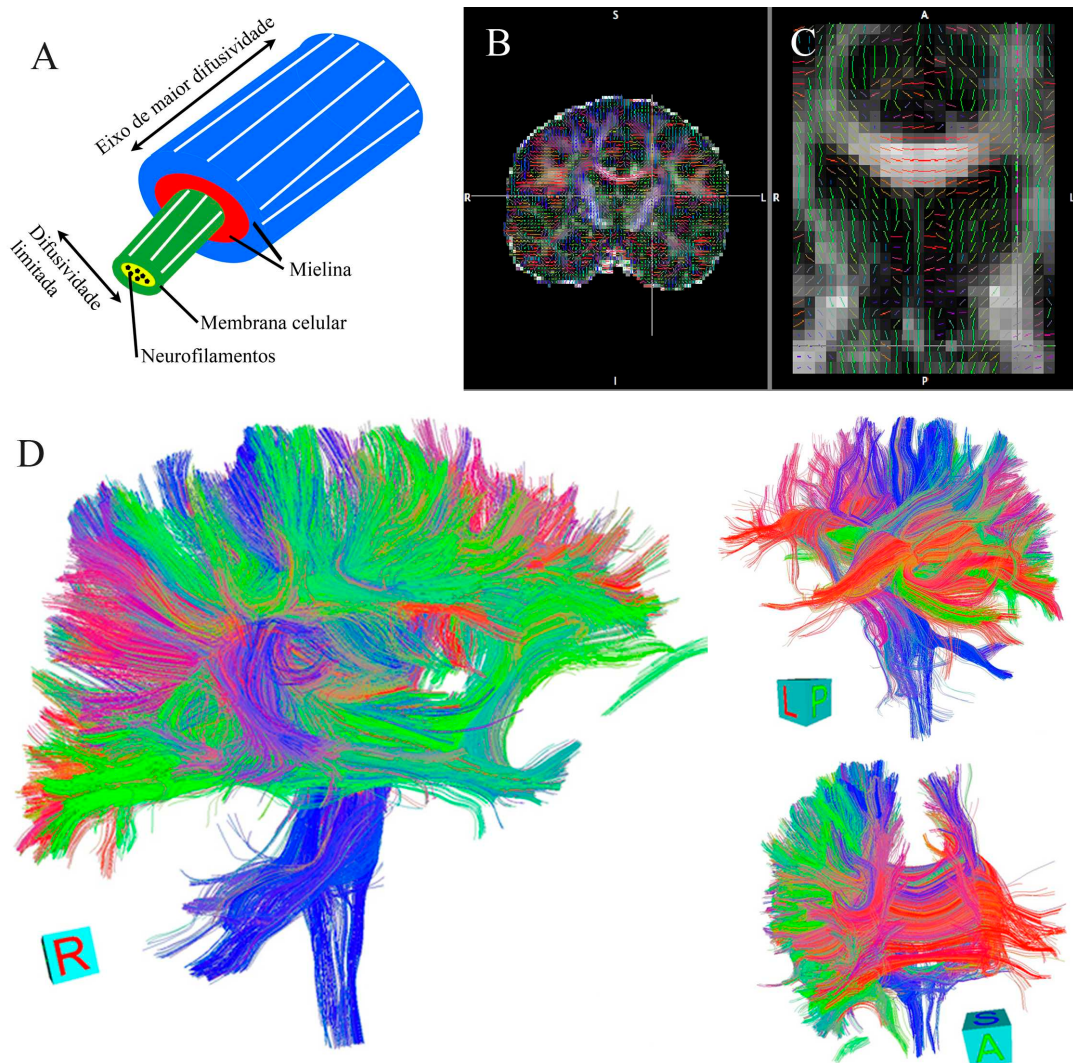
$$D = \begin{pmatrix} 663 & -29 & 108 \\ -29 & 1105 & -0.9 \\ 108 & -0.9 & 909 \end{pmatrix}$$

Figura 5: Representação elipsoidal e respectivos valores de FA, MD e RD estimados pelo com Tensor de Difusão “D” na (A) Radiação Talâmica Anterior, no (B) Pólo Frontal, no (C) Fórceps Maior, no (D) Líquido Cefalorraquidiano e no (E) Corpo Caloso.

Coordenadas registradas no espaço padrão do Instituto Neurológico de Montreal (MNI).

Obs.: Os eixos ortogonais não são os eixos do ressonador, e estão orientados nas direções pósterio-anterior (x), látero-lateral (y) e ínfero-superior (z).

Os índices de difusividade refletem as características de anisotropia local e, no cérebro, essas características dizem respeito às informações micro-estruturais do tecido. Regiões com alto índice de anisotropia, como os tratos, podem ser concatenados para permitir o rastreamento das vias que ligam duas regiões remotas. A **Figura 6** ilustra a fisiologia do trato, com elevado alto índice de anisotropia. Propriedade que permite seu rastreamento (tratografia) através do cerebral.



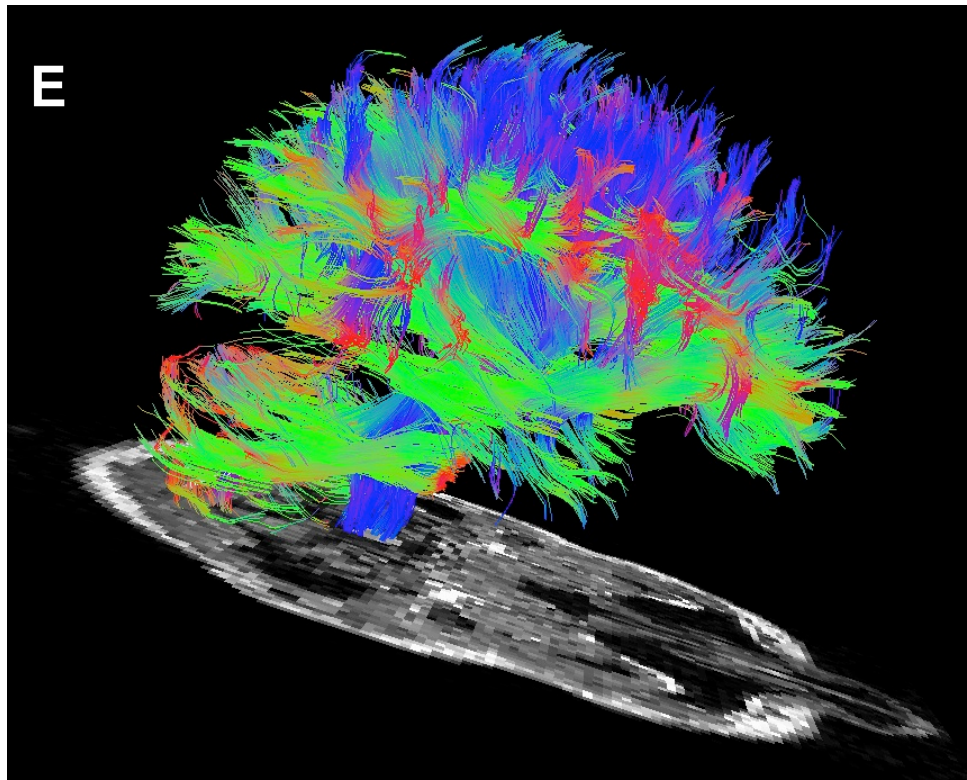


Figura 6: Visualização dos tratos cerebrais. Modelo da fisiologia micro-estrutural dos tratos revelando propriedades anisotrópicas ao longo do feixe (A). Ilustração das direções dos feixes neuronais sobre um corte coronal (B) com detalhe sobre o corpo caloso (C).

Reconstrução dos tratos no hemisfério direito e as respectivas projeções para o hemisfério direito – tratografia (D). Registro de tratos conectando cérebro e coluna espinhal através da ponte. Tons em vermelho representam a direção látero-lateral. Tons em verde indicam direção ânterio-posterior. Tons de azul significa direção ínfero-superior.

## **Conectividade Funcional (fcMRI)**

A definição de conectividade funcional é dada pela correlação entre eventos neurofisiológicos remotos (Friston et al., 1993b). O conceito, apesar de oferece informações sobre sincronia entre as regiões corticais envolvidas na emulação de eventos neurofisiológicos, não lida diretamente com a relação de causa-efeito desses eventos.

Os processos neurais não seguem necessariamente padrões gaussianos entretanto, pode-se caracterizá-los em termos da dependência estatística de segunda ordem, e assim, utilizar correlações para estimar a conectividade funcional (Friston, 2007). Ao assumir que as medidas neurofisiológicas dispersam-se conforme a distribuição Gaussiana basta estimar os valores da covariância para se obter os parâmetros de conectividade funcional. O índice de correlação é representado pela covariância normalizada.

O ponto crítico para evoluir a análise da conectividade funcional está associado com o fato de que a simples correlação de um voxel com os demais não é de grande interesse no estudo, a menos que a série temporal descritas por único voxel seja representativa de uma região de interesse ou de uma estrutura cerebral, ou ainda, que nele expresse-se um valor significativo de mapas estatísticos oriundos de análises prévias, como mapas estatísticos de **fMRI**. Apenas absorvendo estas considerações é que a série temporal de um único voxel pode ser suficiente para se entender fenômenos fisiológicos.

Tratando-se da estrutura de covariância, o mais importante aspecto é a estimativa de padrões de atividade, correlacionados em um grande número de pares co-variantes. Diversas estratégias podem ser empregadas para se mensurar tais padrões, desde as mais elementares, como a média das séries temporais de uma região

de interesse, até as mais elaboradas, como estratégias não-lineares. Um maior aprofundamento dessa técnica pode ser obtido na dissertação mestrado publicada pelo autor há dois anos (Pereira, 2011).

Dentre as diversas metodologias disponíveis para se estimar o padrões de conectividade funcional, três em especial têm se destacado na literatura por não requisitarem informações *a priori* sobre o sistema. A primeira, denominada, *Regional Homogeneity* (ReHo), aborda aspectos locais na busca por de homogeneidade nas flutuações hemodinâmicas enquanto a segunda, *Independent Component Analysis* (ICA) é capaz de separar redes neurais que foram originadas por uma mesma fonte de frequência, como as próprias oscilações hemodinâmicas. Uma terceira metodologia denominada *Temporal Clustering Analysis* (TCA) também tem sido utilizada para extrair uma série temporal sem hipótese definida *à priori* mas que se relaciona com a resposta hemodinâmica e consequentemente, passível de modelagem com as imagens de fMRI.

### ***Homogeneidade regional ( ReHo – regional homogeneity )***

Os parâmetros de homogeneidade regional são estimados pelo coeficiente de correlação de kendall (Kendall and Gibbons, 1990) definidos pela *Equação13*. Esse teste avalia a similaridade entre séries temporais encapsuladas pelos voxels vizinhos. Usa-se estatística não paramétrica sob a forma de ordenamento discreto para cada ponto no tempo das séries temporais e produzem valores entre 0 e 1. A **Figura 7** ilustra a definição de voxels vizinhos para uma dada aquisição em EPI.

*Equação 13*

$$KCC = \frac{\sum R_i^2 - n\bar{R}^2}{\frac{1}{12}K^2(n^3 - n)}$$

$$\bar{R} \equiv \frac{(n+1)K}{2}$$

*KCC*  $\equiv$  *coeficiente de correlação de Kendall*

*R<sub>i</sub>*  $\equiv$  *soma do ordenamento em cada i-ésimo ponto temporal*

*K*  $\equiv$  *número de séries temporais avaliadas (voxels vizinhos).*

*n*  $\equiv$  *total de pontos no tempo*

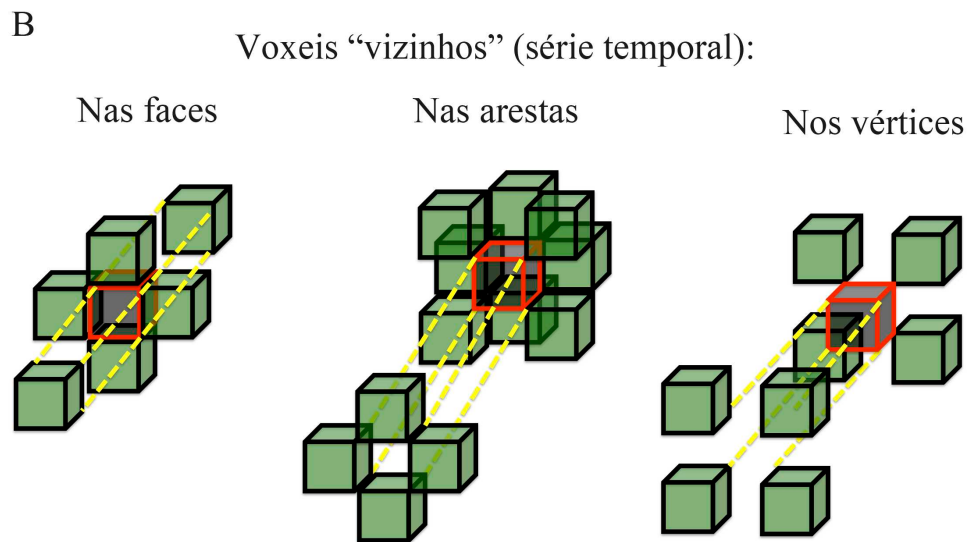
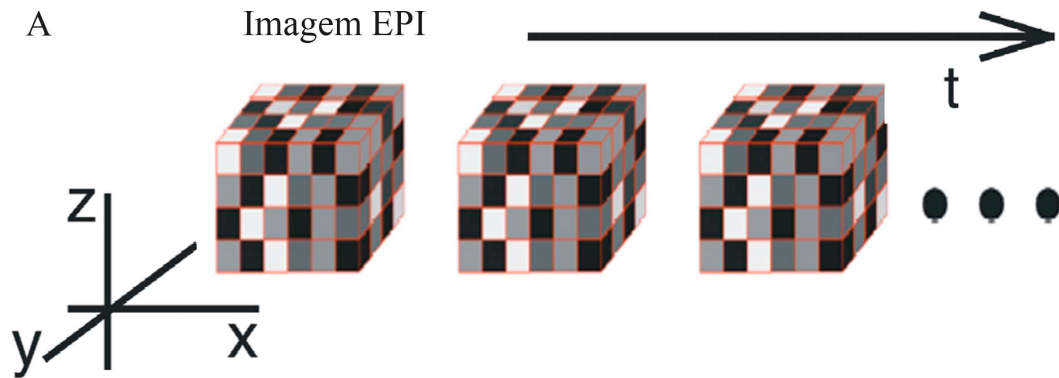


Figura 7: Representação de uma aquisição de série temporal em EPI. Voxels apresentados em níveis de cinza (A). Definição de “vizinhos” para um determinado voxel (vermelho). Cada voxel tem seis vizinhos nas faces, doze vizinhos nas arestas e oito vizinhos nos vértices (B).

*Análise por componente independente (ICA – independent component analysis )*

O método de ICA é uma potente ferramenta empregada para separar fontes (flutuações hemodinâmicas) independentes que estejam linearmente misturadas. Consiste em representar um sistema matricial (e.g. Figura 7A) sem manter necessariamente a ortogonalidade entre esses eixos. Mais informação sobre separação de componentes podem ser obtidos na dissertação de mestrado do autor, em especial uma ferramenta semelhante ao ICA denominada *Principal Componente Analysis* (PCA).

Diversas redes funcionais foram identificadas nos cérebro de jovens controles. As mais utilizadas na literatura com objetivo de investigação em sistemas patológico são apresentadas na **Figura 8**.

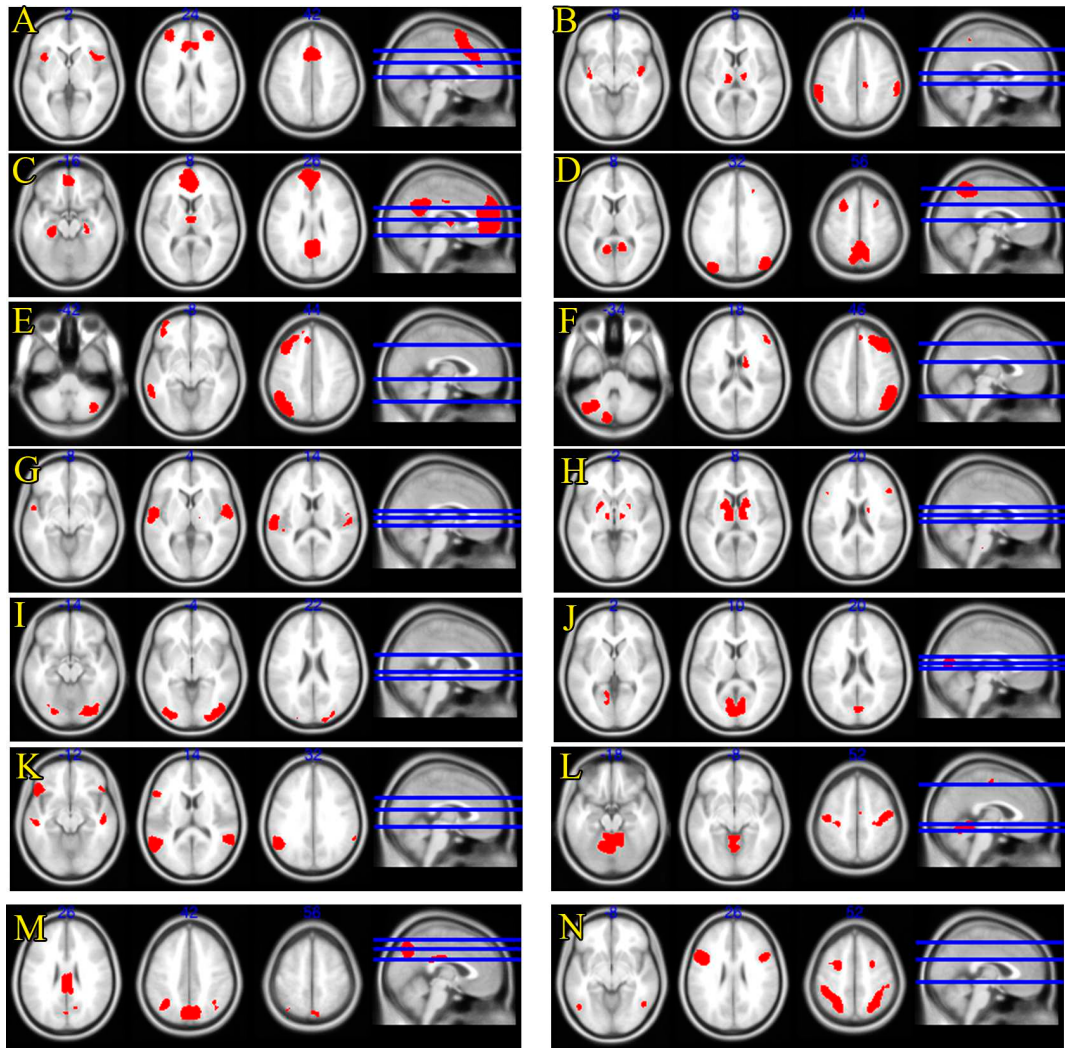


Figura 8: Principais redes funcionais humanas identificadas pela técnica de separação de componentes. Redes de saliência anterior (A) e posterior (B), de modo padrão dorsal (C) e ventral (D), de controle executivo direito (E) e esquerdo (F), de audição (G), do gânglios da base (H), visual superior (I) e primária (J), de linguagem (K), sensoriomotor (L), pré-cuneus (M) e visoespacial (N).

*Análise por clusterização temporal ( TCA – temporal clustering analysis )*

Por fim, a metodologia de *Temporal Clustering Analysis* (TCA) computa uma série temporal a partir dos dados de fMRI. Essa técnica consiste em três fases: identificar o maior valor de intensidade de sinal para cada série temporal, zerar todos os pontos no tempo da respectiva série temporal que não possuem esse valor máximo e somar todos os valores remanescentes em um dado ponto no tempo.

Matematicamente, as operações empregada no TCA são as seguintes:

Seja as séries temporais descritas pela *Equação 14*.

*Equação 14*

$$F_{(x,y,z,t)}$$

$F \equiv$  intensidade do sinal em um dado ponto no espaço e tempo

$x,y,z \equiv$  coordenadas espaciais relacionadas ao voxel

$t \equiv$  coordenada temporal

Aplica-se uma transformada na *Equação 14* para converter diretamente o espaço de quatro dimensões (x,y,z,t) em duas (s,t) descritas pela *Equação 15*. Na operação  $\mathfrak{R}^4 \Rightarrow \mathfrak{R}^2$  o número de voxel permanece constante calculado pelo produto dos números de voxéis nas três dimensões espaciais (x,y,z).

*Equação 15*

$$\oplus F_{(x,y,z,t)} = G_{(s,t)}$$

$\oplus \equiv$  operador espacial

$s \equiv$  coordenada espacial relacionadas ao voxel

$S \equiv X.Y.Z$

Desse modo, a matriz de dados transformados  $G$  pode ser escrita como apresentado na *Equação 16*.

*Equação 16*

$$G_{(s,t)} = \begin{bmatrix} G_{1,1} & G_{1,2} & \dots & G_{1,T} \\ G_{2,1} & G_{2,2} & \dots & G_{2,T} \\ \vdots & \vdots & \vdots & \vdots \\ G_{S,1} & G_{S,2} & \dots & G_{S,T} \end{bmatrix}$$

A primeira etapa do TCA caracteriza-se pela identificação dos valores máximos em cada serie temporal. Essa etapa pode ser representada pela *Equação 17*.

*Equação 17*

$$H_{(s)} = \begin{bmatrix} \max(G_{1,1}, G_{1,2}, \dots, G_{1,T}) \\ \max(G_{2,1}, G_{2,2}, \dots, G_{2,T}) \\ \vdots \\ \max(G_{S,1}, G_{S,2}, \dots, G_{S,T}) \end{bmatrix} = \begin{bmatrix} H_1 \\ H_2 \\ \vdots \\ H_S \end{bmatrix}$$

A segunda etapa do TCA anula os valores para cada ponto no tempo da respectiva série temporal que não possuem valores máximos. Essa etapa é descrita pela *Equação 18*.

*Equação 18*

$$L_{s,t} = \begin{cases} G_{s,t} & \text{se } G_{s,t} = H_s \\ 0 & \text{outro caso} \end{cases}$$

A ultima etapa do TCA estabelece a soma para cada t-ésimo. Essa etapa é descrita pela *Equação 19*.

*Equação 19*

$$Q_t = \sum_{t=1}^T L_{s,t}$$

A Figura 9 ilustra as três etapas descritas anteriormente.

Primeira etapa: identificação dos máximos das séries temporais

$$G(s,t) = \begin{array}{|c|c|c|} \hline 79 & 3 & 67 \\ \hline 95 & 84 & 75 \\ \hline 65 & 93 & 74 \\ \hline \end{array} \quad \begin{array}{|c|c|c|} \hline 39 & 70 & 4 \\ \hline 65 & 3 & 9 \\ \hline 17 & 27 & 82 \\ \hline \end{array} \quad \begin{array}{|c|c|c|} \hline 69 & 3 & 76 \\ \hline 31 & 43 & 79 \\ \hline 95 & 38 & 18 \\ \hline \end{array} \quad \begin{array}{|c|c|c|} \hline 48 & 70 & 67 \\ \hline 44 & 75 & 65 \\ \hline 64 & 27 & 16 \\ \hline \end{array}$$

Tempo (s) →

$$H(s) = \begin{array}{|c|c|c|} \hline 79 & 70 & 76 \\ \hline 95 & 84 & 79 \\ \hline 95 & 93 & 82 \\ \hline \end{array} \quad \text{Matriz de máximos}$$

Segunda etapa: anulação dos valores diferentes do máximos

$$L(s,t) = \begin{array}{|c|c|c|} \hline 79 & 0 & 0 \\ \hline 95 & 84 & 0 \\ \hline 0 & 93 & 0 \\ \hline \end{array} \quad \begin{array}{|c|c|c|} \hline 0 & 70 & 0 \\ \hline 0 & 0 & 0 \\ \hline 0 & 0 & 82 \\ \hline \end{array} \quad \begin{array}{|c|c|c|} \hline 0 & 0 & 76 \\ \hline 0 & 0 & 79 \\ \hline 95 & 0 & 0 \\ \hline \end{array} \quad \begin{array}{|c|c|c|} \hline 0 & 70 & 0 \\ \hline 0 & 0 & 0 \\ \hline 0 & 0 & 0 \\ \hline \end{array}$$

Terceira etapa: soma das intensidades não anuladas

$$Q(t) = \quad 351 \quad \quad 152 \quad \quad 250 \quad \quad 70$$

Figura 9: Operações para obtenção de série temporal a partir dos dados de fMRI pela técnica de TCA.

### **Conectividade Efetiva (ecMRI)**

O conceito de conectividade efetiva foi definido como a influência que um sistema neural exerce sobre outro, de forma direta ou indireta (Friston et al., 1993a, Aertsen et al., 1991, Friston, 1994). Trata-se da estimativa de parâmetros associados a modelos estruturais. Esses parâmetros expressam relações de causa-efeito sejam acionadas por estímulos externos que atuam sobre os sistemas neurais, sejam apenas operados entre os próprios sistemas onde, tanto a causa como o efeito são elementos exclusivos da rede neuronal. Os parâmetros apontam quantidades dinâmicas utilizadas para identificar os níveis de influência sobre um sistema físico em respostas às forças, ações ou estímulos externos, bem como repercussões secundárias no sistema neural causada anteriormente por um outro elemento desse sistema.

Nas dimensões do neurônio, o conceito traduz-se em como a atividade pré-sináptica influencia a resposta pós-sináptica, fenômeno também conhecido como eficácia sináptica. Na escala temporal operada pela **fMRI**, o conceito deve ser entendido em como a resposta hemodinâmica de uma determinada região é perturbada pela ação de outra série temporal, seja esta, de uma estrutura cerebral remota ou de um estímulo externo. Ambas as opções exigem, *a priori*, um modelo estrutural em que se busca estimar os parâmetros de conectividade.

A técnica ainda permite tanto identificar mudanças na influência entre as componentes cerebrais interconectadas bem como selecionar modelos estruturais mais adequados aos fenômenos neurais estudados. Aquele, surge como uma medida indireta de plasticidade ou de modulação por uma função cerebral enquanto esta, fazendo-se uso de inferências bayesianas, responde pela otimização do modelo estrutural.

Em resumo, no estudo de conectividade efetiva é possível obter as seguintes informações: 1) como uma região de interesse influencia outra – medida estática; 2)

como um estímulo modula a interação entre regiões de interesse – medida dinâmica e;

3) qual o modelo estrutural mais apropriado dentre um conjunto de opções – inferência bayesiana.

*Modelagem por equações estruturais (SEM – structural equation modelling)*

Uma forma de estimar os parâmetros de conectividade é através de regressões na estrutura da matriz de variância-covariância (Buchel and Friston, 1997, McIntosh and Gonzalez-Lima, 1994). Compara-se a matriz de covariância representada no modelo estrutural (matriz predita) com a matriz de covariância oriunda diretamente das séries temporais (matriz observada). A obtenção dos coeficientes utilizando modelos de equações estruturais (**SEM** – *Structural Equation Modelling*) implica em assumir que a conectividade efetiva seja constante em toda observação. Este é um fator limitante, e é incapaz de propiciar abordagens de experiências cujo cerne esteja focado na dinâmica das conectividades neurais (e.g. estudos de aprendizado, de plasticidade cerebral, etc) a menos que os dados sejam padronizados, o que leva a perda significativa de informações. Para contornar metodologicamente esta limitação, alguns trabalhos têm proposto parâmetros de regressão variáveis (Buchel and Friston, 1997, Buchel and Friston, 1998) outros, a aplicação de filtros aos dados (e.g. Filtros de kalman (Garbade, 1977) em seus casos especiais (Kalman, 1960)). Se por um lado há a desvantagem na análise por **SEM** de interpretar o modelo estrutural de forma estática, por outro a mesma análise é eficiente para comparar o mesmo modelo anatômico em grupos distintos, como pacientes versus controles.

De forma geral, as equações do modelo estrutural podem ser expressas na seguinte forma matricial:

*Equação 20*

$$\eta = \alpha + \beta\eta + \Gamma\xi + \zeta$$

$\boldsymbol{\eta}$   $\equiv$  variáveis latentes endógenas (vetor coluna com **m** elementos)

$\xi$   $\equiv$  variáveis latentes exógenas (vetor coluna com  $n$  elementos)

$\zeta$   $\equiv$  termo residual (vetor coluna com  $m$  elementos)

MÉDIA( $\xi$ )=  $\kappa$ ; COVARIÂNCIA( $\xi$ ) =  $\Phi$

MÉDIA( $\zeta$ )= 0; COVARIÂNCIA( $\zeta$ ) =  $\Psi$

Os termos  $\xi$  e  $\zeta$  são considerados independentes e, portanto, com covariância nula; os parâmetros  $\alpha$ ,  $\mathbf{B}$  e  $\mathbf{\Gamma}$  são respectivamente: o termo constante, que pode ser eliminado na simplificação do modelo estrutural; os coeficientes estruturais que relacionam as variáveis latentes endógenas e; os coeficientes estruturais que relacionam as variáveis latentes exógenas.

Isolando  $\eta$  e substituindo  $(\mathbf{I} - \mathbf{B})^{-1}$  por  $\mathbf{A}$  tem-se que:

*Equação 21*

$$\eta = \mathbf{A} (\alpha + \mathbf{\Gamma}\xi + \zeta)$$

$$\mathbf{A} \equiv (\mathbf{I} - \mathbf{B})^{-1}$$

A média das variáveis latentes endógenas pode ser expressa por:

*Equação 22*

$$\mu_{\eta} = \mathbf{A} (\alpha + \mathbf{\Gamma}\kappa)$$

$\kappa$   $\equiv$  média das variáveis latentes exógenas ( $\xi$ )

A matriz predita pode ser expressa pela a covariância das variáveis latentes endógenas representada por:

*Equação 23*

$$\text{COV}(\eta) = A (\Gamma \Phi \Gamma^T + \Psi) A^T$$

$\Gamma$   $\equiv$  coeficientes estruturais relacionados às variáveis latentes exógenas

$\Phi$   $\equiv$  covariância das variáveis latentes exógenas

$\Psi$   $\equiv$  covariância dos termos residuais

As equações que representam as variáveis observadas podem ser expressas na seguinte forma matricial:

*Equação 24*

$$y = \tau_y + \Lambda_y \eta + \varepsilon$$

$$x = \tau_x + \Lambda_x \xi + \delta$$

$y$   $\equiv$  variáveis endógenas observadas (vetor  $p$  elementos)

$x$   $\equiv$  variáveis exógenas observadas (vetor  $q$  elementos)

$$E(\varepsilon) = \mathbf{0}; \text{COV}(\varepsilon) = \Theta_y$$

$$E(\delta) = \mathbf{0}; \text{COV}(\delta) = \Theta_x$$

A matriz  $y$  representa um vetor com  $p$  elementos das variáveis endógenas observadas;  $x$  representa o vetor com  $q$  elementos das variáveis exógenas observadas;  $\varepsilon$  e  $\delta$  são os erros medidos respectivamente em  $y$  e  $x$ ;  $\tau_y$  e  $\tau_x$  são termos constantes associados respectivamente a  $y$  e  $x$ ;  $\Lambda_y$  e  $\Lambda_x$  são os parâmetros das variáveis observadas endógena e exógena.

As médias dessas variáveis são expressas por:

*Equação 25*

$$\begin{aligned}\mu_y &= \tau_y + \Lambda_y A (\alpha + \Gamma \kappa); \\ \mu_x &= \tau_x + \Lambda_x \kappa\end{aligned}$$

$\mu_y \equiv$  média das variáveis endógenas observadas

$\mu_x \equiv$  média das variáveis exógenas observadas

A matriz de variâncias e covariâncias é:

*Equação 26*

$$\begin{aligned}\Sigma_{yy} &= \Lambda_y [A (\Gamma \Phi \Gamma^T + \Psi) A^T] \Lambda_y^T + \Theta_y ; \\ \Sigma_{xx} &= \Lambda_x \Theta \Lambda_x^T + \Theta_x ; \\ \Sigma_{yx} &= \Sigma_{xy} = \Lambda_y A \Gamma \Theta \Lambda_x^T\end{aligned}$$

$$\Sigma = \begin{bmatrix} \Sigma_{xx} & \Sigma_{xy} \\ \Sigma_{yx} & \Sigma_{yy} \end{bmatrix}$$

$\Sigma \equiv$  matriz de covariância predita

Esta matriz ( $\Sigma$ ), também chamada de “predita”, contém os parâmetros de conectividade a serem comparados com a matriz de covariância ( $S$ ), calculada a partir das séries temporais.

Raros modelos estruturais podem ser resolvidos analiticamente dado que a inclusão de componentes e de parâmetros, que aproximam o modelo anatômico do fenômeno neural, incorre na definição de equações de ordem superior. Outra consequência bastante comum desta inserção é a não convergência dos parâmetros, nas estimativas baseadas em cálculo numérico. Os modelos estruturais não convergentes são imprestáveis para solucionar as equações estruturais e, conseqüentemente, incapaz de explicar o fenômeno neural. A solução numérica oferecida pelo Máximo Verossímil (**ML** – *Maximun Likelihood*) tem sido empregada

largamente, mas há outras propostas de soluções numéricas para as equações estruturais, como quadrados mínimos e a livre distribuição assintótica.

A Função de Máximo Verossímil (**MLF** – *Maximun Likelihood Function*) é um método estatístico iterativo utilizado principalmente para ajustar um modelo matemático em um conjunto de dados. O método consiste em estimar o valor que maximiza a função de densidade de probabilidade (**PDF** – *Probability Density Function*) para um valor que faz os dados observados mais parecidos.

Sejam os dados representados por um vetor **Y** com **m** medidas independentes entre si. Considere que as medidas seguem distribuição gaussiana com média  $\mu$  e variância  $\sigma^2$ . Matematicamente pode-se escrever:

*Equação 27*

$$Y = (y_1, y_2, y_3, \dots, y_m) \approx N(\mu, \sigma^2)$$

$N(\mu, \sigma^2) \equiv$  Distribuição normal

$\mu \equiv$  Média;  $\sigma^2 \equiv$  variância

$Y \equiv$  vetor representando as medidas (eventos)

$y_i \equiv$  eventos independentes

$m \equiv$  número total de eventos

Seja  $p(Y | \mu, \sigma^2)$  a função densidade de probabilidade que especifica a probabilidade de encontrar os dados **Y** para determinados parâmetros  $\mu$  e  $\sigma^2$ . Pode-se escrever a função como:

*Equação 28*

$$p_{(y)} = \frac{1}{\sigma\sqrt{2\pi}} \exp\left[-\frac{(y-\mu)^2}{2\sigma^2}\right]$$

$p \equiv$  Função densidade de probabilidade normal

Como cada evento ( $y_i$ ) é estatisticamente independente entre si e, de acordo com a teoria da probabilidade, a função da densidade de probabilidade do vetor  $\mathbf{Y}$ , ou seja,  $\mathbf{p}(\mathbf{Y})$ , pode ser expressa como a multiplicação das densidades de probabilidades de cada evento. Portanto:

*Equação 29*

$$P_{(y = (y_1, y_2, y_3, \dots, y_m) | \mu, \sigma^2)} = P_{(y_1 | \mu, \sigma^2)} P_{(y_2 | \mu, \sigma^2)} P_{(y_3 | \mu, \sigma^2)} \dots P_{(y_m | \mu, \sigma^2)} = \prod_{i=1}^m p_{(y_i | \mu, \sigma^2)}$$

$p \equiv$  Função densidade de probabilidade normal

Na prática, tem-se um conjunto de eventos, sob os quais se deseja estimar os parâmetros  $\mu$  e  $\sigma^2$  de uma população, em uma função específica, ou seja, tem-se o problema inverso ao apresentado nas *Equações 27, 28 e 29*. A função que descreve esse problema inverso é denominada Função de Máximo Verossímil (**MLF**), representada matematicamente por:

*Equação 30*

$$L_{(\mu, \sigma^2 | Y)} = P_{(Y | \mu, \sigma^2)} = \prod_{i=1}^m p_{(y_i | \mu, \sigma^2)}$$

$L(\mu, \sigma^2 | Y) \equiv$  Função de máximo verossímil (**MLF**)

Ambas as funções, **PDF** e **MLF**, tratam dos mesmos elementos, entretanto, os parâmetros em uma são os eventos da outra. Ademais, as duas funções são definidas

em abscissas diferentes, por isso não são diretamente comparáveis. Especificamente, por um lado a **PDF** é uma função que descreve o comportamento dos eventos para um dado conjunto de parâmetros. Por outro lado, a **MLF** é uma função que descreve o comportamento dos parâmetros dado um conjunto de elementos. Esta função é definida na escala (abscissa) dos parâmetros enquanto aquela na escala dos dados.

Extraindo o logaritmo neperiano na *Equação 30*, a fim de converter a função produtória em somatória, tem-se que:

*Equação 31*

$$\ln L = \ln \prod_{i=1}^m p_i = \sum_{i=1}^m \ln p_i$$

$L \equiv$  Função de máximo verossímil (**MLF**)

As funções  $\ln L$  (*log-likelihood*) e  $L$  são monotonicamente relacionadas entre si, e por isso, a maximização de uma refere-se também à outra. Assumindo que a função *log-likelihood* seja diferenciável, somente se existir um conjunto de parâmetros ( $\mathbf{w}$ ) que satisfaçam a seguinte equação diferencial:

*Equação 32*

$$\frac{\partial \ln L_{(\mathbf{w} | Y)}}{\partial w_j} = 0$$

$\mathbf{w} \equiv$  Conjunto de parâmetros

$j \equiv$  índice de parâmetros

O ponto de inflexão obtido pela *Equação 32* pode ser de mínimo ou de máximo, assim faz-se necessário impor uma segunda condição para garantir que o ponto de inflexão almejado seja de máximo.

*Equação 33*

$$\frac{\partial^2 \ln L_{(w|Y)}}{\partial w_j^2} < 0$$

$w \equiv$  Conjunto de parâmetros

$j \equiv$  índice de parâmetros

Na prática, nem sempre é possível obter analiticamente a solução das *Equações 32 e 33*, como por exemplo, quando os modelos envolvem muitos parâmetros. Nestes casos, a **PDF** geralmente é ‘muito não-linear’. Para se estimar os parâmetros nestas ocasiões, faz-se uso de processos numéricos como sucessivas interações.

Portanto, a comparação entre  $\Sigma$  e  $S$  é feita pela escolha iterativa dos parâmetros em  $\Sigma$  que maximizam o valor **ML** da seguinte equação:

*Equação 34*

$$ML = \ln(|\Sigma|) - \ln(|S|) - \text{trace}(S\Sigma^{-1}) - p$$

*trace*  $\equiv$  soma dos elementos da diagonal principal;

*p*  $\equiv$  número de variáveis medidas

O método da **SEM** é uma técnica cuja característica principal é confirmatória (não exploratória). Sua aplicação em **fMRI** é comumente empregada com a eliminação dos termos latentes da equação geral acima apresentada, preservando apenas os termos observados e suas respectivas relações. Esta simplificação é conhecida como *Path Analysis*.

### *Modelagem causal dinâmica (DCM – Dinamic Causal Modelling)*

Outra forma de caracterizar os parâmetros de conectividade é através da modelagem causal dinâmica (**DCM** – *Dinamic Causal Modelling*) (Friston et al., 2003). O **DCM** faz distinção entre os níveis neuronal e hemodinâmico, modelando as interações de populações de neurônio, no nível cortical, a partir de séries temporais (hemodinâmica – no **fMRI**, ou eletrofisiológicas – no **EEG**). Essa tarefa é realizada com o auxílio de modelos suplementares que sugerem a forma de como a atividade neuronal é transformada na resposta medida, permitindo que os parâmetros do modelo neuronal sejam estimados através dos dados observados. Esquemáticamente, a informação flui partindo dos estímulos de entrada (*input*) – constituídos por funções convencionais codificadas no desenho experimental, passando ao estado neural (*state*) – representado pelas atividades neuronais e outras variáveis neurofisiológicas e biofísicas e, finalmente, sendo medidas (*output*). Os estímulos de entrada induzem respostas neurais de duas formas. Primeira, eles podem induzir respostas através de influências diretas sobre uma região de interesse no modelo estrutural (estímulo intrínseco). Segunda, eles podem modular conexões existentes no modelo estrutural (estímulo contextual) (Friston and Buchel, 2000). Ao se observar mudanças de conectividade em função de um longo período de tempo, pode-se obter a outra vantagem do método: a medida indireta de plasticidade neural. A classe de estímulos contextuais emula respostas claramente não lineares cuja modelagem, nas equações do **DCM**, são representadas por aproximações em sistemas bilineares. Resumidamente, o **DCM** é um procedimento de identificação de padrões em sistemas não-lineares usando a estimativa Bayesiana em parâmetros de um sistema dinâmico e determinista tipo *input-state-output*.

Matematicamente, as equações de estado neuronal são definidas como:

*Equação 35*

$$\mathbf{z} = [z_1, z_2, z_3, \dots, z_i]^T$$

$\mathbf{z} \equiv$  conjunto de estados neuronais

$z_i \equiv$  estado neuronal da região  $i$

$i \equiv$  número total de regiões (nós no modelo estrutural)

Como o **DCM** é um método dinâmico, a derivada temporal do conjunto dos estados neuronais ( $\mathbf{z}$ ) recai na função neuronal que será aproximada. Portanto:

*Equação 36*

$$\frac{\partial \mathbf{z}}{\partial t} = \dot{\mathbf{z}} = \mathbf{F}_{(z, u, \theta)}$$

$\mathbf{F} \equiv$  Função neuronal não linear

$\mathbf{u} \equiv$  inputs

$\boldsymbol{\theta} \equiv$  Parâmetros

A função  $\mathbf{F}$  é a função não-linear que descreve a influência neurofisiológica sofrida pelo conjunto de regiões ( $\mathbf{z}$ ) e estímulos externos ( $\mathbf{u}$ ). Os parâmetros expressos em  $\boldsymbol{\theta}$  são utilizados na inferência bayesiana. Como, a função  $\mathbf{F}$  será aproximada da equação bilinear, as componentes  $\mathbf{z}$ ,  $\mathbf{u}$  e  $\boldsymbol{\theta}$  serão novamente parametrizados em termos de conectividade efetiva. A aproximação bilinear pode ser expressa por:

*Equação 37*

$$\dot{z} \approx Az + \sum u_j B^j z + Cu = \left( A + \sum u_j B^j \right) z + Cu$$

$A \equiv$  Parâmetros de conectividade intrínsecos (na ausência de inputs)

$B \equiv$  Parâmetros de conectividade modulatória (regulam as conexões)

$C \equiv$  Parâmetros de conectividade extrínsecas (associadas diretamente aos inputs)

$j \equiv$  Número de inputs

Os parâmetros A, B e C podem ser obtidos a partir das seguintes derivadas

parciais: x

*Equação 38*

$$A = \frac{\partial F}{\partial z} = \frac{\partial \dot{z}}{\partial z} ;$$

$$B^j = \frac{\partial^2 F}{\partial x \partial u_j} = \frac{\partial}{\partial u_j} \frac{\partial \dot{z}}{\partial x} ;$$

$$C = \frac{\partial F}{\partial u}$$

$A \equiv$  Parâmetros de conectividade intrínsecos (na ausência de inputs)

$B \equiv$  Parâmetros de conectividade modulatória (regulam as conexões)

$C \equiv$  Parâmetros de conectividade extrínsecas (associadas diretamente aos inputs)

**A** pode ser entendida como o acoplamento intrínseco entre as regiões cerebrais na ausência de *inputs*. Pela *Equação 38* pode-se observar que **A** representa a conectividade de primeira ordem. **B** representa o conjunto dos parâmetros que modificam as conectividades intrínsecas. Com a *Equação 38* observa-se que a

obtenção destes parâmetros pode ser feita pela derivada de segunda ordem. **C** representa o conjunto de parâmetros associados diretamente aos *inputs* que levam a atividade neuronal. O conjunto dos parâmetros **A**, **B** e **C**, ou simplesmente matriz de acoplamento  $\theta_c$ , define a arquitetura e as interações no nível neuronal a serem estimadas.

Esse três níveis de conectividade cerebral podem ser utilizados para explorar diversas condições neuropsiquiátricas e podem constituir-se em um importante marcador para esses transtornos. O potencial dessas técnicas eleva-se ainda mais por serem metodologias não invasivas e com poucas contra indicações. Esses conceitos tomados conjuntamente, motivaram o desenvolvimento dessas técnicas no intuito de se observar padrões ainda não conhecidos de diversas doenças cerebrais e transtornos mentais.

## **OBJETIVOS**

**Objetivos Gerais:**

- Estudar e estimar conectoma cerebral com imageamento por ressonância magnética nuclear
- Modelar interações cerebrais em distintas condições cerebrais e mentais

**Objetivos Específicos:**

- Correlacionar mapas estáticos de ressonância magnética funcional e de conectividade anatômica, funcional e efetiva;
- Estabelecer metodologia inovadora para aquisição, processamento e análise de fMRI, acMRI, fcMRI e ecMRI;
- Estimar mapas de conectividade e comparar grupos de indivíduos controle e pacientes com epilepsia mesial temporal unilateral para as tarefas:
  - Memória verbal (codificação, reconhecimento e evocações imediata e tardia);
  - Memória visual (codificação, reconhecimento e evocações imediata e tardia) e
  - Repouso (resting state)
- Avaliar a conectividade nas regiões mediais temporais com dependência do envelhecimento e codificação de palavras com conteúdo emocional positivas, negativas e neutras.
- Estimar mapas de conectividade anatômica e comparar grupos de controles, sujeitos idosos com depressão e pacientes portadores de mutação no gene SPG11.
- Comparar mapas de conectividade de sujeitos controles, pacientes com doença de Alzheimer e déficit cognitivo leve e correlacionar esses mapas com perfis neuropsicológicos.

## **METODOLOGIA**

Em razão de cada experimento deter métodos e resultados específicos, ambas as etapas serão descritas em cada experimento. O trabalhos que se tornaram artigos publicados em revistas indexadas são apresentados na sequência.

## **Experimento 1 – Conectividade efetiva: SEM aplicado à plasticidade etária e codificação de palavras com conteúdos emocionais.**

### **MATERIAIS E MÉTODOS**

#### **Sujeitos**

Participaram deste trabalho 44 indivíduos adultos sadios (22 mulheres) idade média de  $21,98 \pm 3,82$  e 23 sujeitos mais velhos sadios (15 mulheres) idade média de  $71,91 \pm 7,06$ . Rastreou-se a existência de eventos patológicos de ordens neurológica, cardiovascular ou presença de depressão. A média do inventário de depressão de Beck (*Beck Depression Inventory - BDI*)(Beck, 1979) foi estimada em  $1,31 \pm 1,98$  para os indivíduos adultos jovens, enquanto a escala de depressão geriátrica (*Geriatric Depression Scale – GDS*) (Yesavage et al., 1983, Sheikh et al., 1991) foi calculada em  $2,72 \pm 2,32$  para os sujeitos mais velhos. A média de escolaridade foi de  $14,94 \pm 1,92$  nos jovens e de  $17,09 \pm 2,22$  nos mais velhos. Testes de vocabulário foram aplicados aos participantes. Os adultos jovens obtiveram a pontuação média de  $56,71 \pm 5,71$  enquanto os adultos mais velhos pontuaram a média de  $57,74 \pm 4,59$ . Nenhum participante estava sob a administração de medicamentos que compromettesse funções cognitivas ou de atenção.

#### **Ética**

Os participantes receberam o termo de consentimento para fazerem parte do estudo e foram pagos em \$25,00 (vinte e cinco dólares) por hora pelo tempo empregado despendido no experimento. O estudo foi revisado e aprovado pelo comitê sobre uso de humanos como

sujeitos experimentais (*Committee on the Use of Humans as Experimental Subjects – COUHES*) do Instituto de Tecnologia de Massachusetts (*Massachusetts Institute of Technology – MIT*).

### Aquisição de dados

Imagens em eco planar (EPI) foram coletadas utilizando o sistema Trio 3T da Siemens em dimensões isotrópicas de 5mm, FOV 200x200, tempo de repetição 2000ms e tempo de eco 30ms.

### Codificação

Foram extraídas 324 palavras das “normas afetivas de palavras inglesas” (*The affective norms for english words - ANEW*)(Bradley and Lang, 1999) cujo conteúdo emocional poderia ser classificado exclusivamente como negativo (102 palavras), neutro (116 palavras) ou positivo (102 palavras); formando 2 conjuntos, cada um com 52, 58 e 52 palavras respectivamente aos conteúdos emocionais relacionados. Durante a codificação, cada participante viu um dos grupos de 162 palavras (52 negativas, 58 neutras e 52 positivas). Adicionalmente, 16 palavras foram utilizadas para intercalar eventos e controlar os efeitos de apresentações recentes. Os participantes compuseram um dos 8 grupos para realizarem a tarefa de codificação, ilustrados pela **Figura 10**.

<b>Codificação 1</b> POS Conjunto 1 NEU Conjunto 2 NEG Conjunto 2	<b>Codificação 2</b> POS Conjunto 1 NEU Conjunto 1 NEG Conjunto 2	<b>Codificação 3</b> POS Conjunto 1 NEU Conjunto 2 NEG Conjunto 1	<b>Codificação 4</b> POS Conjunto 2 NEU Conjunto 2 NEG Conjunto 2
<b>Codificação 5</b> POS Conjunto 1 NEU Conjunto 1 NEG Conjunto 1	<b>Codificação 6</b> POS Conjunto 2 NEU Conjunto 1 NEG Conjunto 2	<b>Codificação 7</b> POS Conjunto 2 NEU Conjunto 2 NEG Conjunto 1	<b>Codificação 8</b> POS Conjunto 2 NEU Conjunto 1 NEG Conjunto 1

Figura 10 – Oito grupos de codificação de palavras com conteúdo emocional (positiva, neutra ou negativa), fracionados em dois conjuntos.

As palavras foram projetadas dentro da bobina do aparelho de ressonância magnética e visualizadas através de um espelho colocado sobre a bobina de crânio. O teste foi fracionado em duas aquisições com 81 palavras, respeitando o tamanho e a freqüência no idioma inglês. As palavras foram apresentadas durante dois segundos para os indivíduos jovens e de três segundos para os adultos mais velhos. Foi solicitado aos participantes para julgarem as palavras em concretas, abstratas ou incertas com o propósito de intensificar a codificação. Os participantes manifestaram esse julgamento a partir de um botão colocado em sua mão direita. A ordem de apresentação das palavras foi randomizada. Solicitou-se aos indivíduos lembrarem das palavras pois estes seriam testados mais tarde em outro experimento.

### **Pré-processamento das imagens funcionais**

Todas as imagens foram pré-processadas com o software FreeSurfer ([www.surfer.nmr.mgh.harvard.edu](http://www.surfer.nmr.mgh.harvard.edu)) associado ao software FSL ([www.fmrib.ox.ac.uk/fsl/](http://www.fmrib.ox.ac.uk/fsl/)) de acordo com os seguintes passos: correção de movimento por modelo de corpo rígido (Singh et al., 1998); normalização espacial para o padrão do MNI (Carmack et al., 2004) e suavização espacial com função gaussiana tridimensional de FWHM de 10mm. O pré-processamento objetivou a preparação das imagens individuais para que possam alimentar a comparação os entre grupos.

### **Análise dos dados**

#### **Definição dos volumes anatômicos de interesse (AVOI)**

Foram criados mapas probabilísticos estruturais (Fischl et al., 2004, Fischl et al.,

2008, Fischl et al., 2002, Deskan et al., 2006), de ambos os hemisférios, das estruturas apresentadas na **Tabela 1** e ilustradas na **Figura 11**.

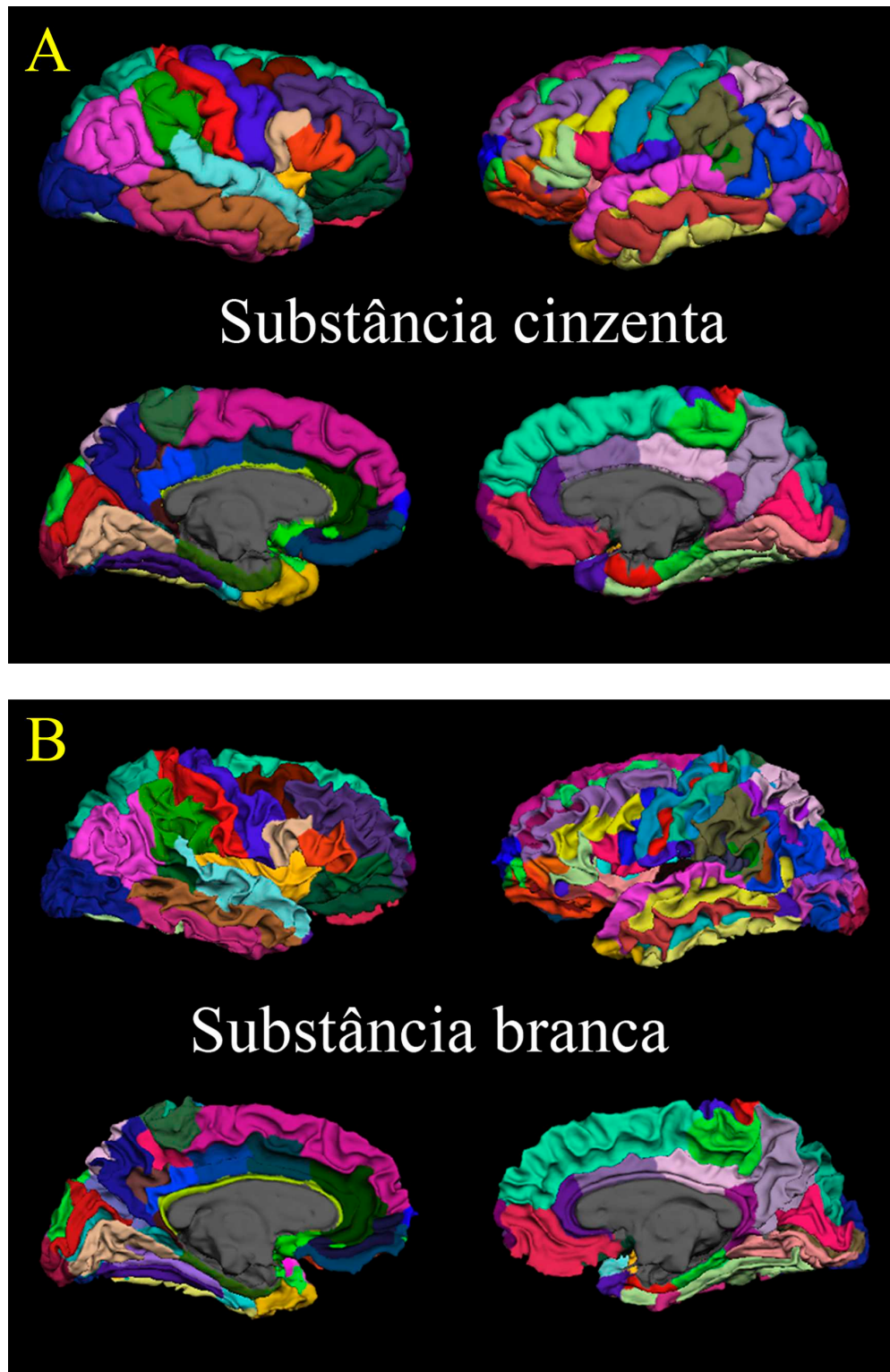


Figura 11 – Ilustração de substâncias cinzenta (A) e branca (B) segmentadas pelo programa

Tabela 1: Lista das estruturas seguímentadas no FreeSurfer

**Regiões parceladas no FreeSurfer**

**LÓBO TEMPORAL**

Superfície medial  
 córtex entorhinal  
 giro parahipocampal  
 pólo temporal  
 giro fusiforme  
 Superfície lateral  
 giro temporal superior  
 giro temporal médio  
 giro temporal inferior  
 córtex temporal transverso

**LÓBO FRONTAL**

giro frontal superior  
 giro frontal médio  
 parte rostral  
 parte caudal  
 giro frontal inferior  
 parte opercular  
 parte triangular  
 parte orbital  
 córtex orbitofrontal  
 divisão lateral  
 divisão média  
 pólo frontal  
 giro pré-central  
 lóbulo paracentral

**LÓBO PARIETAL**

Giro pós-central  
 Giro supramarginal  
 córtex parietal superior  
 córtex parietal inferior  
 córtex percuneus

**LÓBO OCIPITAL**

Giro lingual  
 córtex pericalcanino  
 córtex do cúneos  
 córtex ocipital lateral

**OUTRAS ESTRUTURAS**

giro do cíngulo  
 divisão rostral anterior  
 divisão caudal anterior  
 divisão posterior  
 divisão do ístimo  
 tálamo  
 núcleo caudato  
 núcleo putamen  
 núcleo pálido  
 hipocampo  
 amídala

Rotinas desenvolvidas em Matlab ([www.mathworks.com](http://www.mathworks.com)) foram desenvolvidas para calcular a componente principal (PCA) em cada volume anatômico de interesse (AVOI) (Wang et al., 2006). Cada vetor, relacionado univocamente com uma das estruturas descritas na tabela 1, foi utilizado para na regressão de quadrados mínimos parcial (*partial least square* – PLS) (Rayens and Andersen, 2006) para cada indivíduo separadamente. As duas

estruturas mais significativamente correlacionadas foram os hipocampus e as amídalas. Esses quatro vetores foram utilizados como semente na estimativa dos parâmetros de conectividade efetiva.

### **Modelo anatômico de conectividade efetiva**

Guiados pelo resultados obtidos pela aplicação da técnica de PLS, definiu-se o modelo anatômico de inter-relação hipocampo-amígdala, ipsilateral em ambos os hemisférios (**Figura 12**). Os parâmetros de conectividade efetiva foram estimados através da técnica de modelagem de equação estrutural (*Structural Equation Modelling* – SEM) (Astolfi et al., 2004) utilizando o programa Lisrel versão 8.8 ([www.ssicentral.com](http://www.ssicentral.com)).

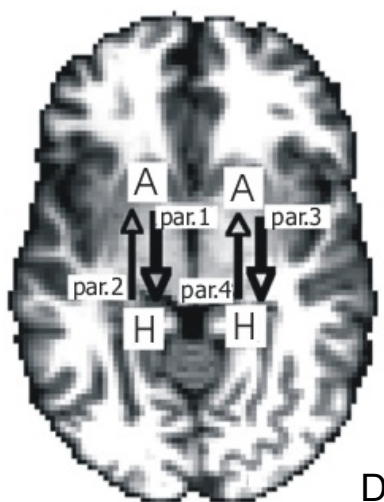


Figura 12 – Modelo anatômico utilizado na modelagem de equação estrutural para se estimar os parâmetros de conectividade (de par.1 a par.4) entre os hipocampus e amídalas.

### **RESULTADOS**

Foram encontrados basicamente três importantes resultados. Primeiro; verificou-se que os parâmetros de conectividade efetiva, na direção das amídalas para os hipocampus ipsilaterais, alcançaram valores superiores àqueles em sentido contrário, sugerindo o predomínio da influência das amídalas sobre o hipocampo, em ambos os grupos (jovens e

mais velhos sadios), durante a tarefa com conteúdo emocional (Gallagher and Chiba, 1996). Segundo; quantitativamente, a influência dos hipocampus sobre as amígdalas foi significativamente maior no grupo de indivíduos jovens que no grupo de indivíduos mais velhos. Terceiro; ao se comparar os parâmetros de conectividade nos hemisférios esquerdo e direito, percebeu-se não haver diferença significativa entre ambos os hemisférios para o grupo de indivíduos jovens enquanto uma significativa distinção ocorreu nos indivíduos mais velhos, cujos parâmetros de conectividade expressaram-se maiores à direita. Esses resultados estão ilustrados na **Figura 13** abaixo.

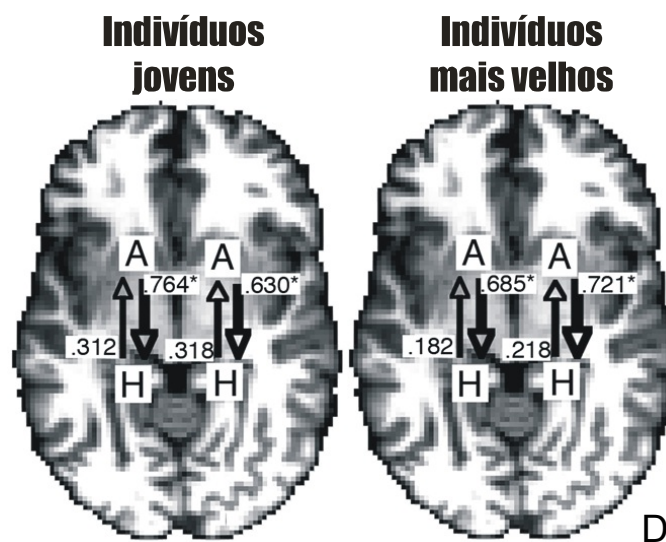


Figura 13 –Parâmetros de conectividade entre os hipocampus e amídalas (ipsilaterais) nos grupos de indivíduos jovens e indivíduos mais velhos. (\* $p < 0.001$ )

## **Experimento 2 – Conectividade efetiva: SEM aplicado a epilepsia de lobo temporal medial esquerdo com codificação de palavras neutras e abstratas**

### **MATERIAIS E MÉTODOS**

#### **Sujeitos**

Participaram deste trabalho 7 indivíduos com ELTM esquerda (6 mulheres; idade média de  $38,57 \pm 8,75$ ; escolaridade média de  $9,57 \pm 3,55$ ) e 7 indivíduos controles (5 mulheres; idade média de  $33,00 \pm 10,75$ ; escolaridade média de  $10,67 \pm 4,59$ ). Os pacientes foram selecionados com base em evidências clínicas, exames físicos e por investigações por MRI e EEG. O diagnóstico de epilepsia foi baseado no critério da liga internacional contra epilepsia (ILAE) (ILAE, 1989). Investigou-se a lateralização das crises com bases na história clínica, exames de EEG interictal e vídeo-EEG. Para constituírem o grupo de pacientes com ELTM esquerda, crises consistentes com a lateralização foram observadas em pelo menos 6 EEGs interictais e 2 crises no vídeo-EEG. Ademais, análises visuais de imagens estruturais em RM demonstraram atrofia hipocampal unilateral (Wieser, 2004) à esquerda, bem como sinais de esclerose hipocampal unilateral também à esquerda. Os pacientes foram considerados refratários à medicação. O grupo controle foi constituído de indivíduos sem prévias manifestações anormais neurológicas nem cardíacas.

#### **Ética**

Todos os participantes do trabalho receberam orientações pertinentes aos riscos potenciais e às contra-indicações, bem como assinaram o termo de consentimento apresentado no **Anexo A**, que foi aprovado pelo comitê da ética da faculdade de ciências médicas (CEP/FCM/UNICAMP) em 4 de dezembro de 2006, no parecer número 678/2006 e no certificado de apresentação para apreciação de ética (CAAE) de número 0546.0.146.000-

06. Concomitante à aquisição dos dados de RM, uma equipe formada por uma neurologista, uma psicóloga, uma enfermeira e uma biomédica colocava-se à disposição para eventuais ocorrências com os indivíduos.

### **Aquisição de dados**

Foram coletadas imagens funcionais em protocolo de eco planar (EPI) utilizando o sistema Prestige da Elscint 2T. Cada volume foi composto de 20 cortes axiais (interleaved botton-up) com FOV (*Field of View*) de 3x3mm, espessura de 6mm sem gap, ângulo de excitação de 90°, matriz de 128x72, TR de 2s e TE de 45ms.

Imagens estruturais, ponderadas por T1, foram adquiridas no mesmo sistema de ressonância, em cortes sagitais isotrópicos de 1mm sem gap, utilizando sequência de pulso em gradiente eco com TR de 22ms, TE de 9ms, ângulo de excitação de 35° e matrix 256x256.

Simultaneamente à aquisição das imagens funcionais, foram coletados dados de EEG com resolução de 32 canais e alta frequência de amostragem.

Durante a aquisição das imagens funcionais, foi solicitado ao individuo a realização de uma determinada tarefa, cujo resultado era expresso através de um botão, colocado na mão direita deste indivíduo. Deste modo, a recepção das respostas emitidas durante o exame fez parte da etapa de aquisição dos dados.

### **Paradigmas**

As aquisições das imagens funcionais foram particionadas em duas etapas (com intervalos de tempo idênticos) em referência ao material específico a ser investigado. Na primeira etapa, buscou-se investigar aspectos de memória verbal enquanto na segunda, de memória visual. Nesta, utilizou-se figuras abstratas em preto e branco, naquela, a intermediação foi alcançada com uso de palavras abstratas, sendo projetadas em letras brancas com fundo preto. Cada etapa foi adquirida de forma ininterrupta. Didaticamente,

dividiu-se cada etapa em três fases: 1) uma aquisição de codificação e evocação imediata; 2) 5 aquisições em *resting state* e 3) uma aquisição de evocação tardia e reconhecimento. Entre as duas etapas, o indivíduo era retirado da máquina de RM para um breve descanso de 30 minutos e para ajustar as impedâncias do sistema de EEG, que foi acoplado no início da aquisição. Após este intervalo, o indivíduo retornava à máquina de RM para prosseguir com as aquisições da segunda etapa. Cada etapa durou 47 minutos e 14 segundos, desconsiderando o breve intervalo entre as aquisições.

### Memória verbal: codificação e evocação imediata

A **Figura 14** ilustra o paradigma desenvolvido nesta fase.

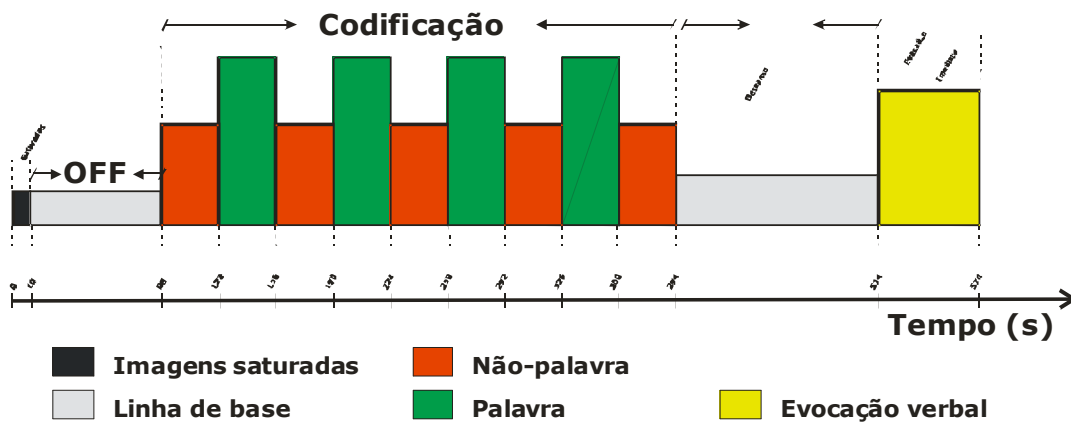


Figura 14 – Paradigma de codificação e evocação imediata para memória verbal.

Apenas uma aquisição (*run*) foi obtida em cada indivíduo, de acordo com a seguinte ordem: 5 volumes iniciais, a serem descartados no processo de análise (Saturadas); 39 volumes, sem que o indivíduo desempenhe tarefa a ele sugerida (OFF); 5 repetições, cada uma contendo 17 volumes, com apresentação visual de uma não-palavra intercalada com 4 repetições de 17 palavras. A taxa de apresentação das palavras foi de 2 segundos por palavra

enquanto uma única não-palavra estimulou o indivíduo por 34 segundos em cada apresentação. O processo de codificação totalizou 153 volumes (Codificação). A lista das palavras e a não-palavra estão apresentadas na **Tabela 2**. Seguiu-se com a aquisição de 60 volumes que objetivaram dois itens, primeiro, o completo decaimento da resposta hemodinâmica originada com a tarefa de codificação e segundo, a promoção de um pequeno intervalo de tempo para evitar conflitos entre codificação e evocação. Por fim, uma fraca mensagem luminosa, com duração de 2 segundos, solicitava do participante o início da tarefa de evocação imediata, a qual se estendeu por 30 volumes. Durante toda esta fase foram feitos os registros de EEG dos indivíduos participantes. A fase de codificação e evocação imediata durou 9 minutos e 34 segundos.

Tabela 2: Lista de palavras e não-palavra utilizada na emulação de memória verbal

Palavras utilizadas na codificação		Palavras utilizadas no reconhecimento		Não-palavra utilizada na codificação e reconhecimento
HONRA	ACASO	FAVOR	SERVIÇO	ARLTIP
OPINIÃO	SIMPATIA	TEORIA	MORAL	
PROBLEMA	ORGULHO	VALOR	FAMA	
DEVER	DECISÃO	RAZÃO	SERMÃO	
INTERESSE	CRITÉRIO	EXAME	DEFESA	
PACIÊNCIA	SISTEMA	LUXO	LEALDADE	
ALMA	VIDA	SEGREDO	PROSA	
LEI	MÉTODO	ASPECTO	ORDEM	
OPÇÃO		ESQUEMA		

### **Memória verbal: *resting state***

A **Figura 15** explica o paradigma utilizado nesta segunda fase.

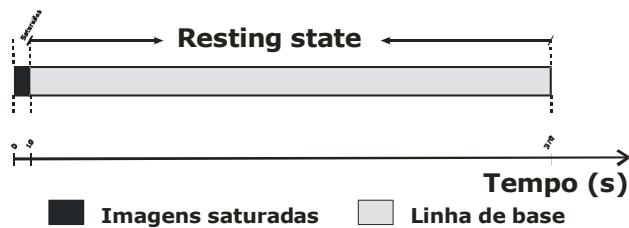


Figura 15 – Paradigma de *resting state*.

Imediatamente após a fase de codificação e evocação imediata, foram realizadas 5 aquisições (*runs*) em *resting state* de cada indivíduo. Os 5 volumes iniciais de cada aquisição (Saturadas) foram obtidos com o propósito de serem descartados na análise dos dados. Os 180 volumes restantes (*Resting state*) foram adquiridos sem que o indivíduo desempenhasse alguma tarefa a ele sugerida e sem receber qualquer estímulo externo. Igualmente à fase anterior, registros de EEG foram obtidos simultaneamente com a aquisição das imagens em EPI. A fase de *resting state*, que inclui as 5 aquisições, durou 30 minutos e 50 segundos, desconsiderando o breve intervalo entre uma e outra aquisição.

### **Memória verbal: evocação tardia e reconhecimento**

A **Figura 16** descreve o paradigma aplicado nesta terceira fase

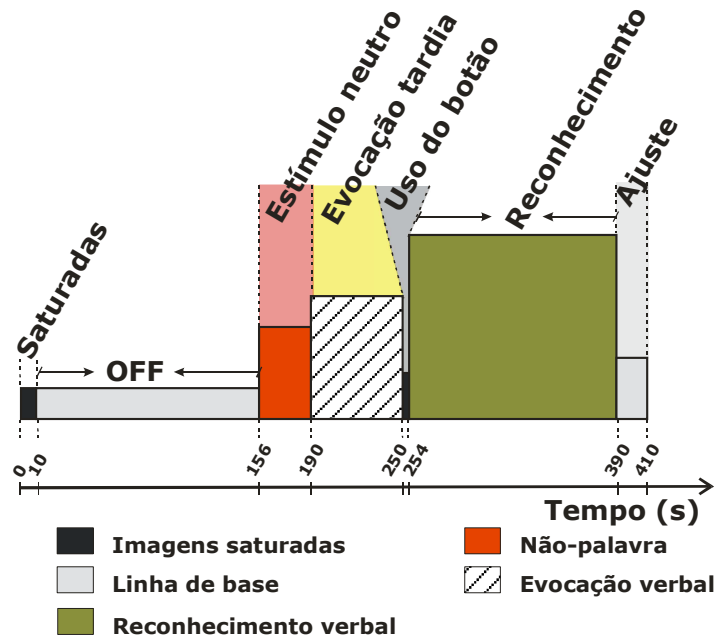


Figura 16 – Paradigma de evocação tardia e reconhecimento.

Uma única aquisição (*run*) foi obtida para cada indivíduo, de acordo com a seguinte sequência: 5 volumes iniciais, descartados durante a análise dos dados (Saturadas); 73 volumes, sem que o indivíduo desenvolvesse alguma tarefa a ele sugerida (OFF); 17 volumes com a apresentação visual da mesma não-palavra apresentada na primeira fase – descrita na **Tabela 2**, (Estímulo neutro); 30 volumes adquiridos, sem estímulo externo, em que o indivíduo tentava recuperar as palavras a ele apresentadas durante a fase de codificação (Evocação tardia); 2 volumes coletados durante o momento em que o participante recebia uma mensagem, com fraca luminosidade, informando que deveria apertar o botão que foi previamente colocado em sua mão direita, quando reconhecesse uma palavra da lista apresentada durante a codificação (Uso do botão); seguiu-se com a obtenção de 68 volumes dos quais o participante respondia afirmativamente (apertando o botão) caso a palavra projetada pertencesse à lista de palavras da primeira fase (Reconhecimento). A taxa de apresentação das palavras foi de 1 a cada 2 segundos, o que totalizou 34 palavras apresentadas, 17 destas compunham a lista inicial (da primeira fase) enquanto as demais

representam nova lista. Para evitar adaptação, a ordem de apresentação das palavras, de ambos as listas, foi randomizada. A **Tabela 2** contém ambas as listas de palavras. Por fim, seguiu-se com a aquisição de 10 volumes sem que o indivíduo recebesse alguma estimulação externa nem que desempenhasse alguma tarefa (Ajuste). Estes 10 volumes finais objetivaram o completo decaimento da resposta hemodinâmica originada com o reconhecimento. Durante toda esta fase foram feitos os registros de EEG. Esta fase durou 6 minutos e 50 segundos.

### Memória visual: codificação e evocação imediata

A **Figura 17** ilustra o paradigma desenvolvido nesta fase.

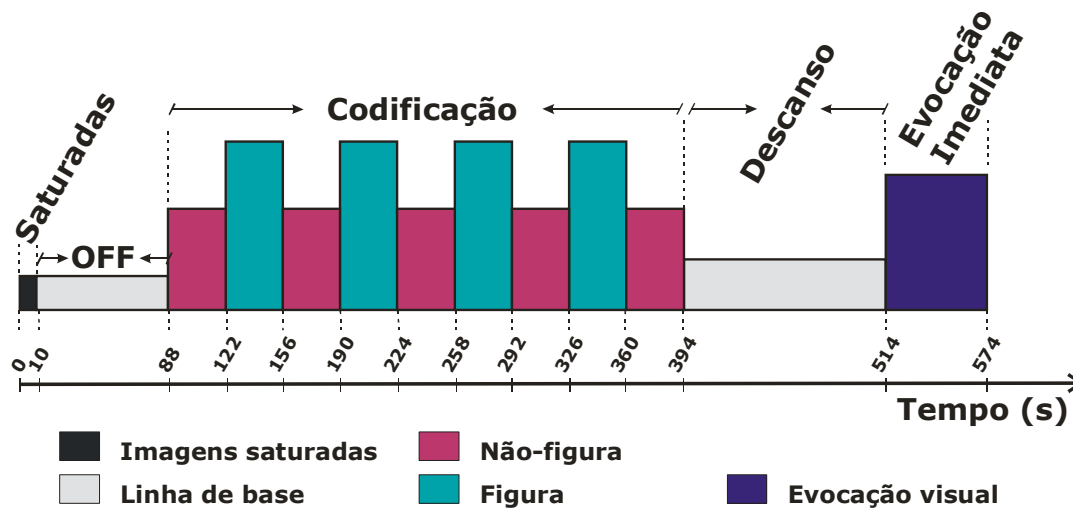


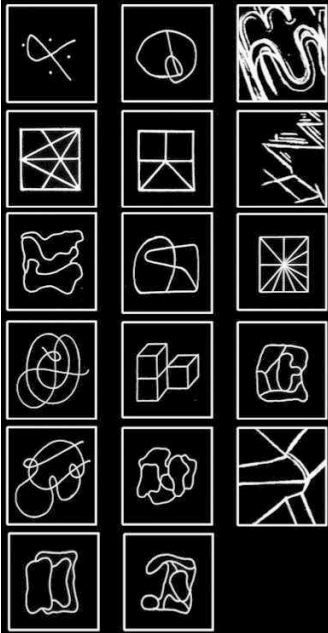
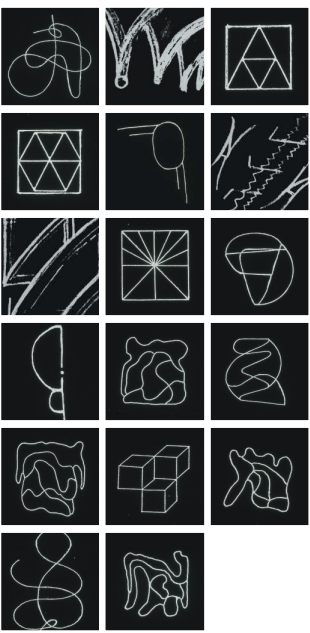
Figura 17 – Paradigma de codificação e evocação imediata para memória visual.

Apenas uma aquisição (*run*) foi obtida para cada indivíduo, de acordo com a seguinte ordem: 5 volumes iniciais, descartados na análise (Saturadas); 39 volumes, sem que o indivíduo desempenhasse alguma tarefa a ele sugerida (OFF); 5 repetições, cada uma contendo 17 volumes, com apresentação visual de uma “não-figura” (cruz) intercalada com 4 repetições de 17 figuras. A taxa de apresentação das figuras foi de 2 segundos para cada

figura enquanto a única “não-figura” estimulou o indivíduo por 34 segundos em cada apresentação. O processo de codificação totalizou 153 volumes (Codificação). A lista das figuras e da “não-figura” está apresentada na **Tabela 3**.

Seguiu-se com a aquisição de 60 volumes que objetivaram o completo decaimento da resposta hemodinâmica originada com a tarefa de codificação bem como a promoção de um pequeno intervalo de tempo para evitar conflitos entre codificação e evocação. Por fim, uma fraca mensagem luminosa solicitava do participante o início da tarefa de evocação imediata, a qual se estendeu por 30 volumes. Em toda esta fase, que durou 9 minutos e 34 segundos, foram feitos registros de EEG.

Tabela 3: Lista de figuras e “não-figura” utilizada na emulação de memória visual

Figuras utilizadas na codificação	Figuras utilizadas no reconhecimento	“Não-figura” utilizada na codificação e reconhecimento
		

**Memória visual: *resting state***

Esta etapa foi idêntica àquela relatada na fase de *resting state* durante a etapa de memória verbal. Ilustrado na **Figura 15**.

### Memória visual: evocação tardia e reconhecimento

A **Figura 18** descreve o paradigma aplicado nesta terceira fase

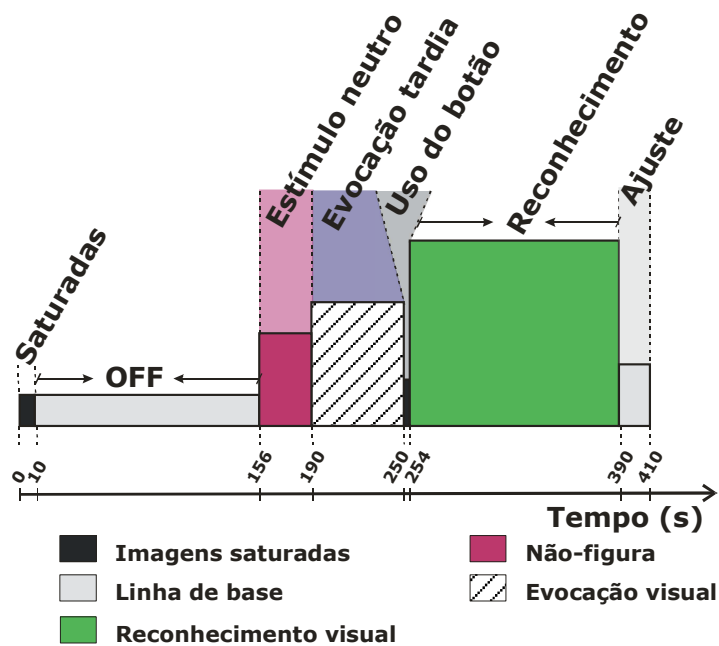


Figura 18 – Paradigma de evocação tardia e reconhecimento.

Uma única aquisição (*run*) foi obtida em cada indivíduo, de acordo com a seguinte sequência: 5 volumes iniciais, descartados durante a análise dos dados (Saturadas); 73 volumes, sem que o participante desenvolvesse alguma tarefa a ele designada (OFF); 17 volumes com a apresentação visual da mesma “não-figura” (cruz) apresentada na primeira fase – descrita na **Tabela 3**, (Estímulo neutro); 30 volumes adquiridos, sem estímulo externo, em que o indivíduo tentava recuperar as figuras a ele apresentadas durante a fase de codificação (Evocação tardia); 2 volumes coletados durante o momento em que o participante

recebia uma mensagem, com fraca luminosidade, informando que deveria apertar o botão, quando reconhecesse uma figura da lista apresentada durante a codificação (Uso do botão); seguiu-se com a obtenção de 68 volumes, dos quais, o participante respondia afirmativamente (apertando o botão) caso a figura projetada pertencesse à lista da primeira fase (Reconhecimento). A taxa de apresentação das figuras foi de uma a cada 2 segundo, o que totalizou 34 figuras apresentadas, 17 destas compunham a lista inicial (da primeira fase) enquanto as demais representam nova lista. Para evitar adaptação, a ordem de apresentação das figuras, de ambas as listas, foi embaralhada. A **Tabela 3** contém ambas as listas de figuras. Por fim, seguiu-se com a aquisição de 10 volumes sem que o indivíduo recebesse alguma estimulação externa e nem que desempenhasse alguma tarefa (Ajuste). Estes 10 volumes finais objetivaram o completo decaimento da resposta hemodinâmica originada com o reconhecimento. Durante toda esta fase, que durou 6 minutos e 50 segundos, foram feitos registros de EEG.

### **Pré-processamento das imagens funcionais**

As imagens funcionais foram coletadas no espaço k, reconstruídas para espaço anatômico (Mccoll et al., 1992) utilizando rotinas locais desenvolvidas no software matlab ([www.matworks.com](http://www.matworks.com)) e reordenadas em formato DICOM. Posteriormente foram convertidas para o formato ANALYZE utilizando o software MRIcro ([www.sph.sc.edu/comd/rorden](http://www.sph.sc.edu/comd/rorden)). Os 5 primeiros volumes de cada aquisição foram descartados dos processamentos seguintes. Utilizando o software SPM5 ([www.fil.ion.ucl.ac.uk/spm](http://www.fil.ion.ucl.ac.uk/spm)) as imagens foram orientadas temporalmente (*slice timing*), realinhadas com o modelo de corpo rígido (Singh et al., 1998), normalizadas para o espaço padrão do MNI (Carmack et al., 2004) e suavizadas espacialmente com função gaussiana tridimensional de FWHM de 6mm.

### **Análise dos dados**

### Definição dos volumes anatômicos de interesse (AVOI)

A análise de grupo dos dados de fMRI dos controles, considerando o contraste na fase de codificação da etapa de memória verbal, revelou áreas frontais e temporais como regiões significativamente correlacionadas ao paradigma expresso na **Figura 14** ( $p < 0,001$  com correção de Bonferroni). Com o atlas binário *automated anatomical labeling* – AAL (Tzourio-Mazoyer et al., 2002), provido pelo software MRICro, foram selecionadas as seguintes regiões no hemisfério esquerdo: hipocampo (HIP), giro parahipocampal (PHIP), giro frontal médio (F2), porção opercular do giro frontal inferior (F3-Oper) e porção triangular do giro frontal inferior (F3-Triang). A seguir, rotinas escritas em matlab permitiram extrair a série temporal de maior significância em cada uma destas regiões para cada indivíduo.

### Conectividade funcional e modelo estrutural

A conectividade funcional intra e inter-regiões frontais e temporais foi estabelecida calculando-se o índice de correlação de Pearson das séries temporais das AVOIs, duas a duas. A média dos valores de conectividade funcional, estimada no grupo controle, foi utilizada para desenhar o modelo estrutural apresentado na **Figura 18**. Os valores dos parâmetros de conectividade efetiva deste modelo estrutural foram estimados utilizando o software Lisrel.

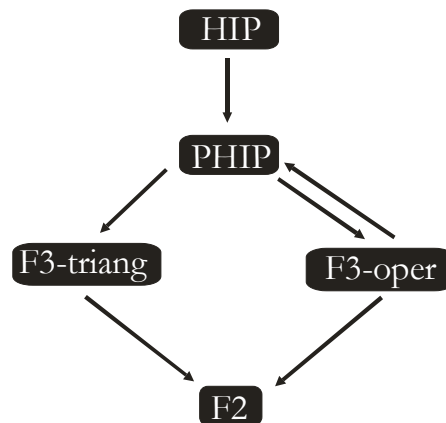


Figura 19 – Modelo estrutural de conectividade efetiva inter e intra-regiões frontais e mesiais temporais no hemisfério esquerdo para codificação de memória verbal.

## RESULTADOS

Foram encontrados resultados de duas ordens que diferenciam o grupo de controles do grupo de indivíduos com ELTM esquerda durante a codificação de palavras. A primeira diferença foi detectada em termos de conectividade funcional. Nos controles, o padrão de conectividade funcional entre as regiões frontais e mesiais temporais expressaram valores negativos, enquanto nos pacientes, esse padrão foi expresso positivamente. A **tabela 4** apresenta todos os resultados de conectividade funcional estabelecidos entre as AVOIs de ambos os grupos de indivíduos.

Tabela 4 – Parâmetros de conectividade funcional estimados entre regiões frontais e mesiais temporais para os grupo de controles (azul) e de pacientes com ELTM esquerda (vermelho).

	Controle	HIP	PHIP	F3-oper	F3-triang	F2
Paciente		X	68±18	-21±29	-13±33	-32±31
HIP		X	68±18	-21±29	-13±33	-32±31
PHIP		71±15	X	-19±18	-14±20	-26±26
F3-oper		01±32	11±22	X	88±09	60±22
F3-triang		09±37	13±28	68±23	X	47±28
F2		06±16	08±13	60±22	48±25	X

Legenda (hemisfério esquerdo): hipocampo (HIP); giro parahipocampal (PHIP); porção opercular do giro frontal inferior (F3-oper); porção triangular do giro frontal inferior (F3-triang) e giro frontal médio (F2).

Valores expressos em  $10^{-2}$ .

A segunda diferença entre o grupo de controles e o de pacientes com ELTM esquerda foi detectada em termos de conectividade efetiva. Nos controles, o padrão de conectividade

efetiva apresentou valores relativamente mais intensos que o padrão dos pacientes, inclusive quando a influência era negativa. A **Figura 20** apresenta todos os parâmetros de conectividade efetiva estabelecidos com o modelo estrutural apresentado na **Figura 19**.

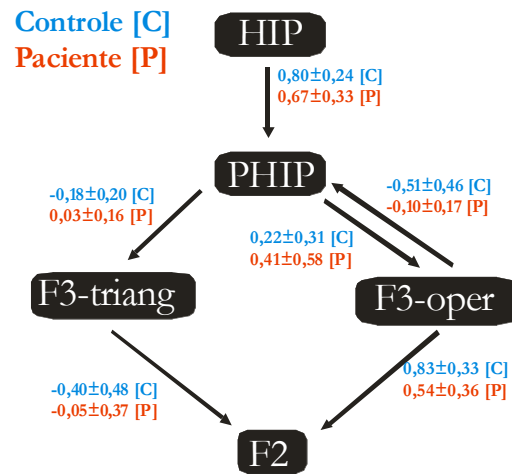


Figura 20 – Parâmetros de conectividade efetiva em sujeitos controles e pacientes com ELTM esquerda.

## **Experimento 3 – Modulação de conectividade efetiva por codificação de palavras neutras e abstratas**

### **MATERIAIS E MÉTODOS**

#### **Sujeitos**

Participaram deste trabalho 9 sujeitos controle (4 mulheres; idade média de 33,00±9,37) e 9 indivíduos com ELTM direita (5 mulheres; idade média de 39,67±6,22) e 9 indivíduos com ELTM esquerda (8 mulheres; idade média de 35,67±9,91). Os pacientes foram selecionados seguindo os mesmos critérios estabelecidos no experimento 2 com a ressalva de que cada grupo de pacientes apresentou esclerose hipocampal unilateral e ipsilateral com a lateralização dos focos epileptogênicos. O grupo controle, por sua vez, foi constituído de forma idêntica ao apresentado no experimento 2.

Todos os participantes apresentaram dominância hemisférica esquerda para linguagem determinada através de teste de audição dicótica além de serem considerados destros pelo inventário de Edinburgh (Oldfield, 1971).

#### **Ética**

Idem ao experimento 2.

#### **Aquisição de dados**

Idem ao experimento 2.

#### **Paradigmas**

Utilizou-se o paradigma de codificação de memória verbal ilustrado pela **Figura 14**.

#### **Pré-processamento das imagens**

Os processos de preparação das imagens para serem analisadas seguiram caminhos semelhantes àqueles descritos no experimento 2, entretanto, as etapas de orientação temporal (*slice timing*), correção de movimento, normalização para o espaço padrão e suavização das imagens funcionais foram realizadas com o software SPM8 ([www.fil.ion.ucl.ac.uk/spm](http://www.fil.ion.ucl.ac.uk/spm)). Após a etapa de pré-processamento, as imagens funcionais apresentaram resolução isométrica de 1mm<sup>3</sup>, enquanto a resolução no experimento anterior foi de 2mm<sup>3</sup> isométricos.

## **Análise dos dados**

### **Definição dos volumes anatômicos de interesse (AVOI)**

Para verificar a modulação na conectividade efetiva provocada pela codificação de palavras, utilizaram-se as seguintes AVOIs do hemisfério esquerdo: área visual primária (área de Brodmann 17 – AB17), porção caudal do giro temporal superior (área de Wernicke ou área de Brodmann 22 – AB22), córtex pré-frontal dorsolateral (área de Brodmann 46 – AB46) e o hipocampo (HIP). Estas regiões foram descritas previamente como correlacionadas à memória episódica (Dupont et al., 2000) bem como foram observadas na análise de grupo dos dados de fMRI dos controles na fase de codificação da etapa de memória verbal, cujo paradigma está ilustrado na **Figura 15**.

Analisadas as imagens funcionais dos três grupos individualmente (contraste na codificação), elegeu-se o voxel de maior significância em cada uma das regiões anteriormente mencionadas. As posições destes voxels foram utilizadas para marcar o centro de uma esfera (5mm de raio) nas imagens funcionais dos indivíduos em seus respectivos grupos. Extraíu-se cada série temporal encapsulada pela esfera e calculou-se sua componente principal (PCA). Esses vetores, 4 para cada indivíduo, foram utilizados para se estimar a conectividade efetiva e a modulação provocada pela codificação verbal em cada indivíduo.

### **Modulação por codificação verbal.**

Com o propósito de se verificar a modulação dos parâmetros de conectividade efetiva (intrínseco, modulatório e extrínseco) provocada pela realização da tarefa de codificação verbal, estimou-se o modelo anatômico apresentado na **Figura 21** utilizando a modelagem causal dinâmica.

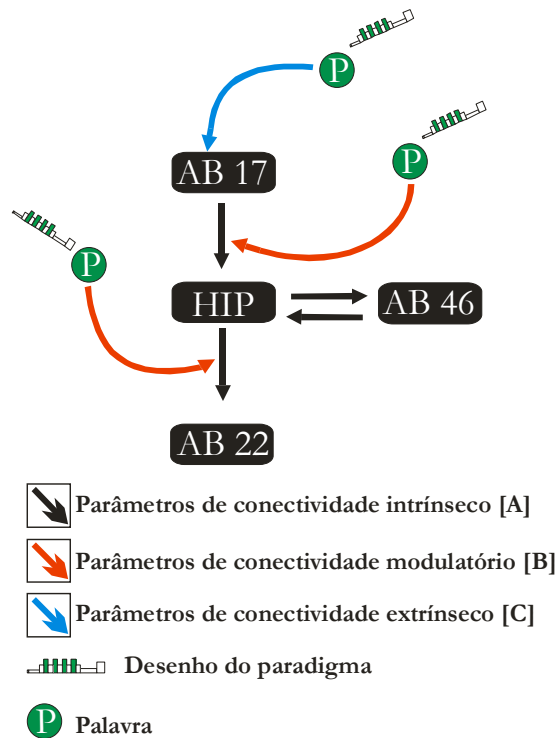


Figura 21 – Modelo anatômico com as áreas de Brodmann 17, 46 e 22 (AB17, AB46 e AB22 respectivamente) e hipocampo (HIP). Parâmetros de conectividade (A, B e C) da equação 14.

## RESULTADOS

Foram observadas diferenças, em termos de conectividade efetiva, na maioria das conexões estabelecidas entre as regiões apresentadas na **Figura 21** para o grupo controle versus os grupos de pacientes. O parâmetro de conectividade da área visual primária ao

hipocampo esquerdo foi significativamente maior nos controles que nos pacientes. O mesmo padrão, mas com sinal oposto, foi observado entre a porção dorsolateral do córtex pré-frontal e o hipocampo esquerdo. Encontrou-se também que a conectividade modulatória, produzida pela codificação verbal, foi significativamente pronunciada nos controles mas não nos pacientes. A **Figura 22** ilustra detalhadamente de forma quantitativa esses resultados.

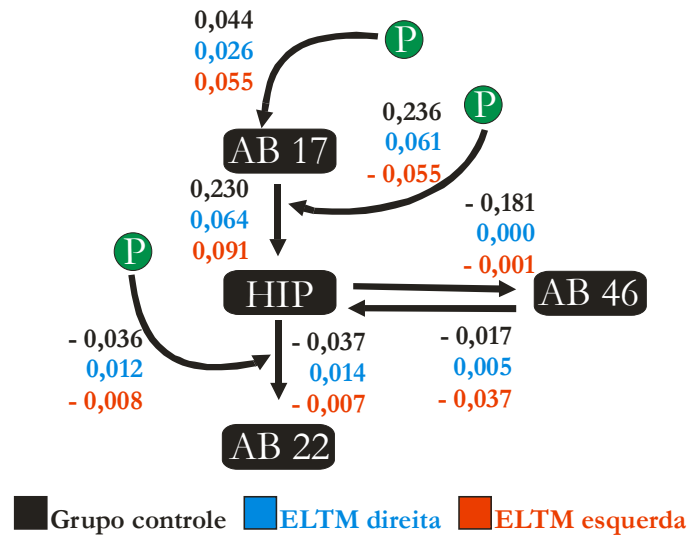


Figura 22 – Parâmetros de conectividade efetiva modulados pela codificação verbal em indivíduos controles (preto) e pacientes com ELTM direita (azul) e esquerda (vermelho).

# Experimento 4 – Análise de imageamento por tensor de difusão em pacientes idosos com e sem diagnóstico de depressão

Journal of Psychiatric Research 46 (2012) 1643–1649



Contents lists available at SciVerse ScienceDirect

Journal of Psychiatric Research

journal homepage: [www.elsevier.com/locate/psychires](http://www.elsevier.com/locate/psychires)



## DTI voxelwise analysis did not differentiate older depressed patients from older subjects without depression

Diana Moitinho Bezerra<sup>a,\*</sup>, Fabrício R.S. Pereira<sup>b</sup>, Fernando Cendes<sup>b</sup>, Marcel Parolin Jackowski<sup>c</sup>, Eduardo Y. Nakano<sup>d</sup>, Marco A.A. Moscoso<sup>a</sup>, Salma R.I. Ribeiz<sup>a</sup>, Renata Ávila<sup>a</sup>, Cláudio Campi de Castro<sup>e</sup>, Cássio M.C. Bottino<sup>a</sup>

<sup>a</sup> Old Age Research Group – PROTER, Institute and Department of Psychiatry, University of São Paulo, São Paulo, Brazil

<sup>b</sup> Neurology Department, Neuroimaging Laboratory, University of Campinas – UNICAMP, Campinas, São Paulo, Brazil

<sup>c</sup> Computer Science, Institute of Mathematics and Statistics, University of São Paulo, São Paulo, Brazil

<sup>d</sup> Department of Statistics, University of Brasília – UnB, Brasília, Brazil

<sup>e</sup> Department of Diagnostic Imaging, Heart Institute – InCor, Hospital das Clínicas at University of São Paulo, São Paulo, Brazil

### ARTICLE INFO

#### Article history:

Received 13 June 2012

Received in revised form

19 August 2012

Accepted 1 September 2012

#### Keywords:

Elderly

Major depressive disorder

Diffusion tensor imaging

Fractional anisotropy

Tract-based spatial statistics

Voxelwise analysis

### ABSTRACT

**Introduction:** Neuroimaging has been widely used in studies to investigate depression in the elderly because it is a noninvasive technique, and it allows the detection of structural and functional brain alterations. Fractional anisotropy (FA) and mean diffusivity (MD) are neuroimaging indexes of the microstructural integrity of white matter, which are measured using diffusion tensor imaging (DTI). The aim of this study was to investigate differences in FA or MD in the entire brain without a previously determined region of interest (ROI) between depressed and non-depressed elderly patients.

**Method:** Brain magnetic resonance imaging scans were obtained from 47 depressed elderly patients, diagnosed according to DSM-IV criteria, and 36 healthy elderly patients as controls. Voxelwise statistical analysis of FA data was performed using tract-based spatial statistics (TBSS).

**Results:** After controlling for age, no significant differences among FA and MD parameters were observed in the depressed elderly patients. No significant correlations were found between cognitive performance and FA or MD parameters.

**Conclusion:** There were no significant differences among FA or MD values between mildly or moderately depressed and non-depressed elderly patients when the brain was analyzed without a previously determined ROI.

© 2012 Elsevier Ltd. All rights reserved.

### 1. Introduction

Depression is the most common psychiatric disorder found in elderly patients, and prevalence rates range from 4.7 to 36.8%, considering different forms and severities of depression (Barcelos-Ferreira et al., 2009).

Depression is clearly associated with cognitive and functional deficits (Blazer et al., 1991), even when the symptoms are moderate (Kiosses et al., 2000), and these are usually present during the depressive episode and after remission of the same (Butters et al., 2000; Alexopoulos et al., 1993). Furthermore, the degree of cognitive impairment seems to follow the severity of symptoms (Baudic

et al., 2004). Recent research suggests that changes in white matter integrity throughout life are associated with cognitive impairments too (Schiavone et al., 2009).

Diffusion tensor imaging (DTI) is a variation of structural magnetic resonance imaging (MRI) examination that measures the rate and determines the direction of water diffusion in tissues, which permits the quantification of brain tissue microstructures. DTI is commonly used to study the organization of brain regions such as white matter and neuronal tract fibers because it is able to detect subtle changes in white matter (Taylor et al., 2004a; Mori and Zhang, 2006). Fractional anisotropy (FA) is a measure of directionally dependent restriction of water diffusion and mean diffusivity (MD) is the average of water diffusion in all directions (Mettenberg et al., 2012). These two measurements combined may assist in an indirect way the characterization of tissue integrity. DTI abnormalities typically manifest as increased MD and/or reduced FA.

Several DTI studies on major depressive disorder have showed that abnormalities in frontal-subcortical circuits are common and

\* Corresponding author. Faculty of Medicine, University of São Paulo, R. Dr. Ovidio Pires de Campos, 785, 3º andar sala 14, Caixa Postal 3671, CEP 01060-970, São Paulo – SP, Brazil. Tel.: +55 11972877087.  
E-mail address: [di\\_piparoti@yahoo.com.br](mailto:di_piparoti@yahoo.com.br) (D.M. Bezerra).

may play an important role in the pathophysiology of this disorder (Nobuhara et al., 2004, 2006; Shimony et al., 2009; Taylor et al., 2004b; Yang et al., 2007).

Recent evidence demonstrated significant correlation between DTI parameters and decreased global cognition in elderly patients (Vernooij et al., 2009).

Generally, DTI images may be analyzed by examining one or more regions of interest (ROI) or by voxel-based analysis (VBA). Analysis by ROI is a manual or semiautomated method that analyses predetermined regions of the brain (Sexton et al., 2009), whereas VBA analysis is an observer-independent method that explores the entire brain without a previous hypothesis (Smith et al., 2006, 2007). Voxel-based morphometry (VBM) is one of the most widely used VBA approaches to study the volume of white and gray matter (Ashburner and Friston, 2000). However, this method has significant limitations in processing anisotropic parameters (Smith et al., 2006; Afzali et al., 2011).

Smith et al. (2006) have recently suggested a new automatized method, tract-based space statistics (TBSS), as a part of the FSL program. This tool is expected to improve objectivity and simplicity in the interpretation of DTI analysis because it utilizes diffusion parameters for image registration.

Most of the studies investigating diffusion parameters and depression in the elderly have used the ROI method for image evaluation and observed changes mainly in frontal and temporal regions of brain (Nobuhara et al., 2004, 2006; Shimony et al., 2009; Taylor et al., 2004b; Yang et al., 2007). However, because researchers have only analyzed predetermined areas of the brain, the existence of difference in unevaluated regions remains unknown. Conversely, studies investigating alterations in the entire white matter through DTI in depressed elderly patients are scarce and inconclusive (Dalby et al., 2010; Yuan et al., 2007).

The objective of this study was to investigate changes in white matter through fractional anisotropy (FA) and mean diffusivity (MD), using voxelwise analysis of DTIs in depressed and non-depressed elderly patients. The study also aimed to investigate correlations among FA and MD data to scores obtained from cognitive and functional evaluations.

## 2. Methods

### 2.1. Sample

Forty-seven elderly patients aged 60 years and over who were diagnosed with major depression or depressive episodes according to the diagnostic criteria of the Diagnostic and Statistical Manual-IV (DSM-IV) (APA, 1994) participated in this study. The study subjects were selected from a pool of outpatients treated by the Old Age Research Group at the Institute of Psychiatry, "Hospital das Clínicas" at School of Medicine at the University of São Paulo (HC-FMUSP). Of the 47 elderly with depressive disorders, 8 (17.0%) received some type of antidepressant and 8 (17.0%) were taking benzodiazepines.

We included elderly patients who met the DSM-IV criteria for depressive disorders, based on a diagnostic interview (CAM-DEX) (Bottino et al., 1999) administered by two trained geriatric psychiatrists, who also applied the cognitive tests and depression scales. The clinical evaluation and MRI scanning occurred in two weeks.

The exclusion criteria for the elderly depressed group were: diagnoses of dementia or other organic mental disorders; and DSM-IV criteria-based diagnoses of any psychiatric disorder other than depression (although patients with anxiety disorders comorbid to depression were not excluded) or the inability to perform an MR examination.

To ensure that any subjects with incipient dementia would be excluded from the elderly depressed group, the Bayer Activities of Daily Living Scale (B-ADL) (Lehfeld et al., 1997) was applied to informants. According to a previous study with Brazilian patients (Folquitto et al., 2007), the cutoff point of B-ADL  $\geq 3.12$  provides adequate sensitivity, specificity, positive and negative predictive values to discriminate patients with mild to moderate dementia from non-demented elderly subjects. Patients were monitored for a year to guarantee that no dementia cases were included in the depressed elderly group. Cognitive evaluations were performed every three months, and none of the patients developed dementia during this period.

Thirty-six elderly patients aged 60 years and over without depression or any other psychiatric disorders were also included in this study as the control group. Members of control group were recruited from Geriatric Department at HC-FMUSP. No member of control group was taking psychotropic medications. The following exclusion criteria were used for the control group: current DSM-IV criteria-based diagnoses of any psychiatric disorders; and previous history of depressive disorders at any point in their lives; dementia syndrome; another organic brain syndrome and the inability to perform an MR examination.

All of the participants gave their written informed consent following a detailed description of study's procedures. This study was approved by the Institute of Psychiatry's Ethics Committee of HC-FMUSP.

### 2.2. Clinical, cognitive and functional assessment

The following instruments were used to evaluate cognitive aspects: Cambridge Examination for Mental Disorders of the Elderly (CAMDEX) (Roth et al., 1986; Bottino et al., 1999), which includes CAMCOG (Cambridge Cognitive Test) and Mini-Mental State Examination (MMSE) (Folstein et al., 1975). To measure depressive symptomatology, the Montgomery–Asberg Depression Rating Scale (MADRS) (Montgomery and Asberg, 1979) and Hamilton Rating Scale of Depression (HAM-D) (Hamilton, 1960) were utilized. Bayer Activities of Daily Living Scale (B-ADL) (Lehfeld et al., 1997) was used to evaluate functional activity. Finally, clinical comorbidities were measured using Cumulative Illness Rating Scale (CIRS) (Linn et al., 1968).

Patients with late onset depression (LOD) (after age 60) more frequently present structural and functional abnormalities in the brain in comparison to early onset depression (EOD) (Blazer, 2003). Because of this, an analysis to verify the existence of significant DTI alterations between EOD, LOD and the control group will be performed.

### 2.3. DTI acquisition

Structural MR examinations were performed at the Diagnostic Imaging Division of the Heart Institution (INCOR) of HC-FMUSP using a GE 1.5 T (Signa, GE Medical Systems, Horizon, LX) MR instrument.

Diffusion protocol used to produce DTI images consisted of a diffusion sequence in 25 directions ( $b = 0$  and  $b = 1000$  s/mm<sup>2</sup>), echo time (TE) of 100 ms, repetition time (TR) of 10,000 ms, field of view of 26, a 128 × 128 matrix, and 5.0 mm slice thickness.

### 2.4. Image processing

DTI data processing and analysis were performed using software tools from FMRIB Software Library (FSL) 4.1 (<http://www.fmrib.ox.ac.uk/fsl/>) (Smith et al., 2004). The main tool used for voxel-to-voxel comparison of diffusion data was TBSS (Smith et al., 2006) v1.2.

All images were initially aligned to the reference image at  $b = 0$  so that the sequence created a mask. The main objective in using the mask was to extract all of the elements that were not a part of the brain (for example, the eye socket) to identify exactly which voxels should be included in the analysis. This was referred to as the preprocessing stage.

FA and MD maps, three auto-values and three auto-vectors were estimated. In next step, the parameters for normalization of these data into a common space of  $1 \times 1 \times 1$  mm were calculated.

The results using these parameters were applied to the images through linear and nonlinear transformations to complete the normalization. These parameters corrected differences caused by slight movements during image acquisition along with slight distortions due to field induction in different acquisitional directions caused by MR coil itself. FMRIB58\_FA atlas was used as the reference for normalization. This step was necessary to ensure that all of the individuals were in the same space (compatible with Montreal Neurological Institute (MNI) atlas (Mazziotta et al., 2001), assuming that FMRIB58\_FA anisotropy atlas possessed the same coordinates as MNI atlas) for future statistical comparisons. This stage was referred to as "Registration".

The next step was to calculate the average FA to create a mean FA skeleton. This mean FA skeleton was formed using the average points of the FA tracts. Once created, the mean FA skeleton was applied to each patient to produce individual mean FA skeletons. The threshold selected for the creation of mean skeletons was 0.2; therefore, the program used every voxel with an FA greater than 0.2 to calculate the mean skeleton. The final result obtained from this process was used for statistical analysis; thus, only the voxels belonging to the skeleton were considered for statistics.

In the next step, voxel-to-voxel comparisons were performed among the groups, and statistical maps were generated.

### 2.5. Statistical analysis

The following tests were used to analyze clinical and socio-demographic data: MADRS, HAM-D, B-ADL, CIRS, age and education. Student's  $t$ -test was used to compare means when variables were normally distributed. Mann–Whitney  $U$ -test was used to compare groups when normality could not be established. Normality of the data was tested using Kolmogorov–Smirnov nonparametric test. Pearson's Chi-square test was used to compare frequencies for gender and civil status. Finally, analysis of covariance (ANCOVA) was used for MMSE and CAMDEX variables controlling for education because an initial analysis revealed that these parameters differed between the groups.

Voxel-to-voxel statistical comparisons were performed to compare the entire white matter skeleton of the groups (patients

vs. controls) using the TBSS tool from FSL program and the Student's  $t$ -test. Statistical maps were created to show anatomical brain location of the clusters of significantly different voxels between the groups ( $p < 0.001$ ). The statistical maps were created using a statistical threshold corrected for 1000 multiple comparisons. Pearson's correlation coefficient was used to measure associations among anisotropy parameters and clinical data.

### 3. Results

Sociodemographic data of the subjects are shown in Table 1. "Education" was the only sociodemographic variable that differed significantly between groups.

The results obtained from cognitive evaluations, depressive symptom scales, functional activity and clinical comorbidities are shown in Table 2.

Nonsignificant differences were observed between the two groups following the analysis of diffusivity, which was quantified by FA, and the diffusion of water molecules in every direction, which was quantified by MD.

Regarding the possible association between anisotropy parameters and cognitive evaluation (CAMDEX and MMSE) nonsignificant findings were observed. Similar results were observed for the association among functional activity (measured by B-ADL scale) and FA or MD parameters.

The analysis performed between EOD, LOD and control group showed nonsignificant differences, same results were obtained between EOD and LOD without the control group.

Statistical maps obtained from the results revealed nonsignificant reductions in FA nor increases in MD in depressed elderly patients and a nonsignificant association between MMSE and FA reduction in the whole sample (Figs. 1–3).

### 4. Discussion

The present study showed nonsignificant differences in FA neither MD parameters between depressed and non-depressed elderly patients. Although previous studies have demonstrated conflicting results, it should be noted that among studies reviewed that investigated depression and anisotropy parameters in the elderly (Alexopoulos et al., 1993; Bae et al., 2006; Dalby et al., 2010; Nobuhara et al., 2004, 2006; Shimony et al., 2009; Taylor et al., 2004b; Yang et al., 2007; Yuan et al., 2007), only one utilized an evaluation similar to the current study (Dalby et al., 2010). Dalby et al. (2010) used voxel-based non-morphometric analysis to investigate these parameters between depressed and non-depressed elderly patients and obtained results consistent with our study. They reported nonsignificant differences in anisotropy

**Table 1**  
Sample data.

Variable		Depressed elderly ( $n = 47$ )	Non-depressed elderly ( $n = 36$ )	Statistical test and $p$ -value
Gender	M	11 (23.4%)	9 (25.0%)	$\chi^2 = 0.028$ ( $df = 1$ )
$n$ (%)	F	36 (76.6%)	27 (75.0%)	
Age		70.94 (6.98)	69.39 (7.21)	$t = 0.866$ ( $df = 81$ )
Mean (SD)				
Education		6.31 (5.60)	9.08 (4.75)	$t = -2.378$ ( $df = 81$ )
Mean (SD)				
Number of previous depressive episodes <sup>a</sup>		1.45 (2.33)	–	<b><math>p = 0.020</math></b>
Age of onset of symptoms <sup>a</sup>		LOD = 17 (36.2%) EOD = 30 (63.8%)	–	

$n$  = number of patients; F = female; M = male; LOD = Late-onset depression; EOD = Early-onset depression;  $\chi^2$ : Pearson's chi-square;  $t$ : Student's  $t$ -test;  $p$ -value. Bold means the only significance difference found in ( $p < 0.05$ ).

<sup>a</sup> These variables refer only to patients.

**Table 2**  
Cognitive and functional assessment, severity of depressive symptoms and clinical comorbidity.

Variable	Depressed elderly (n = 47)	Non-depressed elderly (n = 36)	Statistical test and p-value
MMSE	25.21 (±) 3.74	27.86 (±) 1.99	$F = 8.612$ ( $fd = 1;80$ ) $p = \mathbf{0.004^a}$
CAMDEX	82.94 (±) 13.95	90.83 (±) 8.88	$F = 5.352$ ( $fd = 1;80$ ) $p = \mathbf{0.017^a}$
B-ADL	2.25 (±) 1.01	1.32 (±) 0.56	$t = 4.966$ ( $fd = 81$ ) $p < 0.001^b$
MADRS	23.23 (±) 8.60	1.39 (±) 1.20	$t = 15.111$ ( $fd = 81$ ) $p < 0.001^b$
HAM-D	18.64 (±) 6.17	2.67 (±) 1.57	$t = 15.151$ $p < 0.001^b$
CIRS-index	0.65 (±) 0.92	0.56 (±) 0.97	$U = 754.0$ $p = 0.427^c$
CIRS-severity	1.23 (±) 0.21	1.25 (±) 0.22	$U = 790.5$ $p = 0.724^c$

MMSE = Mini-Mental State Examination; CAMDEX = Cambridge Examination for Mental Disorders of the Elderly; B-ADL = Bayer Activities of Daily Living Scale; HAM-D = Hamilton Depression Scale; MADRS = Montgomery–Asberg Depression Rating Scale; CIRS = Cumulative Illness Rating Scale.  $fd$  = freedom degree  $p$ -value. Bold means significance ( $p < 0.05$ ) and italics means differentiate the symbol of statistical test.

<sup>a</sup> Analysis of covariance (ANCOVA) controlling for years of education.

<sup>b</sup> Student's  $t$ -test.

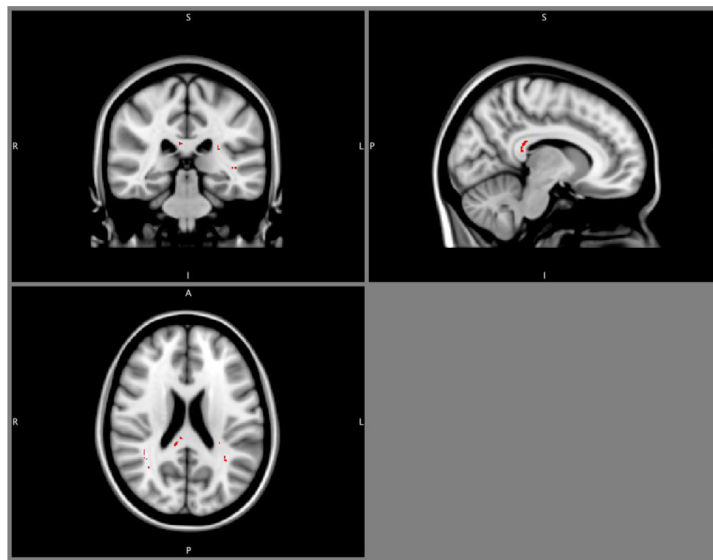
<sup>c</sup> Mann–Whitney  $U$ -test.

parameters between groups. Yuan et al. (2007) used morphometric analysis of FA to investigate the association between remission and changes in anisotropy parameters and to compare depressed elderly patients who achieved remission to non-depressed controls. In a study conducted by Alexopoulos et al. (2008), VBA analysis was used to compare elderly patients who achieved remission from depressive symptoms to elderly patients who did not achieve remission. In the remaining studies, investigations were conducted by delineating ROI (Bae et al., 2006; Nobuhara et al., 2004, 2006; Shimony et al., 2009; Taylor et al., 2004b; Yang et al., 2007).

Kieseppä et al. (2010) did not observe changes between depressed and non-depressed patients while investigating depression and anisotropy parameters using the same processing methodology used in our study (TBSS). However, this group (Kieseppä et al., 2010) investigated younger patients with a mean age of 40 years. Study conducted with even younger individuals (mean age of 20 years), who were not yet medicated for depression and were experiencing their first depressive episode, showed significant differences in the anterior part of internal capsule and parahippocampal gyrus using TBSS analysis (Zhu et al., 2011).

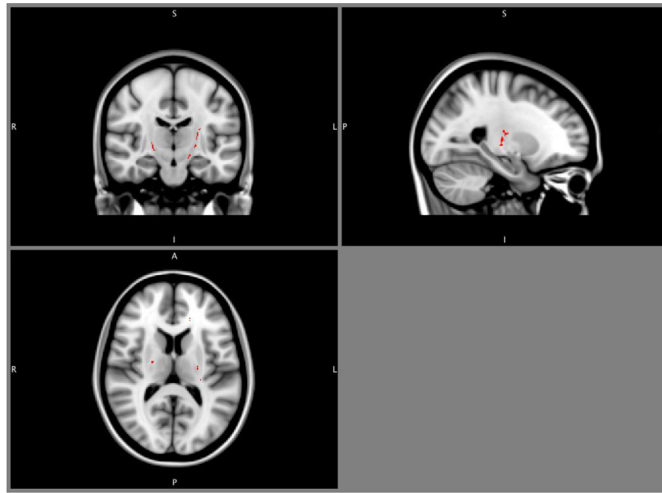
Table 3 displays data obtained from studies published to date on the study of depressed and non-depressed elderly patients using anisotropy parameters.

The same participants used in this study were previously investigated regarding changes in white and gray matter density as part of another research project (Avila et al., 2011). In this study,



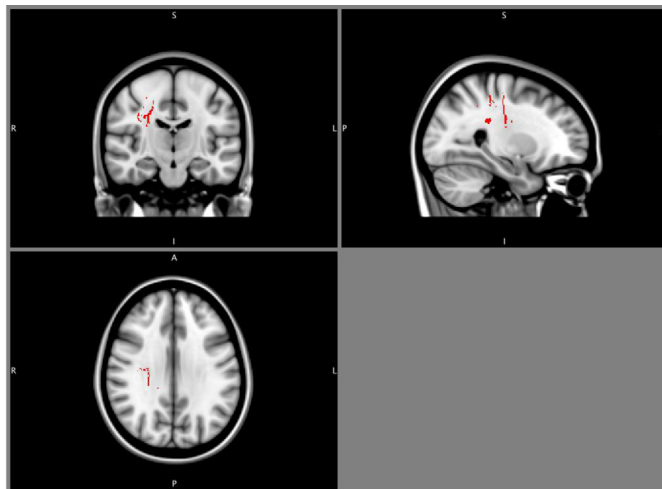
MNI coordinates of the most significant voxel  $x=11$   $y=-36$  and  $z=21$

**Fig. 1.** Nonsignificant reduction of FA in the splenium of the corpus callosum in depressed elderly compared to non-depressed elderly ( $p = 0.48$ ).



MNI coordinates of the most significant voxel X=-24 y=-17 and z=12

Fig. 2. Nonsignificant increase in MD at the posterior limb of the right internal capsule in depressed elderly compared to non-depressed elderly ( $p = 0.45$ ).



MNI coordinates of the most significant voxel x=11 y=-36 and z=21

Fig. 3. Nonsignificant positive associations between FA in temporal regions and cognition through MMSE data ( $p = 0.35$ ). The association between the anisotropy parameters and the other tests and scales did not result in statistical maps and was not significant.

**Table 3**  
Summary of the literature on DTI parameters and depressed elderly compared to non-depressed elderly.

Study	n P/C	Age mean (SD)	Study design	Methods	Significant results in depressed elderly
Taylor et al., 2004b	17	67.5 (6.1)	Depressed × non-depressed	ROI	↓ FA in the right superior frontal gyrus
Nobuhara et al., 2004	16	69.8 (6.4)	Depressed × non-depressed	ROI	↓ FA in widespread frontal and temporal regions
	8	62.9 (5.8)			
Nobuhara et al., 2006	12	60.9 (4.6)	Depressed × non-depressed	ROI	↓ FA in widespread regions of the frontal and temporal lobes Association between severity and FA in frontal lobe
	13	62.8 (6.6)			
Bae et al., 2006	13	61.5 (4.8)	Depressed × non-depressed	ROI	↓ FA in white matter of the right anterior cingulate cortex, bilateral superior frontal gyri, and left middle frontal gyrus Absence of association between severity and FA
	106	70.4 (6.4)			
Yang et al., 2007	84	71.7 (6.0)	Depressed × non-depressed	ROI	↓ FA in frontal (superior and middle frontal gyrus), and temporal (right parahippocampal gyrus) regions
	31	64.6 (5.2)			
Shimony et al., 2009	15	64.3 (4.2)	Depressed × non-depressed	ROI	↓ RA (similar to FA) in pre-frontal ROIs ↑ MD in pre-frontal ROIs and deep white matter ↑ MD in combined non-prefrontal regions (temporal, parietal, occipital and motor regions)
	78	68.6 (7.2)			
Dalby et al., 2010	23	70.0 (5.9)	Depressed × non-depressed	VBA	There is <b>no significant difference</b> in FA when compared both groups Association between FA and severity in deep white matter lesions
	22	59.2 (7.3)			
Colloby et al., 2011	38	74.1 (6.1)	Depressed × non-depressed	TBSS	Corrected maps showed <b>no significant differences</b> in FA neither MD parameters when compared both groups
	30	74.4 (6.4)			

nonsignificant differences were observed between depressed and non-depressed elderly following VBM analysis of the entire brain.

A possible explanation for the absence of significant differences between groups in this present study is the similar profiles of these groups regarding clinical comorbidities and cardiovascular factors, such as hypertension, diabetes and heart diseases, which involve major changes in white and gray matter (de Toledo Ferraz Alves et al., 2010).

Another aspect that may partially explain these findings is the small number of previous depressive episodes among the study population. Most of the patients (40.4%) were being treated for their first depressive episode, and a significant portion (25.5%) was experiencing their second depressive episode. Although no studies about the association between number of depressive episodes and diffusion parameters were found in the literature, a relationship between greater numbers of episodes and greater brain atrophy has been suggested (Janssen et al., 2007).

The present study did not observe an association between anisotropy parameters and cognitive evaluation. Although a previous study demonstrated significant correlation between microstructural white matter damage measured by diffusivity parameters and decreased global cognition in elderly patients (Vernooij et al., 2009), the relationship between white matter integrity and cognitive function has not been clearly established (Madden et al., 2004).

The current study has some important limitations: the slice width in MR examination; group heterogeneity regarding education; a majority of patients with mild to moderate depressive symptoms and a lack of data concerning duration of disease and duration of the antidepressant therapy of patients.

However, regarding abovementioned limitations, the same slice width of 5.0 mm (Abe et al., 2010; Kiesepää et al., 2010) or very similar slice widths (4.0 mm) (Ma et al., 2007; Wu et al., 2011; Yuan et al., 2007; Zhu et al., 2011) were used in several studies that investigated depression and anisotropy parameters. About severity of depressive symptoms, Dalby et al. (2010) reported a positive correlation between severity of depressive symptoms and FA changes in fiber tracts affected by deep white matter lesions, however, no association was observed in a study that correlated depression severity and FA values in younger patients (Abe et al., 2010). Moreover, when considering duration of disease, no relationships between FA parameters and the duration of depressive disorders were observed (Ma et al., 2007).

The discrepancy in the results of neuroimaging studies of major depressive disorder may reflect the clinical heterogeneity of the

samples and also possible heterogeneities intrinsic to the pathophysiology of the disorder itself.

## 5. Conclusion

Data obtained from this study suggest that there is nonsignificant difference in diffusion parameters (FA and MD) between mild to moderately depressed and non-depressed elderly patients.

It may also be concluded that diffusion parameters in the elderly (both FA and MD) are not associated with cognitive function.

## Role of funding source

This study received financial support from "Fundação de Amparo à Pesquisa do Estado de São Paulo" (FAPESP), grant no. 04/09586-9. Diana M. Bezerra was particularly supported by the "Coordenação de Aperfeiçoamento de Pessoal de Nível Superior" (CAPES).

## Contributors

Authors Cássio Machado de Campos Bottino and Diana Moitinho Bezerra designed the study.

Authors Cássio Machado de Campos Bottino, Diana Moitinho Bezerra, Fabrício Ramos Silvestre Pereira, Fernando Cendes, Marcel Parolin Jackowski wrote the protocol.

Authors Diana Moitinho Bezerra, Marco Antonio Aparício Moscoso, Salma R. I. Ribeiz, Renata Ávila, Cláudio Campi managed the literature searches and analyses.

Authors Eduardo Yoshio Nakano and Diana Moitinho Bezerra undertook the statistical analysis, and authors Diana Moitinho Bezerra and Cássio Machado de Campos Bottino wrote the first draft of the manuscript.

All authors contributed to and have approved the final manuscript.

## Conflict of interest

Authors declare no conflict of interests affecting this manuscript.

## Acknowledgments

We would like to thank Professor Edson Amaro Junior by his advices during this research.

## References

- Abe O, Yamasue H, Kasai K, Yamada H, Aoki S, Inoue H, et al. Voxel-based analyses of gray/white matter volume and diffusion tensor data in major depression. *Psychiatry Research* 2010;181(1):64–70.
- Afzall M, Soltanian-Zadeh H, Elisevich KV. Tract based spatial statistical analysis and voxel based morphometry of diffusion indices in temporal lobe epilepsy. *Computers in Biology and Medicine* 2011;41(12):1082–91.
- Alexopoulos GS, Meyers BS, Young RC, Mattis S, Kakuma T. The course of geriatric depression with “reversible dementia”: a controlled study. *American Journal of Psychiatry* 1993;150(11):1693–9.
- Alexopoulos GS, Murphy CF, Gunning-Dixon FM, Latoussakis V, Kanellopoulos D, Klimstra S, et al. Microstructural white matter abnormalities and remission of geriatric depression. *American Journal of Psychiatry* 2008;165(2):238–44.
- American Psychiatric Association Committee on Nomenclature and Statistics. *Diagnostic and statistical manual of mental disorders*. 4th ed. Washington, DC: American Psychiatric Association; 1994.
- Ashburner J, Friston KJ. Voxel-based morphometry—the methods. *NeuroImage* 2000;11:805–21.
- Avila R, Ribetz S, Duran FL, Arrais JP, Moscoso MA, Bezerra DM, et al. Effect of temporal lobe structure volume on memory in elderly depressed patients. *Neurobiology of Aging* 2011;32(10):1857–67.
- Bae JN, MacFall JR, Krishnan KR, Payne ME, Steffens DC, Taylor WD. Dorsolateral prefrontal cortex and anterior cingulate cortex white matter alterations in late-life depression. *Biological Psychiatry* 2006;60(12):1356–63.
- Barcelos-Ferreira R, Pinto Jr JA, Nakano EY, Steffens DC, Litvov J, Bottino CM. Clinically significant depressive symptoms and associated factors in community elderly subjects from Sao Paulo, Brazil. *American Journal of Geriatric Psychiatry* 2009;17(7):582–90.
- Baudis S, Tzortzis C, Barba GD, Traykov L. Executive deficits in elderly patients with major unipolar depression. *Journal of Geriatric Psychiatry and Neurology* 2004;17(4):195–201.
- Blazer D, Burchett B, Service C, George LK. The association of age and depression among the elderly: an epidemiologic exploration. *Journal of Gerontology* 1991 Nov;46(6):210–5.
- Blazer DG. Depression in late life: review and commentary. *Journals of Gerontology, Series A, Biological Sciences and Medical Sciences* 2003;58(3):249–65. Review.
- Bottino CMC, Almeida OP, Tamai S, Fortezza OV, Scalco MZ, Carvalho IAM. Entrevista estruturada para diagnóstico de transtornos mentais em idosos – CAMDEX (translated and adapted on behalf of the editors). São Paulo: Cambridge University Press; 1999.
- Butters MA, Becker JT, Nebes RD, Zmuda MD, Mulsant BH, Pollock BG, et al. Changes in cognitive functioning following treatment of late-life depression. *American Journal of Psychiatry* 2000;157(12):1949–54.
- Colloby SJ, Firbank MJ, Thomas AJ, Vasudev A, Parry SW, O'Brien JT. White matter changes in late-life depression: a diffusion tensor imaging study. *Journal of Affective Disorders* 2011;135(1–3):216–20.
- Dalby RB, Frandsen J, Chakravarty MM, Ahlidan J, Sørensen L, Rosenberg R, et al. Depression severity is correlated to the integrity of white matter fiber tracts in late-onset major depression. *Psychiatry Research* 2010;184(1):38–48.
- de Toledo Ferraz Alves TC, Ferreira LK, Busatto GF. Vascular diseases and old age mental disorders: an update of neuroimaging findings. *Current Opinion in Psychiatry* 2010;23(6):491–7. Review.
- Folquito JC, Bustamante SEZ, Barros SB, Azevedo D, Lopes MA, Hototian SR, et al. The Bayer-Activities of Daily Living Scale (B-ADL) in the differentiation between mild to moderate dementia and normal aging. *Revista Brasileira de Psiquiatria* 2007;29:350–3.
- Folstein MF, Folstein SE, McHugh PR. Mini mental state: a practical method for grading the cognitive state of patients for the clinician. *Journal of Psychiatric Research* 1975;12:129–38.
- Hamilton M. A rating scale for depression. *Journal of Neurology, Neurosurgery, and Psychiatry* 1960;23:56–9.
- Janssen J, Hulshoff Pol HE, de Leeuw FE, Schnack HG, Lampe IK, Kok RM, et al. Hippocampal volume and subcortical white matter lesions in late life depression: comparison of early and late onset depression. *Journal of Neurology, Neurosurgery, and Psychiatry* 2007;78(6):638–40.
- Kiosses DN, Alexopoulos GS, Murphy C. Symptoms of striatofrontal dysfunction contribute to disability in geriatric depression. *International Journal of Geriatric Psychiatry* 2000;15(11):992–9.
- Kieseppä T, Eerola M, Mäntylä R, Neuvonen T, Poutanen V, Tuoma K, et al. Major depressive disorder and white matter abnormalities: a diffusion tensor imaging study with tract-based spatial statistics. *Journal of Affective Disorders* 2010;120(1–3):240–4.
- Lehfeld H, Reisberg B, Finkel S, Kanowski S, Wied V, Pittas J, et al. Informant-rated activities of daily living (ADL) assessments: results of a study of 141 items in the USA, Germany, Russia and Greece from the International ADL Scale Development Project. *Alzheimer Disease and Associated Disorders* 1997;11(4):39–44.
- Linn BS, Linn MW, Currell L. Cumulative illness rating scale. *Journal of the American Geriatrics Society* 1968;16:622–5.
- Ma N, Li L, Shu N, Liu J, Gong G, He Z, et al. White matter abnormalities in first-episode, treatment-naive young adults with major depressive disorder. *American Journal of Psychiatry* 2007;164:823–6.
- Madden DJ, Whiting WL, Huettel SA, White LE, MacFall JR, Provenzale JM. Diffusion tensor imaging of adult age differences in cerebral white matter: relation to response time. *NeuroImage* 2004;21:1174–81.
- Mazziotta J, Toga A, Evans A, Fox P, Lancaster J, Zilles K, et al. A probabilistic atlas and reference system for the human brain: International Consortium for Brain Mapping (ICBM). *Philosophical Transactions of the Royal Society of London B Biological Sciences* 2001;1412:1293–322.
- Mettenberg JM, Benzinger TL, Shimony JS, Snyder AZ, Sheline YI. Diminished performance on neuropsychological testing in late life depression is correlated with microstructural white matter abnormalities. *NeuroImage* 2012;60(4):2182–90.
- Montgomery SA, Asberg M. A new depression scale designed to be sensitive to change. *British Journal of Psychiatry* 1979;134:382–9.
- Mori S, Zhang J. Principles of diffusion tensor imaging and its applications to basic neuroscience research. *Neuron* 2006;51(5):527–39. Review.
- Nobuhara K, Okugawa G, Minami T, Takase K, Yoshida T, Yagyu T, et al. Effects of electroconvulsive therapy on frontal white matter in late-life depression: a diffusion tensor imaging study. *Neuropsychobiology* 2004;50(1):48–53.
- Nobuhara K, Okugawa G, Sugimoto T, Minami T, Tamagaki C, Takase K, et al. Frontal white matter anisotropy and symptom severity of late-life depression: a magnetic resonance diffusion tensor imaging study. *Journal of Neurology, Neurosurgery, and Psychiatry* 2006;77:120–2.
- Roth M, Tym E, Mountjoy CQ, Huppert FA, Hendrie H, Verma S, et al. CAMDEX. A standardised instrument for the diagnosis of mental disorder in the elderly with special reference to the early detection of dementia. *British Journal of Psychiatry* 1986;149:698–709.
- Schiavone F, Charlton RA, Barrick TR, Morris RG, Markus HS. Imaging age-related cognitive decline: a comparison of diffusion tensor and magnetization transfer MRI. *Journal of Magnetic Resonance Imaging* 2009;29(1):23–30.
- Sexton CE, Mackay CE, Ebmeier KP. A systematic review of diffusion tensor imaging studies in affective disorders. *Biological Psychiatry* 2009;66:814–23.
- Shimony JS, Sheline YI, D'Angelo G, Epstein AA, Benzinger TL, Mintun MA, et al. Diffuse microstructural abnormalities of normal-appearing white matter in late life depression: a diffusion tensor imaging study. *Biological Psychiatry* 2009;66(3):245–52.
- Smith SM, Jenkinson M, Woolrich MW, Beckmann CF, Behrens TE, Johansen-Berg H, et al. Advances in functional and structural MR image analysis and implementation as FSL. *NeuroImage* 2004;23(S1):208–19.
- Smith SM, Jenkinson M, Johansen-Berg H, Rueckert D, Nichols TE, Mackay CE, et al. Tract-based spatial statistics: voxelwise analysis of multi-subject diffusion data. *NeuroImage* 2006;31(4):1487–505.
- Smith SM, Johansen-Berg H, Jenkinson M, Rueckert D, Nichols TE, Miller KL, et al. Acquisition and voxelwise analysis of multi-subject diffusion data with tract-based spatial statistics. *Nature Protocols* 2007;2:499–503.
- Taylor WD, Hsu E, Krishnan KR, MacFall JR. Diffusion tensor imaging: background, potential, and utility in psychiatric research. *Biological Psychiatry* 2004a;55(3):201–7. Review.
- Taylor WD, MacFall JR, Payne ME, McQuoid DR, Provenzale JM, Steffens DC, et al. Late-life depression and microstructural abnormalities in dorsolateral prefrontal cortex white matter. *American Journal of Psychiatry* 2004b;161:1293–6.
- Vernooij MW, Ikram MA, Vrooman HA, Wielopolski PA, Krestin GP, Hofman A, et al. White matter microstructural integrity and cognitive function in a general elderly population. *Archives of General Psychiatry* 2009;66(5):545–53.
- Wu F, Tang Y, Xu K, Kong L, Sun W, Wang F, et al. White matter abnormalities in medication-naive subjects with a single short-duration episode of major depressive disorder. *Psychiatry Research* 2011;191(1):80–3.
- Yang Q, Huang X, Hong N, Yu X. White matter microstructural abnormalities in late-life depression. *International Psychogeriatrics* 2007;19:757–66.
- Yuan Y, Zhang Z, Bai F, Yu H, Shi Y, Qian Y, et al. White matter integrity of the whole brain is disrupted in first-episode remitted geriatric depression. *NeuroReport* 2007;18:1845–9.
- Zhu X, Wang X, Xiao J, Zhong M, Liao J, Yao S. Altered white matter integrity in first-episode, treatment-naive young adults with major depressive disorder: a tract-based spatial statistics study. *Brain Research* 2011;19(1369):223–9.

# Experimento 5 – Anormalidade em substância branca e cinzenta em pacientes com mutação do gene SPG11.

JNNP Online First, published on June 13, 2012 as 10.1136/jnnp-2011-300129

Neurogenetics

## RESEARCH PAPER

### White and grey matter abnormalities in patients with SPG11 mutations

Marcondes C França Jr,<sup>1</sup> Clarissa L Yasuda,<sup>1</sup> Fabrício R S Pereira,<sup>1</sup> Anelyssa D'Abreu,<sup>1</sup> Camila M Lopes-Ramos,<sup>2</sup> Madalena V Rosa,<sup>2</sup> Fernando Cendes,<sup>1</sup> Iscia Lopes-Cendes<sup>2</sup>

<sup>1</sup>Department of Neurology and Neuroimaging Laboratory, Faculty of Medicine, University of Campinas—UNICAMP, Campinas, São Paulo, Brazil  
<sup>2</sup>Department of Medical Genetics, Faculty of Medicine, University of Campinas—UNICAMP, Campinas, São Paulo, Brazil

**Correspondence to**  
Dr I Lopes-Cendes, Department of Medical Genetics, University of Campinas—UNICAMP, Rua Tessália Vieira de Camargo, 126 Cidade Universitária Zefelino Vaz, Campinas, São Paulo, Brazil; icendes@unicamp.br

Received 24 March 2011  
Revised 22 February 2012  
Accepted 13 May 2012

#### ABSTRACT

**Background** Mutations in *SPG11* are the most frequent known cause of autosomal recessive hereditary spastic paraplegia. Corpus callosum thinning is a hallmark of the condition but little is known about damage to other structures in the CNS.

**Objective** To evaluate in vivo cerebral damage in patients with *SPG11* mutations.

**Methods** 5 patients and 15 age and sex matched healthy controls underwent high resolution diffusion tensor imaging (32 directions) and a T1 volumetric (1 mm slices) acquisition protocol in a 3 T scanner (Philips Achieva). These sequences were then analysed through voxel based morphometry (VBM) and tract based spatial statistics (TBSS).

**Results** Mean age of the patients was  $23.6 \pm 4.5$  years (range 14–45) and mean duration of disease was 12 years (range 5–15). All patients presented with progressive spastic paraplegia and three were already wheelchair bound when first evaluated. Mutations found were: c.529\_533delATATT, c.704\_705delAT, c.733\_734delAT, c.118C>T and c.7256A>G. VBM identified significant grey matter atrophy in both the thalamus and lentiform nuclei. TBSS analyses revealed reduced fractional anisotropy involving symmetrically subcortical white matter of the temporal and frontal lobes, the cingulate gyrus, cuneus, striatum, corpus callosum and brainstem.

**Conclusions** Widespread white matter damage in patients with *SPG11* mutations has been demonstrated. Grey matter atrophy was prominent in both the thalamus and basal ganglia but not in the cerebral cortex. These findings suggest that neuronal damage/dysfunction is more widespread than previously recognised in this condition.

#### INTRODUCTION

Hereditary spastic paraplegia (HSP) is a heterogeneous group of neurodegenerative disorders characterised by progressive lower limb weakness and spasticity.<sup>1</sup> In some patients, these are the sole clinical findings and these patients are classified as pure HSP. In contrast, some additional systemic (cataracts) or neurological (dementia, ataxia, epilepsy) features may be found in other patients; these in turn are classified as complicated HSP. At present, there are at least 48 loci associated with HSP and 17 identified genes.<sup>1,2</sup> HSP may segregate as an autosomal dominant, autosomal recessive or X linked trait.

Mutations in the *SPG11* gene located on chromosome 15q13-15 are now recognised as the most frequent cause of autosomal recessive HSP.<sup>3</sup> Patients typically present with gait complaints in

the first or second decades but ultimately develop cognitive impairment and peripheral manifestations. Ataxia, parkinsonism and motor neuron disease have lately been described as frequent findings in individuals bearing *SPG11* mutations.<sup>4–6</sup>

MRI usually shows severe corpus callosum thinning and sparse white matter hyperintense foci in this disease.<sup>4</sup> The clinical variability that is otherwise characteristic of HSP due to *SPG11* mutations suggests that neuronal damage is not restricted to these structures but this has not yet been proved. Modern neuroimaging techniques, including voxel based morphometry (VBM) and diffusion tensor imaging (DTI), make it possible to perform automated and unbiased whole brain analyses and to determine in vivo the distribution of damage to neural structures.<sup>7,8</sup> These have been successfully used to study similar neurodegenerative disorders, such as Niemann–Pick type C and inherited ataxias.<sup>9,10</sup> Therefore, we designed an MRI based study to characterise white matter and grey matter abnormalities in a cohort of patients with confirmed *SPG11* mutations.

#### METHODS

##### Subject selection

We recruited 11 consecutive adult patients with autosomal recessive HSP, thin corpus callosum and cognitive decline that were regularly followed at the Neurogenetics Outpatient Clinic at UNICAMP hospital between 2007 and 2010. From this group, we found five patients with mutations in the *SPG11* gene that underwent detailed clinical and MRI analyses. Severity of disease was quantified with the Spastic Paraplegia Rating Scale.<sup>11</sup>

Imaging findings were compared with a control group of 15 age and sex matched individuals with no neurological abnormalities (men/women ratio 7/8 and mean age  $24.0 \pm 3.8$  years). These were mostly relatives of patients and volunteers from the local community and were recruited during the study period. None of the patients or controls had significant motion artefacts on MRI scans.

This study was approved by our institutional ethics committee and written informed consent was obtained from all participants.

##### Molecular studies

Genomic DNA from each subject was isolated from lymphocytes of fresh blood by standard methods using phenol–chloroform extraction. We used previously designed forward and reverse primers to perform PCR analyses, as described elsewhere.<sup>3,4</sup>

Copyright Article author (or their employer) 2012. Produced by BMJ Publishing Group Ltd under licence. 1 of 6

## Neurogenetics

**Table 1** Demographic, genetic and clinical data for the SPG11 patients included in the study

Patient No	Mutation	Age (years)	Duration (years)	Gender	PN	Parkinsonism	Dementia	MMSE	SPRS
1	c.529_533delATATT (Exon 3)	19	13	F	–	+	++	14	37
2	c.733_734delAT (Exon 4)	31	15	M	++	–	++	19	38
3	c.704_705delAT (Exon 4)	23	14	F	–	–	++	18	32
4	c.118C>T (Exon 1)	21	5	M	–	+	+	23	19
5	c.A7256G/c.733_734delAT (Exon 40/Exon 4)	24	13	F	+	–	+	22	26

MMSE, Mini-Mental State Examination; PN, peripheral neuropathy; SPRS, Spastic Paraplegia Rating Scale.

Purified PCR products were then sequenced on an automatic sequencer MegaBACE 1000 (Amersham Bioscience, Piscataway, New Jersey). All 40 exons and exon–intron boundaries of the *SPG11* gene were investigated for each individual.

### MRI acquisition protocol

All patients and controls underwent MRI scans on a Phillips Achieva-Intera 3 T scanner at UNICAMP hospital. T1 and T2 weighted images were acquired in axial, coronal and sagittal planes with thin cuts. We also obtained two specific sequences that were later employed for VBM and DTI analyses, respectively.

1. Volumetric (three-dimensional) T1 gradient echo images—acquired in the sagittal plane with 1 mm slice thickness (flip angle=35°, TR=7.1 ms, TE=3.2 ms, matrix=240 × 240, field of view=24 × 24 cm).
2. DTI—undertaken via a 32 direction non-collinear echoplanar sequence (flip angle=90°, voxel size=2×2×2 mm<sup>3</sup>, TR=8500 ms, TE=61 ms, matrix=128 × 128, field of

view=256 × 256 mm, 70 slices with 3 mm thickness, b value=1000).

### VBM protocol and analysis

MRI scans produce images in DICOM format. These images were converted into ANALYSE format using the MRICro software (<http://www.microw.com>). We used the SPM8 package (Wellcome Department of Imaging Neuroscience, London, UK, <http://www.fil.ion.ucl.ac.uk>) running on MaTLab 8.0 to perform the preprocessing steps that are required before statistical analyses are performed. These include spatial normalisation of all image data to the same stereotaxic space; segmentation and tissue extraction; spatial smoothing; and correction for volume changes induced by spatial normalisation (modulation). The SPM8 package has improved some of the algorithms needed to perform these initial steps. Regarding spatial normalisation, it now includes a more sophisticated registration model (the DARTEL algorithm) that substantially reduces the imprecision of intersubject registration.<sup>12</sup>

**Figure 1** Results of voxelwise analysis showing areas of grey matter volumetric reduction in patients with *SPG11* mutations after comparison with age and sex matched controls. Results are shown on the MNI152 1 mm template. MNI z axis coordinates are shown (in mm) above each image. The colour coded bar represents the Z score.

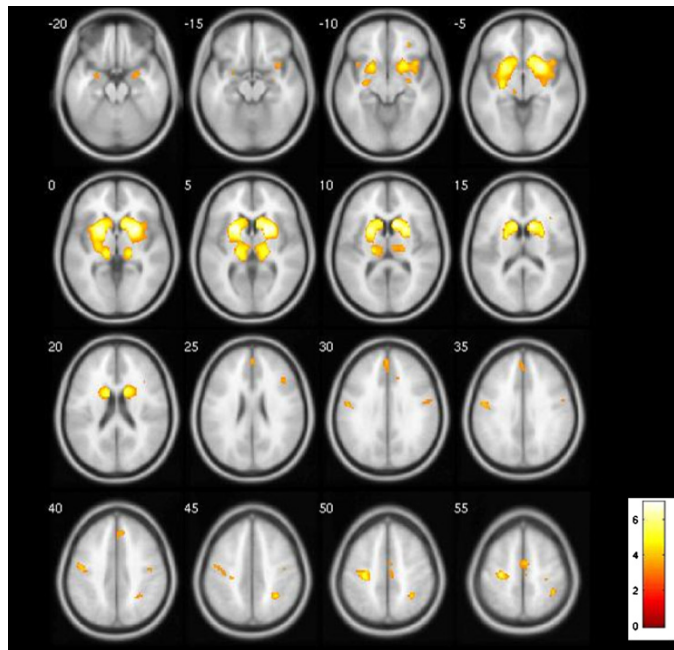


**Table 2** Voxel based morphometry results for volumes of grey matter in patients with SPG11

Cluster size (voxels)	MNI coordinates (local maxima)			Areas
	X	Y	Z	
3765	12	13.5	13.5	R caudate nucleus, lentiform nucleus, putamen
48	39	15	-9	R insula, frontal inferior gyri
4280	-19.5	9	4.5	L caudate nucleus, lentiform nucleus, putamen, globus pallidus, thalamus, claustrum
573	18	-24	3	R thalamus, mammillary body
33	-46.5	-12	40.5	L precentral gyrus
48	31.5	-49.5	46.5	R inferior parietal lobule
406	-30	-22.5	52.5	L precentral and postcentral gyri, middle frontal gyrus
23	39	-43.5	60	R inferior parietal lobule
12	4.5	-6	57	R medial frontal gyrus, supplementary motor area

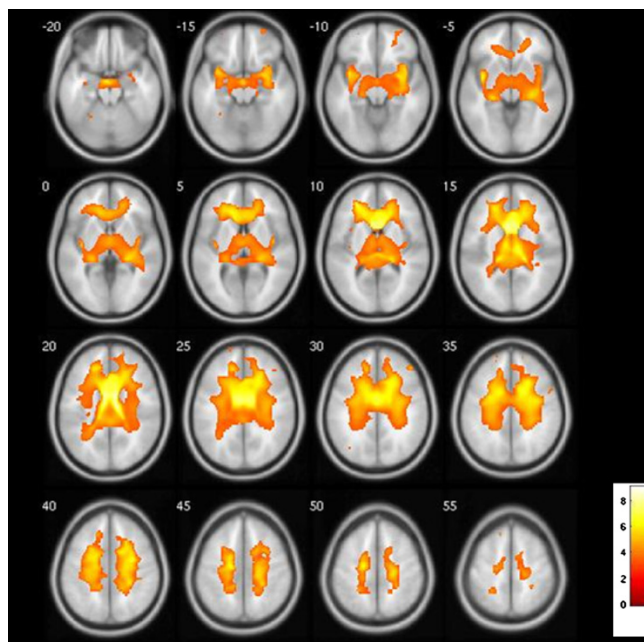
Processed images of patients and controls were compared using a voxelwise statistical analysis. We looked for differences in white and grey matter volumes between the two groups. We defined the contrast searching for areas of reduced and increased volumes both in white and grey matter. The results were corrected for multiple comparisons using a false discovery rate of 5% and significant differences were set at  $\alpha < 0.05$ . We used *xjView8* (<http://www.alivelearn.net/xjview8/>), a MatLab toolbox to display our results.

#### Tract based spatial statistics

We obtained maps of fractional anisotropy (FA), mean diffusivity (MD), radial diffusivity (RD) and axial diffusivity (AD) using the FMRIB diffusion toolbox which is part of the FSL

software V4.1.4.<sup>13</sup> Comparison of groups was then carried out using tract based spatial statistics (TBSS) on the FSL software V4.1.4.<sup>14</sup> TBSS involves several preprocessing steps before final analyses. All FA images are first aligned to a standard space using the non-linear registration. The next step involves the creation of a mean FA template which then enables the creation of the mean FA skeleton. Thereafter, each patient's aligned FA map is then projected over this skeleton; this is an essential step in the processing algorithm because it removes the effect of cross subject spatial variability. These final data are then used to perform the voxelwise statistics. A similar procedure was performed for the other DTI parameters (MD, RD and AD). We performed a two sample t test to compare group of patients and controls, searching for areas with FA, MD, RD and AD

**Figure 2** Results of voxelwise analysis showing areas of white matter volumetric reduction in patients with *SPG11* mutations after comparison with age and sex matched controls. Results are shown on the MNI152 1 mm template. MNI z axis coordinates are shown (in mm) above each image. The colour coded bar represents the Z score.



differences between the two groups. In order to control for multiple comparisons, we applied a family wise error correction, accepting  $p$  values  $<0.05$ . We used the Johns Hopkins white matter DTI based atlas within the FSL toolbox to identify the abnormal white matter fibre tracts.

### RESULTS

We observed that four patients were homozygous and one was compound heterozygous for mutations in *SPG11* (table 1). All mutations found had been previously reported in patients with autosomal recessive HSP and thinning of the corpus callosum.<sup>3 4 15 16</sup> They were of the non-sense type, leading to premature protein truncation. Mean age of the patients was  $23.6 \pm 4.5$  years (range 19–31) and mean duration of disease was 12 years (range 5–15). All patients presented with progressive spastic paraplegia and three were already wheelchair bound when first evaluated. Cognitive decline was evident in all patients according to the Mini-Mental State Examination scores (adjusted for age and educational level). Detailed information for each patient is depicted in table 1.

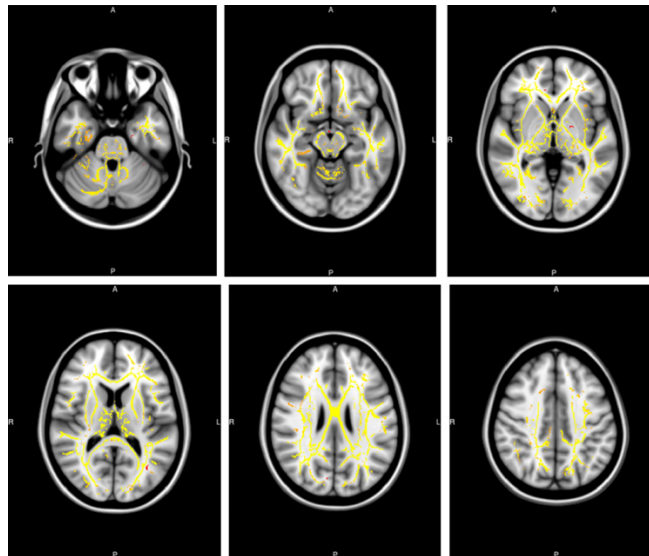
#### Grey matter results

VBM analysis identified symmetrical and significant grey matter volumetric reduction in both the thalamus, caudate and lentiform nuclei of patients with *SPG11* compared with controls (figure 1). We found small areas of cortical volumetric reduction, essentially restricted to the precentral and postcentral gyri (table 2). There were no regions with grey matter volumetric increases.

#### White matter results

Cerebral white matter was assessed both with VBM and TBSS. These are essentially complementary tools as VBM provides a macroscopic map of atrophy whereas DTI based analyses enable the identification of microstructural damage.

**Figure 3** Results of tract based spatial statistics voxelwise analysis showing areas of reduced fractional anisotropy (FA) in patients with *SPG11* mutations after comparison with age and sex matched controls. Areas with reduced FA are shown in yellow—red and represent cluster based values ( $p < 0.05$ , corrected). Results are shown on the MNI152 1 mm template.



VBM identified severe white matter volumetric reduction around the corpus callosum (figure 2). TBSS, however, revealed reduced FA involving symmetrically subcortical white matter of the temporal and frontal lobes, the cingulate gyrus, cuneus, striatum, corpus callosum, cerebellum and brainstem (figure 3). There was no region of significantly increased FA. MD maps also revealed diffuse white matter abnormalities (figure 4). There were also widespread areas of increased RD, especially involving subcortical white matter of the posterior temporal and occipital lobes (figure 4). We found areas of significantly increased AD around the thalamus and frontal deep white matter, but not in the posterior regions (figure 4).

### DISCUSSION

In this study, we investigated *SPG11* mutations in all patients with typical HSP with the thin corpus callosum phenotype<sup>17</sup> from our centre, and found that 45% (5/11) of the families tested positive. This confirms that *SPG11* is a rather common cause of HSP but that there is also locus heterogeneity within the limits of this phenotype. All mutations identified in this study had been previously reported in a large survey of patients from different ethnic origins.<sup>3 4 15 16</sup> This indicates that the genotypes of Brazilian patients with *SPG11* related HSP are not different from other populations.<sup>18</sup>

Damage to grey and white matter structures other than the corpus callosum in a cohort of genetically proven *SPG11* patients has not been systematically investigated. We thus used two validated and unbiased methods—VBM and TBSS—to perform whole brain analysis in patients with *SPG11* without a priori hypotheses. We were also able to scan these patients on a high field MRI scanner (3 T), which is more sensitive in detecting subtle abnormalities.<sup>19</sup> In addition, processing of images to run VBM was accomplished by SPM8 running on MaLab 8.0. This version of the software improved several of the

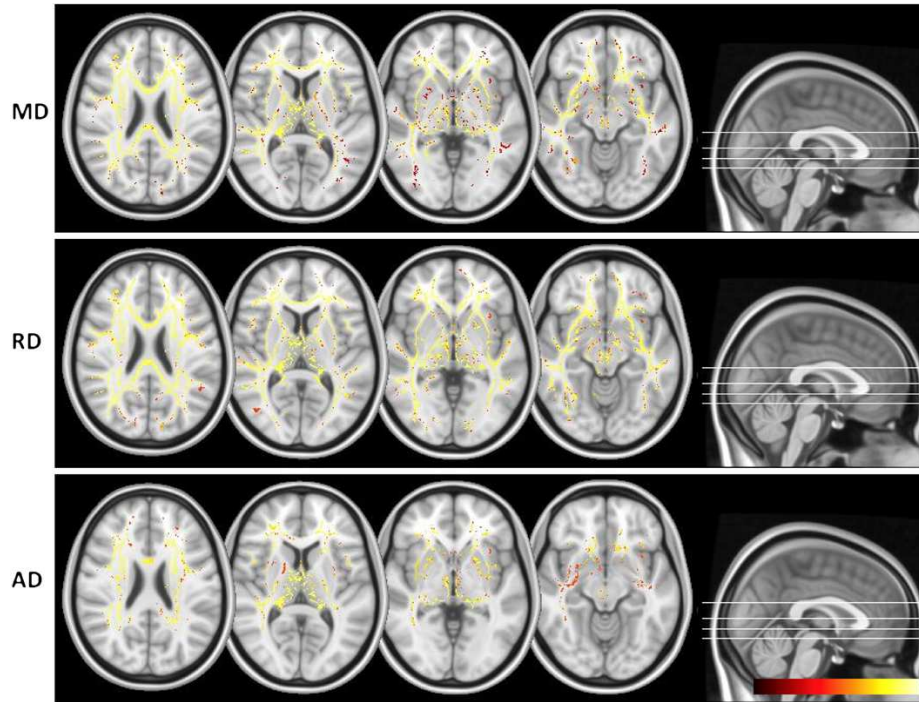


**Figure 4** Results of tract based spatial statistics voxelwise analysis showing areas of increased mean diffusivity (MD), radial diffusivity (RD) and axial diffusivity (AD) in patients with *SPG11* mutations after comparison with age and sex matched controls. Areas with increased MD, RD and AD are shown in red–yellow and represent cluster based values ( $p < 0.05$ , corrected). Results are shown on the MNI152 1 mm template.

required preprocessing steps but especially the spatial normalisation algorithm.<sup>20</sup> There is a single previous DTI based study in *SPG11* but the authors included only two patients.<sup>21</sup> They performed a voxelwise analysis but without an algorithm to adjust for the alignment of images from multiple subjects. These are major limitations of the study and preclude the extrapolation of the findings. Our study, in turn, enrolled a larger sample of patients and used TBSS analysis, which improves the sensitivity, objectivity and interpretability of DTI data.<sup>14</sup>

We have found restricted areas of grey matter atrophy in patients with mutations in *SPG11*. These were symmetrical and included the thalamus and basal ganglia. It is noteworthy that significant volumetric reduction was only found over small regions of the cortical mantle. These findings suggest that neurons in different regions of the CNS may present distinct vulnerability to *SPG11* related damage. This possibility is further supported by gene expression data which show much higher spatacsin mRNA levels in subcortical structures than in the cortex.<sup>5</sup> This suggests that neuronal populations of deep nuclei require higher spatacsin expression for proper functioning and integrity. Although not widespread, grey matter damage involves key subcortical structures that take part in motor and

cognitive networks. Thalamic damage in combination with corpus callosum atrophy might result in dementia and behavioural disturbances in these patients. In addition, we found significant volumetric reduction of the lentiform nuclei but not of the substantia nigra. This suggests that parkinsonism, which has been increasingly recognised in *SPG11*,<sup>5</sup> may be due to dysfunction in the dopaminergic receptors located in the putamen and not in the dopamine producing neurons of the midbrain. This helps to explain why levodopa and dopaminergic agonists do not improve parkinsonian features in many patients with *SPG11*.

In striking contrast to the grey matter results, we found remarkable and diffuse white matter abnormalities. As predicted, gross structural data provided by VBM confirmed severe corpus callosum atrophy in these individuals. However, we should emphasise the microstructural damage identified by DTI on the cerebellum, corpus callosum, cingulate gyrus and subcortical white matter of the temporal and occipital lobes. These results are similar to those reported by Chen *et al* in two patients with *SPG11* mutations.<sup>21</sup> In addition, we found abnormal FA in areas not described previously, such as the brainstem, and internal and external capsulae. Reduced FA

indicates disruption of nerve fibre bundles, either due to axonal or myelin compromise. Experimental evidence indicates that axonal damage takes part in this process. In a zebrafish model, Southgate *et al* used morpholino antisense nucleotides to knock-down *SPG11* in embryos, and found severe abnormalities of neuronal differentiation, especially in motor pathways.<sup>22</sup> Cranial and spinal motor nerves appeared thinner and with reduced numbers of axons. Oligodendrocyte and myelin abnormalities probably also contribute to white matter microstructural alterations. Proton magnetic resonance spectroscopy of frontal white matter showed mild reduction of N-acetylaspartate (NAA) levels but a prominent increase in choline (Cho) levels in a patient bearing the c.1951C>T mutation at *SPG11*.<sup>4</sup>

Analysis of AD and RD maps also provides some insight into the substrate of white matter damage in SPG11 related HSP. AD measures diffusivity along the main direction of diffusion and is considered a marker of axonal damage.<sup>23</sup> By contrast, RD evaluates diffusion that is orthogonal to the principal diffusion direction. Experimental data indicate that RD abnormalities are associated with myelin and/or oligodendrocyte damage.<sup>24</sup> In our patients, we found increased AD and RD, which indicates that both axonal damage and demyelination indeed take place in SPG11. RD abnormalities were, however, much more widespread than those related to AD, suggesting that CNS myelin is severely affected in the condition and this is especially prominent in posterior white matter.

An unsettled issue about SPG11 is the nature of corpus callosum thinning as it is not clear whether it is due to true atrophy or hypoplasia. Although we are not able to definitively answer this question with the present data, we had the opportunity of studying two patients who had been part of a previous prospective study.<sup>25</sup> Indeed, we could document that both patients presented with progressive volumetric reduction of the corpus callosum over a 1 year period (data not shown). This suggests that progressive corpus callosum atrophy occurs at least in some patients with *SPG11* mutations.

HSP due to *SPG11* mutations is a relatively new and rare condition, thus enabling us to enrol only a small number of patients for MRI scans. Regarding group comparisons, we tried to mitigate this with a large number of age and sex matched controls and a conservative statistical approach. Despite these limitations, our results provide insight into the neurobiology of the disease and help to understand many of the symptoms presented by these patients. Further studies are needed to evaluate the usefulness of MRI as a progression biomarker in SPG11 related HSP.

**Contributors** 1—Research project: (A) conception, (B) organisation, (C) execution. 2—Statistical analysis: (A) design, (B) execution, (C) review and critique. 3—Manuscript: (A) writing of the first draft, (B) review and critique. MCF: 1, 2A, 2B and 3A. CLY: 1C, 2B, 2C and 3B. FRSP: 1C, 2B, 2C and 3B. AD: 1A, 2C and 3B. CML-R: 1B, 1C, 2B and 3B. MVR: 1B, 1C and 2B. FC: 1A, 1B, 2C and 3B. IL-C: 1A, 1B, 2C and 3B.

**Funding** MCF received a post-doctoral fellowship from Fundação de Amparo à Pesquisa do Estado de São Paulo—FAPESP, São Paulo, Brazil (2008/58605-7). IL-C and FC are supported by FAPESP and Conselho Nacional de Pesquisa (CNPq, Brazil). The funding agencies did not interfere with the design of the study, collection of the data or drafting of the manuscript.

**Competing interests** None.

**Ethics approval** Ethics approval was provided by Comitê de Ética da Faculdade de Ciências Médicas (UNICAMP).

**Provenance and peer review** Not commissioned; externally peer reviewed.

**Data sharing statement** There are no additional unpublished data from this research. All information is included in the manuscript, tables and figures.

## REFERENCES

- Salinas S, Proukakis C, Crosby A, *et al*. Hereditary spastic paraplegia: clinical features and pathogenetic mechanisms. *Lancet Neurol* 2008;**7**:1127–38.
- Slabicki M, Theis M, Krastev DB, *et al*. A genome-scale DNA repair RNAi screen identifies SPG48 as a novel gene associated with hereditary spastic paraplegia. *PLoS Biol* 2010;**8**:e1000408.
- Stevanin G, Santorelli FM, Azzedine H, *et al*. Mutations in SPG11, encoding spatacsin, are a major cause of spastic paraplegia with thin corpus callosum. *Nat Genet* 2007;**39**:366–72.
- Hehr U, Bauer P, Wimmer B, *et al*. Long-term course and mutational spectrum of spatacsin-linked spastic paraplegia. *Ann Neurol* 2007;**62**:656–65.
- Anheim M, Lagier-Tourenne C, Stevanin G, *et al*. SPG11 spastic paraplegia. A new cause of juvenile parkinsonism. *J Neurol* 2009;**256**:104–8.
- Orlacchio A, Babalini C, Borreca A, *et al*. SPATACSN mutations cause autosomal recessive juvenile amyotrophic lateral sclerosis. *Brain* 2010;**133**:591–8.
- Ashburner J, Friston KJ. Voxel-based morphometry—the methods. *Neuroimage* 2000;**11**:805–21.
- Le Bihan D, Mangin JF, Poupon C, *et al*. Diffusion tensor imaging: concepts and applications. *J Magn Reson Imaging* 2001;**13**:534–46.
- Walterfang M, Fahey M, Desmond P, *et al*. White and grey matter alterations in adults with Niemann–Pick disease type C: a cross-sectional study. *Neurology* 2010;**75**:49–56.
- Alcauter S, Barrios FA, Diaz R, *et al*. Gray and white matter alterations in spinocerebellar ataxia type 7: an in vivo DTI and VBM study. *Neuroimage* 2011;**55**:1–7.
- Schüle R, Holland-Letz T, Klumpp S, *et al*. The Spastic Paraplegia Rating Scale (SPRS): a reliable and valid measure of disease severity. *Neurology* 2006;**67**:430–4.
- Yasuda CL, Betting LE, Cendes F. Voxel-based morphometry and epilepsy. *Expert Rev Neurother* 2010;**10**:975–84.
- Smith SM, Jenkinson M, Woolrich MW, *et al*. Advances in functional and structural MR image analysis and implementation as FSL. *Neuroimage* 2004;**23**(Suppl 1):S208–19.
- Smith SM, Jenkinson M, Johansen-Berg H, *et al*. Tract-based spatial statistics: voxelwise analysis of multi-subject diffusion data. *Neuroimage* 2006;**31**:1487–505.
- Stevanin G, Azzedine H, Denora P, *et al*. SPATAX consortium. Mutations in SPG11 are frequent in autosomal recessive spastic paraplegia with thin corpus callosum, cognitive decline and lower motor neuron degeneration. *Brain* 2008;**131**:772–84.
- Paisan-Ruiz C, Dogu O, Yilmaz A, *et al*. SPG11 mutations are common in familial cases of complicated hereditary spastic paraplegia. *Neurology* 2008;**70**:1384–9.
- Nakamura A, Izumi K, Umehara F, *et al*. Familial spastic paraplegia with mental impairment and thin corpus callosum. *J Neurol Sci* 1995;**131**:35–42.
- Denora PS, Schlesinger D, Casali C, *et al*. Screening of ARHSP-TCC patients expands the spectrum of SPG11 mutations and includes a large scale gene deletion. *Hum Mutat* 2009;**30**:E500–19.
- Alvarez-Linera J. 3T MRI: advances in brain imaging. *Eur J Radiol* 2008;**67**:415–26.
- Ashburner J. A fast diffeomorphic image registration algorithm. *Neuroimage* 2007;**38**:95–113.
- Chen Q, Lui S, Wang JG, *et al*. Diffusion tensor imaging of two unrelated Chinese men with hereditary spastic paraplegia associated with thin corpus callosum. *Neurosci Lett* 2008;**441**:21–4.
- Southgate L, Dafou D, Hoyle J, *et al*. Novel SPG11 mutations in Asian kindreds and disruption of spatacsin function in the zebrafish. *Neurogenetics* 2010;**11**:379–89.
- Song SK, Sun SW, Ju WK, *et al*. Diffusion tensor imaging detects and differentiates axon and myelin degeneration in mouse optic nerve after retinal ischemia. *Neuroimage* 2003;**20**:1714–22.
- Song SK, Yoshino J, Le TQ, *et al*. Demyelination increases radial diffusivity in corpus callosum of mouse brain. *Neuroimage* 2005;**26**:132–40.
- França MC Jr, D'Abreu A, Maurer-Morelli CV, *et al*. Prospective neuroimaging study in hereditary spastic paraplegia with thin corpus callosum. *Mov Disord* 2007;**22**:1556–62.

## White matter abnormalities associated with Alzheimer's disease and mild cognitive impairment: a critical review of MRI studies

*Expert Rev. Neurother.* 13(5), 483–493 (2013)

Marcia Radanovic\*<sup>1,2</sup>,  
Fabrício Ramos  
Silvestre Pereira<sup>2,3</sup>,  
Florindo Stella<sup>1,2,4</sup>,  
Ivan Aprahamian<sup>1</sup>,  
Luiz Kobuti Ferreira<sup>2,3</sup>,  
Orestes Vicente  
Forlenza<sup>1,2</sup> and Geraldo  
F Busatto<sup>2,3</sup>

<sup>1</sup>Laboratory of Neurosciences, Institute of Psychiatry, Faculty of Medicine, University of São Paulo, São Paulo, Brazil

<sup>2</sup>Center for Interdisciplinary Research on Applied Neurosciences (INAPNA), University of São Paulo, São Paulo, Brazil

<sup>3</sup>Laboratory of Psychiatric Neuroimaging, Faculty of Medicine, University of São Paulo, São Paulo, Brazil

<sup>4</sup>Biosciences Institute, Universidade Estadual Paulista, Campus of Rio Claro, São Paulo, Brazil

\*Author for correspondence:  
Tel.: +55 2661 7283  
[marciaradanovic@gmail.com](mailto:marciaradanovic@gmail.com)

In this article, the authors aim to present a critical review of recent MRI studies addressing white matter (WM) abnormalities in Alzheimer's disease (AD) and mild cognitive impairment (MCI), by searching PubMed and reviewing MRI studies evaluating subjects with AD or MCI using WM volumetric methods, diffusion tensor imaging and assessment of WM hyperintensities. Studies have found that, compared with healthy controls, AD and MCI samples display WM volumetric reductions and diffusion tensor imaging findings suggestive of reduced WM integrity. These changes affect complex networks relevant to episodic memory and other cognitive processes, including fiber connections that directly link medial temporal structures and the corpus callosum. Abnormalities in cortico–cortical and cortico–subcortical WM interconnections are associated with an increased risk of progression from MCI to dementia. It can be concluded that WM abnormalities are detectable in early stages of AD and MCI. Degeneration of WM networks causes disconnection among neural cells and the degree of such changes is related to cognitive decline.

**KEYWORDS:** Alzheimer's disease • brain connections • diffusion tensor imaging • mild cognitive impairment • voxel-based morphometry • white matter

Alzheimer's disease (AD) is a neurodegenerative disorder characterized by a progressive decline in memory associated with impairment in other cognitive functions, such as judgment, abstraction, decision-making, language, attention and visuospatial abilities. It is preceded by a prodromal condition compatible with the clinical diagnosis of mild cognitive impairment (MCI), in which patients present cognitive and functional disabilities without fulfilling the criteria for dementia diagnosis [1,2].

Traditionally, neuroimaging examinations using MRI have been used in clinical practice to rule out nondegenerative forms of dementia, to identify unusual forms of dementia or to detect cerebrovascular disease contributing to cognitive impairment. In addition, morphological MRI scans are used to detect gray matter abnormalities that provide supportive features for the early diagnosis of AD, including atrophy of the whole

brain, hippocampal formation and entorhinal cortex, as well as enlargement of the temporal horn of the lateral ventricles [3]. However, many MRI investigations to date have shown that AD patients may also present with white matter (WM) abnormalities including WM hyperintensities [4], WM volume deficits and disruption of the integrity of WM pathways. WM hyperintensities are easily identified through basic structural T2-weighted or fluid attenuated inversion recovery MRI scanning [5], while microstructural integrity of WM can be assessed through MRI techniques based on diffusion tensor imaging (DTI) [6].

The present article aims to provide a critical review of recent MRI studies in this field.

### WM hyperintensities & AD

Focal WM abnormalities such as MRI hyperintensities are a common feature in the overall

elderly population: although variable, the prevalence-estimates of these lesions are very high, reaching 95% [7,8]. WM hyperintensities can be measured by visual rating scales [9,10] or quantitative methods [11], which take into account the location and volume of WM lesions. In this section, the authors review the relationship of WM hyperintensities with AD, cognitive decline, neuropathology and diagnosis of dementia.

The neuropathological correlates of WM hyperintensities are still not completely understood and may reflect local demyelination, loss of axons and oligodendroglial cells, astrogliosis, fibrohyaline arterioles, and dilatation of perivascular spaces, corresponding to incomplete infarctions [8]. In the general population, the presence of WM hyperintensities is related to major vascular-related risk factors, such as hypertension, diabetes, smoking and hypercholesterolemia, as well as with signs of endothelial dysfunction [12]. WM hyperintensities are frequently taken as due to cerebrovascular disease, given such association with cardiovascular risk factors; also, a number of histopathological studies have found signs of microinfarcts and markers of hypoxia in the regions where WM hyperintensities are located [13]. However, it is important to note that some studies did not find evidence of ischemia in association with such lesions, even in extensive deep WM hyperintensities [13]. Apart from ischemia, there are indications that WM hyperintensities may be related to blood-brain barrier dysfunction [14] and microglial activation [15]. Thus, there is evidence suggesting that the etiopathological substrate of WM hyperintensities is heterogeneous and the common assumption that their causality is fully explained by cerebrovascular changes may lead to an oversimplification of the phenomena.

The interaction between cerebrovascular disease and AD is quite frequent and complex, and may occur in two ways: firstly by the presence of vascular lesions in patients with AD and secondly, by the sharing of major vascular-related risk factors [16]. In addition, endothelial damage and amyloid angiopathy may be present in AD. The pattern of WM changes found in AD seems to be more subtle than that associated with vascular dementia (VD), but nonetheless the differentiation between AD and VD may be difficult [17]. This is a relevant topic because cerebrovascular disease is the second main cause of cognitive decline [18]. One of the most commonly used methods to characterize the cerebrovascular risk and to distinguish between AD and VD is the Hachinski Ischemic Score (HIS) [19] or its modified version [20,21]. The sensitivity and specificity of the HIS to distinguish AD from VD was high (89%) in a study of 312 patients with dementia but it was not accurate in distinguishing AD or VD from mixed dementia [22]. More recently, a longitudinal study showed that higher HIS scores significantly increased the odds of incident VD relative to AD within 5 years [23].

The relationship between the presence and intensity of WM hyperintensities and the existence or severity of cognitive deficits is still controversial. Cross-sectional studies of elderly individuals have reported an association of WM abnormalities with episodic and working memory deficits, executive dysfunction, and neuropsychiatric symptoms, particularly depression [24–27]. However, there are also studies that could not demonstrate any relationship

between WM hyperintensities and cognitive deficits [28,29]. Motor impairments such as decreased postural and gait stability have also been associated with WM hyperintensities [30].

Amyloid deposition in the brain, a hallmark of AD [31], is seen initially and most prominently in the entorhinal and perirhinal cortex [32,33] and can nowadays be evaluated *in vivo* with molecular imaging methods using PET [34]. Two recent neuroimaging studies could not find significant correlations between WM hyperintensities and brain amyloid burden *in vivo* [25,28]. Conversely, in a study that combined MRI and amyloid deposition imaging with PET [35], the authors showed that, among elderly individuals with significant brain amyloidosis, those with clinically defined AD presented increased volumes of WM hyperintensities when compared with normal elders, thus suggesting that clinical dementia may be the result of a 'double hit' on the brain: amyloid deposition and WM degeneration [35]. This is in accordance with a longitudinal study of 804 elderly individuals from the AD neuroimaging initiative, which reported that higher baseline WM hyperintensity volumes were associated with decreases in global measures of cognition [36] and also with a community-based epidemiological study that reported that volume of parietal WM hyperintensities predicted incident AD [37]. Another relevant finding of the aforementioned study is that the volume of WM hyperintensities did not differ between subjects with and without significant amyloid deposition [35]. In other words, although WM hyperintensities seem to occur independently of AD pathology, they may increase the risk of developing cognitive decline, especially in those who have undergone other brain insults such as extensive amyloid deposition [35,38].

In conclusion, WM hyperintensities are very common in both AD and in the general elderly population. These brain lesions cannot be taken as specific to AD, but rather may indicate increased cerebrovascular brain damage and vulnerability to cognitive decline [35,39]. It is also important to note that there are other brain lesions caused by vascular pathology – such as gross infarcts detectable with MRI – that may have strong effects on cognition [28]. In fact, a recent study has shown that in a sample of elderly subjects – including those with normal cognition and those with cognitive impairment – the relationship of cognition (executive function, verbal and nonverbal memory) with brain infarcts was stronger than its association with amyloid deposition [28].

#### **Volumetric abnormalities of WM in AD & MCI**

T1-weighted MRI scans can detect quantitative changes in WM volume of separate regions in groups of patients with neuropsychiatric disorders compared with healthy control groups matched for demographic variables. Two strategies have most often been employed to perform such quantitative measurements and between-group comparisons: the delineation of regions-of-interest (ROI) around selected brain structures (manually or in an automated fashion); or voxel-based morphometry (VBM), an automated technique that uses T1-weighted images to perform voxel-wise statistical tests with the purpose of uncovering subtle brain volume changes in association with neuropsychiatric disorders [40,41].

Morphometric MRI studies of AD using the ROI-based approach have focused on the detection of volume deficits of the hippocampus and other medial temporal lobe regions, as well as other selected cortical regions. Differently, VBM analyses are performed separately on either gray or WM tissue compartments across the whole brain [42,43]. Suitable for group comparisons, the application of VBM has been widespread to identify gray matter volume abnormalities in AD samples relative to elderly healthy control groups [41,43–46]. The VBM approach has also been used to investigate the risk for dementia in premorbid conditions such as MCI [9], and recent meta-analyses of VBM studies demonstrated atrophy of the hippocampus and parahippocampal gyrus as the most reliable predictors of progression from amnesic MCI to AD [47].

In the first VBM study that investigated the topography of WM volume deficits affecting the corpus callosum in AD subjects, Chaim *et al.* showed that callosal atrophy was most significant in the anterior splenium and isthmus, which are crucial callosal fiber tracts that interconnect the two cortical hemispheres [43]. Although less significantly, there were also volume reductions in the rostral genu as well as the anterior and posterior regions of the callosal body in AD patients relative to controls [43]. There was also a positive correlation between the degree of cognitive decline as assessed by the Mini-Mental State Examination and the volume of the anterior body of the corpus callosum. VBM-based findings of corpus callosum volume deficits in association with AD [48] complement findings of callosal shape abnormalities as assessed in sophisticated MRI studies that used high-dimensional warping methods [49], as well as the results of earlier ROI-based morphometric MRI investigations comparing AD patients to elderly healthy controls [50–52].

Several other morphometric MRI studies of AD, using either the ROI-based approach or VBM, have reported WM atrophy of subcortical regions in AD patients compared with healthy elderly individuals affecting temporal lobe structures in addition to the corpus callosum [53–55], as well as other WM tracts including the inferior longitudinal fasciculus [56]. A recent meta-analysis including eight VBM studies reported significant WM volume reduction in temporal lobe regions including the parahippocampal gyrus bilaterally, as well as the posterior corpus callosum in AD patients relative to elderly controls [48].

Structural abnormalities of the splenial portion of the corpus callosum in AD may be related to findings of neuronal loss in the temporoparietal cortical regions that are interconnected by this callosal subregion, with an unfavorable impact on episodic memory performance among other cognitive aspects. Additionally, volume reduction of the anterior corpus callosum may explain the decline of executive functions that may be seen even at early stages of AD, as this brain region connects interhemispheric frontal cortical regions [43]. WM volume increase in samples of AD patients relative to healthy controls has not been detected in VBM investigations to date [48].

A few VBM studies have also investigated groups of MCI individuals in regard to WM volumes, but to date, these studies have reported conflicting findings. For instance, one VBM study

reported WM atrophy in periventricular areas in a group of AD patients relative to controls (mainly in the anterior corpus callosum and the WM of associative cortical regions), but no WM volume deficits in a sample of amnesic MCI subjects compared with the same healthy control group [44]. Conversely, there have been reports of WM volume decrements in the medial temporal lobe in a group of amnesic MCI subjects compared with age-matched controls, which predicted significantly episodic memory decline as much as gray matter volumes in the hippocampal region [56]. In individuals at risk for AD, dysfunction of episodic memory might be influenced by changes in WM pathways connecting the hippocampus and neocortical regions.

Finally, another point of interest refers to the relationship between volumetric deficits in gray and WM compartments in the same samples of AD patients or MCI subjects [55,57]. One such VBM investigation showed that the degree of gray matter hippocampal atrophy in AD patients was specifically correlated to decreased WM volume in the cingulum bundle. As the same AD sample was also investigated with PET after injection of <sup>18</sup>F-fluorodeoxyglucose, the authors were able to demonstrate that the WM cingulum disruption was significantly correlated with the degree of glucose hypometabolism in the posterior cingulate cortex (a very early functional imaging feature associated with the diagnosis of AD), as well as with hypometabolism in other subcortical and cortical regions. These findings provide support to the notion that gray matter abnormalities and deficits in long WM tracts are related to each other in AD, leading to disconnection of multifocal neural networks relevant to cognitive processing [58].

Despite the interest raised by the above data, limitations of the VBM approach to assess WM volumes need to be acknowledged. In regard to the corpus callosum, for instance, inter-subject variations in callosal location may emerge secondary to ventricle dilatation or between-group differences in callosal shape [59], interfering with the process of spatial normalization and potentially confounding VBM-based group comparisons. The spatial normalization step in the VBM methodology, whereby images are warped to conform to a standardized anatomical space, may be prone to inaccuracies that are more likely to occur when the degree of brain structural inter-subject variations is wider (as in the case of neurodegenerative disorders) [59].

One additional approach of demonstrated validity to investigate morphometric brain abnormalities associated with AD and MCI consists of analyzing the nonlinear deformation fields that result from registering the MRI datasets of individual subjects to a standardized reference brain space, using such information to infer local differences in brain volume or shape [60,61]. Two techniques based on this principle, referred to as deformation-based morphometry and tensor-based morphometry, have been infrequently applied to demonstrate WM morphological abnormalities in AD and MCI patients relative to healthy controls [62].

Finally, computational methods for measuring regional brain thickness changes have also been applied to investigate WM abnormalities associated with AD using structural MRI datasets. These include: mesh-based geometrical modeling methods, recently used to demonstrate reduced callosal thickness

in patients with severe AD relative to unaffected controls [49]; and the FreeSurfer suite, a surface-based approach that allows thickness and volume measurements of separate regions across the entire brain to be obtained on an automated fashion, after segmentation of separate gray matter, WM and cerebrospinal fluid compartments [63]. Several studies using FreeSurfer software have confirmed and extended VBM findings of gray matter changes associated with AD and MCI, revealing reductions in both volume and thickness of key brain regions [64,65]. The FreeSurfer approach has also been applied in a study that identified differences of WM volume between AD patients and elderly controls: AD-related decreases in WM volume were found in parahippocampal, entorhinal, precuneus, inferior parietal and middle frontal WM [66]. The FreeSurfer methodology provides volumetric measures in native space and information can be extracted for individual subjects, rather than solely for statistical group comparisons. Moreover, there is evidence that FreeSurfer may be more suitable for longitudinal investigations of regional brain volume changes over time as compared with voxel-based methods [67].

#### Microstructural WM abnormalities as assessed by DTI

Despite the usefulness of the above MRI methods employed to assess WM, either by quantifying hyperintense lesions or measuring WM volumes and thickness, DTI methods have a greater potential to provide detailed information about the structural characteristics of WM tracts in the brain. DTI is a technique based on the concept of random movement of water molecules in brain tissue, which is altered when there are microstructural lesions in WM fiber bundles. Indices of WM integrity are afforded by measuring mean diffusivity (MD) and fractional anisotropy (FA) [68]. There is recent empirical demonstration that volumetric and DTI analyses of WM yield different and complementary results in regard to the pathophysiology of AD [69].

Since the development of DTI methods, there have been a large number of cross-sectional DTI studies comparing samples of AD patients and MCI subjects relative to elderly control groups [70–76]. The DTI literature has been evaluated in recent meta-analyses, which have indicated that both in AD and MCI samples relative to healthy controls, there are significant changes in WM microstructure in the corpus callosum as well as in other brain regions including the cingulum and parahippocampal region [77,78], as well as the longitudinal and uncinate fascicule [74–76]. As expected, DTI investigations have indicated greater loss of WM integrity in AD patients relative to MCI individuals, affecting key brain regions such as the corpus callosum and fornix (which contains efferent fibers from the hippocampal region) [71,74,79]. WM microstructural changes as assessed by DTI are significantly associated with the degree of cognitive decline, and might be considered as predictors of AD pathology [71]. There is also indication that DTI indices (particularly MD) provide high levels of diagnostic accuracy to differentiate MCI subjects from healthy controls, possibly with larger effect sizes in comparison to measures of hippocampal volume [77]. On the other hand, a recent study showed that FA indices in the fornix predicted conversion to AD in a sample of 23 MCI

subjects (from which six developed AD over 2.5 years) with an impressive accuracy of 95% [80]. However, more studies with greater samples are needed to replicate and confirm these findings.

High-resolution DTI scanning enables the investigation of specific WM tracts such as the perforant path, which connects the entorhinal cortex to the hippocampus [73,81,82]. The entorhinal cortex is seen as critically relevant to memory processing as it provides the main input from the cortex to the hippocampal formation [83,84]. Postmortem studies have documented neuropathological findings characteristic of AD (i.e., neurofibrillary tangles) and decreased neuronal density in the entorhinal cortex of patients in the earliest stages of AD [32,33]; such degenerative changes are thought to affect the perforant path and lead to an isolation of the hippocampus from cortical input [85,86]. *In vivo* DTI studies identified decreased FA and increased MD – suggestive of WM damage and/or loss of fibers – in normally appearing WM of the perforant path in AD and MCI [73,82]. Moreover, DTI indices of the perforant path integrity have been shown to correlate with declarative memory performance [82].

One important DTI question arises with regards to the assessment of the relationship between changes in WM microstructure and gray matter atrophy. A common multimodal integration that deals with such issue regards to the combination of DTI indices with gray matter volume indices as assessed using VBM. A pioneering study that used this approach detected widespread WM changes in AD patients as assessed with DTI; however, these degenerative changes were largely unrelated with gray matter volume measurements, suggesting that both features would be independent pathological aspects in the progression of AD [87]. A relative independence between altered diffusivity in the parahippocampal WM as assessed with DTI and volumetric measurements of the hippocampal region were also reported in a subsequent investigation [73]. Conversely, in one other study, FA indices both in anterior and posterior regions of the corpus callosum in AD patients (but not in healthy controls) were significantly correlated with gray matter volumes in several cortical regions [70]. The latter findings support a view that axonal impairments in the corpus callosum are closely linked to gray matter degeneration in the cortical areas interconnected by these callosal fibers in AD [43,70]. Moreover, a study that investigated whole brain WM also found correlations between regional gray matter volume and DTI indices of WM degeneration, this time in the left frontal and temporal cortices [82].

One other important, but as yet relatively unexplored, issue in regard to the possibility that WM abnormalities, as detected by reduced FA, may also be significantly related to gray matter volume deficits as assessed by VBM in patients with MCI due to AD. Further MRI studies with complementary information from such gray and WM measurements may improve the accuracy to distinguish AD patients from MCI subjects and healthy controls.

Finally, one of the methods used most often recently to quantify diffusion images is Tract-Based Spatial Statistics (TBSS), which allows comparisons of the integrity of WM tracts across different groups by means of projecting the FA onto an alignment tract representation, with improved sensitivity [88]. The TBSS

methodology is a promising approach to examine the integrity of WM tracts and it may also be used to classify distinct groups of subjects. This procedure has been applied to infer WM microstructural changes in MCI that may predict conversion to AD [89–91]. Significant FA differences in the fornix, cingulum and corpus callosum have been observed between MCI subjects that converted to AD and those that did not [89]. The TBSS approach has also shown that amnesic MCI patients display FA abnormalities relative to healthy controls consistent with pathological findings of AD (involving the temporal lobe, corpus callosum and fornix, among other regions), while non-amnesic MCI patients display more widespread and variable patterns of WM abnormalities, but relatively sparing the temporal lobe [90].

#### Limitations & caveats in the interpretation of DTI findings

When interpreting WM results from neuroimaging studies, it is important to remember that these findings represent indirect estimates of the brain anatomy. Therefore, one type of neuroimaging finding may result from different changes in the brain microstructure [92,93]. For instance, as addressed above, WM hyperintensities may be associated with different pathological findings, such as cerebrovascular disease, microglial activation and/or blood–brain barrier dysfunction.

In DTI studies, findings of regional lower FA have been interpreted as indicating decreased WM integrity (an unspecific term that generally encompasses loss of myelination, axonal degeneration or atrophy and/or increased membrane permeability). However, one other plausible explanation is that FA changes would be due to variations in axonal diameter or atypical packing density of axons [92–94]. Moreover, decreased anisotropy may simply result from different axonal alignment: regional anisotropy differences may indicate, in one group of subjects, that the axons are all aligned in the same direction, while in another group this same brain region contains branching or crossing fibers [92]. As noted elsewhere, in its current state, 'DTI is useful for localizing and quantifying the anatomical abnormalities, but it is apparently not adequate to investigate the histopathological background of the diseases' [93]. For a recent and thorough review of the limitations of DTI methods, the reader is referred to Jones *et al.* [92].

#### Relationship between WM changes & neuropsychiatric syndromes in AD

Although MRI studies of AD have predominantly concentrated on investigating the relationship between brain abnormalities and measures of cognitive decline, it is also critical to drive attention to neuropsychiatric symptoms (such as psychosis, agitation, depression and apathy). These are highly frequent in AD patients, being associated with greater disease severity and increased mortality [95].

Morphometric MRI studies, by means of VBM, have demonstrated that distinct patterns of gray matter abnormalities are correlated with the presence of neuropsychiatric syndromes in mild AD, including associations between: delusions and gray matter reduction in fronto-parietal regions; agitation and gray matter reduction in the insula and anterior cingulate cortex; and apathy

and decreased gray matter volume in frontal, anterior cingulate and striatal regions [96]. Similar regional-specific associations have been reported in more recent morphometric MRI investigations using large AD and MCI samples [97]. However, these studies did not investigate if degenerative WM volume deficits could also be associated with neuropsychiatric syndromes.

Such investigations of WM abnormalities would be highly relevant, since the neural substrate underlying neuropsychiatric syndromes in neurodegenerative diseases has not yet been clearly defined. Using a sample of AD patients who displayed delusions over a period of 2 years, an interesting VBM study recently examined neuroanatomical changes both in gray matter and WM compartments before delusions onset [98]. The authors found significantly smaller gray matter volume bilaterally in the parahippocampal gyrus, inferior frontal gyrus, right orbitofrontal cortex, and left insula in AD patients who developed delusions compared with those without delusions. Conversely, the authors did not observe significant WM changes in any brain regions among patients who developed delusions compared with those without psychotic symptoms. Thus, the role of WM degenerative changes to predict the emergence of neuropsychiatric syndromes in AD patients remains to be clarified.

More recently, neuropsychiatric symptoms have also been addressed in DTI studies investigating relatively modest MCI and AD samples. In one of these studies, the relationship between neuropsychiatric symptoms and WM integrity was examined in the fornix, cingulum bundle and splenium of the corpus callosum [99]. Expecting similar associations across AD and MCI subjects, the authors combined both groups in their analyses. Patients in the lowest tertile regarding anterior cingulum FA were more likely to exhibit irritability, agitation, dysphoria, apathy, and night-time behavioral disturbances. After accounting for the influence of the degree of cognitive decline using Mini-Mental State Examination scores, only irritability remained significantly associated with reduced FA in the cingulum [99]. Another DTI study explored the association between apathy and WM integrity in AD patients. The authors found negative statistical correlations between scores on an apathy scale and FA in the right anterior cingulum as well as in the right thalamus and bilateral parietal regions, after taking into account the influence of demographic and cognitive decline variables [100].

#### Possible mechanisms underlying volume deficits & integrity changes of WM tracts in AD & MCI

It has not yet been possible to fully clarify the mechanisms that specifically underlie the AD-related pathological changes in WM tracts detected in the MRI studies reviewed herein, nor the relationship between the degeneration of such subcortical WM interconnections and the gray matter changes that characterize AD.

One proposed mechanism is that gray matter degeneration would lead to WM deficits through demyelination in efferent pathways connecting the hippocampus and amygdala to the parahippocampal gyrus and the temporal lobe neocortex, extending towards the corpus callosum. Amyloid plaques and neurofibrillary tangles affecting gray matter could drive anterograde Wallerian

degenerative changes in WM tracts [101], particularly in close proximity to cortical regions. Wallerian degeneration affecting the posterior portion of the corpus callosum would disorganize axonal interconnections among temporo-parietal regions, which are known to be affected early over the course of AD [45].

One alternative explanation is that primary, AD-related pathological WM changes would lead to decreased WM volume and contribute to cortical gray matter degeneration. Within this framework, damage to WM is seen as an early phenomenon in AD, caused either by microvascular ischemic events or other myelin-related defects, with amyloid and tau pathologies representing secondary effects [102]. Such primary WM abnormalities would lead to interconnection deficits and axonal injuries reducing synaptic activity, even in prodromal MCI stages. This myelin model of AD, proposed by Bartzokis, is based on the observation that the myelination of the human brain is dynamic and presents an inverted U-shaped trajectory throughout the lifespan [102]. According to this model, it is necessary to understand the pathophysiology of AD in light of age-related myelin toxicity, which has been suggested to be an earlier event that may not only be induced by, but also promote  $\beta$ -amyloid aggregation and tau deposits [102]. According to this model, brain amyloidosis can be considered a late pathological event and therefore treatments aiming at amyloidosis may not be successful.

Recently, a retrogenesis model has been proposed to explain the decreased WM integrity in AD [103], according to which there is firstly degeneration of the late-myelinating WM tracts, such as the inferior and superior longitudinal fascicule and the uncinate fasciculus, a proposition supported by findings of reduced FA in these regions in AD patients [74,76,87]. Early-myelinating tracts would only be affected later in the course of AD. According to the retrogenesis model, dropping off WM integrity reflects myelin breakdown occurring as a reverse pattern of the myelogenic process [102].

It is actually possible that both primary and secondary WM degeneration processes are present in AD and MCI [72,73]. Moreover, the fact that oligodendrocytes – the cells that produce myelin – are vulnerable to a diversity of insults, such as hypoperfusion, iron toxicity, oxidative damage, glucocorticoids, alcohol, cocaine, brain trauma and  $\beta$ -amyloid oligomers makes WM degeneration a pivotal element of the neuropathology of cognitive decline and AD (for a thorough review, see Bartzokis [104]). Regardless of the underlying nature and sequencing of white and gray matter changes over the disease course, WM abnormalities undoubtedly reduce cortico-cortical and cortico-subcortical connectivity in AD subjects. Future neuroimaging studies with improved methods are likely to better delineate how critically such WM changes contribute, not only to cognitive decline but also, to the emergence of neuropsychiatric syndromes. These studies are also expected to contribute further to improve the accuracy of diagnosis of AD and MCI.

#### Five-year view

This review shows that current neuroimaging technology allows the quantification of regional indices of human WM structure reliably *in vivo*. The MRI studies addressed herein have

demonstrated unequivocally that WM abnormalities in the brain are detectable in early stages of AD and in MCI. Between-group differences have been clearly identified when comparing AD and/or MCI patients to elderly controls, and significant associations between WM structure and cognitive performance and prognosis have been documented. These changes affect key components of a complex brain network relevant to episodic memory and other cognitive processes, including fiber connections that directly link medial temporal structures and different regions of the corpus callosum. Abnormalities in these network nodes may influence one another, and the profile of cognitive deficits and emergence of neuropsychiatric syndromes may be best explained in terms of disturbances of such brain networks rather than by damage to a specific subcortical structure. Degeneration of WM fiber pathways causes disconnection among neural cells, with loss of myelinated axons resulting in reduced signaling and synaptic activity [105]. Overall, these findings encourage the exploration of a number of important novel research avenues in the field of WM investigations in AD and MCI.

The literature on WM changes associated with AD has led some authors to suggest that such abnormalities could be an important target for aiding in the diagnosis and disease monitoring in AD [93]. DTI studies have provided interesting results regarding: identification of WM differences between AD and VD [106]; discrimination between individual AD or MCI patients and controls [62,107–110]; distinction of individual patients with AD from those with frontotemporal lobar degeneration [111] and characterization of treatment effects of galantamine – a cholinesterase inhibitor approved for the treatment of AD – in the WM of AD patients [112]. However, despite such encouraging findings, DTI methods are still not developed as robust clinical tools in the field of brain aging and dementia [113]. Though much progress has been made in the past years, there is still much to be improved in terms of *in vivo* WM imaging methods before MRI indices of WM integrity can be established as accurate and reliable biomarkers in the AD field [114]. A number of these limitations have been evoked in the reasoning why DTI was not included in the MRI core of the AD neuroimaging initiative [114]. These issues were 'uncertainty about long-term test-retest precision', 'absence of widely available phantoms to calibrate measurements of diffusion' and 'minimal evidence of diagnostic efficacy in AD' [113]. In other words, advances in multiple fronts are required before DTI can be implemented in clinical practice for AD diagnosis and monitoring. One important research field that must be explored further in the near future regards to the assessment of advanced acquisition methods to increase spatial resolution of DTI data and more accurately extract information from specific small WM tracts of critical relevance to AD and MCI, such as the perforant path [115].

One other important issue for future research refers to multimodal neuroimaging approaches. By applying different acquisition protocols in the same imaging session, MRI techniques may provide complimentary information about brain structure and function in one single cohort of individuals. Sophisticated computational and statistical methods also allow the combination

of information from MRI data with other imaging modalities, including the use of PET for measuring regional glucose metabolism and molecular imaging. For instance, structural connectivity – measured with DTI – can provide useful information to assist the interpretation of neurofunctional results as assessed with functional MRI or PET imaging, as it is known that structural and functional connectivity are intimately related [116]. In accordance with this idea, glucose hypometabolism in the posterior cingulate cortex – a common feature of AD – was associated with decreased FA in the descending cingulum in a study that acquired DTI and PET data from MCI and AD patients [107]. These fibers connect the hippocampus to neocortical regions; thus, these results provide further support to the notion that disconnection between the medial temporal lobe and medial parietal cortex contributes to the hypometabolism in the posterior cingulate cortex found in AD [117]. Another example of a multimodal study is one recent report showing that regional decreased FA in the cingulum of amnesic MCI patients was associated with failure to deactivate the inferior parietal lobe and precuneus, during an object recognition task as assessed with functional MRI [118]. These two regions comprise the default mode network, which is thought to present normal deactivations during externally oriented tasks in healthy controls [119,120]. Multimodal imaging studies may afford greater accuracy for the distinction of AD from other forms of dementia [111,121], as well as for the prediction of the transition from pre-dementia stages to AD [122,123]. Given the wealth of recent data indicating the relevance of WM abnormalities in MCI and AD, we foresee a greater emphasis on the inclusion of MRI protocols dedicated to the assessment of WM among the methods selected for use in future multimodal studies evaluating these disorders.

We also expect to see an exponential growth of studies integrating neuroimaging data on WM changes with findings obtained with other research methods. Though the cognitive decline of AD and MCI emerges from brain changes that can be assessed

using neuroimaging techniques, there are several determinants of brain abnormalities that are better evaluated with methods from other research fields. Perhaps the best example of this is provided by the emerging field of imaging genetics, which investigates how single or combined molecular genetic characteristics may influence the variability of structural and/or functional neuroimaging phenotypes. For instance, it is known that the APOE  $\epsilon$ 2 allele is associated with a lower risk for AD [124]; in a recent DTI study of healthy elderly individuals, APOE  $\epsilon$ 2 carriers presented increased FA in the posterior cingulate cortex and in the corpus callosum compared with homozygous for the APOE  $\epsilon$ 3 allele, suggesting that the protective effect of APOE  $\epsilon$ 2 against the incidence of AD may be exerted through a greater degree of WM integrity [125].

Finally, a number of CSF and plasma biomarkers have been identified as potentially useful to aid in the early diagnosis and prediction of AD [126,127], and they have been investigated in conjunction with imaging biomarkers in recent studies [111,128–130]. Given the salience of WM abnormalities in AD and MCI as shown in the present report, we expect that future studies investigating multiple peripheral, CSF and neuroimaging markers in large samples will place greater emphasis on the role of WM changes in association with those clinical conditions.

#### Financial & competing interests disclosure

The authors were partially funded by the University of São Paulo (Grant #2011.1.9333.1.3, Center for Interdisciplinary Research on Applied Neurosciences - NAPNA). GF Busatto and OV Forlenza are supported by the National Council of Technological and Scientific Development (CNPq), Brazil. LK Ferreira is supported by Fundação de Amparo à Pesquisa do Estado de São Paulo (FAPESP). The authors have no other relevant affiliations or financial involvement with any organization or entity with a financial interest in or financial conflict with the subject matter or materials discussed in the manuscript apart from those disclosed.

No writing assistance was utilized in the production of this manuscript.

#### Key issues

- Recent MRI investigations using volumetric measurements and diffusion tensor imaging clearly indicate the presence of white matter (WM) abnormalities in Alzheimer's disease (AD), even at early stages such as minor cognitive impairment.
- WM changes in AD have been found to affect tracts that interconnect relevant networks for cognition such as the perforant pathway, the corpus callosum, fornix, the cingulum bundle and other cortico-cortical tracts.
- Degeneration of WM causes disconnection among neural cells, damage to cortico-cortical and cortico-subcortical pathways, as well as loss of myelinated axons resulting in reduced signaling and synaptic activity, even at early AD stages.
- The degree of WM abnormalities in AD (hyperintense lesions on T2/FLAIR and diffusion tensor imaging indices of WM disruption) are related to the severity of cognitive impairment, and these WM changes may predict the progression from minor cognitive impairment to AD.
- The possible relationship between WM abnormalities and the emergence of neuropsychiatric symptoms in AD remains to be clarified.

#### References

Papers of special note have been highlighted as:

- of interest
- of considerable interest

1 Dubois B, Feldman HH, Jacova C *et al.* Revising the definition of Alzheimer's

disease: a new lexicon. *Lancet Neurol.* 9(11), 1118–1127 (2010).

2 Sperling RA, Aisen PS, Beckett LA *et al.* Toward defining the preclinical stages of Alzheimer's disease: recommendations from the National Institute on Aging – Alzheimer's Association workgroups on

diagnostic guidelines for Alzheimer's disease. *Alzheimers Dement.* 7(3), 280–292 (2011).

3 Dickerson BC, Sperling RA. Neuroimaging biomarkers for clinical trials of disease-modifying therapies in Alzheimer's disease. *NeuroRx* 2(2), 348–360 (2005).

- 4 Hommet C, Mondon K, Constans T *et al.* Review of cerebral microangiopathy and Alzheimer's disease: relation between white matter hyperintensities and microbleeds. *Dement. Geriatr. Cogn. Disord.* 32(6), 367–378 (2011).
- 5 Admiraal-Behloul F, van den Heuvel DM, Olofsen H *et al.* Fully automatic segmentation of white matter hyperintensities in MR images of the elderly. *Neuroimage* 28(3), 607–617 (2005).
- 6 Gold BT, Powell DK, Andersen AH, Smith CD. Alterations in multiple measures of white matter integrity in normal women at high risk for Alzheimer's disease. *Neuroimage* 52(4), 1487–1494 (2010).
- 7 Longstreth WT Jr, Manolio TA, Arnold A *et al.* Clinical correlates of white matter findings on cranial magnetic resonance imaging of 3301 elderly people. The Cardiovascular Health Study. *Stroke* 27(8), 1274–1282 (1996).
- 8 Schmidt R, Schmidt H, Haybaeck J *et al.* Heterogeneity in age-related white matter changes. *Acta Neuropathol.* 122(2), 171–185 (2011).
- **A review about white matter (WM) hyperintensities in the aging brain, including imaging findings, neuropathology and genetic aspects.**
- 9 Fazekas F, Chawluk JB, Alavi A, Hurtig HI, Zimmerman RA. MR signal abnormalities at 1.5 T in Alzheimer's dementia and normal aging. *AJR. Am. J. Roentgenol.* 149(2), 351–356 (1987).
- 10 Wahlund LO, Barkhof F, Fazekas F *et al.*; European Task Force on Age-Related White Matter Changes. A new rating scale for age-related white matter changes applicable to MRI and CT. *Stroke* 32(6), 1318–1322 (2001).
- 11 Brickman AM, Sneed JR, Provenzano FA *et al.* Quantitative approaches for assessment of white matter hyperintensities in elderly populations. *Psychiatry Res.* 193(2), 101–106 (2011).
- 12 Rostrup E, Gouw AA, Vrenken H *et al.*; LADIS study group. The spatial distribution of age-related white matter changes as a function of vascular risk factors – results from the LADIS study. *Neuroimage* 60(3), 1597–1607 (2012).
- 13 Gouw AA, Seewann A, van der Flier WM *et al.* Heterogeneity of small vessel disease: a systematic review of MRI and histopathology correlations. *J. Neurol. Neurosurg. Psychiatr.* 82(2), 126–135 (2011).
- 14 Simpson JE, Fernando MS, Clark L *et al.*; MRC Cognitive Function and Ageing Neuropathology Study Group. White matter lesions in an unselected cohort of the elderly: astrocytic, microglial and oligodendrocyte precursor cell responses. *Neuropathol. Appl. Neurobiol.* 33(4), 410–419 (2007).
- 15 Simpson JE, Ince PG, Higham CE *et al.*; MRC Cognitive Function and Ageing Neuropathology Study Group. Microglial activation in white matter lesions and nonlesional white matter of ageing brains. *Neuropathol. Appl. Neurobiol.* 33(6), 670–683 (2007).
- 16 Elias MF, Elias PK, Sullivan LM, Wolf PA, D'Agostino RB. Lower cognitive function in the presence of obesity and hypertension: the Framingham heart study. *Int. J. Obes. Relat. Metab. Disord.* 27(2), 260–268 (2003).
- 17 de la Torre JC. Three postulates to help identify the cause of Alzheimer's disease. *J. Alzheimers Dis.* 24(4), 657–668 (2011).
- 18 O'Brien JT, Erkinjuntti T, Reisberg B *et al.* Cerebral blood flow in dementia. *Lancet Neurol.* 2(2), 89–98 (2003).
- 19 Hachinski VC, Iliff LD, Zilhka E *et al.* Cerebral blood flow in dementia. *Arch. Neurol.* 32(9), 632–637 (1975).
- 20 Loeb C, Gandolfo C. Diagnostic evaluation of degenerative and vascular dementia. *Stroke* 14(3), 399–401 (1983).
- 21 Rosen WG, Terry RD, Fuld PA, Katzman R, Peck A. Pathological verification of ischemic score in differentiation of dementias. *Ann. Neurol.* 7(5), 486–488 (1980).
- 22 Moroney JT, Bagiella E, Desmond DW *et al.* Meta-analysis of the Hachinski Ischemic Score in pathologically verified dementias. *Neurology* 49(4), 1096–1105 (1997).
- 23 Brewster PW, McDowell I, Moineddin R, Tierney MC. Differential prediction of vascular dementia and Alzheimer's disease in nondemented older adults within 5 years of initial testing. *Alzheimers. Dement.* 8(6), 528–535 (2012).
- 24 Gunning-Dixon FM, Raz N. The cognitive correlates of white matter abnormalities in normal aging: a quantitative review. *Neuropsychology* 14(2), 224–232 (2000).
- 25 Hedden T, Mormino EC, Amariglio RE *et al.* Cognitive profile of amyloid burden and white matter hyperintensities in cognitively normal older adults. *J. Neurosci.* 32(46), 16233–16242 (2012).
- 26 Herrmann LL, Le Masurier M, Ebmeier KP. White matter hyperintensities in late life depression: a systematic review. *J. Neurol. Neurosurg. Psychiatr.* 79(6), 619–624 (2008).
- 27 Tamashiro JH, Zung S, Zanetti MV *et al.* Increased rates of white matter hyperintensities in late-onset bipolar disorder. *Bipolar Disord.* 10(7), 765–775 (2008).
- 28 Marchant NL, Reed BR, Sanossian N *et al.* The aging brain and cognition: contribution of vascular injury and A $\beta$  to mild cognitive dysfunction. *JAMA Neurol.* 70(4), 488–495 (2013).
- 29 Wahlund LO, Almkvist O, Basun H, Julin P. MRI in successful aging, a 5-year follow-up study from the eighth to ninth decade of life. *Magn. Reson. Imaging* 14(6), 601–608 (1996).
- 30 Murray ME, Senjem ML, Petersen RC *et al.* Functional impact of white matter hyperintensities in cognitively normal elderly subjects. *Arch. Neurol.* 67(11), 1379–1385 (2010).
- 31 Hardy J, Selkoe DJ. The amyloid hypothesis of Alzheimer's disease: progress and problems on the road to therapeutics. *Science* 297(5580), 353–356 (2002).
- 32 Braak H, Braak E. Frequency of stages of Alzheimer-related lesions in different age categories. *Neurobiol. Aging* 18(4), 351–357 (1997).
- 33 Price JL, Morris JC. Tangles and plaques in nondemented aging and 'preclinical' Alzheimer's disease. *Ann. Neurol.* 45(3), 358–368 (1999).
- 34 Ferreira LK, Busatto GF. Neuroimaging in Alzheimer's disease: current role in clinical practice and potential future applications. *Clinics (Sao. Paulo)*. 66(Suppl. 1), 19–24 (2011).
- 35 Provenzano FA, Muraskin J, Tosto G *et al.*; for the Alzheimer's Disease Neuroimaging Initiative. White matter hyperintensities and cerebral amyloidosis: necessary and sufficient for clinical expression of Alzheimer disease? *JAMA Neurol.* 70(4), 455–461 (2013).
- **A recent study addressing the relationship between amyloid deposition and WM hyperintensities using amyloid imaging and MRI.**
- 36 Carmichael O, Schwarz C, Drucker D *et al.*; Alzheimer's Disease Neuroimaging Initiative. Longitudinal changes in white matter disease and cognition in the first year of the Alzheimer disease neuroimaging initiative. *Arch. Neurol.* 67(11), 1370–1378 (2010).

- 37 Brickman AM, Provenzano FA, Muraskin J *et al.* Regional white matter hyperintensity volume, not hippocampal atrophy, predicts incident Alzheimer disease in the community. *Arch. Neurol.* 69(12), 1621–1627 (2012).
- 38 Gorelick PB, Scuteri A, Black SE *et al.*; American Heart Association Stroke Council, Council on Epidemiology and Prevention, Council on Cardiovascular Nursing, Council on Cardiovascular Radiology and Intervention, and Council on Cardiovascular Surgery and Anesthesia. Vascular contributions to cognitive impairment and dementia: a statement for healthcare professionals from the American Heart Association/American Stroke Association. *Stroke* 42(9), 2672–2713 (2011).
- 39 Debetre S, Markus HS. The clinical importance of white matter hyperintensities on brain magnetic resonance imaging: systematic review and meta-analysis. *BMJ* 341, c3666 (2010).
- 40 Mechelli A, Price CJ, Friston KJ, Ashburner J. Voxel-based morphometry of the human brain: methods and applications. *Curr. Med. Imag. Rev.* 1(2), 105–113 (2005).
- 41 Busatto GF, Diniz BS, Zanetti MV. Voxel-based morphometry in Alzheimer's disease. *Expert Rev. Neurother.* 8(11), 1691–1702 (2008).
- 42 Whitwell JL. Voxel-based morphometry: an automated technique for assessing structural changes in the brain. *J. Neurosci.* 29(31), 9661–9664 (2009).
- 43 Chaim TM, Duran FL, Uchida RR, Périco CA, de Castro CC, Busatto GF. Volumetric reduction of the corpus callosum in Alzheimer's disease *in vivo* as assessed with voxel-based morphometry. *Psychiatry Res.* 154(1), 59–68 (2007).
- 44 Balthazar ML, Yasuda CL, Pereira FR, Pedro T, Damasceno BP, Cendes F. Differences in grey and white matter atrophy in amnesic mild cognitive impairment and mild Alzheimer's disease. *Eur. J. Neurol.* 16(4), 468–474 (2009).
- 45 Busatto GF, Garrido GE, Almeida OP *et al.* A voxel-based morphometry study of temporal lobe gray matter reductions in Alzheimer's disease. *Neurobiol. Aging* 24(2), 221–231 (2003).
- 46 Balthazar ML, Yasuda CL, Cendes F, Damasceno BP. Learning, retrieval, and recognition are compromised in aMCI and mild AD: are distinct episodic memory processes mediated by the same anatomical structures? *J. Int. Neuropsychol. Soc.* 16(1), 205–209 (2010).
- 47 Ferreira LK, Diniz BS, Forlenza OV, Busatto GF, Zanetti MV. Neurostructural predictors of Alzheimer's disease: a meta-analysis of VBM studies. *Neurobiol. Aging* 32(10), 1733–1741 (2011).
- 48 Li J, Pan P, Huang R, Shang H. A meta-analysis of voxel-based morphometry studies of white matter volume alterations in Alzheimer's disease. *Neurosci. Biobehav. Rev.* 36(2), 757–763 (2012).
- A recent meta-analysis of voxel-based morphometry studies addressing WM volume differences between patients and controls.
- 49 Di Paola M, Luders E, Di Iulio F *et al.* Callosal atrophy in mild cognitive impairment and Alzheimer's disease: different effects in different stages. *Neuroimage* 49(1), 141–149 (2010).
- 50 Hampel H, Teipel SJ, Alexander GE, Pogarell O, Rapoport SI, Möller HJ. *In vivo* imaging of region and cell type specific neocortical neurodegeneration in Alzheimer's disease. Perspectives of MRI derived corpus callosum measurement for mapping disease progression and effects of therapy. Evidence from studies with MRI, EEG and PET. *J. Neural Transm.* 109(5–6), 837–855 (2002).
- 51 Teipel SJ, Bayer W, Alexander GE *et al.* Regional pattern of hippocampus and corpus callosum atrophy in Alzheimer's disease in relation to dementia severity: evidence for early neocortical degeneration. *Neurobiol. Aging* 24(1), 85–94 (2003).
- 52 Teipel SJ, Bayer W, Alexander GE *et al.* Progression of corpus callosum atrophy in Alzheimer disease. *Arch. Neurol.* 59(2), 243–248 (2002).
- 53 Li S, Pu F, Shi F, Xie S, Wang Y, Jiang T. Regional white matter decreases in Alzheimer's disease using optimized voxel-based morphometry. *Acta Radiol.* 49(1), 84–90 (2008).
- 54 Matsuda H. Voxel-based morphometry of brain MRI in normal aging and Alzheimer's disease. *Aging Dis.* 4(1), 29–37 (2013).
- 55 Di Paola M, Spalletta G, Caltagirone C. *In vivo* structural neuroanatomy of corpus callosum in Alzheimer's disease and mild cognitive impairment using different MRI techniques: a review. *J. Alzheimers Dis.* 20(1), 67–95 (2010).
- 56 Stoub TR, deToledo-Morrell L, Stebbins GT, Leurgans S, Bennett DA, Shah RC. Hippocampal disconnection contributes to memory dysfunction in individuals at risk for Alzheimer's disease. *Proc. Natl. Acad. Sci. USA* 103(26), 10041–10045 (2006).
- 57 Guo X, Wang Z, Li K *et al.* Voxel-based assessment of gray and white matter volumes in Alzheimer's disease. *Neurosci. Lett.* 468(2), 146–150 (2010).
- 58 Villain N, Desgranges B, Viader F *et al.* Relationships between hippocampal atrophy, white matter disruption, and gray matter hypometabolism in Alzheimer's disease. *J. Neurosci.* 28(24), 6174–6181 (2008).
- 59 Pereira JM, Xiong L, Acosta-Cabrero J, Pengas G, Williams GB, Nestor PJ. Registration accuracy for VBM studies varies according to region and degenerative disease grouping. *Neuroimage* 49(3), 2205–2215 (2010).
- 60 Davatzikos C, Vaillant M, Resnick SM, Prince JL, Letovsky S, Bryan RN. A computerized approach for morphological analysis of the corpus callosum. *J. Comput. Assist. Tomogr.* 20(1), 88–97 (1996).
- 61 Leporé N, Brun C, Pennec X *et al.* Mean template for tensor-based morphometry using deformation tensors. *Med. Image Comput. Comput. Assist. Interv.* 10(Pt 2), 826–833 (2007).
- 62 Friese U, Meindl T, Herpertz SC, Reiser MF, Hampel H, Teipel SJ. Diagnostic utility of novel MRI-based biomarkers for Alzheimer's disease: diffusion tensor imaging and deformation-based morphometry. *J. Alzheimers Dis.* 20(2), 477–490 (2010).
- 63 Fischl B. FreeSurfer. *Neuroimage* 62(2), 774–781 (2012).
- 64 Westman E, Muehlboeck JS, Simmons A. Combining MRI and CSF measures for classification of Alzheimer's disease and prediction of mild cognitive impairment conversion. *Neuroimage* 62(1), 229–238 (2012).
- 65 Ridgway GR, Lehmann M, Barnes J *et al.* Early-onset Alzheimer disease clinical variants: multivariate analyses of cortical thickness. *Neurology* 79(1), 80–84 (2012).
- 66 Salat DH, Greve DN, Pacheco JL *et al.* Regional white matter volume differences in nondemented aging and Alzheimer's disease. *Neuroimage* 44(4), 1247–1258 (2009).
- 67 Clarkson MJ, Cardoso MJ, Ridgway GR *et al.* A comparison of voxel and surface based cortical thickness estimation methods. *Neuroimage* 57(3), 856–865 (2011).

- 68 Masutani Y, Aoki S, Abe O, Hayashi N, Otomo K. MR diffusion tensor imaging: recent advance and new techniques for diffusion tensor visualization. *Eur. J. Radiol.* 46(1), 53–66 (2003).
- 69 Yoon B, Shim YS, Hong YJ *et al.* Comparison of diffusion tensor imaging and voxel-based morphometry to detect white matter damage in Alzheimer's disease. *J. Neurol. Sci.* 302(1–2), 89–95 (2011).
- 70 Sydykova D, Stahl R, Dietrich O *et al.* Fiber connections between the cerebral cortex and the corpus callosum in Alzheimer's disease: a diffusion tensor imaging and voxel-based morphometry study. *Cereb. Cortex* 17(10), 2276–2282 (2007).
- 71 Mielke MM, Kozauer NA, Chan KC *et al.* Regionally-specific diffusion tensor imaging in mild cognitive impairment and Alzheimer's disease. *Neuroimage* 46(1), 47–55 (2009).
- 72 Cho H, Yang DW, Shon YM *et al.* Abnormal integrity of corticocortical tracts in mild cognitive impairment: a diffusion tensor imaging study. *J. Korean Med. Sci.* 23(3), 477–483 (2008).
- 73 Salat DH, Tuch DS, van der Kouwe AJ *et al.* White matter pathology isolates the hippocampal formation in Alzheimer's disease. *Neurobiol. Aging* 31(2), 244–256 (2010).
- 74 O'Dwyer L, Lambertson F, Bokde AL *et al.* Multiple indices of diffusion identifies white matter damage in mild cognitive impairment and Alzheimer's disease. *PLoS ONE* 6(6), e21745 (2011).
- 75 Alves GS, O'Dwyer L, Jurcoane A *et al.* Different patterns of white matter degeneration using multiple diffusion indices and volumetric data in mild cognitive impairment and Alzheimer patients. *PLoS ONE* 7(12), e52859 (2012).
- 76 Stricker NH, Schweinsburg BC, Delano-Wood L *et al.* Decreased white matter integrity in late-myelinating fiber pathways in Alzheimer's disease supports retrogenesis. *Neuroimage* 45(1), 10–16 (2009).
- 77 Sexton CE, Kalu UG, Filippini N, Mackay CE, Ebmeier KP. A meta-analysis of diffusion tensor imaging in mild cognitive impairment and Alzheimer's disease. *Neurobiol. Aging* 32(12), 2322.e5–2322.18 (2011).
- 78 Clerx L, Visser PJ, Verhey F, Aalten P. New MRI markers for Alzheimer's disease: a meta-analysis of diffusion tensor imaging and a comparison with medial temporal lobe measurements. *J. Alzheimers Dis.* 29(2), 405–429 (2012).
- 79 Shu N, Wang Z, Qi Z, Li K, He Y. Multiple diffusion indices reveals white matter degeneration in Alzheimer's disease and mild cognitive impairment: a tract-based spatial statistics study. *J. Alzheimers Dis.* 26(Suppl. 3), 275–285 (2011).
- 80 Mielke MM, Okonkwo OC, Oishi K *et al.* Fornix integrity and hippocampal volume predict memory decline and progression to Alzheimer's disease. *Alzheimers. Dement.* 8(2), 105–113 (2012).
- 81 Kalus P, Slotboom J, Gallinat J *et al.* Examining the gateway to the limbic system with diffusion tensor imaging: the perforant pathway in dementia. *Neuroimage* 30(3), 713–720 (2006).
- 82 Wang J, Zuo X, Dai Z *et al.* Disrupted functional brain connectome in individuals at risk for Alzheimer's disease. *Biol. Psychiatr.* 73(5), 472–481 (2012).
- 83 Heinemann U, Schmitz D, Eder C, Gloveli T. Properties of entorhinal cortex projection cells to the hippocampal formation. *Ann. N. Y. Acad. Sci.* 911, 112–126 (2000).
- 84 Witter MP. The perforant path: projections from the entorhinal cortex to the dentate gyrus. *Prog. Brain Res.* 163, 43–61 (2007).
- 85 Hyman BT, Van Hoesen GW, Kromer LJ, Damasio AR. Perforant pathway changes and the memory impairment of Alzheimer's disease. *Ann. Neurol.* 20(4), 472–481 (1986).
- 86 Morys J, Sadowski M, Barcikowska M, Maciejewska B, Narkiewicz O. The second layer neurones of the entorhinal cortex and the perforant path in physiological ageing and Alzheimer's disease. *Acta Neurol. Exp. (Wars)* 54(1), 47–53 (1994).
- 87 Xie S, Xiao JX, Gong GL *et al.* Voxel-based detection of white matter abnormalities in mild Alzheimer disease. *Neurology* 66(12), 1845–1849 (2006).
- 88 Smith SM, Jenkinson M, Johansen-Berg H *et al.* Tract-based spatial statistics: voxelwise analysis of multi-subject diffusion data. *Neuroimage* 31(4), 1487–1505 (2006).
- 89 van Bruggen T, Stieltjes B, Thomann PA, Parzer P, Meinzer HP, Fritzsche KH. Do Alzheimer-specific microstructural changes in mild cognitive impairment predict conversion? *Psychiatry Res.* 203(2–3), 184–193 (2012).
- 90 Zhuang L, Wen W, Zhu W *et al.* White matter integrity in mild cognitive impairment: a tract-based spatial statistics study. *Neuroimage* 53(1), 16–25 (2010).
- 91 Liu Y, Spulber G, Lehtimäki KK *et al.* Diffusion tensor imaging and tract-based spatial statistics in Alzheimer's disease and mild cognitive impairment. *Neurobiol. Aging* 32(9), 1558–1571 (2011).
- 92 Jones DK, Knösche TR, Turner R. White matter integrity, fiber count, and other fallacies: the do's and don'ts of diffusion MRI. *Neuroimage* 73, 239–254 (2013).
- A review paper on diffusion tensor imaging (DTI) methodology explaining the limits of interpreting DTI findings.
- 93 Oishi K, Mielke MM, Albert M, Lyketsos CG, Mori S. DTI analyses and clinical applications in Alzheimer's disease. *J. Alzheimers Dis.* 26(Suppl. 3), 287–296 (2011).
- A review of DTI studies in Alzheimer's disease (AD).
- 94 Takahashi M, Hackney DB, Zhang G *et al.* Magnetic resonance microimaging of intraaxonal water diffusion in live excised lamprey spinal cord. *Proc. Natl Acad. Sci. USA* 99(25), 16192–16196 (2002).
- 95 Lyketsos CG, Carrillo MC, Ryan JM *et al.* Neuropsychiatric symptoms in Alzheimer's disease. *Alzheimers. Dement.* 7(5), 532–539 (2011).
- 96 Bruen PD, McGeown WJ, Shanks MF, Venneri A. Neuroanatomical correlates of neuropsychiatric symptoms in Alzheimer's disease. *Brain* 131(Pt 9), 2455–2463 (2008).
- 97 Trzepacz PT, Yu P, Bhamidipati PK *et al.* Alzheimer's Disease Neuroimaging Initiative. Frontolimbic atrophy is associated with agitation and aggression in mild cognitive impairment and Alzheimer's disease. *Alzheimers. Dement.* doi:10.1016/j.jalz.2012.10.005 (2012) (Epub ahead of print).
- 98 Nakaaki S, Sato J, Torii K *et al.* Neuro-anatomical abnormalities before onset of delusions in patients with Alzheimer's disease: a voxel-based morphometry study. *Neuropsychiatr. Dis. Treat.* 9, 1–8 (2013).
- 99 Tighe SK, Oishi K, Mori S *et al.* Diffusion tensor imaging of neuropsychiatric symptoms in mild cognitive impairment and Alzheimer's dementia. *J. Neuropsychiatry Clin. Neurosci.* 24(4), 484–488 (2012).
- 100 Ota M, Sato N, Nakata Y, Arima K, Uno M. Relationship between apathy and diffusion tensor imaging metrics of the brain in Alzheimer's disease. *Int. J. Geriatr. Psychiatry* 27(7), 722–726 (2012).
- 101 Tomimoto H, Lin JX, Matsuo A *et al.* Different mechanisms of corpus callosum

- atrophy in Alzheimer's disease and vascular dementia. *J. Neurol.* 251(4), 398–406 (2004).
- 102 Bartzokis G. Alzheimer's disease as homeostatic responses to age-related myelin breakdown. *Neurobiol. Aging* 32(8), 1341–1371 (2011).
- Thorough review about the relationship between WM degeneration and neurodegeneration, including alternative relationships between the amyloid hypothesis of AD and WM.
- 103 Brickman AM, Meier IB, Korgaonkar MS *et al.* Testing the white matter retrogenesis hypothesis of cognitive aging. *Neurobiol. Aging* 33(8), 1699–1715 (2012).
- 104 Bartzokis G. Age-related myelin breakdown: a developmental model of cognitive decline and Alzheimer's disease. *Neurobiol. Aging* 25(1), 5–18; author reply 49 (2004).
- A proposal for a developmental model of cognitive decline and AD centered on WM pathology.
- 105 Kuceyeski A, Zhang Y, Raj A. Linking white matter integrity loss to associated cortical regions using structural connectivity information in Alzheimer's disease and fronto-temporal dementia: the Loss in Connectivity (LoCo) score. *Neuroimage* 61(4), 1311–1323 (2012).
- 106 Fu JL, Zhang T, Chang C, Zhang YZ, Li WB. The value of diffusion tensor imaging in the differential diagnosis of subcortical ischemic vascular dementia and Alzheimer's disease in patients with only mild white matter alterations on T2-weighted images. *Acta Radiol.* 53(3), 312–317 (2012).
- 107 Bozoki AC, Korolev IO, Davis NC, Hoisington LA, Berger KL. Disruption of limbic white matter pathways in mild cognitive impairment and Alzheimer's disease: a DTI/FDG-PET study. *Hum. Brain Mapp.* 33(8), 1792–1802 (2012).
- 108 Müller MJ, Greverus D, Weibrich C *et al.* Diagnostic utility of hippocampal size and mean diffusivity in amnesic MCI. *Neurobiol. Aging* 28(3), 398–403 (2007).
- 109 O'Dwyer L, Lamberton F, Bokde AL *et al.* Using support vector machines with multiple indices of diffusion for automated classification of mild cognitive impairment. *PLoS ONE* 7(2), e32441 (2012).
- 110 Wang L, Goldstein FC, Veledar E *et al.* Alterations in cortical thickness and white matter integrity in mild cognitive impairment measured by whole-brain cortical thickness mapping and diffusion tensor imaging. *AJNR. Am. J. Neuroradiol.* 30(5), 893–899 (2009).
- 111 McMillan CT, Brun C, Siddiqui S *et al.* White matter imaging contributes to the multimodal diagnosis of frontotemporal lobar degeneration. *Neurology* 78(22), 1761–1768 (2012).
- 112 Likitjaroen Y, Meindl T, Friese U *et al.* Longitudinal changes of fractional anisotropy in Alzheimer's disease patients treated with galantamine: a 12-month randomized, placebo-controlled, double-blinded study. *Eur. Arch. Psychiatry Clin. Neurosci.* 262(4), 341–350 (2012).
- 113 Jack CR Jr, Bernstein MA, Borowski BJ *et al.*; Alzheimer's Disease Neuroimaging Initiative. Update on the magnetic resonance imaging core of the Alzheimer's disease neuroimaging initiative. *Alzheimers. Dement.* 6(3), 212–220 (2010).
- 114 Jack CR Jr. Alzheimer disease: new concepts on its neurobiology and the clinical role imaging will play. *Radiology* 263(2), 344–361 (2012).
- 115 Yassa MA, Muftuler LT, Stark CE. Ultrahigh-resolution microstructural diffusion tensor imaging reveals perforant path degradation in aged humans *in vivo*. *Proc. Natl Acad. Sci. USA* 107(28), 12687–12691 (2010).
- 116 Greicius MD, Supekar K, Menon V, Dougherty RF. Resting-state functional connectivity reflects structural connectivity in the default mode network. *Cereb. Cortex* 19(1), 72–78 (2009).
- 117 Chételat G, Desgranges B, Landeau B *et al.* Direct voxel-based comparison between grey matter hypometabolism and atrophy in Alzheimer's disease. *Brain* 131(Pt 1), 60–71 (2008).
- 118 Jacobs HI, Gronenschild EH, Evers EA *et al.* Visuospatial processing in early Alzheimer's disease: a multimodal neuroimaging study. *Cortex*. doi:10.1016/j.cortex.2012.01.005 (2012) (Epub ahead of print).
- 119 Buckner RL, Andrews-Hanna JR, Schacter DL. The brain's default network: anatomy, function, and relevance to disease. *Ann. N. Y. Acad. Sci.* 1124, 1–38 (2008).
- 120 Raichle ME, MacLeod AM, Snyder AZ, Powers WJ, Gusnard DA, Shulman GL. A default mode of brain function. *Proc. Natl Acad. Sci. USA* 98(2), 676–682 (2001).
- 121 Kantarci K, Lowe VJ, Boeve BF *et al.* Multimodality imaging characteristics of dementia with Lewy bodies. *Neurobiol. Aging* 33(9), 2091–2105 (2012).
- 122 Shaffer JL, Petrella JR, Sheldon FC *et al.*; Alzheimer's Disease Neuroimaging Initiative. Predicting cognitive decline in subjects at risk for Alzheimer disease by using combined cerebrospinal fluid, MR imaging, and PET biomarkers. *Radiology* 266(2), 583–591 (2013).
- 123 Zhang D, Shen D. Predicting future clinical changes of MCI patients using longitudinal and multimodal biomarkers. *PLoS ONE* 7(3), e33182 (2012).
- 124 Kim J, Basak JM, Holtzman DM. The role of apolipoprotein E in Alzheimer's disease. *Neuron* 63(3), 287–303 (2009).
- 125 Chiang GC, Zhan W, Schuff N, Weiner MW. White matter alterations in cognitively normal apoE ε2 carriers: insight into Alzheimer resistance? *AJNR. Am. J. Neuroradiol.* 33(7), 1392–1397 (2012).
- 126 Forlenza OV, Diniz BS, Gattaz WF. Diagnosis and biomarkers of predementia in Alzheimer's disease. *BMC Med.* 8, 89 (2010).
- 127 Hu WT, Holtzman DM, Fagan AM *et al.*; Alzheimer's Disease Neuroimaging Initiative. Plasma multianalyte profiling in mild cognitive impairment and Alzheimer disease. *Neurology* 79(9), 897–905 (2012).
- 128 Mielke MM, Haughey NJ, Ratnam Bandaru VV *et al.* Plasma ceramides are altered in mild cognitive impairment and predict cognitive decline and hippocampal volume loss. *Alzheimers. Dement.* 6(5), 378–385 (2010).
- 129 Vemuri P, Wiste HJ, Weigand SD *et al.*; Alzheimer's Disease Neuroimaging Initiative. MRI and CSF biomarkers in normal, MCI, and AD subjects: predicting future clinical change. *Neurology* 73(4), 294–301 (2009).
- 130 Thambisetty M, An Y, Kinsey A *et al.* Plasma clusterin concentration is associated with longitudinal brain atrophy in mild cognitive impairment. *Neuroimage* 59(1), 212–217 (2012).

**Experimento 7 – Alterações neuropsiquiátricas associados com danos de redes funcionais em pacientes com doença de Alzheimer e transtorno cognitivo leve.**

♦ Human Brain Mapping 000:00–00 (2013) ♦

**Neuropsychiatric Symptoms in Alzheimer’s Disease Are Related to Functional Connectivity Alterations in the Salience Network**

**Marcio L. F. Balthazar,<sup>1</sup> Fabrício R. S. Pereira,<sup>1</sup> Tátila M. Lopes,<sup>1</sup> Elvis L. da Silva,<sup>1</sup> Ana Carolina Coan,<sup>1</sup> Brunno M. Campos,<sup>1</sup> Niall W. Duncan,<sup>2</sup> Florindo Stella,<sup>3</sup> Georg Northoff,<sup>2</sup> Benito P. Damasceno,<sup>1</sup> and Fernando Cendes<sup>1\*</sup>**

<sup>1</sup>Neuroimaging Laboratory, Department of Neurology, Medical Sciences School, University of Campinas (UNICAMP), Brazil

<sup>2</sup>Institute of Mental Health Research, University of Ottawa, Ottawa, Ontario, Canada

<sup>3</sup>Biosciences Institute, São Paulo State University (UNESP), Brazil

---

**Abstract:** Neuropsychiatric syndromes are highly prevalent in Alzheimer’s disease (AD), but their neurobiology is not completely understood. New methods in functional magnetic resonance imaging, such as intrinsic functional connectivity or “resting-state” analysis, may help to clarify this issue. Using such approaches, alterations in the default-mode and salience networks (SNs) have been described in Alzheimer’s, although their relationship with specific symptoms remains unclear. We therefore carried out resting-state functional connectivity analysis with 20 patients with mild to moderate AD, and correlated their scores on neuropsychiatric inventory syndromes (apathy, hyperactivity, affective syndrome, and psychosis) with maps of connectivity in the default mode network and SN. In addition, we compared network connectivity in these patients with that in 17 healthy elderly control subjects. All analyses were controlled for gray matter density and other potential confounds. Alzheimer’s patients showed increased functional connectivity within the SN compared with controls (right anterior cingulate cortex and left medial frontal gyrus), along with reduced functional connectivity in the default-mode network (bilateral precuneus). A correlation between increased connectivity in anterior cingulate cortex and right insula areas of the SN and hyperactivity syndrome (agitation, irritability, aberrant motor behavior, euphoria, and disinhibition) was found. These findings demonstrate an association between specific network changes in AD and particular neuropsychiatric symptom types. This underlines the potential clinical significance of resting state alterations in future diagnosis and therapy. *Hum Brain Mapp* 00:000–000, 2013. © 2013 Wiley Periodicals Inc.

**Key words:** Alzheimer’s disease; default mode network; salience network; functional connectivity; neuropsychiatric symptoms

---

Contract grant sponsor: São Paulo Research Foundation (FAPESP), Brazil; Contract grant number: 2009/02179-2.

\*Correspondence to: Fernando Cendes, Department of Neurology, FCM, University of Campinas (UNICAMP), Cidade Universitária, Campinas-SP, Brazil, 13083-970. E-mail: fcendes@unicamp.br

Received for publication 22 February 2012; Revised 6 November 2012; Accepted 3 December 2012

DOI: 10.1002/hbm.22248

Published online in Wiley Online Library (wileyonlinelibrary.com).

© 2013 Wiley Periodicals, Inc.

---



---

**INTRODUCTION**

Neuropsychiatric symptoms (NPS) are highly prevalent in patients with dementia. This is particularly the case in those with Alzheimer's disease (AD), where studies report a prevalence of NPS that varies from 60 to 90% during the course of the disease [Youn et al., 2011]. However, despite this high prevalence, the neurobiology underlying these symptoms is poorly understood. The most widespread theories about the genesis of cognitive deficits and NPS in AD relate to anatomic-structural changes, associated with pathological features (neuritic plaques, neurofibrillary tangles, and loss of synaptic density, among others), in the limbic, paralimbic, and neocortical regions. In addition, NPS may be associated with dysfunction of various neurotransmitter systems due to neuronal death in specific transmitter source nuclei (cholinergic, serotonergic, noradrenergic, etc.) [Cummings, 2000].

In addition to the observed anatomical deficits, recent advances in the neuroimaging of dementia have highlighted concurrent dysfunctions in functional networks. Such networks have been identified across a number of imaging modalities, most prominently fMRI, and are characterized by inter-regional correlations in spontaneous BOLD fluctuations (known as functional connectivity) in the absence of an experimental paradigm or any other explicit stimulus [van den Heuvel and Pol, 2010]. Different networks are spatially distinct but functionally related and have been found to be present at rest, during tasks, and even during sleep and anesthesia [Deshpande et al., 2010; Fox and Raichle, 2007; van den Heuvel and Pol, 2010]. Neurodegenerative diseases, such as AD, can disrupt activity within the networks [Seeley et al., 2009], as well as the complex system of interconnections between the different networks, causing cognitive problems (memory, attention, language, praxis, and executive functions), and NPS (apathy, depression, agitation, disinhibition, etc.) [Bruen et al., 2008; Gauthier et al., 2010; Lyketsos et al., 2011]. In the case of AD, one of the most relevant networks appears to be the default mode network (DMN). The role of the DMN, which consists of regions such as the posterior cingulate cortex (PCC), precuneus, ventromedial prefrontal cortex, and the hippocampal formation, remains unclear; however, it is widely accepted that this system shows increased activity when a person is not focused on activities directed to the external environment (e.g., when an individual recalls autobiographical facts and events, or plans the future) [Buckner et al., 2008]. Some studies in AD have shown a breakdown in functional connectivity in the DMN, even at early stages of the disease [Greicius et al., 2004; Zhang et al., 2010]. In addition, Celone et al. [2006] reported associations between DMN connectivity and memory performance assessed outside of the scanner, whereas Westlye et al. [2011] showed a negative correlation between DMN synchronization and performance on memory tests, suggesting a neurocognitive significance of brain activity patterns during rest in healthy elderly

individuals who are carriers of the AD-related apolipoprotein  $\epsilon 4$  gene (APOE4).

A second network that seems to be relevant in AD is the salience network (SN), which comprises the anterior cingulate cortex (ACC), the frontal insula, the amygdala and the striatum. Activity in the SN is related to emotionally relevant stimuli, which can originate either internally or from the external environment [Seeley et al., 2007]. In the case of AD (and the behavioral variant of frontotemporal dementia), Zhou et al. [2010] showed a negative correlation between the connectivity of the SN and the DMN, meaning that decreasing activity in the DMN is related to increased activity in the SN and vice versa). A dynamic interaction between these networks may provide regulation of shifts in attention, as well as access to personal resources for general cognitive processing and specific cognitive domains. Such mechanisms would have important implications for psychopathological disorders involving dysfunctional saliency processing, which can diminish the ability to direct attentional resources and goal-relevant cognition [Menon, 2011].

Several unanswered questions remain, however, regarding the role of these functional networks in the development of AD symptoms. To our knowledge, no studies have investigated the correlation between neuropsychiatric syndromes and disruptions in the DMN or SN in AD. One study by Seeley et al. [2007] did find significant correlations between the level of anxiety in healthy adults before MRI scanning and the degree of connectivity of the ACC (an important part of the SN). The authors proposed that behavioral symptoms in AD, which often involve early emotional sensitizations such as irritability and anxiety, might be associated with functional alterations in SN [Zhou et al., 2010].

We based our study hypothesis on the following premises: (1) alterations in functional networks may be related to NPS; and (2) disruptions in one network may interfere with other networks (e.g., the negative correlation in connectivity patterns between DMN and SN). We hypothesized that alterations in DMN and SN connectivity may be responsible at least in part for the NPS of AD patients. More specifically, we sought to determine whether an increase in connectivity in the SN could lead to hyperactivity behaviors, such as agitation and irritability. With regard to the DMN, we hypothesized that a decrease in connectivity within this network could lead to apathy, potentially through deficits in forming expectations for the future or recounting recent events [Buckner et al., 2008]. Given the anticorrelation between SN and DMN, it is plausible to hypothesize that decreases in DMN connectivity might also be related to hyperactivity behaviors, which would fit with observations of combined apathy and agitation in patients with dementia.

To test our hypotheses, we correlated the scores of the neuropsychiatric inventory (NPI) subsyndromes, as defined by Aalten et al. [2007], with individual maps SN and DMN connectivity in patients with mild to moderate AD,

considering age, atrophy, and dementia severity as covariates. The subsyndromes used were apathy, hyperactivity, affective syndrome, and psychosis. The use of NPI subsyndromes, rather than unitary symptoms, is supported by the fact that various individual symptoms usually manifest together and have a similar course over time, suggesting a common biological basis. In addition, pharmacological studies have shown that drug treatments have an effect on behavioral features in dementia when neuropsychiatric subsyndromes are considered but not when individual symptoms are considered [Gauthier et al., 2005; Herrmann et al., 2005]. We also compared the patterns of connectivity between patients and a group of healthy elderly people.

## MATERIALS AND METHODS

### Subjects

We studied 37 subjects over the age of 50 years ( $73.85 \pm 8.19$ ). Of those subjects, 20 had mild to moderate AD and were treated at the Neuropsychology and Dementia Outpatient Clinic (UNICAMP University Hospital). The remaining 17 subjects were healthy control subjects, matched for age and sex. Routine laboratory studies, including B12 levels, folate levels, syphilis serology, and thyroid hormone levels, were performed for all patients. The local ethics committee approved these experiments. The diagnosis of probable AD was based on criteria established by the National Institute of Neurological and Communicative Disorders, and the Stroke/Alzheimer's Disease and Related Disorders Association [McKhann et al., 1984]. We only included patients who were classified as clinical dementia rating (CDR) 1 (13 patients) and 2 (seven patients). All patients had at least one psychiatric symptom, as measured by the NPI. Exclusion criteria included a history of other neurological or psychiatric diseases, previous head injury with loss of consciousness, drug or alcohol addiction, prior chronic exposure to neurotoxic substances, and a Hachinski ischemic score  $>4$ . Patients who met the clinical criteria for probable AD but had extensive white matter hyperintensities on  $T_2$ -weighted MRI were also excluded. Fifteen patients underwent MRI scanning on the same day that their caregivers completed the NPI interview. In the remaining five cases, the interviews were performed 2 days before the MRI scanning. The control group consisted of subjects who were classified as CDR 0 and had no history of neurological diseases, psychiatric diseases, or memory complaints.

### Neuropsychological, Neuropsychiatric, and Functional Evaluations

Global cognitive status was measured using the Mini Mental Status Examination [MMSE, Folstein et al., 1975; Brazilian version by Brucki et al., 2003]. Episodic memory was evaluated by the Rey auditory verbal learning test

[Rey, 1964]. Visual perception was assessed with subtests of Luria's Neuropsychological Investigation (LNI), using items G12, G13, G14 (the patient is asked to examine and name pictures of objects that are scribbled over or superimposed on another picture), along with G17 (an item from Raven's test) and one item for mental rotation of figures (in both items, the patient is asked to complete a structure, a portion of which is missing, by choosing from various options) [Christensen, 1975]. Four items from the Ratcliff's manikin test for mental rotation were also used [Ratcliff, 1979]. Constructive praxis was evaluated using the Rey-Osterrieth's Complex Figure test [Osterrieth, 1944]. Language tests included the Boston Naming Test [Kaplan et al., 1983] and verbal fluency for category words (animals) and phonology (FAS). Working memory was assessed by the forward (FDS) and backward digit span subtest of the WAIS-R [Wechsler, 1987]. Executive functions were evaluated using the Trail Making Test A and B, Stroop color-word test and Clock drawing test.

The neuropsychiatric assessment consisted of the Neuropsychiatric Inventory (NPI) [Cummings et al., 1994] based on an interview with the closest caregiver. The NPI consists of a detailed evaluation of the following 12 neuropsychiatric domains: hallucinations, delusions, agitation/aggression, depression, anxiety, irritability, disinhibition, euphoria, apathy, aberrant motor behavior, change in night-time sleep behavior, and changes in appetite and eating. The questions were read to the caregiver exactly as written. If the caregiver failed to comprehend the question, we repeated it in alternate terms. After reading the screening question, the caregiver was asked if the behavior described had been observed. If the answer was "no" then we proceeded to the next section and read the next screening question. If the answer was "yes," then the subquestions were read, and yes/no responses were obtained. The caregiver was then asked to rate the frequency and severity of the behaviors within that domain, based on the most abnormal behavior revealed in the subquestions. The scores were calculated by multiplying the frequency of the symptoms (from 1 to 4: rarely, sometimes, often and very often) by the intensity (from 1 to 3: mild, moderate and severe). Each NPI domain score may thus vary from 0 to 12. Based on a study by Aalten et al. [2007], we considered the following four subsyndromes: apathy, hyperactivity (the sum of agitation, disinhibition, irritability, euphoria, and aberrant motor behavior scores), psychosis (delusions, hallucinations, and night-time behavior disturbances) and affective syndrome (depression and anxiety). We also applied the CDR using a semistructured interview and Pfeffer's daily-life activities questionnaire.

Data analysis was performed using Systat software 12.0. Student's *t*-tests were performed for intergroup comparisons of the demographic and cognitive scores. On occasions where the data violated the assumptions of parametric tests, we performed the Mann Whitney test. The results were considered to be statistically significant when  $P < 0.05$ .

---

**Magnetic Resonance Image Acquisition**

Structural and functional images were acquired on a 3T MRI scanner (Philips Achieva, Best, The Netherlands). A set of structural images was composed with the following sequences: (a) sagittal high-resolution  $T_1$ -weighted with gradient echo images that were acquired with TR/TE = 7/3.2 ms, FOV =  $240 \times 240$ , and isotropic voxels of  $1 \text{ mm}^3$ ; (b) coronal and axial FLAIR (fluid-attenuated inversion recovery)  $T_2$ -weighted images, anatomically aligned at the hippocampus with image parameters set to TR/TE/TI = 12,000/140/2,850 ms, FOV =  $220 \times 206$ , voxels reconstructed to  $0.45 \times 0.45 \times 4.00 \text{ mm}^3$  with the gap between slices set to 1 mm; (c) coronal IR (inversion recovery)  $T_1$ -weighted images with TR/TE/TI = 3,550/15/400 ms, FOV =  $180 \times 180$  and voxels reconstructed to  $0.42 \times 0.42 \times 3.00 \text{ mm}^3$ ; (d) coronal multiecho (five echos)  $T_2$ -weighted images with TR/TE = 3,300/30 ms, FOV =  $180 \times 180$ , voxels reconstructed to  $0.42 \times 0.42 \times 3.00 \text{ mm}^3$ .

Functional images were acquired during rest. Subjects were instructed to keep their eyes closed and to not think of anything in particular. Axial  $T_2^*$ -weighted images had TR/TE = 2,000/30 ms, FOV =  $240 \times 240$ , 40 axial slices per volume, and isotropic voxels set to  $3 \times 3 \times 3 \text{ mm}^3$ . For each participant, we acquired 10-min of echo planar images (300 volumes) and discarded the first three volumes.

The participants' sensory stimulation was limited to the noise of the scanner during image acquisitions. To reduce noise, all subjects wore earplugs. In addition, all subjects had their head movements restricted by a soft Velcro strap.

**Structural Imaging Analysis**

To exclude the influence of structural abnormalities, we evaluated gray matter (GM) density through voxel-based morphometry (VBM) analysis. VBM is a technique that allows the assessment of the volume or concentration of gray and white matter across the whole brain through an automated postprocessing MRI evaluation [Ashburner and Friston, 2000]. The voxelwise approach does not require prior information about GM [Good et al., 2001]. We carried out VBM analysis on 3D, sagittal  $T_1$ -weighted images, with a thickness of 1 mm (TR/TE = 22/9 ms, flip angle =  $35^\circ$ , matrix =  $256 \times 220$ ) using the FSL toolbox (<http://www.fmrib.ox.ac.uk/fsl/>) [Smith et al., 2004]. Images were skull stripped using the BET algorithm [Smith, 2002] and GM was automatically segmented using the FAST4 algorithm [Zhang et al., 2001]. GM maps were then normalized to MNI standard space with affine registration [Jenkinson et al., 2002; Jenkinson and Smith, 2001]. Registered images were divided by the Jacobian of the warp field in order to correct local deformation. Resulting images were smoothed with an 8-mm FWHM isotropic Gaussian kernel. Smoothed GM images were then used in subsequent analysis.

**Functional Imaging Analysis**

Functional images were converted from DICOM to the NIfTI format using Philips scanner software. Images were preprocessed by removing linear trends before slice timing and motion correction algorithms were applied. The motion correction step took the first volume of the time series as its reference and output six parameters of head movement, three related to head translation and three associated to the head rotation (yaw, pitch, and roll). Subsequently, images were normalized to MNI standard space and smoothed with a 6 mm FWHM Gaussian kernel. We applied Fourier filters on smoothed images, setting a bandpass from 0.01 to 0.1 Hz, and regressed these data with the motion parameters previously calculated. All of these steps were done with the AFNI software package (<http://afni.nimh.nih.gov/>). Subsequently, probabilistic independent component (IC) analysis (pICA) [Beckmann and Smith, 2004; Guo, 2011] was estimated in order to extract independent spatial maps (IC) for each subject. ICs were obtained with the FSL toolbox, Multivariate Exploratory Linear Optimized Decomposition into Independent Components (MELODIC v3.0). We allowed the MELODIC algorithm to determine as many ICs as was necessary to explain 99% of the variability of preprocessed data (default option).

The set of ICs components was masked with the atlas of functional ROIs (fROI) available on the Stanford's Functional Imaging in Neuropsychiatric Disorders website (<http://findlab.stanford.edu/index.html>) [Shirer et al., 2012]. We used the "ventral and dorsal DMN" (vDMN and dDMN) and the "anterior and posterior SN" (aSN and pSN) to extract z-values of ICs within and outside of the fROIs. To do this, we used a linear template-matching procedure that involves taking the average z-score of voxels falling within the template minus the average z-score of voxels outside the template and selecting the component in which this difference (the goodness-of-fit) was the greatest. The z-scores here reflect the degree to which a given voxel's time series correlates with the overall component time series, scaled by the standard deviation of the residual Gaussian noise [Greicius et al., 2004]. This procedure was estimated by the following equation:

$$\text{GoF} = (\bar{I} - \bar{O}) \times 100 \times \left( \frac{PN_I}{N_I} - \frac{PN_O}{N_O} \right)$$

$\bar{I}$  = Average z - scores from voxels inside the ROI

$\bar{O}$  = Average z - scores from voxels outside the ROI

$PN_I$  = Number of voxels with positive score inside the ROI

$PN_O$  = Number of voxels with positive score outside the ROI

$N_I$  = Number of voxels inside the ROI

$N_O$  = Number of voxels outside the ROI

Among the set of ICs, we selected the one with the highest value of GOF to use for the second level of analysis

**TABLE I. Demographic, functional, and neuropsychological data**

	AD	Controls	<i>P</i>
Age (years)	73.85 ± 8.19	72.33 ± 6.37	0.43*
Education (years)	6.95 ± 4.45	10.16 ± 5.36	<0.05
CDR-SB	6.72 ± 2.74	0	
Pfeffer Functional Activity Questionnaire	18.45 ± 7.83	0	
MMSE	16.35 ± 6.22	28.55 ± 1.85	<0.0001
RAVLT: COD	18.83 ± 7.53	45.66 ± 8.46	<0.0001
RAVLT: A7	0.55 ± 1.09	8.26 ± 0.61	<0.0001
BNT	29.53 ± 13.80	52.46 ± 4.89	<0.0001
Semantic VF	6.88 ± 3.12	18.00 ± 4.20	<0.0001*
Phonologic VF (FAS)	13.82 ± 9.76	33.46 ± 13.19	<0.0001
VSP-LNI	13.25 ± 3.76	18.13 ± 1.24	<0.0001
FDS	3.82 ± 1.70	5.40 ± 2.16	0.02*
BDS	2.05 ± 1.81	4.33 ± 1.54	0.002*
TMT-A (s)	225.67 ± 98.66	66.73 ± 20.32	<0.0001
TMT-B (s)	278.73 ± 56.60	123.07 ± 83.34	<0.0001
Stroop test: Congruent (s)	98.52 ± 41.51	58.06 ± 18.69	0.004
Stroop test: Congruent (errors)	0.23 ± 0.75	0.06 ± 0.25	0.62
Stroop test: Incongruent (s)	216.24 ± 59.00	108.20 ± 28.20	0.008
Stroop test: Incongruent (errors)	34.52 ± 23.93	2.53 ± 3.75	<0.0001
Clock drawing test (0-10)	5.53 ± 0.79	9.46 ± 0.35	0.0004
Rey complex figure (copy)	14.00 ± 3.37	34.60 ± 1.19	<0.0001

Data presented as mean ± SD.  
 \*Mann-Whitney test was applied due to non-normal distribution. MMSE, mini-mental status examination; RAVLT-COD, encoding of Rey auditory verbal learning test (sum of A1 + A2 + ... + A5); RAVLT -A7, delayed recall of RAVLT; BNT, Boston naming test; VF, verbal fluency; VSP-LNI, visuospatial perception item of Luria's neuropsychological investigation; FDS, forward digit span; BDS, backward digit span; TMT, Trail Making Test. Significance levels of comparisons between AD and healthy groups are given in the final column.

and to calculate correlations with NPI scores. Thus, one IC was chosen for each fROI (vDMN, dDMN, aSN, and pSN) to enter subsequent analyses.

Differences between controls and patients were estimated by nonparametric permutation tests (RANDOMISE - 5000 permutations) [Nichols and Holmes, 2002]. The *P* values calculated were corrected for multiple comparisons according to the threshold-free cluster enhancement algorithm implemented in FSL [Anderson and Robinson, 2001; Bullmore et al., 1999; Hayasaka and Nichols, 2003]. We included each subject's 3D map of GM in this analysis to correct the results for atrophy on a voxelwise basis.

**Correlations Between NPI and DMN and SN Connectivity**

We used the same nonparametric approach to evaluate the correlation between patients' selected ICs (vDMN, dDMN, aSN, and pSN) and NPI syndromes (apathy, hyperactivity, affective syndrome, and psychosis). Age, dementia severity (as measured by CDR sum of boxes (memory, orientation, judgment, and problem solving, community affairs, home and hobbies, and personal care), and GM maps were entered for nuisance variables. Statistical maps were then corrected for multiple comparisons with *P* < 0.01, FDR corrected.

**RESULTS**

**Cognitive and Neuropsychiatric Evaluations**

As shown in Table I, there was no difference between the AD group and the controls with regard to age (*P* = 0.43), but there was a significant difference in the two groups regarding education (*P* < 0.05). The AD patients performed worse in all tests, which included episodic memory, attention and working memory, visuospatial skills, executive functions, and language (Table I). Distribution of NPI symptoms and subsyndromes are shown in Table II and Figure 1.

**Differences in the DMN and SN in AD Patients and Healthy Elderly**

We found areas of decreased connectivity in the dorsal DMN (atrophy corrected), and in particular in its posterior anatomical structures, when comparing the AD group to the control subjects (*P* < 0.01, corrected for multiple comparisons). These were the right precuneus (MNI

**TABLE II. Neuropsychiatric inventory syndromes and symptoms**

NPI subsyndromes	NPI symptoms	Mean ± SD	% of patients with symptom
Apathy	Apathy	4.25 ± 3.22	90
	Appetite and eating abnormalities	1.70 ± 2.93	35
Hyperactivity	Agitation	1.10 ± 2.75	30
	Disinhibition	0.30 ± 1.34	5
	Irritability	1.2 ± 2.19	40
	Euphoria	0.2 ± 0.89	5
	Aberrant motor behavior	1.45 ± 2.32	35
Affective	Depression	1.55 ± 2.28	35
	Anxiety	0.95 ± 2.25	25
Psychosis	Hallucinations	0.10 ± 0.30	10
	Delusions	0.15 ± 0.48	10
	Night time behavior disturbances	1.20 ± 2.17	30

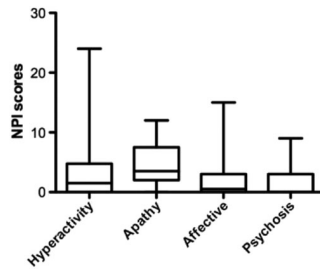


**Figure 1.** Box and whiskers plot showing the distribution of NPI syndromes scores: hyperactivity (mean  $\pm$  SD:  $4.05 \pm 6.18$ ), apathy ( $4.25 \pm 3.22$ ), affective syndrome ( $2.50 \pm 4.28$ ), and psychosis ( $1.45 \pm 2.41$ ). The box extends from the 25th percentile to the 75th percentile, with a horizontal line at the median. Whiskers extend down to the smallest value and up to the largest.

coordinates: 6, -66, 24; 205 voxels;  $z = 4.12$ ) and left precuneus (-2, -64, 54; 160 voxels;  $z = 3.82$ ) (Fig. 2A). The same analysis did not show any areas of increased connectivity in the DMN in AD patients.

The opposite pattern was found in relation to the anterior SN. AD patients showed areas of increased con-

nectivity (atrophy corrected) in the right cingulate gyrus (18, 20, 38; 96 voxels;  $z = 4.42$ ;  $P < 0.01$ , corrected) and left medial frontal gyrus (-8, 32, 38; 79 voxels;  $z = 4.08$ ;  $P < 0.01$ , corrected) (Fig. 2B). We did not find any significant differences between AD and controls in the connectivity of the ventral DMN and posterior SN.

#### Multiple Regressions of NPI Syndromes With DMN and SN

We performed multiple regressions between the dorsal and ventral DMN and anterior and posterior SN maps and the NPI syndromes of apathy, affective symptoms, hyperactivity, and psychosis. We found significant areas of positive correlation with hyperactivity in the anterior SN (atrophy corrected), specifically in the right ACC (MNI: 8, 28, 18; 180 voxels;  $z = 4.82$ ;  $P < 0.01$ , corrected) and right insula (44, 10, -6; 68 voxels;  $z = 4.36$ ;  $P < 0.01$ , corrected) (Fig. 3). All other regressions did not show any significant correlation between dorsal/ventral DMN or anterior/posterior SN with NPI syndromes following correction for multiple comparisons and GM atrophy.

#### DISCUSSION

Using resting-state fMRI in a group of patients with mild to moderate AD and age and sex matched controls, we showed that alterations in the intrinsic connectivity of the anterior SN predict behavioral symptoms in AD

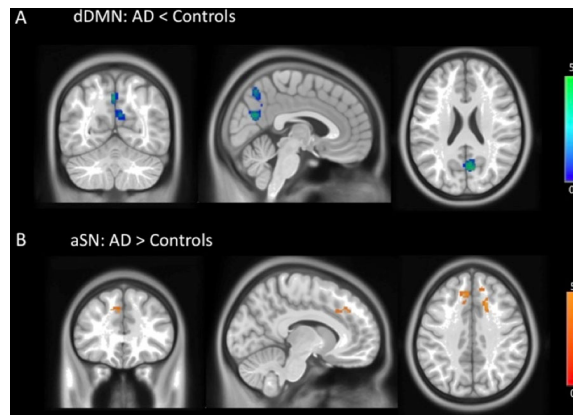


**Figure 2.**

**(A)** Dorsal DMN areas of decreased functional connectivity in AD patients (atrophy corrected): right precuneus (MNI coordinates: 6, -66, 24) and left precuneus (-2, -64, 54);  $P < 0.01$ , corrected for multiple comparisons. **(B)** Anterior SN areas of increased connectivity in AD patients (atrophy corrected): right cingulate gyrus (18, 20, 38) and left medial frontal gyrus (-8, 32, 38);  $P < 0.01$ , corrected.

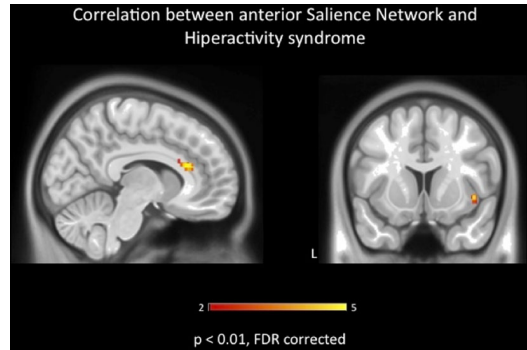


**Figure 3.**

Areas of positive correlations between anterior SN and hyperactivity syndrome (atrophy corrected): right ACC (MNI: 8, 28, 18) and right insula (44, 10, -6);  $P < 0.01$ , corrected for multiple comparisons.

patients. Specifically, we demonstrated that hyperactivity syndrome is associated with aSN hyperconnectivity in the ACC and right insula. This correlation remains even after correction for GM atrophy. No correlations were found between DMN connectivity and NPS, or between SN connectivity and other NPS (apathy, psychosis, and affective syndromes) following correction for atrophy.

To our knowledge, our study is the first to report a correlation between alterations in SN connectivity and a specific NPS in AD. The relevance of the role of functional networks in psychopathology has been increasingly recognized, especially the SN, which is important in the appropriate assignment of saliency to external stimuli or internal mental events. The SN, with the anterior insula as its integral outflow hub, assists target brain regions in the generation of appropriate behavioral responses to salient stimuli [Menon, 2011]. This property of detecting salient events (from the external environment or internally) may be susceptible to dysfunction (ineffective or enhanced detection) leading to inappropriate behaviors. We found that hyperactivity syndrome (composed of symptoms of agitation, disinhibition, irritability, euphoria, and aberrant motor behavior symptoms) is related to enhanced connectivity in SN nodes such as the ACC and right AI. This syndrome, at least in part, could be a manifestation of an anxiety disorder, in which hyperactivity of AI has been consistently implicated [Menon, 2011; Paulus and Stein, 2006].

In accordance to Menon's triple network model, we suggest that in AD patients, enhanced saliency detection might cause misperception of common events as if they were emotionally relevant. This might cause symptoms such as agitation, euphoria, and irritability, which more

directly involve emotional sensations. Furthermore, aberrant motor behavior also seems to involve stereotypical features (e.g., rummaging through drawers, manipulation of buttons, etc.); since the SN also receives information about representations of goals and motor plans (Palaniyappan and Liddle, 2012), this kind of behavior may be associated with dysfunctional representations of complex movements. We also propose that dysfunctional processing of stimuli by a hypoconnected DMN, as occurs in AD patients, might compromise the conscious awareness of the sensation caused by the stimuli. For example, a person who is walking incessantly may be in pain or be thirsty, although they cannot consciously process these sensations properly. Therefore, AD patients seem to have an altered response to a wide array of internal and external stimuli, as well as problems in the conscious awareness of the sensations caused by these stimuli. Considering the entire set of findings, it is possible that an alteration in the balance of functional connectivity networks in SN and DMN will predict the behaviors of hyperactivity observed in our patients.

In this regard, another plausible explanation could be based on a neurobiological account of Freudian constructs. According to Carhart-Harris and Friston [2010], Freud's descriptions of the primary and secondary processes are consistent with self-organized activity in hierarchical cortical systems, where the secondary process entailed by ego functions are associated with the suppressive effect of the DMN on its subcortical nodes and anticorrelated networks, such as the SN with its limbic and paralimbic components (frontoinsula cortices, amygdala). The hyperactivity syndrome of our AD patients could thus be equated with a

primitive, at least partly unconscious, primary process thinking and behavior. Our finding of hypoconnectivity in the dorsal DMN and hyperconnectivity in the SN suggests that there have been a weakening or loss of top-down DMN-associated ego control over limbic activity in those hierarchically lower systems involved with the primary process. In our view, Carhart-Harris and Friston's neurobiological Freudian account and Menon's triple network model complement each other in explaining our findings. Previous authors have found associations between SN connectivity and NP symptoms. For example, Seeley et al. [2007] found a correlation between stressor-associated anticipatory anxiety levels before MRI scanning and ACC connectivity in young subjects without neurologic or psychiatric diseases. In AD patients, Zhou et al. [2010] also found increased SN connectivity in the ACC, and suggested that this finding may be related to behavioral symptoms involving emotional sensations such as irritability and anxiety. In addition, a number of authors have suggested that the SN may also be involved in other psychiatric diseases, such as schizophrenia, especially those with the major features of psychosis [Palaniyappan and Liddle, 2011].

Regarding the neurobiology of hyperactivity syndrome, there are few studies about the neural correlates of agitation, irritability, and aberrant motor behavior in AD. Tekin et al. [2001] demonstrated that neurofibrillary tangles in the ACC were related to agitation in AD patients, while in a SPECT study, Rolland et al. [2005] found a correlation between wandering behavior and left parietotemporal hypoperfusion. However, Bruen et al. [2008], who found a correlation between agitation scores and low GM density in bilateral ACC, noted that neuropathological evidence did not coincide with the appearance of the symptom. It is possible that hyperconnectivity in the ACC of AD patients (and hyperactivity syndrome) may precede the pathological findings described by these authors. Moreover, they did not find a correlation with other symptoms of hyperactivity syndrome. More work to support this hypothesis is required, however.

Regarding the relevance of functional connectivity disruptions in AD, some authors speculate that DMN problems may precede beta-amyloid pathology. This hypothesis is supported by recent studies which have demonstrated that disconnection precedes atrophy in the PCC [Gili et al., 2011] and that asymptomatic carriers of APOE4 have a reduction in PCC connectivity, along with increased SN connectivity [Machulda et al., 2011]. Another possibility is that typical AD pathology may disrupt functional networks, with atrophy in some key DMN components, secondary to classic AD pathology, potentially initiating connectivity alterations in the whole network. Should this be the case, atrophy in the hippocampi may have led to a decrease in connectivity in the PCC; for example, studies using diffusion tensor imaging in patients with medial temporal lobe epilepsy with hippocampal sclerosis showed dysfunctions in the uncinate and

arcuate fasciculus, involving frontal and posterior parietal regions in addition to the corpus callosum and cingulum [Thivard et al., 2005]. Following this model, it is possible that a decrease in DMN connectivity may cause an increase in other networks, including the SN. This is supported by a number of studies that have shown a negative correlation between the SN and DMN [Greicius and Krasnow, 2003; Fox et al., 2005; Zhou et al., 2010], with our study providing additional evidence. This correlation between DMN and SN activity has led some authors to suggest that they are functionally related, proposing that the SN plays a role in switching brain states from the internally guided DMN to an external task-related activity mode [Sridharan et al., 2008; Palaniyappan and Liddle, 2011].

Our study has some limitations. First, we studied a relatively small cohort, although our findings were robust to a wide range of potential confounds and to multiple comparison correction, suggesting a reasonable degree of power. Second, it would be better to assess NPS symptoms during MRI scanning rather than through indirect methods; however, in most cases, we performed the NPI interview on the same day as the scan procedure, which could minimize this problem. Finally, future studies could test the validity of the method used here for evaluating clinical responses to pharmacological and nonpharmacological treatments of NP syndromes in AD and other forms of dementia.

## CONCLUSIONS

Our findings demonstrate a correlation between hyperactivity syndrome and alterations in the connectivity of the SN in areas without anatomic atrophy. These results underline the potential clinical significance of resting state alterations in future diagnosis and therapy. However, these findings do not explain the whole phenomenon of NPS symptoms in AD—several other well-established causes, including structural, genetic, biochemical, and environmental factors, are also related to these complex mental dysfunctions and may influence intrinsic connectivity patterns.

## REFERENCES

- Aalten P, Verhey FR, Boziki M, Bullock R, Byrne EJ, Camus V, Caputo M, Collins D, De Deyn PP, Elina K, Frisoni G, Girtler N, Holmes C, Hurt C, Marriott A, Mecocci P, Nobili F, Ousset PJ, Reynish E, Salmon E, Tsolaki M, Vellas B, Robert PH (2007): Neuropsychiatric syndromes in dementia. Results from the European Alzheimer Disease Consortium: Part I. *Dement Geriatr Cogn Disord* 24:457–463.
- Anderson MJ, Robinson J (2001): Permutation tests for linear models. *Aust NZ J Stat* 43:75–78.
- Ashburner J, Friston KJ (2000): Voxel-based morphometry—The methods. *Neuroimage* 11(6 Pt 1):805–821.
- Beckmann CF, Smith SM (2004): Probabilistic independent component analysis for functional magnetic resonance imaging. *IEEE Trans Med Imaging* 23:137–152.

- Brucki SM, Nitrini R, Caramelli P, Bertolucci PH, Okamoto IH (2003): [Suggestions for utilization of the mini-mental state examination in Brazil]. *Arq Neuropsiquiatr* 61:777-781.
- Bruen PD, McGeown WJ, Shanks MF, Venneri A (2008): Neuroanatomical correlates of neuropsychiatric symptoms in Alzheimer's disease. *Brain* 131(Pt 9):2455-2463.
- Buckner RL, Andrews-Hanna JR, Schacter DL (2008): The brain's default network: Anatomy, function, and relevance to disease. *Ann NY Acad Sci* 1124:1-1138.
- Bullmore ET, Suckling J, Overmeyer S, Rabe-Hesketh S, Taylor E, Brammer MJ (1999): Global, voxel, and cluster tests, by theory and permutation, for a difference between two groups of structural MR images of the brain. *IEEE Trans Med Imaging* 18:32-42.
- Carhart-Harris RL, Friston KJ (2010): The default-mode, ego-functions and free-energy: A neurobiological account of Freudian ideas. *Brain* 133:1265-1283.
- Celone KA, Calhoun VD, Dickerson BC, Atri A, Chua EF, Miller SL, DePeau K, Rentz DM, Selkoe DJ, Blacker D, Albert MS, Sperling RA (2006): Alterations in memory networks in mild cognitive impairment and Alzheimer's disease: An independent component analysis. *J Neurosci* 26:10222-10231.
- Christensen A-L. 1975. Luria's Neuropsychological Investigation, Manual and Test Material, 4th ed. Copenhagen: Munksgaard.
- Cummings JL, Mega M, Gray K, Rosenberg-Thompson S, Carusi DA, Gornbein J (1994): The Neuropsychiatric Inventory: Comprehensive assessment of psychopathology in dementia. *Neurology* 44:2308-2314.
- Cummings JL (2000): Cognitive and behavioral heterogeneity in Alzheimer's disease: Seeking the neurobiological basis. *Neurobiol Aging* 21:845-861.
- Deshpande G, Kerssens C, Sebel PS, Hu X (2010): Altered local coherence in the default mode network due to sevoflurane anesthesia. *Brain Res* 1318:110-121.
- Folstein MF, Folstein SE, McHugh PR (1975): "Mini-mental state". A practical method for grading the cognitive state of patients for the clinician. *J Psychiatr Res* 12:129-138.
- Fox MD, Snyder AZ, Vincent JL, Corbetta M, Van Essen DC, Raichle ME (2005): The human brain is intrinsically organized into dynamic, anticorrelated functional networks. *Proc Natl Acad Sci USA* 102:9673-9678.
- Fox MD, Raichle ME (2007): Spontaneous fluctuations in brain activity observed with functional magnetic resonance imaging. *Nat Rev Neurosci* 8:700-711.
- Gauthier S, Wirth Y, Mobius HJ (2005): Effects of memantine on behavioural symptoms in Alzheimer's disease patients: An analysis of the Neuropsychiatric Inventory (NPI) data of two randomised, controlled studies. *Int J Geriatr Psychiatry* 20:459-464.
- Gauthier S, Cummings J, Ballard C, Brodaty H, Grossberg G, Robert P, Lyketsos C (2010): Management of behavioral problems in Alzheimer's disease. *Int Psychogeriatr* 22:346-372.
- Gili T, Cercignani M, Serra L, Perri R, Giove F, Maraviglia B, Caltagirone C, Bozzali M (2011): Regional brain atrophy and functional disconnection across Alzheimer's disease evolution. *J Neurol Neurosurg Psychiatry* 82:58-66.
- Good CD, Johnsrude IS, Ashburner J, Henson RN, Friston KJ, Frackowiak RS (2001): A voxel-based morphometric study of ageing in 465 normal adult human brains. *Neuroimage* 14(1 Pt 1):21-36.
- Greicius MD, Krasnow B, Reiss AL, Menon V (2003): Functional connectivity in the resting brain: A network analysis of the default mode hypothesis. *Proc Natl Acad Sci U S A* 100:253-258.
- Greicius MD, Srivastava G, Reiss AL, Menon V (2004): Default-mode network activity distinguishes Alzheimer's disease from healthy aging: Evidence from functional MRI. *Proc Natl Acad Sci U S A* 101:4637-4642.
- Guo Y (2011): A general probabilistic model for group independent component analysis and its estimation methods. *Biometrics* 67:1532-1542.
- Hayasaka S, Nichols TE (2003): Validating cluster size inference: Random field and permutation methods. *Neuroimage* 20:2343-2356.
- Herrmann N, Rabheru K, Wang J, Binder C (2005): Galantamine treatment of problematic behavior in Alzheimer disease: Post-hoc analysis of pooled data from three large trials. *Am J Geriatr Psychiatry* 13:527-534.
- Jenkinson M, Bannister P, Brady M, Smith S (2002): Improved optimization for the robust and accurate linear registration and motion correction of brain images. *Neuroimage* 17:825-841.
- Jenkinson M, Smith S (2001): A global optimisation method for robust affine registration of brain images. *Med Image Anal* 5:143-156.
- Kaplan EF, Goodglass H, Weintraub S (1983). *The Boston Naming Test*, 2nd ed. Philadelphia: Lea & Febiger.
- Lyketsos CG, Carrillo MC, Ryan JM, Khachaturian AS, Trzepacz P, Amatniek J, Cedarbaum J, Brashear R, Miller DS (2011): Neuropsychiatric symptoms in Alzheimer's disease. *Alzheimer Dement* 7:532-539.
- Machulda MM, Jones DT, Vemuri P, McDade E, Avula R, Przybelski S, Boeve BF, Knopman DS, Petersen RC, Jack CR Jr (2011): Effect of APOE epsilon4 status on intrinsic network connectivity in cognitively normal elderly subjects. *Arch Neurol* 68:1131-1136.
- McKhann G, Drachman D, Folstein M, Katzman R, Price D, Stadlan EM (1984): Clinical diagnosis of Alzheimer's disease: Report of the NINCDS-ADRDA Work Group under the auspices of Department of Health and Human Services Task Force on Alzheimer's Disease. *Neurology* 34:939-944.
- Menon V (2011): Large-scale brain networks and psychopathology: A unifying triple network model. *Trends Cogn Sci* 15:483-506.
- Nichols TE, Holmes AP (2002): Nonparametric permutation tests for functional neuroimaging: A primer with examples. *Hum Brain Mapp* 15:1-25.
- Osterrieth PA (1944): [The test of copying a complex figure: A contribution to the study of perception and memory]. *Arch Psychol* 30:286-356.
- Palaniyappan L, Liddle PF (2012): Does the salience network play a cardinal role in psychosis? An emerging hypothesis of insular dysfunction. *J Psychiatry Neurosci* 37:17-27.
- Paulus MP, Stein MB (2006): An insular view of anxiety. *Biol Psychiatry* 60:383-387.
- Ratcliff G (1979): Spatial thought, mental rotation and the right cerebral hemisphere. *Neuropsychologia* 17:49-54.
- Rey A. 1964. [Clinical examination in psychology]. Paris: Press Universitaire de France.
- Rolland Y, Payoux P, Lauwers-Cances V, Voisin T, Esquerre JP, Vellas B (2005): A SPECT study of wandering behavior in Alzheimer's disease. *Int J Geriatr Psychiatry* 20:816-820.
- Seeley WW, Menon V, Schatzberg AF, Keller J, Glover GH, Kenna H, Reiss AL, Greicius MD (2007): Dissociable intrinsic

- connectivity networks for salience processing and executive control. *J Neurosci* 27:2349–2356.
- Seeley WW, Crawford RK, Zhou J, Miller BL, Greicius MD (2009): Neurodegenerative diseases target large-scale human brain networks. *Neuron* 62:42–52.
- Shirer WR, Ryali S, Rykhlevskaia E, Menon V, Greicius MD (2012): Decoding subject driven cognitive states with whole-brain connectivity patterns. *Cereb Cortex* 22:158–165.
- Smith SM (2002): Fast robust automated brain extraction. *Hum Brain Mapp* 17:143–155.
- Smith SM, Jenkinson M, Woolrich MW, Beckmann CF, Behrens TE, Johansen-Berg H, Bannister PR, De Luca M, Drobnjak I, Flitney DE, Niazy RK, Saunders J, Vickers J, Zhang Y, De Stefano N, Brady JM, Matthews PM (2004): Advances in functional and structural MR image analysis and implementation as FSL. *Neuroimage* 23(Suppl 1):S208–S219.
- Sridharan D, Levitin DJ, Menon V (2008): A critical role for the right fronto-insular cortex in switching between central-executive and default-mode networks. *Proc Natl Acad Sci U S A* 105:12569–12574.
- Tekin S, Mega MS, Masterman DM, Chow T, Garakian J, Vinters HV, Cummings JL (2001): Orbitofrontal and anterior cingulate cortex neurofibrillary tangle burden is associated with agitation in Alzheimer disease. *Ann Neurol* 49:355–361.
- Thivard L, Lehericy S, Krainik A, Adam C, Dormont D, Chiras J, Baulac M, Dupont S (2005): Diffusion tensor imaging in medial temporal lobe epilepsy with hippocampal sclerosis. *Neuroimage* 28:682–690.
- van den Heuvel MP, Hulshoff Pol HE (2010): Exploring the brain network: A review on resting-state fMRI functional connectivity. *Eur Neuropsychopharmacol* 20:519–534.
- Wechsler D (1987). *Manual for the Wechsler Memory Scale-Revised (WMS-R)*. San Antonio: The Psychological Corporation.
- Westlye ET, Lundervold A, Rootwelt H, Lundervold AJ, Westlye LT (2011): Increased hippocampal default mode synchronization during rest in middle-aged and elderly APOE epsilon4 carriers: Relationships with memory performance. *J Neurosci* 31:7775–7783.
- Youn JC, Lee DY, Jhoo JH, Kim KW, Choo IH, Woo JI (2011): Prevalence of neuropsychiatric syndromes in Alzheimer's disease (AD). *Arch Gerontol Geriatr* 52:258–263.
- Zhang HY, Wang SJ, Liu B, Ma ZL, Yang M, Zhang ZJ, Teng GJ (2010): Resting brain connectivity: Changes during the progress of Alzheimer disease. *Radiology* 256:598–606.
- Zhang Y, Brady M, Smith S (2001): Segmentation of brain MR images through a hidden Markov random field model and the expectation-maximization algorithm. *IEEE Trans Med Imaging* 20:45–57.
- Zhou J, Greicius MD, Gennatas ED, Growdon ME, Jang JY, Rabinovici GD, Kramer JH, Weiner M, Miller BL, Seeley WW (2010): Divergent network connectivity changes in behavioural variant frontotemporal dementia and Alzheimer's disease. *Brain* 133(Pt 5):1352–67.

# Experimento 8 – Pasticidade cerebral em codificação de memória verbal e visual de pacientes com epilepsia medial temporal.

◆ Human Brain Mapping 00:000–000 (2011) ◆

## Brain Plasticity for Verbal and Visual Memories in Patients with Mesial Temporal Lobe Epilepsy and Hippocampal Sclerosis: An fMRI Study

Andréa Alessio,<sup>1,2</sup> Fabricio R.S. Pereira,<sup>1</sup> Maurício S. Sercheli,<sup>2</sup>  
Jane M. Rondina,<sup>1,2</sup> Helka B. Ozelo,<sup>1,2</sup> Elisabeth Bilevicius,<sup>1</sup>  
Tatiane Pedro,<sup>1</sup> Roberto J.M. Covolan,<sup>2</sup> Benito P. Damasceno,<sup>1</sup>  
and Fernando Cendes<sup>1\*</sup>

<sup>1</sup>Neuroimaging Laboratory, School of Medical Sciences, University of Campinas, Unicamp, Campinas, Brazil

<sup>2</sup>Neurophysics Group, Gleb Wataghin Physics Institute, University of Campinas, Unicamp, Campinas, Brazil



**Abstract:** We aimed to identify the brain areas involved in verbal and visual memory processing in normal controls and patients with unilateral mesial temporal lobe epilepsy (MTLE) associated with unilateral hippocampal sclerosis (HS) by means of functional magnetic resonance imaging (fMRI). The sample comprised nine normal controls, eight patients with right MTLE, and nine patients with left MTLE. All subjects underwent fMRI with verbal and visual memory paradigms, consisting of encoding and immediate recall of 17 abstract words and 17 abstract drawings. A complex network including parietal, temporal, and frontal cortices seems to be involved in verbal memory encoding and retrieval in normal controls. Although similar areas of activation were identified in both patient groups, the extension of such activations was larger in the left-HS group. Patients with left HS also tended to exhibit more bilateral or right lateralized encoding related activations. This finding suggests a functional reorganization of verbal memory processing areas in these patients due to the failure of left MTL system. As regards visual memory encoding and retrieval, our findings support the hypothesis of a more diffuse and bilateral representation of this cognitive function in the brain. Compared to normal controls, encoding in the left-HS group recruited more widespread cortical areas, which were even more widespread in the right-HS group probably to compensate for their right mesial temporal dysfunction. In contrast, the right-HS group exhibited fewer activated areas during immediate recall than the other two groups, probably related to their greater difficulty in dealing with visual memory content. Hum Brain Mapp 00:000–000, 2011. © 2011 Wiley Periodicals, Inc.

**Key words:** cognitive functions; neuropsychological evaluation; hippocampal atrophy; functional reorganization



Contract grant sponsor: Fundação de Amparo à Pesquisa do Estado de São Paulo—FAPESP; Contract grant number: 05/54908-7.

\*Correspondence to: Fernando Cendes, Department of Neurology, FCM-UNICAMP, Cidade Universitária, Campinas, SP, Brazil, CEP 13083-970. E-mail: fcendes@unicamp.br

Received for publication 18 January 2010; Revised 13 June 2011; Accepted 8 July 2011

DOI: 10.1002/hbm.21432

Published online in Wiley Online Library (wileyonlinelibrary.com).

© 2011 Wiley Periodicals, Inc.

## INTRODUCTION

Neuropsychological evaluation of patients with refractory mesial temporal lobe epilepsy (MTLE) associated with hippocampal atrophy (HA) and other MRI signs of hippocampal sclerosis (HS) usually reveal a mild-to-moderate memory deficit [Engel et al., 1997; French et al., 1993]. According to the classic material-specific model of memory, lesions in the hippocampus of the left temporal lobe (dominant for language) may implicate in verbal memory deficits [Meyer and Yates, 1955; Milner, 1972; Novelly et al., 1984] and those of the right temporal lobe, in visual memory deficits [Jones-Gotman, 1987; Kimura, 1963; Milner et al., 1962]. However, more recent studies in epilepsy surgery have shown that the relationship between lateralized hippocampal pathology and memory dysfunction is more evident in left MTLE than in right MTLE [Alessio et al., 2004a,b; Hermann et al., 1997; Jones-Gotman, 1996; Lencz et al., 1992; Saling et al., 1993; Trenerry et al., 1995]. Evidences have suggested that the most important predictor factor for postoperative memory decline is the functional capacity of the ipsilateral mesial temporal lobe (MTL; hippocampal adequacy model) rather than the functional reserve of the contralateral MTL (hippocampal reserve model) to sustain memory performance [Powell et al., 2007; Rabin et al., 2004]. However, MRI findings associated with neuropsychological data are not always sufficient to determine the risk of language and/or memory impairment following mesial temporal resection. Application of more invasive procedures, such as intracranial monitoring with depth electrodes (SEEG) and intracarotid sodium amytal test (IAT or Wada test), may be considered necessary [Dinner, 1991; Golby et al., 2002; Lineweaver et al., 2006; Rausch and Langfitt, 1991].

Even though considered the gold standard, the IAT has a series of limitations, including its invasiveness, poor spatial resolution, insufficient time for detailed evaluation of language and memory functions and limited ability to distinguish verbal versus visual memory deficits [Dade and Jones-Gotman, 1997; Gotman et al., 1992; Loring et al., 1990; Lukban et al., 1994; Rausch, 2002]. Because of these limitations of IAT, some researchers have aimed to explore alternative methods, such as fMRI [Aldenkamp et al., 2003; Golby et al., 2002; Rausch, 2002].

Although the role of fMRI in the lateralization of hemispheric dominance for language is relatively well-established, such an application has so far not been proved reliable in the lateralization of verbal and visual memories [Jokeit et al., 2001]. fMRI evaluation of memory is more difficult than fMRI evaluation of other cognitive functions due to some neuropsychological and technical issues [Alessio et al., 2004b; Detre et al., 1998; Jones-Gotman, 1996; Powell et al., 2004, 2005; Strange, 2002; Richardson et al., 2003].

Keeping all the above factors in mind, the purposes of this study were: (1) to identify the brain areas involved in verbal and visual memory processing in normal controls

and patients with unilateral MTLE associated with ipsilateral HS, by means of fMRI; and (2) to assess the sensitivity and potential clinical role of memory tests applied during fMRI experiments in lateralizing and localizing verbal and visual memory functions, during two distinct stages of memory processing, namely: encoding and retrieval.

## PATIENTS AND METHODS

### Ascertainment of Subjects

In this study we included patients with diagnosis of refractory MTLE followed at our epilepsy clinic. We also included a control group, which were submitted to the same protocols. All individuals signed a written consent, approved by the ethics committee of UNICAMP Medical School.

The clinical criterion was a history of simple partial and/or complex partial seizures with characteristics of MTL origin, such as: rising epigastric sensation, fear, experiential phenomena, and autonomic signs and symptoms. As a complement of this clinical criterion, no suggestion of any other partial epilepsy syndrome could be present. The EEG criterion was the presence of interictal epileptiform discharges over mid-inferomesial temporal regions and no clear-cut epileptiform abnormalities elsewhere.

The selected 26 individuals were divided into three groups, as follows: control group, composed of nine normal controls with no history of epilepsy or any other neurological and/or psychiatric pathology, and at ages and education level similar to the patient groups; right-HS group, composed of eight patients who fulfilled clinical-EEG criteria for right MTLE and who had right HA and other signs of unilateral right HS on MRI; and finally, left-HS group, composed of nine patients who also had clinical and EEG diagnosis of left MTLE and had left HA and other signs of unilateral left HS on MRI. All patients had normal hippocampal volumes contralateral to the EEG lateralization, determined by MRI volumetric analysis according to a previously defined protocol [Bonilha et al., 2004]. Other MRI signs of HS, including hyperintense T2 signal were evaluated clinically by one of the authors with experience in neuroimaging investigation in epilepsies (F.C.).

### Neuropsychological Evaluation

Both patient groups were submitted to an extensive neuropsychological evaluation, which included: (1) vocabulary and block design subtests of the Wechsler adult intelligence scale-revised (WAIS-R) to estimate IQ; (2) the Edinburgh handedness inventory and dichotic listening test to determine hemispheric dominance for language and, by inference, to lateralize verbal and visual memories; (3) the logical memory and verbal paired associates of the Wechsler memory scale-revised (WMS-R) to investigate verbal

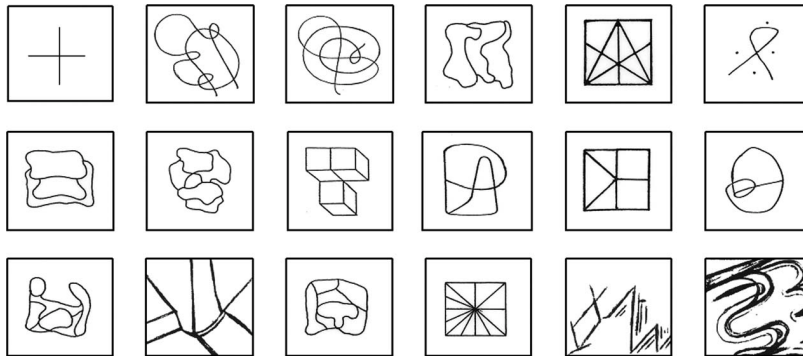


**Figure 1.**  
The cross and the 17 abstract drawings.

memory; and (4) the figural memory, visual reproduction, and visual paired associates of the WMS-R to investigate visual memory. To control other cognitive functions that could somehow influence memory tasks, they were also submitted to tests for language (verbal fluency test and Boston naming test/BNT), and attention [Strub and Black Vigilance Test; Fromm-Auch and Yeudall, 1983; Kaplan et al., 1983; Oldfield, 1971; Spreen and Strauss, 1998; Strub and Black, 1993; Wechsler, 1981, 1987]. These tests were adapted for our population by means of few stimuli substitutions. However, the procedures were kept the same as the originals. The results of each test were compared with results for normal controls matched by age and educational level. We did not use the same fMRI control group for neuropsychological data.

#### Verbal and Visual Memory Tests During fMRI

Verbal memory evaluation during fMRI consisted of encoding and immediate recall of 17 abstract and emotionally neutral words [the equivalent Portuguese translations for HONOR, OPINION, PROBLEM, DUTY, INTEREST, PATIENCE, SOUL, LAW, OPTION, HAZARD, SYMPATHY, PRIDE, DECISION, CRITERIA, SYSTEM, LIFE, METHOD, as proposed by Jones-Gotman et al., 1997] presented in four blocks alternating with a non-word string (ARLTIP) presented in five blocks. Likewise, visual memory evaluation consisted of encoding and immediate recall of 17 abstract drawings presented in four blocks alternating with a fixation point (“+”) presented in five blocks [Damaseno et al., 2005; Jones-Gotman et al., 1997; see Fig. 1].

Individuals were instructed to focus their attention on the non-word/fixation point for 34 s during the baseline

condition, and to try to memorize the 17 words/drawings in 34 s during the experimental condition. At the end of this encoding period, they rested for 120 s and, soon afterward, they attempted to recall silently all words/drawings during 60 s (see Fig. 2). After this immediate recall period, the individuals were requested to try to recognize, by pressing a push-button, the 17 memorized words/drawings among another 17 new abstract words/drawings.

#### fMRI Acquisition and Data Analysis

Before getting into the MR scanner, all subjects received complete instructions about the verbal and visual memory tests they were supposed to perform inside the machine.

Images were acquired in a bottom/up interleaved mode, using a 2T Elscint Prestige (Haifa, Israel) MR scanner with an EPI protocol (TR = 2 s, TE = 45 ms, voxel size =  $3 \times 3 \times 6 \text{ mm}^3$ ). Two hundred and ninety cerebral volumes with 20 slices each were obtained in the run.

The functional images acquired were then (1) reconstructed and temporally reorganized, (2) transformed from DICOM-2D into ANALYSE-3D format by using the MRIcro software, and finally (3) slice timed, realigned, normalized (MNI standard template), smoothed (6 mm/FWHM) and analyzed by using the SPM2 software package (<http://www.fil.ion.ucl.ac.uk/spm/>). The imaging preprocessing was carried out individually for each subject and run, while the data analysis was performed putting together all subjects of the same group (control group, right-HS group and left-HS group).

We attempted to maximize the signal-to-noise ratio before acquiring the EPI images by following a semi-automatic shimming procedure to homogenize the magnetic

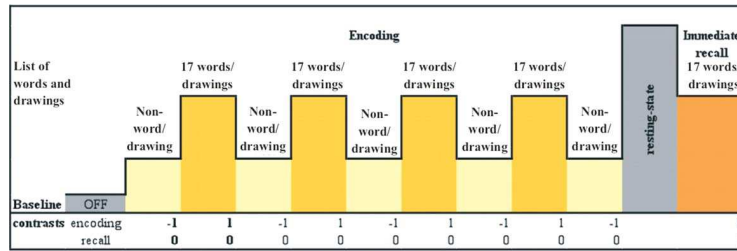


**Figure 2.** Verbal and visual memory paradigms. [Color figure can be viewed in the online issue, which is available at [wileyonlinelibrary.com](http://wileyonlinelibrary.com).]

field strength in the brain region to the sub-ppm level. In order to reduce the chance for ghost artifacts, we have made use of an algorithm proposed by Buonocore and Gao [1997] during the image reconstruction stage.

For data analysis, the following parameters were adopted: gamma function with window length of 32 and order 1, whereas model interaction, parametric modulation, other regressors, removal of global effects, high-pass filter and correction for serial correlations were left aside. Three *T*-test contrasts were created in order to identify cerebral areas related to verbal memory encoding (word blocks—*minus*—nonword blocks) and immediate recall (words recall). The same procedure was adopted for visual memory encoding and immediate recall (see Fig. 2). In other words, the first two contrasts designed were word blocks and nonword blocks and the third one, immediate recall. In order to identify the cerebral areas activated during encoding stage, we assigned the value “1” to the word blocks and the value “-1” to the nonword blocks, while no value was assigned to the baseline condition (OFF). We also assigned the value “0” to the immediate recall block because in doing so it was left aside of this analysis. Then, the program performed not only the subtraction of word blocks—*minus*—nonword blocks but also compared this result to the baseline condition result. Soon afterwards, to identify the cerebral regions activated during immediate recall stage, we assigned the value “1” to the immediate recall block and no value to the baseline condition. Once again, the value “0” was assigned to the word and nonword blocks, which were left aside of this second analysis.

Finally, for the results visualization a threshold of  $P < 0.001$ , uncorrected for multiple comparisons, and clusters of 125/0 voxels were used for the encoding/retrieval phase.

### RESULTS

The three groups had similar age and educational level (Table I). The two patient groups were similar in age of

seizure onset, duration of epilepsy, seizure frequency, and number of antiepileptic drugs used, as well as in the results of the Edinburgh handedness inventory, dichotic listening test, Boston naming test, verbal fluency test, Strub&Black vigilance test, visual memory tests, and fMRI recognition tests. The only difference between them was that patients with left HS had lower IQ ( $F = 9.656$ ;  $P = 0.008$ ) and worse performance on tests of general memory ( $F = 15.387$ ;  $P = 0.002$ ), verbal memory ( $F = 14.510$ ;  $P = 0.002$ ), and delayed recall ( $F = 6.345$ ;  $P = 0.025$ ) than patients with right HS (Table II).

As already mentioned, three contrasts were designed during the SPM2 analysis aiming to visualize the results for encoding [-1 1 0] and immediate recall [0 0 1] stages. The differences between cerebral areas activated during encoding and immediate recall of verbal versus visual memories are shown in Table III.

#### Verbal Memory Test

The data analysis of the encoding stage revealed activations of: (1) bilateral occipital cortices in the three groups; (2) right parietal cortex in control group, and bilateral parietal cortices in right-HS and left-HS groups; (3) left superior temporal cortex in control group, bilateral superior temporal cortices in right-HS group, and right superior temporal cortex in left-HS group; (4) bilateral middle frontal cortices in control and left-HS groups, and left middle frontal cortex in right-HS group (see Fig. 3); and (5) bilateral>left ventro-lateral frontal cortices in right-HS group and bilateral>right ventro-lateral frontal cortices in left-HS group, while there was no such activation in control group (see Fig. 4).

The data analysis of immediate recall showed activations of: (1) left occipital cortex in control and right-HS groups, and bilateral occipital cortices in left-HS group; (2) left parietal cortex in the three groups; (3) right superior temporal cortex in control and left-HS groups, whereas no

TABLE I. Demographic and fMRI data of subjects

Subjects	Age (years)	Education (years)	fMRI verbal memory (correct answers)	fMRI visual memory (correct answers)	Edinburgh handedness inventory
<b>Controls</b>					
1	38	4	7	13	right
2	23	16	17	14	right
3	19	11	12	8	right
4	29	15	10	8	right
5	31	11	10	16	right
6	50	7	12	11	right
7	40	15	17	17	right
8	35	5	12	8	right
9	31	11	16	12	right
<b>Right-HS group</b>					
1	34	11	12	12	right
2	32	11	5	NA	right
3	43	11	13	11	right
4	49	11	14	14	left
5	50	16	14	15	right
6	41	13	15	11	right
7	38	8	12	13	right
8	35	8	17	16	right
<b>Left-HS group</b>					
1	48	15	15	14	right
2	42	4	7	11	right
3	24	11	14	11	right
4	34	11	8	13	right
5	47	8	11	13	left
6	33	11	8	9	right
7	42	7	0	NA	right
8	20	4	15	14	Right
9	31	5	11	12	Right
<i>F</i> and	1.5	1.574	1.402	0.508	0.536
<i>P</i> values	0.244	0.229	0.266	0.609	0.592

NA, not available.

such activation was detected in right-HS group; (4) bilateral>right infero-medial temporal cortices in control group and right infero-medial temporal cortex in right-HS group, and absence of such activation in left-HS group (see Fig. 5); (5) right ventro-lateral frontal cortex in right-HS and left-HS groups, while no such activation was identified in control group (see Fig. 6); and (6) right prefrontal cortex in control and right-HS groups, and bilateral prefrontal cortices in left-HS group.

#### Visual Memory Test

The data analysis of the encoding stage revealed activations of: (1) bilateral occipital and parietal cortices in the three groups, (2) right frontal cortex in control group, and bilateral superior and inferior frontal and prefrontal cortices in right-HS and left-HS groups (see Fig. 7); and (3) bilateral inferior temporal cortices in right-HS group (see Fig. 8), while there was no such activation in control and left-HS groups.

The data analysis of immediate recall showed activations of: (1) bilateral cerebellum in the three groups; (2) right occipital cortex in control group, and left occipital cortex in left-HS and right-HS groups; (3) bilateral parietal cortices in control group, and left parietal cortices in left-HS and right-HS groups; (4) right prefrontal cortex in control group and bilateral prefrontal cortex in left-HS group (see Fig. 9), whereas no such activation was detected in right-HS; (5) bilateral inferior temporal cortices in control group, and right inferior temporal cortex in left-HS and right-HS groups; (6) right mid-temporal cortex in control and left-HS groups, while there was no such activation in right-HS; and (7) bilateral hippocampal cortices in control group (see Fig. 10).

#### DISCUSSION

As already well-established in the literature, neuropsychological evaluation of patients with refractory MTLE

TABLE II. MRI, clinical, and neuropsychological data of patients

Patients	MRI	Side of TL spikes on EEG	Age at seizure onset (years)	Duration of epilepsy (years)	Seizure frequency (P/month)	AEDs	Dichotic listening test	WAIS-R estimated IQ	Boston naming test (z score)	Verbal fluency test (z score)	Vigilance test (errors)	WMS-R general memory (z score)	WMS-R verbal memory (z score)	WMS-R visual memory (z score)	WMS-R delayed recall (z score)
<b>Right-HS group</b>															
1	RHA	right	4	30	20	CBZ; CLN	left	100	0.12	-0.63	0	1.23	1.53	-0.05	1.95
2	RHA	right	8	24	12	CBZ; CLB	NA	97	-4.8	-0.63	0	0.4	0.68	-0.37	-0.24
3	RHA	right	7	36	2	PNT; CLB	left	86	-3.39	-0.19	0	-0.55	-0.54	-0.76	-1.02
4	RHA	right	0	49	14	CBZ; CLB	left	100	-2.13	-0.85	1	0.46	-0.02	1.68	-0.45
5	RHA	right	19	31	2	LMT; CLB	left	115	-0.11	0.02	0	2.38	2.96	0.46	3.16
6	RHA	right	6	34	12	CBZ; CLB	left	100	1.32	0.46	1	0.9	0.77	0.63	0.48
7	RHA	right	4	34	30	CBZ	left	92	-1.11	NA	0	-0.04	0.07	-0.11	-1
8	RHA	right	4	31	4	CBZ; CLB	left	97	-0.58	-0.85	0	1.29	1.07	1.04	1.88
<b>Left-HS group</b>															
1	LHA	left	1	47	2	OXC; CLB	NA	94	-1.26	-0.85	0	-0.76	-1.19	0.78	-0.77
2	LHA	left	20	22	40	CBZ; CLB	left	80	-501	-1.02	1	-0.23	-0.22	-0.24	-1.3
3	LHA	left	2	22	6	CBZ; TPM	left	88	-4.49	-0.85	0	-1.25	-1.12	-0.5	-0.24
4	LHA	left	4	29	1	CBZ; PNT; CLB	left	94	-2.69	-0.19	0	-0.83	-1.55	0.59	-0.65
5	LHA	left	3	44	5	CBZ; CLB	left	89	-1.27	0.46	0	-0.04	-0.22	0.27	-0.03
6	LHA	left	7	26	2	LMT; TPM; CLB	left	89	-1	1.34	0	-0.04	-0.09	0.01	-0.59
7	LHA	left	2	40	4	CBZ; CLB	left	80	-7.97	-1.64	0	-1.83	-2.3	0.01	-1.73
8	LHA	left	2	18	11	CBZ	left	NA	NA	NA	NA	NA	NA	NA	NA
9	LHA	left	4	27	4	CBZ	left	86	-4.45	NA	0	-1.51	-1.12	-1.53	-3.15
<i>F</i> and			0.287	0.482	0.461	0.204		<b>9.656</b>	3.855	0.001	0.368	<b>15.387</b>	<b>14.51</b>	1.061	<b>6.345</b>
<i>P</i> values			0.600	0.498	0.508	0.658		<b>0.008</b>	0.07	0.979	0.554	<b>0.002</b>	<b>0.002</b>	0.32	<b>0.025</b>

TL, temporal lobe; RHA, right hippocampal atrophy; LHA, left hippocampal atrophy; AEDs, antiepileptic drugs; CBZ, carbamazepine; CLB, clobazam; PNT, phenytoin; LMT, lamotrigine; TPM, topiramate; CLN, clonazepam; NA, not available.

◆ Brain Plasticity for Verbal and Visual Memories ◆

**TABLE III. Comparison of verbal and visual memories activation areas**

Activation areas	Encoding of verbal memory									Immediate recall of verbal memory								
	Control group			Right-HS group			Left-HS group			Control group			Right-HS group			Left-HS group		
	R	L	B	R	L	B	R	L	B	R	L	B	R	L	B	R	L	B
Superior temporal cortex		*				*	*	*		*								*
Infero-medial temporal cortex					*				*		*	*						*
Middle frontal cortex				*					*					*	*			
Ventro-lateral frontal cortex						*			*			*		*	*		*	*
Parietal cortex	*					*			*	*			*	*	*		*	*
Occipital cortex				*			*		*	*			*		*			*
	Encoding of visual memory									Immediate recall of visual memory								
Inferior temporal cortex						*			*	*	*	*			*			*
Mid-temporal cortex									*	*		*			*			*
Hippocampal cortex									*	*		*			*			*
Superior and inferior frontal cortex	*					*			*	*	*	*			*			*
Prefrontal cortex	*					*			*	*	*	*			*			*
Parietal cortex				*		*			*	*	*	*		*	*		*	*
Occipital cortex				*		*			*	*	*	*		*	*		*	*
Cerebellum									*	*	*	*		*	*		*	*

R, right; L, left; B, bilateral; \* presence of activation.

associated with HA usually reveals a mild-to-moderate memory deficit [Engel et al., 1997; French et al., 1993]. According to our previous studies [Alessio et al., 2004a,b], patients with refractory MTLE have more memory deficits than those with drug-responsive MTLE, regardless of the presence and degree of HA on MRI. On the other hand, individuals with HA on MRI exhibit more memory impairment than individuals with normal MRI, regardless of the presence and frequency of seizures. However, the

interaction of refractory seizures and HA is related to the worst memory performance [Alessio et al., 2004a,b].

**Verbal Memory**

A matter of less agreement in the literature concerns the classic material-specific model of memory. More recent studies in epilepsy surgery have shown that the

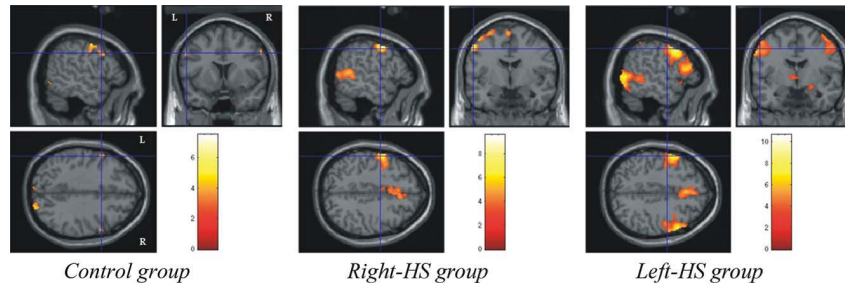


**Figure 3.** Encoding activations of bilateral middle frontal cortices in control and Left-HS groups, and left middle frontal cortex in Right-HS group.

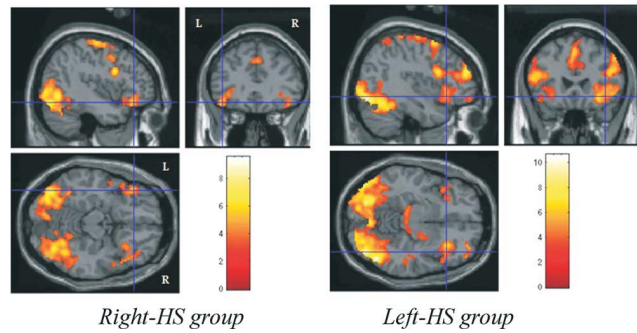


**Figure 4.**

Encoding activations of bilateral > left ventro-lateral frontal cortices in Right-HS group and bilateral > right ventro-lateral frontal cortices in Left-HS group.

relationship between lateralized hippocampal pathology and memory dysfunction is more evident in left MTL for verbal memory deficits than in right MTL for visual memory [Alessio et al., 2004a,b]. However, it is not well established what kind of verbal memory process (encoding, consolidation, or retrieval) is related to which cortical brain regions in these patients, and this issue is particularly important when selecting candidates for resection of mesial temporal lobe structures.

Hence, one of the purposes of this study was to identify and compare the cerebral areas involved in verbal memory processing in normal controls and in patients with refrac-

tory MTL by means of fMRI. More specifically, we tried to localize and lateralize verbal memory function, during two distinct stages of memory processing: encoding and retrieval.

The first important result of this study is the fact that the two patient groups were similar as regards several variables which can influence verbal memory performance, such as age of seizure onset, duration of epilepsy, seizure frequency, and number of antiepileptic drugs used, as well as vigilance, language and visual memory functions. Nevertheless, patients with left HS had worse performance on verbal memory, general memory and delayed recall

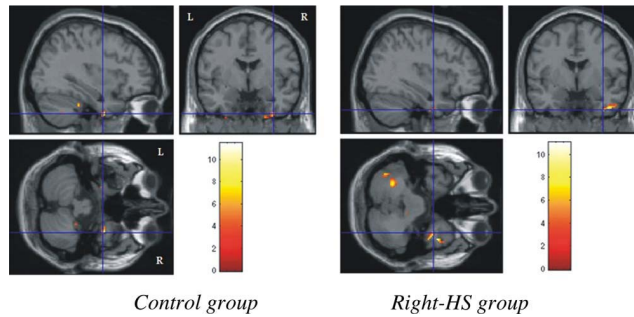


**Figure 5.**

Immediate recall activations of bilateral > right infero-medial temporal cortices in control group and right infero-medial temporal cortex in Right HS group.

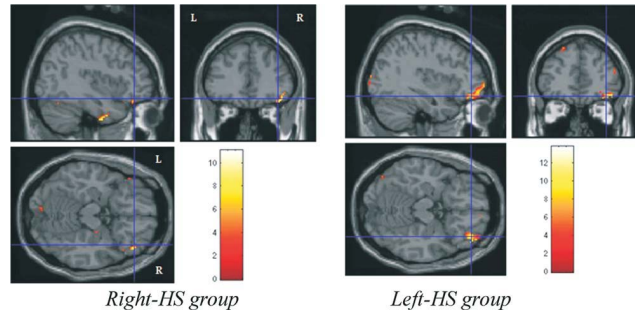


**Figure 6.**

Immediate recall activations of right ventro lateral frontal cortex in Right HS and left HS groups.

than patients with right HS. Moreover, they also had lower IQ, which may have contributed to their inferior memory performance.

In addition, although the three groups were similar in age, educational level, handedness, and hemispheric dominance for language, they exhibited different patterns of activations not only in the encoding stage, but also in the retrieval stage of verbal memory processing.

With regard to the encoding stage, patients with left HS showed more widespread areas of activations than patients with right HS, and even more than normal controls. Although this pattern had been observed in the occipital (Brodmann areas [BA]: 17/18), parietal (BA: 7) and temporal regions (BA: 21/22), it seemed to be mostly remarkable in the middle and ventro-lateral frontal regions

(BA: 6/8 and 44/45, respectively). These findings are in accordance with previous fMRI studies that have demonstrated a larger involvement of frontal cerebral areas in verbal memory processing in patients with left MTLE [Dupont et al., 2000; Golby et al., 2001].

Patients with left HS also tended to exhibit more bilateral or right lateralized encoding related activations (Figs. 3 and 4). This functional reorganization and, consequently, cortical reallocation of verbal memory encoding in more widespread bilateral fronto-parietal, and right temporal areas in patients with left MTLE may indicate a compensatory strategy for the dysfunction of left MTL system [Dupont et al., 2000]. A less evident functional reorganization of verbal memory encoding was also detected in the bilateral parietal, bilateral > left ventro-lateral frontal, left

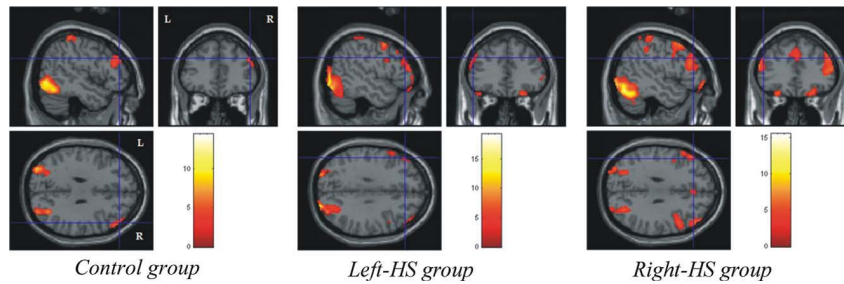
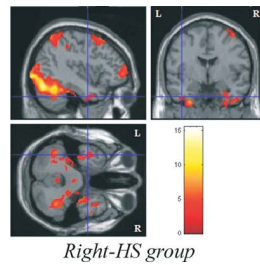


**Figure 7.**

Encoding activations of right frontal cortex in control group, and bilateral superior and inferior frontal and prefrontal cortices in Right HS and left HS groups.



*Right-HS group*

**Figure 8.**

Encoding activations of bilateral inferior temporal cortices in Right HS group.

middle frontal, and bilateral superior temporal cortices in patients with right HS, as compared to normal controls. We could also hypothesize that this functional rearrangement can be secondary to the failure of right MTL system.

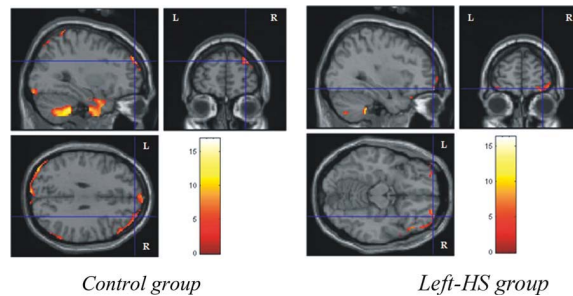
Another interpretation of our regional activation data during verbal encoding is that the block designed visual presentation of the abstracts words could also activate the semantic working memory processing of these words, whose meanings (concepts) are accessed almost automatically. Indeed, a “semantic working memory system” responsible for retrieving, maintaining, monitoring and manipulating semantic representations and composed particularly by the left anterior-inferior prefrontal cortex and the polar region of the left temporal lobe, has been proposed by Gabrieli et al. [1998], Wagner [1999], and Martin and Chao [2001]. Additional evidence for the relevance of the left lateral prefrontal cortex for semantic processing of

abstract words has been yielded afterward by other authors [Fiebach and Friederici, 2004; Goldberg et al., 2007]. In an event-related fMRI study of normal readers Fiebach and Friederici [2004] found that different semantic classes of nouns are processed in distinct cortical regions within the left hemisphere, with concrete nouns activating preferentially the left basal temporal cortex, and abstract nouns the left inferior frontal cortex. In patients with left MTL and HS, on the contrary, similar studies have shown a shift of activations to homologous regions in the right hemisphere during the processing of abstract words as compared to concrete words and non-words [Edwards et al., 2005; Koylu et al., 2006]. Our group of left MTL and HS patients showed similar shifted distribution of activations: right temporal, right or bilateral inferolateral frontal, bilateral middle frontal and bilateral parietal. Thus, this widespread contralateral and ipsilateral cortical activation may be interpreted as resulting not only from the episodic encoding but also from the semantic working memory processing of the words presented.

With respect to the retrieval stage, patients with MTL associated with left HS continued to show more widespread areas of activations than patients with right HS and normal controls. Once more, this pattern was more evident in the frontal region. However, it is important to emphasize that the activation areas observed in the retrieval stage were smaller than those detected in the encoding stage in the three groups.

In the retrieval period, as opposed to the encoding stage, not only patients with left HS, but also patients with right HS and normal controls tended to exhibit more bilateral and right-sided activations (Figs. 5 and 6).

This prevalence of right hemisphere activations during the retrieval stage is in agreement with the hemispheric encoding/retrieval asymmetry (HERA) model, which predicts prefrontal activation during encoding of new



*Control group*

*Left-HS group*

**Figure 9.**

Immediate recall activations of right prefrontal cortex in control group and bilateral prefrontal cortices left HS group.

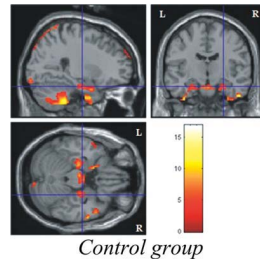


**Figure 10.**  
Immediate recall activations of bilateral hippocampal cortices in control group.

information mainly in the left hemisphere, whereas retrieval of previously learned information is accompanied by increased activity in right prefrontal areas [Dupont et al., 2000; Kapur et al., 1994; Kennepohl et al., 2007; Powell et al., 2004; Tulving et al., 1994]. Although it concerns only to the material-independent lateralization of certain memory tasks in frontal lobes, some authors have recommended that it be extended to temporal lobe regions [Kennepohl et al., 2007]. During retrieval, our group of left MTLE patients showed bilateral prefrontal activation with right frontal ventrolateral predominance, which indicates a reduction of the functional hemispheric asymmetry in this task, similarly to that observed with normal aging (the so called HAROLD, Hemispheric Asymmetry Reduction in Older adults), [Cabeza, 2002]. In patients with left MTLE, the increased (bilateral) prefrontal activation not only may be compensatory, but also may represent a decrease in the level of functional differentiation of the task-relevant neural systems, as proposed by Chen et al. [2002] for the HAROLD model. It remains unexplained why our group of patients with right MTLE presented ipsilateral activation (right prefrontal, frontal ventrolateral, and temporal inferomedial), thus preserving the prevalence of right hemisphere activations during retrieval. It is possible that their long epilepsy duration with early development of right HS has led to intrahemispheric reorganization of cognitive functions.

### Visual Memory

Our previous studies did not show a significant correlation between the degrees of right HA and visual memory deficits in patients with right MTLE [Alessio et al., 2004a,b, 2006; Bonilha et al., 2007]. Two hypotheses have been raised to explain this lack of correlation: (1) the visual memory may have a more diffuse and bilateral representation in the brain [Helmstaedter and Kurthen, 2001;

Jones-Gotman, 1996], and/or (2) the visual memory tests employed may not be robust enough to identify nondominant hippocampal dysfunction [Jones-Gotman, 1996]. We believe in a combination of these two hypotheses, because: (1) we found visual memory deficits in MTLE patients with bilateral HA and rarely in those with right unilateral HA, and (2) we observed that some patients made use of verbal strategies in order to memorize a visual content [Alessio et al., 2004a].

Hence, another purpose of this study was to identify and compare the cerebral areas involved in visual memory processing in normal controls and patients with refractory MTLE by means of fMRI.

With regard to the encoding stage, patients with right MTLE showed more widespread and bilateral areas of activations than patients with left MTLE, and even more than normal controls. Moreover, while normal controls tended to exhibit asymmetrical (bilateral > right) activated regions, patients with right HS tended to show more symmetrical and bilateral activated regions probably to compensate for the failure of their right MTL system (Figs. 7 and 8).

These findings are in agreement with the hypothesis of a more diffuse and bilateral representation of visual memory in the brain. Not only MTL structures, but also temporoparietal and prefrontal areas seem to be involved with the functional neuroanatomy of visual memory, as follows: (1) posterior parietal cortex provides a bridge from perception to recognition, it is related to attention and spatial awareness, and it takes part in spatial memory; and (2) dorsolateral prefrontal cortex is associated with attention, working memory and executive functions that are also critical for memory processes [Burgess et al., 2001; Desgranges et al., 1998].

However, in contrast to some authors [Detre et al., 1998; Stern et al., 1996; Szafarski et al., 2004] who have found bilateral-symmetrical hippocampal activation in normal controls and bilateral-asymmetrical hippocampal activation in MTLE patients, we did not find hippocampal activations in the three groups during encoding stage of a visual content. This discrepancy could be explained by (1) differences in the fMRI task design; and/or (2) lack of MTL activation in our study owing to those technical limitations mentioned before, such as geometric distortions, signal loss artifacts, and partial volume effects [Figueiredo et al., 2008; Powell et al., 2004, 2005, 2007]. For different reasons some other functional studies have also failed to demonstrate hippocampal activation either during encoding or retrieval stages [Cabeza and Nyberg, 2000; Schacter and Wagner, 1999].

With respect to the retrieval stage, the activation patterns found in the three groups were exactly the opposite of those detected in the encoding stage. Compared to patients with right MTLE, left MTLE patients retrieval produced more diffuse activation, which was even more diffuse in normal controls (Figs. 9 and 10). It is important to note that in the retrieval stage we were able to detect

bilateral symmetrical hippocampal activation in the control group [Jokeit et al., 2001]. Again, not only MTL structures but also temporal, parietal and prefrontal areas seem to be involved in visual memory processing [Burgess et al., 2001; Engelsens et al., 2006; Fletcher, 1995; Ungerleider et al., 1998].

In addition, patients with right-HS tended to exhibit more left-sided activated areas during retrieval as opposed to patients with left-HS and normal controls, which tended to show more bilateral and right-sided activations. This prevalence of right hemisphere activations during the retrieval stage in normal controls is in agreement with the hemispheric encoding/retrieval asymmetry (HERA) model. Patients with right MTLE, on the contrary, tended to show more left-sided activated areas probably to compensate for the failure of their right MTL system.

### Limitations

As already mentioned, fMRI evaluation of memory is more difficult than fMRI evaluation of other cognitive functions, due to some neuropsychological and technical issues [Powell et al., 2004, 2005]. As regards the neuropsychological aspects, we polarized as much as possible the verbal versus the nonverbal (visual) memory contents, by using a list of 17 abstract and emotionally neutral words as opposed to a series of 17 abstract drawings. In spite of this, some of the drawings may have led the patients to use verbal strategies in order to memorize the visual content. In addition, the drawings may have led to a different pattern of activation because they were more complex than the fixation point (“+”) of the baseline condition. In addition, the technical aspects could not be so well controlled, because (1) the fMRI acquisitions were made using EPI sequence, which is particularly susceptible to geometric distortions and signal loss, and (2) the BOLD response is naturally lower in the hippocampal regions. All these problems may have contributed to the relative lack of MTL activations, and their solution requires paradigms with even less verbalizable visual-spatial test material and more complex stimulus than a fixation point, as well as fMRI equipments with higher spatial resolution and greater sensitivity.

However, we believe that the restrictive and rigorous statistical analysis that we performed in the present study make our findings quite reliable.

### CONCLUSION

A complex network including parietal, temporal and frontal cortices seems to be involved in verbal memory encoding and retrieval in normal controls. The extension of such activations was larger in patients with right and left HS, more so in patients with left HS. Whereas normal controls and patients with right HS tended to exhibit more left-sided activated areas, patients with left HS tended to

show more bilateral and right-sided activated regions in the encoding stage. These findings can indicate either a dysfunction or a functional reorganization of verbal memory processing in other cerebral regions, particularly in frontal lobes. In contrast, the three groups presented more right-sided activated areas in the retrieval stage, which is in agreement with the HERA model.

As regards visual memory encoding and retrieval, our findings support the hypothesis of a more diffuse and bilateral representation of this cognitive function in the brain. Compared to normal controls, encoding of visual material in patients with left HS recruited more widespread cortical areas, which were even more widespread in patients with right HS probably to compensate for their right mesial temporal dysfunction. On the other hand, when compared to the right MTLE group, the drawing retrieval task produced more diffuse activation in the left MTLE group and even more diffuse activation in the control group (including also both hippocampi). In spite of their effort in memorizing (encoding) the 17 drawings, patients with right MTLE exhibited fewer activated areas during immediate recall probably related to their greater difficulty in dealing with visual memory content.

### REFERENCES

- Aldenkamp AP, Boon PA, Deblaere K, Achten E, Backes WH, Boon P, Hofman P, Troost J, Vandemaele P, Vermeulen J, Vonck K, Wilmink J (2003): Usefulness of language and memory testing during intracarotid amobarbital testing: Observations from an fMRI study. *Acta Neurol Scand* 108:147–152.
- Alessio A, Kobayashi E, Damasceno BP, Lopes-Cendes I, Cendes F (2004a): Evidence of memory impairment in asymptomatic individuals with hippocampal atrophy. *Epilepsy Behav* 5:981–987.
- Alessio A, Damasceno BP, Camargo CHP, Kobayashi E, Guerreiro CAM, Cendes F (2004b): Differences in memory performance and other clinical characteristics in patients with mesial temporal lobe epilepsy with and without hippocampal atrophy. *Epilepsy Behav* 5:22–27.
- Alessio A, Bonilha L, Rorden C, Kobayashi E, Li ML, Damasceno BP, Cendes F (2006): Memory and language impairments and their relationship to hippocampal and perirhinal cortex damage in patients with medial temporal lobe epilepsy. *Epilepsy Behav* 8:593–600.
- Baxendale SA (1997): The role of the hippocampus in recognition memory. *Neuropsychologia* 35:591–598.
- Baxendale SA, Thompson F, Harkness W, Duncan J (2006): Predicting memory decline following epilepsy surgery: A multivariate approach. *Epilepsia* 47:1887–1894.
- Bonilha L, Kobayashi E, Cendes F, Li LM (2004): Protocol for volumetric segmentation of medial temporal structures using high resolution 3D MRI. *Hum Brain Mapp* 22:145–154.
- Bonilha L, Alessio A, Rorden C, Baylis G, Damasceno BP, Li ML, Cendes F (2007): Extrahippocampal gray matter atrophy and memory impairment in patients with medial temporal lobe epilepsy. *Hum Brain Mapp* 28:1376–1390.
- Bunge SA, Ochsner KN, Desmond JE, Glover GH, Gabrieli JD (2001): Prefrontal regions involved in keeping information in and out of mind. *Brain* 124:2074–2086.

- Buonocore MH, Gao L (1997): Ghost artifact reduction for echo planar imaging using image phase correction. *Magn Reson Med* 38:89-100.
- Burgess N, Maguire EA, Spiers HJ, O'Keefe J (2001): A temporo-parietal and prefrontal network for retrieving the spatial context of lifelike events. *Neuroimage* 14:439-453.
- Cabeza R (2002): Hemispheric asymmetry reduction in older adults: The HAROLD model. *Psychol Aging* 17:85-100.
- Cabeza R, Nyberg L (2000): Imaging cognition II: An empirical review of 275 PET and fMRI studies. *J Cogn Neurosci* 12:1-47.
- Chen J, Myerson J, Hale S (2002): Age-related dedifferentiation of visuospatial abilities. *Neuropsychologia* 40:20-50.
- Dade LA, Jones-Gotman M (1997): Sodium amobarbital memory tests: What do they predict? *Brain Cogn* 33:189-209.
- Damaseno A, Alessio A, Damasceno BP, Li LM, Cendes F (2005): Spatial and emotional memory in patients with temporal lobe epilepsy. *Neurology* 64 (Suppl 1):A359-A360.
- Desgranges B, Baron JC, Eustache F (1998): The functional neuroanatomy of episodic memory: The role of the frontal lobes, the hippocampal formation and other areas. *Neuroimage* 8:198-213.
- Detre JA, Maccotta L, King D, Alsop DC, Glosser G, D'Esposito M, Zarahn E, Aguirre GK, French JA (1998): Functional MRI lateralization of memory in temporal lobe epilepsy. *Neurology* 50:926-932.
- Dinner DS (1991): Intracarotid amobarbital test to define language lateralization. In: Luders H, editor. *Epilepsy Surgery*. New York: Raven Press. pp 503-506.
- Dupont S, Van de Moortele PF, Samson S, Hasboun D, Poline JB, Adam C, Lehericy S, Le Bihan D, Samson Y, Baulac M (2000): Episodic memory in left temporal lobe epilepsy: A functional MRI study. *Brain* 123:1722-1732.
- Edwards J, Bass A, Goodyear B, Federico P (2005): An fMRI study of semantic reorganization in temporal lobe epilepsy. *J Neurol Sci* 238 (Suppl 1):S122.
- Engel J, Willimson PD, Wieser HG (1997): Mesial temporal lobe epilepsy. In: Engel J, Pedley TA, editors. *Epilepsy: A Comprehensive Textbook*. Philadelphia: Lippincott-Raven Publishers. pp 2417-2426.
- Engelsen BA, Gramstad A, Thomsen T, Beneventi H, Erstrand L, Smievoll AI, Lundervold A, Hugdahl K (2006): Frontoparietal activation during delayed visuospatial recall in patients with epilepsy due to hippocampal sclerosis. *Epilepsy Behav* 8:565-574.
- Fiebach CJ, Friederici AD (2004): Processing concrete words: fMRI evidence against a specific right-hemisphere involvement. *Neuropsychologia* 42:62-70.
- Figueiredo P, Santana J, Teixeira J, Cunha C, Machado E, Sales F, Almeida E, Castelo-Branco M (2008): Adaptive visual memory reorganization in the right medial temporal lobe epilepsy. *Epilepsia* 49:1395-1408.
- Fletcher PC, Frith CD, Baker SC, Shallice T, Frackowiak RS, Dolan RJ (1995): The mind's eye—Precuneus activation in memory-related imagery. *Neuroimage* 2:195-200.
- French JA, Willimson PD, Thadani VM, Darcey TM, Mattson RH, Spencer SS, Spencer DD (1993): Characteristics of temporal lobe epilepsy: I results of history and physical examination. *Ann Neurol* 34:774-780.
- Fromm-Auch D, Yeudall LT (1983): Normative data for the Halstead-Reitan neuropsychological tests. *J Clin Neuropsychol* 5:221-238.
- Gabrieli JDE, Poldrack RA, Desmond JE (1998): The role of left prefrontal cortex in language and memory. *Proc Natl Acad Sci USA* 95:906-913.
- Gleissner U, Helmstaedter C, Schramm J, Elger CE (2004): Memory outcome after selective amygdalohippocampectomy in patients with temporal lobe epilepsy: One-year follow up. *Epilepsia* 45:960-962.
- Golby AJ, Poldrack RA, Brewer JB, Spencer D, Desmond JE, Aron AP, Gabrieli JDE (2001): Material-specific lateralization in the medial temporal lobe and prefrontal cortex during memory encoding. *Brain* 124:1841-1854.
- Golby AJ, Poldrack RA, Illes J, Chen D, Desmond JE, Gabrieli JDE (2002): Memory lateralization in medial temporal lobe epilepsy assessed by functional MRI. *Epilepsia* 43:855-863.
- Goldberg RF, Perfetti CA, Fiez JA, Schneider W (2007): Selective retrieval of abstract semantic knowledge in left prefrontal cortex. *J Neurosci* 27:3790-3798.
- Gotman J, Bouwer MS, Jones-Gotman M (1992): Intracranial EEG study of brain structures affected by internal carotid injection of sodium amobarbital. *Neurology* 42:2136-2143.
- Helmstaedter C, Kurthen M (2001): Memory and epilepsy: Characteristics, course, and influence of drugs and surgery. *Curr Opin Neurol* 14:211-216.
- Hermann BP, Connell B, Barr WB, Wyler AR (1995): The utility of the Warrington recognition memory test for temporal lobe epilepsy: Pre and postoperative results. *J Epilepsy* 8:139-145.
- Hermann BP, Seidenberg M, Schoenfeld J, Davies K (1997): Neuropsychological characteristics of the syndrome of mesial temporal lobe epilepsy. *Arch Neurol* 54:369-376.
- Jokeit H, Okujava M, Woermann FG (2001): Memory fMRI lateralizes temporal lobe epilepsy. *Neurology* 57:1786-1793.
- Jones-Gotman M (1987): Commentary: Psychological evaluation: Testing hippocampal function. In: Engel JR, editor. *Surgical Treatment of the Epilepsies*. New York: Raven Press. pp 68-76.
- Jones-Gotman M (1996): Psychological evaluation for epilepsy surgery. In: Shorvon S, Dreifuss F, Fish D, Thomas D, editors. *The Treatment of Epilepsy*. Oxford: Blackwell Science. pp 621-630.
- Jones-Gotman M, Zatorre RJ, Olivier A, Andermann F, Cendes F, Staunton H, McMackin D, Siegel A, Wieser HG (1997): Learning and retention of words and designs following excision from medial or lateral temporal-lobe structures. *Neuropsychologia* 35:963-973.
- Kaplan EF, Goodglass H, Weintaub S (1983): *The Boston Naming Test*. Philadelphia: Lea & Febiger.
- Kapur S, Craik FL, Tulving E, Wilson AA, Houle S, Brown GM (1994): Neuroanatomical correlates of encoding in episodic memory: Levels of processing effect. *Proc Natl Acad Sci USA* 91:2008-2011.
- Kennepohl S, Sziklas V, Garver KE, Wagner DD, Jones-Gotman M (2007): Memory and the temporal lobe: Hemispheric specialization reconsidered. *Neuroimage* 36:969-978.
- Kimura D (1963): Right temporal lobe damage. Perception of unfamiliar stimuli after damage. *Arch Neurol* 8:264-271.
- Koylu B, Trinka E, Ischebeck A, Visani P, Trieb T, Kremser C, Bartha L, Schocke M, Benke T (2006): Neural correlates of verbal semantic memory in patients with temporal lobe epilepsy. *Epilepsy Res* 72:178-191.
- Lenz T, McCarthy G, Bronen RA, Scott TM, Inserni JA, Sass KJ, Novelly RA, Kim JH, Spencer DD (1992): Quantitative magnetic resonance imaging in temporal lobe epilepsy: Relationship to neuropathology and neuropsychological function. *Ann Neurol* 31:629-637.
- Lineweaver TT, Morris HH, Naugle RI, Najm IM, Diehl B, Bingaman W (2006): Evaluating the contributions of state-of-the-art

- assessment techniques to predicting memory outcome after unilateral anterior temporal lobectomy. *Epilepsia* 47:1895–1903.
- Loring DW, Lee GP, Meador KJ, Flanigin HF, Smith JR, Figueroa RE, Martin RC (1990): The intracarotid amobarbital procedure as a predictor of memory failure following unilateral temporal lobectomy. *Neurology* 40:605–610.
- Lukban A, Dean G, Lisbona R, Dubeau F, McMackin D, Evans AC (1994): Anatomical localization of seizure foci using registered SPECT/MRI brain volumes. *Neurology* 44:385.
- Martin A, Chao LL (2001): Semantic memory and the brain: Structure and processes. *Curr Opin Neurobiol* 11:194–201.
- Meyer V, Yates AJ (1955): Intellectual changes following temporal lobectomy for psychomotor epilepsy. *J Neurol Neurosurg Psychiatry* 18:44–52.
- Milner B (1972): Disorders of learning and memory after temporal lobe lesions in man. *Clin Neurosurg* 19:421–446.
- Milner B, Branch C, Rasmussen T (1962): Study of short-term memory after intracarotid injection of sodium amytal. *Trans Am Neurol Assoc* 87:224–226.
- Novelly R, Augustine EA, Mattson RH, Glaser GH, Williamson PD, Spencer DD, Spencer SS (1984): Selective memory improvement and impairment in temporal lobectomy for epilepsy. *Ann Neurol* 15:64–67.
- Oldfield RC (1971): The assessment and analysis of handedness: The Edinburgh inventory. *Neuropsychologia* 9:97–113.
- Powell HW, Koeppe MJ, Richardson MP, Symms MR, Thompson PJ, Duncan JS (2004): The application of functional MRI of memory in temporal lobe epilepsy: A clinical review. *Epilepsia* 45:855–863.
- Powell HW, Koeppe MJ, Symms MR, Boulby PA, Salek-Haddadi A, Thompson PJ, Duncan JS, Richardson MP (2005): Material-specific lateralization of memory encoding in the medial temporal lobe: blocked versus event-related design. *Neuroimage* 27:231–239.
- Powell HW, Richardson MP, Symms MR, Boulby PA, Thompson PJ, Duncan JS, Koeppe MJ (2007): Reorganization of verbal and nonverbal memory in temporal lobe epilepsy due to unilateral hippocampal sclerosis. *Epilepsia* 48:1512–1525.
- Rabin ML, Narayan VM, Kimberg DY, Casasanto DJ, Glosser G, Tracy JL, French JA, Sperling MR, Detre JA (2004): Functional MRI predicts post-surgical memory following temporal lobectomy. *Brain* 127:2286–2298.
- Rausch R (2002): Epilepsy surgery within the temporal lobe and its short-term and long-term effects on memory. *Curr Opin Neurol* 15:185–189.
- Rausch R, Langfitt JT (1991): Memory evaluation during the intracarotid sodium amobarbital procedure. In: Luders H, editor. *Epilepsy Surgery*. New York: Raven Press. pp 507–514.
- Richardson MP, Strange BA, Duncan JS, Dolan RJ (2003): Preserved verbal memory function in left medial temporal pathology involves reorganization of function to right medial temporal lobe. *Neuroimage* 20 (Suppl 1):S112–S119.
- Saling MM, Berkovic SF, O'Shea MF, Kalnins RM, Darby DG, Bladin PF (1993): Lateralization of verbal memory and unilateral hippocampal sclerosis. Evidence of task specific effects. *J Clin Exp Neuropsychol* 15:608–618.
- Schacter DL, Wagner AD (1999): Medial temporal lobe activations in fMRI and PET studies of episodic encoding and retrieval. *Hippocampus* 9:7–24.
- Spreen O, Strauss E (1998): Language tests. In: Spreen O, Strauss E, editors. *A Compendium of Neuropsychological Tests: Administration, Norms and Commentary*. New York: Oxford University Press. pp 423–480.
- Stern CE, Corkin S, Gonzalez RG, Guimaraes AR, Baker JR, Jennings PJ, Carr CA, Sugiura RM, Vedantham V, Rosen BR (1996): The hippocampal formation participates in novel picture encoding: Evidence from functional magnetic resonance imaging. *Proc Natl Acad Sci USA* 93:8660–8665.
- Strange BA, Otten LJ, Josephs O, Rugg MD, Dolan RJ (2002): Dissociable human perirhinal, hippocampal, and parahippocampal roles during verbal encoding. *J Neurosci* 22:523–528.
- Strub RL, Black FW (1993): *Mental Status Examination in Neurology*. Philadelphia: FA Davis.
- Szaflarski JP, Holland SK, Schmithorst VJ, Dunn RS, Privitera MD (2004): High-resolution functional MRI at 3T in health and epilepsy subjects: Hippocampal activation with picture encoding task. *Epilepsy Behav* 5:244–252.
- Trener MR, Jack CR Jr, Ivnik RJ, Sharbrough FW, Cascino GD, Hirschorn KA, Marsh WR, Kelly PJ, Meyer FB (1993): MRI hippocampal volumes and memory function before and after temporal lobectomy. *Neurology* 43:1800–1805.
- Trener MR, Westerveld M, Meador KJ (1995): MRI hippocampal volume and neuropsychology in epilepsy surgery. *Magn Reson Imaging* 13:1125–1132.
- Tulving E, Kapur S, Craik FI, Moscovitch M, Houle S (1994): Hemispheric encoding/retrieval asymmetry in episodic memory: Positron emission tomography findings. *Proc Natl Acad Sci USA* 91:2016–2020.
- Ungerleider LG, Courtney SM, Haxby JV (1998): A neural system for human visual working memory. *Proc Natl Acad Sci USA* 95:883–890.
- Wagner AD (1999): Working memory contributions to human learning and remembering. *Neuron* 22:19–22.
- Wechsler D (1981): *Wechsler Adult Intelligence Scale-Revised*. New York: Psychological Corp.
- Wechsler D (1987): *Wechsler Memory Scale-Revised: Manual*. San Diego: Psychological Corp/Harcourt Brace Jovanovich.

BRIEF REPORT

## Partial Reversibility of Hypothalamic Dysfunction and Changes in Brain Activity After Body Mass Reduction in Obese Subjects

Simone van de Sande-Lee,<sup>1</sup> Fabrício R.S. Pereira,<sup>2</sup> Dennys E. Cintra,<sup>1,3</sup> Paula T. Fernandes,<sup>2</sup> Adilson R. Cardoso,<sup>4</sup> Célia R. Garlipp,<sup>5</sup> Eliton A. Chaim,<sup>6</sup> Jose C. Pareja,<sup>6</sup> Bruno Geloneze,<sup>7</sup> Li Min Li,<sup>2</sup> Fernando Cendes,<sup>2</sup> and Lício A. Velloso<sup>1</sup>

**OBJECTIVE**—Inflammation and dysfunction of the hypothalamus are common features of experimental obesity. However, it is unknown whether obesity and massive loss of body mass can modify the immunologic status or the functional activity of the human brain. Therefore, the aim of this study was to determine the effect of body mass reduction on brain functionality.

**RESEARCH DESIGN AND METHODS**—In humans, changes in hypothalamic activity after a meal or glucose intake can be detected by functional magnetic resonance imaging (fMRI). Distinct fMRI analytic methods have been developed to explore changes in the brain's activity in several physiologic and pathologic conditions. We used two analytic methods of fMRI to explore the changes in the brain activity after body mass reduction.

**RESULTS**—Obese patients present distinct functional activity patterns in selected brain regions compared with lean subjects. On massive loss of body mass, after bariatric surgery, increases in the cerebrospinal fluid (CSF) concentrations of interleukin (IL)-10 and IL-6 are accompanied by changes in fMRI patterns, particularly in the hypothalamus.

**CONCLUSIONS**—Massive reduction of body mass promotes a partial reversal of hypothalamic dysfunction and increases anti-inflammatory activity in the CSF. *Diabetes* 60:1699–1704, 2011

Obesity affects more than 300 million people worldwide (1). It is the main risk factor for type 2 diabetes, atherosclerosis, and hypertension, and therefore plays an important role in the overall mortality of modern societies (2). Increased adiposity results from the progressive loss of the homeostatic control of caloric intake and energy expenditure. In animal models, dysfunctional activity of specialized neurons of the hypothalamus is regarded as an important determinant for the development of obesity (3–6). In both genetic and diet-induced obese rodents, the malfunction of the hypothalamus is a consequence of the activation of local inflammation and eventually apoptosis of selected neuronal

populations (3,4,7,8). The inhibition of inflammation by genetic or pharmacologic approaches leads to the reduction of the obese phenotype and correction of the metabolic breakdown, placing hypothalamic inflammation as a potential target for the treatment of obesity (3,4,8–10).

We show that obese patients present distinct functional activity patterns in selected brain regions, compared with lean subjects. On massive loss of body mass, increases in the cerebrospinal fluid (CSF) concentrations of interleukin (IL)-10 and IL-6 are accompanied by changes in functional magnetic resonance imaging (fMRI) patterns, particularly in the hypothalamus.

### RESEARCH DESIGN AND METHODS

Thirteen obese patients (11 females) were recruited from the Obesity Clinic at the University of Campinas. All patients were selected for bariatric surgery according to the National Institutes of Health Consensus Statement (11). The surgical technique used was always the Roux-in-Y gastric bypass (12). Patients were submitted to fMRI plus blood and CSF collection at the time of the surgery and after reduction of body mass. Inclusion criteria for patient selection were men and women between 18 and 60 years of age who met the above-mentioned criteria for surgery. Exclusion criteria for patient selection were diabetes, inflammatory or infectious disease, use of psychotropic or anti-inflammatory drugs, and history of substance addiction. In addition, eight lean control subjects were selected among students of the university. Control subjects were submitted to blood collection and fMRI. Control CSF was obtained from patients referred to the university for headache. Criteria for selection of both control groups were the same used for patients, except for a BMI <25. The fMRI studies were performed on a 1.5 GE MRI scanner (GE Healthcare, Waukesha, WI) in 12-h fasting subjects. The method for image acquisition was the same as previously described (13) except that a total of 500 images were acquired in 30 min. D-glucose (50 g) was ingested after 5 min. Leptin, insulin, and adiponectin were determined in sera using ELISA kits from Millipore (Billerica, MA). Tumor necrosis factor- $\alpha$  (TNF- $\alpha$ ), IL-1 $\beta$ , IL-10, and IL-6 were determined in sera and CSF using ultra-sensitive ELISA kits from BD Biosciences (Bedford, MA) and Cayman Chemical (Ann Arbor, MI). Biochemical and cellular parameters in the blood and CSF were determined using automated methods from F. Hoffmann-La Roche (Basel, Switzerland) and Beckman Coulter (Brea, CA). Temporal clustering analysis (TCA) and spatial analysis were performed as described (13). The fMRI analysis was performed as previously described (14,15) except that the seed (virtual label that defines the target area from or toward which connectivity is evaluated) was placed in the hypothalamus. Student *t* test was used for statistical analysis.

### RESULTS

Patients were evaluated at the time of the surgery and 238  $\pm$  11 days later, when body mass was reduced by 29  $\pm$  4% ( $P < 0.05$ ). Although most patients enrolled in the study were women, both male patients presented similar outcomes; therefore, we have no reason to suspect the data shown in this article represent female-specific phenomena. The nutritional habits of the patients were assessed according to the International Collaborative Study of

From the <sup>1</sup>Laboratory of Cell Signaling, University of Campinas, Campinas, Brazil; the <sup>2</sup>Department of Neurology, University of Campinas, Campinas, Brazil; the <sup>3</sup>Faculty of Applied Sciences, University of Campinas, Campinas, Brazil; the <sup>4</sup>Department of Anesthesiology, University of Campinas, Campinas, Brazil; the <sup>5</sup>Department of Clinical Pathology, University of Campinas, Campinas, Brazil; the <sup>6</sup>Department of Surgery, University of Campinas, Campinas, Brazil; and the <sup>7</sup>Laboratory of Investigation in Metabolism and Diabetes, University of Campinas, Campinas, Brazil.

Corresponding author: Lício A. Velloso, laveloso.unicamp@gmail.com.

Received 23 November 2010 and accepted 13 March 2011.

DOI: 10.2337/db10-1614

© 2011 by the American Diabetes Association. Readers may use this article as long as the work is properly cited, the use is educational and not for profit, and the work is not altered. See <http://creativecommons.org/licenses/by-nc-nd/3.0/> for details.

Macro- and Micronutrients and Blood Pressure 24-h dietary recall (16). Total caloric intake decreased from  $5,602 \pm 3,391$  to  $803 \pm 355$  kCal/day ( $P < 0.05$ ), and the consumption of saturated fats decreased from  $33.6 \pm 6.1$  to  $30.3 \pm 11.6\%$  of total caloric intake ( $P < 0.05$ ). Of special interest, the relative consumption of saturated fats by obese patients was greater than that of lean control subjects on enrollment and reduced by 10.5% after surgery, becoming statistically similar to lean subjects. As expected, all the systemic parameters reflecting the metabolic and inflammatory status of the patients improved significantly after massive body mass loss (Table 1), reflecting the known impact of reduction of adiposity and caloric intake on subclinical inflammation and glucose/lipid homeostasis (17).

Body mass loss produced no effect on cellular and biochemical parameters in the CSF (Table 2). Two distinct ultra-sensitive ELISA methods were used to evaluate TNF- $\alpha$  and IL-1 $\beta$  in CSF, but these rendered no detectable levels in all samples evaluated. However, the CSF levels of IL-10 increased in all patients, and the CSF levels of IL-6 increased in all except one patient, leading to statistically significant increases of both these cytokines after body mass loss (Fig. 1A and B). Both IL-6 and IL-10 levels in the CSF were inversely correlated with BMI (Fig. 1C and D), and IL-6 levels in the CSF were inversely correlated with IL-6 in the blood (Fig. 1E). Compared with lean subjects, IL-10 levels in the CSF of obese subjects were similar before surgery ( $15.9 \pm 8.6$  vs.  $18.1 \pm 7.8$  pg/mL for obese and lean subjects, respectively) and significantly higher after body mass loss ( $29.8 \pm 10.4$  pg/mL,  $P < 0.05$ ). Conversely, IL-6 levels in the CSF of obese patients were significantly lower than in lean control subjects before surgery ( $1.6 \pm 1.3$  vs.  $6.4 \pm 5.3$  pg/mL [ $P < 0.05$ ] for obese and lean subjects, respectively), reaching similar levels after body mass loss ( $5.7 \pm 2.8$  pg/mL). In all groups, the CSF levels of IL-10 were similar or higher than the blood levels of this

cytokine, suggesting that, at least in part, IL-10 was produced in the central nervous system (Fig. 1F). No significant differences in blood monocyte counts were detected among obese and lean subjects and in obese patients before and after surgery.

Two distinct analytic methods were used to evaluate the impact of obesity and body mass loss on the activity of the brain: TCA and functional connectivity MRI (fcMRI). TCA allows for the identification of maximal response to a given stimulus in a combination of signal intensity and spatial extent (13), whereas fcMRI defines temporal correlations between remote neurophysiologic events, which are hemodynamic in nature when evaluated by fMRI (14,18).

For TCA, a mathematic model converts a multiple-dimension data space into a relationship between the number of voxels, reaching maximum signal intensity, and the time (13). On a given time frame, the spatial mapping allows for the anatomic localization of the activity. We found that a first peak of activity occurred right after glucose intake (Fig. 2A), as previously reported (13). This peak was similar in lean and obese subjects both before and after surgery (Fig. 2A). After approximately 5 min of the glucose stimulus, lean subjects presented a second peak that was comparable to previously reported data (13). However, obese patients did not present such a peak, either before or after surgery (Fig. 2A). In addition, during the remaining 20 min of analysis, the number of voxels reaching maximum activity became progressively different among the groups. The highest activity was presented by lean subjects, whereas obese subjects before surgery presented the lowest activity and obese subjects after surgery presented intermediate activity (Fig. 2A). Spatial analysis was then performed at three distinct time windows, labeled in yellow in Fig. 2A. In the first window (W1), which included the first peak after glucose intake, maximum activity was detected in the hypothalamus and orbitofrontal cortex in all three conditions (lean subjects,

TABLE 1  
Blood metabolic and inflammatory parameters

	Lean	Obese before surgery	Obese after surgery
	6 females, 2 males	11 females, 2 males	
Age (years)	29.5 $\pm$ 4		
BMI (kg/m <sup>2</sup> )	20.9 $\pm$ 2.4	39.1 $\pm$ 1.9*	28.1 $\pm$ 2.8*§
WC (cm)	72.2 $\pm$ 9.2	110.3 $\pm$ 9.9*	89.7 $\pm$ 8.7*§
HC (cm)	91.3 $\pm$ 7.3	127.0 $\pm$ 5.2*	105.0 $\pm$ 7.5*§
Glucose (mg/dL)	80.6 $\pm$ 3.1	84.3 $\pm$ 6.1	77.9 $\pm$ 7.3
HbA <sub>1c</sub> (%)	4.8 $\pm$ 0.2	5.2 $\pm$ 0.3	5.1 $\pm$ 0.3
Insulin (pmol/L)	25.0 $\pm$ 10.3	68.7 $\pm$ 38.1*	21.5 $\pm$ 10.4§
HOMA-IR	0.7 $\pm$ 0.3	2.1 $\pm$ 1.2*	0.6 $\pm$ 0.2§
Cholesterol (mg/dL)	189 $\pm$ 28	153 $\pm$ 24	141 $\pm$ 16
HDL (mg/dL)	74.5 $\pm$ 25.7	36.9 $\pm$ 5.8*	52.6 $\pm$ 9.1*§
LDL (mg/dL)	99.5 $\pm$ 22.4	97.6 $\pm$ 26.4	73.6 $\pm$ 16.1
Triglycerides (mg/dL)	75.5 $\pm$ 38.9	94.1 $\pm$ 27.1	76.6 $\pm$ 19.9
CRP (mg/dL)	0.13 $\pm$ 0.02	0.91 $\pm$ 0.70*	0.17 $\pm$ 0.02§
ESR (mm/1 h)	14 $\pm$ 12	26 $\pm$ 16*	16 $\pm$ 9§
Adiponectin ( $\mu$ g/mL)	6.9 $\pm$ 1.7	2.7 $\pm$ 1.8*	7.8 $\pm$ 1.6§
Leptin (ng/mL)	21.4 $\pm$ 6.2	36.8 $\pm$ 12.0*	17.0 $\pm$ 13.9§
TNF- $\alpha$ (pg/mL)	5.8 $\pm$ 5.5	25.6 $\pm$ 10.3*	12.4 $\pm$ 9.8§
IL-1 $\beta$ (pg/mL)	2.0 $\pm$ 1.8	42.9 $\pm$ 26.7*	13.6 $\pm$ 4.3*§
IL-6 (pg/mL)	4.1 $\pm$ 4.2	26.3 $\pm$ 10.2*	8.5 $\pm$ 6.4§
IL-10 (pg/mL)	14.0 $\pm$ 10.1	15.6 $\pm$ 16.5	15.8 $\pm$ 5.5

CRP, C-reactive protein; ESR, erythrocyte sedimentation rate; HC, hip circumference; HOMA-IR, homeostasis model assessment of insulin resistance; WC, waist circumference. \* $P < 0.05$  vs. lean. § $P < 0.05$  vs. obese before surgery.

TABLE 2  
Cerebrospinal fluid cellular and biochemical parameters

	Lean	Obese before surgery	Obese after surgery
Glucose (mg/dL)	59.5 ± 9.6	52.9 ± 8.5	48.5 ± 4.4
Protein (mg/dL)	26.3 ± 6.8	26.6 ± 11.1	23.7 ± 6.8
Leukocytes/mL	1.6 ± 0.8	2.0 ± 1.5	2.5 ± 4.3
Erythrocytes/mL	18 ± 38	37 ± 79	44 ± 57

obese subjects before surgery, and obese subjects after surgery), in the occipital cortex in lean and obese subjects after surgery, and in the somatosensory cortex in obese subjects both before and after surgery (Fig. 2B, W1). Comparisons between the groups revealed that lean and obese subjects before surgery presented different activities in the hypothalamus (*inset graph*, Fig. 2B, W1) and occipital and somatosensory cortices; lean and obese subjects after surgery were mostly similar with discrete differences in the somatosensory cortex; and obese subjects before and after surgery presented different activities in the hypothalamus (*inset graph*, Fig. 2B, W1). In the second window (W2), which included the second peak after glucose intake, lean subjects presented the highest activity in the hypothalamus and somatosensory and occipital cortices; obese subjects before surgery presented the highest activities in the somatosensory and occipital cortices and cerebellum; and obese subjects after surgery presented the highest activity in the somatosensory cortex (Fig. 2B, W2). At W2, the activities in the hypothalamus (*inset graph*, Fig. 2B, W2) and somatosensory cortex were

different between lean and obese subjects before surgery. The comparison between lean and obese subjects after surgery showed a significant difference only in the somatosensory cortex; the comparison between obese subjects before and after surgery showed differences in the hypothalamus (*inset graph*, Fig. 2B, W2) and occipital, somatosensory, and orbitofrontal cortices. In the third window (W3), lean subjects presented the highest activities in the hypothalamus and orbitofrontal and somatosensory cortices; obese subjects before surgery presented the highest activities in the somatosensory and occipital cortices and in the cerebellum; and obese subjects after surgery presented the highest activity only in the somatosensory cortex (Fig. 2B, W3). Somatosensory and orbitofrontal cortices and the hypothalamus (*inset graph*, Fig. 2B, W3) presented different activities when lean subjects were compared with obese subjects before surgery. Only the orbitofrontal cortex was different between lean and obese subjects after surgery, and somatosensory and orbitofrontal cortices were different between obese subjects before and after surgery (Fig. 2B, W3).

At both resting state and after a stimulus, synchronized fluctuations of blood oxygen levels dependent on function in fMRI signals in remote brain areas reflect physiologic or pathologic patterns in a neuronal network (14,15,18). The measurements of such events, which are the basis of fcMRI, provide maps of connectivity that indicate integration and segregation of brain information. Here, a seed was placed on the hypothalamus to explore the connectivity of this anatomic region with other brain areas. In lean subjects, the hypothalamus presented the highest level of functional connectivity with the orbitofrontal and somatosensory cortices (Fig. 3A). In obese subjects before surgery, functional connectivity was detected between

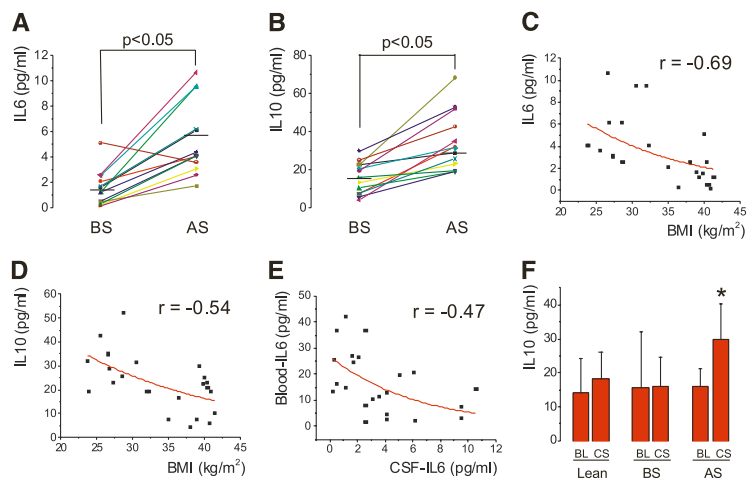
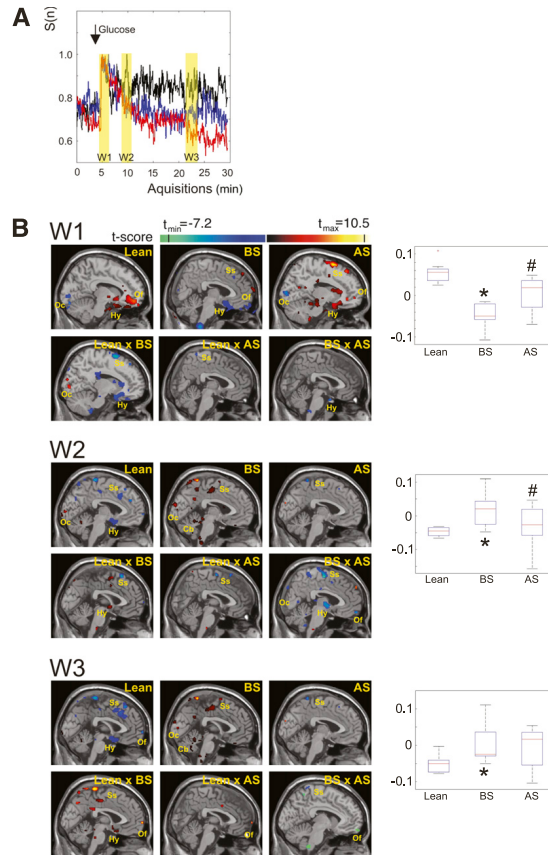


FIG. 1. Inflammatory markers in the CSF. Levels of IL-6 (A) and IL-10 (B) were determined in the CSF of obese patients before and after bariatric surgery. Correlation between IL-6 (C) and IL-10 (D) concentrations in the CSF and BMI, and correlation between IL-6 concentrations in the CSF and blood (E) were obtained. The mean ( $\pm$ SD) levels of IL-10 in the blood and CSF were obtained for lean and obese subjects before and after surgery (F).  $N = 8$  for lean subjects;  $N = 13$  for obese subjects. F: \* $P < 0.05$  vs. blood/after surgery. AS, after surgery; BL, blood; BS, before surgery; CS, cerebrospinal fluid.



**FIG. 2.** TCA of the human brain after glucose intake. **A:** Time course of the activation depicted as the means of all analyzed subjects in the respective groups (black, lean; red, obese before surgery; blue, obese after surgery); W1–W3 represent the time windows selected for spatial analysis. **B:** Spatial mapping of the brain activity at each of the time windows (W1–W3); individual group analyses were performed for lean and obese subjects before and after surgery; comparisons were also performed for all pairs of groups. The inset graphs on the right represent the signal intensity in the region of the hypothalamus for each group.  $N = 8$  for lean subjects;  $N = 13$  for obese subjects. A pixel clustering size of 5 and a  $t$ -threshold of  $|t| > 2.1$  were chosen to afford a  $P < 0.01$  level of statistical significance of the detected signal changes. This is represented by the different colors, as defined by the normalized color bars. Color bars indicate  $t$  value for one-sample  $t$  test (lean, BS, and AS) and two-sample  $t$  test (lean vs. BS, lean vs. AS, and BS vs. AS). In the insets in B, \* $P < 0.01$  vs. lean and # $P < 0.01$  vs. before surgery. AS, after surgery; BS, before surgery; Cb, cerebellum; Hy, hypothalamus; Oc, occipital cortex; Of, orbitofrontal cortex; Ss, somatosensory cortex. (A high-quality digital representation of this figure is available in the online issue.)

the hypothalamus and the orbitofrontal cortex and cerebellum (Fig. 3B). After surgery, functional connectivity of obese patients was highest between the hypothalamus and the orbitofrontal, somatosensory, and occipital cortices (Fig. 3C). Intergroup comparisons revealed the greatest difference in functional connectivity between lean and obese subjects before surgery, particularly in the regions of the cerebellum and somatosensory cortex (Fig. 3D). Functional connectivity was mostly similar between lean and obese patients after surgery (not shown). Finally, some differences in functional connectivity between

obese subjects before and after surgery were detected in the cerebellum, somatosensory, and orbitofrontal cortices (Fig. 3E).

#### DISCUSSION

Both TCA and fcMRI analyses showed distinct patterns of functionality between obese and lean subjects. The differences were mostly confined to a few anatomic regions, predominating in the hypothalamus and somatosensory and orbitofrontal cortices. The hypothalamus harbors

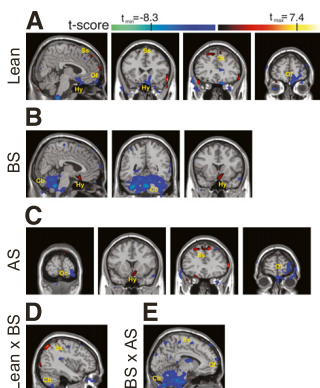


**FIG. 3.** Functional connectivity maps. A seed was placed in the hypothalamus, and intragroup (A–C) and intergroup (D and E) analyses were performed. **A:** Connectivity maps of lean subjects are depicted. **B:** Connectivity maps of obese patients before surgery are depicted. **C:** Connectivity maps of obese patients after surgery are depicted. **D:** Intergroup analysis between lean subjects and obese patients before surgery (lean  $\times$  BS) is depicted. **E:** Intergroup analysis between obese patients before surgery and obese patients after surgery (BS  $\times$  AS) is depicted. Color bars represent  $t$  values. For intragroup analysis (A–C), hot colors indicate the common level of correlation and cold colors indicate the common level of anticorrelation with the time course provided by the seed within each group. For intergroup analysis (D and E), hot colors indicate the level of differences between two groups toward lean and obese patients before surgery, respectively, and cold colors indicate the level of differences between two groups toward obese patients before and after surgery, respectively. AS, after surgery; BS, before surgery; Cb, cerebellum; Hy, hypothalamus; Oc, occipital cortex; Of, orbitofrontal cortex; Ss, somatosensory cortex. (A high-quality digital representation of this figure is available in the online issue.)

hormone and nutrient-sensing neurons and provides the integration for the energy intake and expenditure responses (19). Defective leptin and insulin signaling in this region provides the basis for experimental obesity (5,19). The somatosensory and orbitofrontal cortices integrate feeding cues with gustatory activity and facial movements, respectively. The activities of these regions have been shown to be modulated after a meal or glucose ingestion (13,20,21), and data obtained from experimental animals reinforce their role in the control of feeding and energy homeostasis (5,19). The massive loss of body mass obtained after surgery produced obvious changes in the functionality of the brain. By either analytic method, it is clear that changes occurred toward the patterns found in lean subjects. This is particularly evident in the TCA spatial analysis, which showed only minor differences when lean subjects were compared with obese subjects after surgery (Fig. 2B, W1, W2, and W3 – Lean  $\times$  AS). Another remarkable finding was the increased levels of IL-10 and IL-6 in the CSF of obese subjects after surgery. In a recent study, increased levels of both these cytokines were shown to play a role in the reduction of hypothalamic resistance to leptin after physical activity (22). Although inflammatory cytokines were not detected in the current study, we believe that advancement in measurement methods will allow quantification of these cytokines and a comparison with the findings in animal models, which show reductions in both TNF- $\alpha$  and IL-1 $\beta$  after body mass loss (3,4).

The human brain activity in response to glucose ingestion is modified by obesity, and body mass loss reestablishes some of the parameters. We cannot be sure if a longer period of time elapsed from the surgery or whether the complete restoration of body mass to levels similar to those of lean control subjects would completely correct the dysfunction. As observed in experimental obesity, neuronal apoptosis in the hypothalamus can affect distinct cellular subpopulations, leading to a defective response to hormonal and nutritional inputs (7). Should a similar phenomenon occur in humans, a complete restoration of the functional activity may not be achieved. Nevertheless, the increase in the anti-inflammatory activity detected in the CSF of obese patients after the loss of body mass is remarkable. In addition to the well-known anti-inflammatory activity of IL-10, the inhibition of neuronal degeneration through the reduction of apoptosis has been reported (23). Thus, we can hypothesize that body mass loss or other conditions that increase IL-10 in the brain may reduce neuronal damage resulting in the restoration of functionality. Moreover, these findings place IL-10 and perhaps IL-6 as attractive therapeutic agents for obesity, as recently suggested (22).

In conclusion, reduction of body mass in obese humans increases the anti-inflammatory activity in the CSF and partially corrects the dysfunctional activity in response to glucose in selected brain areas. These data suggest that obesity and body mass loss affect the human brain in a manner similar to the animal models for this disease.

#### ACKNOWLEDGMENTS

This work was supported by grants from the Fundação de Amparo a Pesquisa do Estado de Sao Paulo. The Laboratory of Cell Signaling belongs to the Instituto Nacional de Ciência e Tecnologia–Obesidade e Diabetes. F.R.S.P., P.T.F., L.M.L., and F.C. are affiliated with the Cooperação Interinstitucional de Apoio a Pesquisas sobre o Cerebro.

No potential conflicts of interest relevant to this article were reported.

S.v.d.S.-L. performed patient care and collected clinical and nutritional data. F.R.S.P. performed neuroimaging studies. D.E.C. performed patient care and collected clinical and nutritional data. P.T.F. performed neuroimaging studies. A.R.C. and C.R.G. collected and evaluated data. E.A.C., J.C.P., and B.G. performed surgery and the metabolic studies. L.M.L. and F.C. performed neuroimaging studies. L.A.V. conceived, organized, and wrote the article.

The authors thank Dr. N. Conran, University of Campinas, for editing the English grammar.

#### REFERENCES

1. Kelly T, Yang W, Chen CS, Reynolds K, He J. Global burden of obesity in 2005 and projections to 2030. *Int J Obes (Lond)* 2008;32:1431–1437
2. Després JP, Lemieux I. Abdominal obesity and metabolic syndrome. *Nature* 2006;444:881–887
3. De Souza CT, Araujo EP, Bordin S, et al. Consumption of a fat-rich diet activates a proinflammatory response and induces insulin resistance in the hypothalamus. *Endocrinology* 2005;146:4192–4199
4. Milanski M, Degasperi G, Coope A, et al. Saturated fatty acids produce an inflammatory response predominantly through the activation of TLR4 signaling in hypothalamus: implications for the pathogenesis of obesity. *J Neurosci* 2009;29:359–370
5. Velloso LA, Araujo EP, de Souza CT. Diet-induced inflammation of the hypothalamus in obesity. *Neuroimmunomodulation* 2008;15:189–193
6. Yang L, Hotamisligil GS. Stressing the brain, fattening the body. *Cell* 2008;135:20–22

7. Moraes JC, Coope A, Morari J, et al. High-fat diet induces apoptosis of hypothalamic neurons. *PLoS ONE* 2009;4:e5045
8. Thaler JP, Schwartz MW. Minireview: Inflammation and obesity pathogenesis: the hypothalamus heats up. *Endocrinology* 2010;151:4109–4115
9. Ozcan L, Ergin AS, Lu A, et al. Endoplasmic reticulum stress plays a central role in development of leptin resistance. *Cell Metab* 2009;9:35–51
10. Zhang X, Zhang G, Zhang H, Karin M, Bai H, Cai D. Hypothalamic IKKbeta/NF-kappaB and ER stress link overnutrition to energy imbalance and obesity. *Cell* 2008;135:61–73
11. Gastrointestinal surgery for severe obesity: National Institutes of Health Consensus Development Conference Statement. *Am J Clin Nutr* 1992;55 (Suppl.):615S–619S
12. de Carvalho CP, Marin DM, de Souza AL, et al. GLP-1 and adiponectin: effect of weight loss after dietary restriction and gastric bypass in morbidly obese patients with normal and abnormal glucose metabolism. *Obes Surg* 2009;19:313–320
13. Liu Y, Gao JH, Liu HL, Fox PT. The temporal response of the brain after eating revealed by functional MRI. *Nature* 2000;405:1058–1062
14. Pereira FR, Alessio A, Sercheli MS, et al. Asymmetrical hippocampal connectivity in mesial temporal lobe epilepsy: evidence from resting state fMRI. *BMC Neurosci* 2010;11:66
15. Biswal BB, Van Klyen J, Hyde JS. Simultaneous assessment of flow and BOLD signals in resting-state functional connectivity maps. *NMR Biomed* 1997;10:165–170
16. Robertson C, Conway R, Dennis B, Yarnell J, Stamler J, Elliott P. Attainment of precision in implementation of 24 h dietary recalls: INTERMAP UK. *Br J Nutr* 2005;94:588–594
17. Esposito K, Pontillo A, Di Palo C, et al. Effect of weight loss and lifestyle changes on vascular inflammatory markers in obese women: a randomized trial. *JAMA* 2003;289:1799–1804
18. Colonnese MT, Phillips MA, Constantine-Paton M, Kaila K, Jasanoff A. Development of hemodynamic responses and functional connectivity in rat somatosensory cortex. *Nat Neurosci* 2008;11:72–79
19. Morton GJ, Cummings DE, Baskin DG, Barsh GS, Schwartz MW. Central nervous system control of food intake and body weight. *Nature* 2006;443:289–295
20. Matsuda M, Liu Y, Mahankali S, et al. Altered hypothalamic function in response to glucose ingestion in obese humans. *Diabetes* 1999;48:1801–1806
21. Fühner D, Zysset S, Stumvoll M. Brain activity in hunger and satiety: an exploratory visually stimulated fMRI study. *Obesity (Silver Spring)* 2008;16:945–950
22. Ropelle ER, Flores MB, Cintra DE, et al. IL-6 and IL-10 anti-inflammatory activity links exercise to hypothalamic insulin and leptin sensitivity through IKKbeta and ER stress inhibition. *PLoS Biol* 2010;8:e1000465
23. Bachis A, Colangelo AM, Vicini S, et al. Interleukin-10 prevents glutamate-mediated cerebellar granule cell death by blocking caspase-3-like activity. *J Neurosci* 2001;21:3104–3112



## **DISCUSSÃO**



Neste trabalho buscou-se o desenvolvimento e o aperfeiçoamento de uma sequência de experimentos, em ordem crescente dos níveis de dificuldade, para gerar mapas cerebrais e conectomas diversas condições neurológicas e psiquiátricas. O conjunto de variáveis que permearam o trabalho pode ser apresentado didaticamente em três categorias distintas, apesar de estarem interligadas. A primeira, de ordem fisiológica, é representada pelos os processos cerebrais. As interpretações sobre esses processos têm sido discutidas tanto em escalas microscópicas, da ordem de canais iônicos (Heinzen et al., 2007), de expressões gênicas (Kobayashi et al., 2002), ou de componentes metabólicas (Pascual et al., 2008) como também em dimensões macroscópicas a exemplo, de ordem anatômica, em diferentes níveis de substâncias cinzenta (Keller et al., 2002) ou branca (McMillan et al., 2004) e de conexão (Bonilha et al., 2004). Na presente tese, os exemplos que foram estudados envolveram o processo de envelhecimento normal (Kensinger et al., 2006, Salat et al., 2005, Corkin, 1998), de epilepsia medial temporal (Pereira et al., 2010, Alessio et al., 2011), de doença de Alzheimer (Balthazar et al., 2013), de transtorno cognitivo leve (Radanovic et al., 2013), de pacientes com obesidade mórbida (van de Sande-Lee et al., 2011), de idosos com diagnóstico de depressão (Bezerra et al., 2012) e de indivíduos com mutação gênica (Franca et al., 2012).

Na segunda categoria, de ordem neuropsicológica, residem os processos de funções cognitivas. A base deste conceito fundamenta-se na representação interna de informações, sejam estas obtidas externamente ou processadas internamente (Gazzaniga et al., 2009). As informações, elevadas à esfera mental, podem gerar, elaborar ou mesmo manipular grupos de operações mentais como memória, atenção, linguagem entre outras. As interações entre operações mentais e processos cerebrais compõem um sistema dinâmico de informações denominado sistema funcional complexo (Luria, 1980). Entretanto, as manifestações mentais interdependentes com a matriz cerebral podem ser modeladas apenas se os processos neuronais (como metabolismo ou descargas elétricas), que foram mobilizados pelas funções

mentais, puderem se detectáveis por instrumentação. Visto que a hegemonia dos processos mentais não possui relação unívoca com determinadas regiões cerebrais (Luria, 1973) (como acreditavam os frenologista), associado ao fato de haver uma enorme limitação instrumental e uma prudente orientação ética para se mensurar sinais cerebrais humanos, tem-se que a modelagem de séries temporais, como fMRI ou EEG, é extremamente limitada. Apesar disso, as inferências sobre interações e segregações cerebrais podem ser realizadas e compõem uma nova abordagem da neuropsicologia. Em particular, as funções de memórias verbal e não-verbal, além das sub-categorias de codificação, evocação e reconhecimento foram utilizadas como exemplos para motivar a modelagem cerebral durante a realização deste trabalho.

A terceira categoria, de ordem técnica, caracterizou-se pela modelagem dos fenômenos cerebrais e mentais. Foram estimados esquemas mais simples que a complexidade neural biológica utilizando-se de arcabouços estatísticos e matemáticos aplicados a séries temporais, a exemplos daquelas séries temporais produzidas no imageamento por ressonância magnética funcional e por aquisições de eletroencefalografia. Ambas as técnicas serviram de molde para se verificar integração e segregação ao se calcular mapas de conectividade anatômica (Sporns et al., 2005, Van Essen and Ugurbil, 2012), funcional e efetiva (Friston, 2007).

Nos seres humanos, a natureza dual e interpenetrante dos fenômenos mental e cerebral dificulta uma abordagem individualizada de cada processo. A informação que flui por estes fenômenos não é completamente mensurável devido tanto à própria natureza do fenômeno biológico (mental e cerebral) como à limitação do instrumental disponível. Deste modo, a estratégia para se extrair conhecimento sobre as redes neurais requer maximização e combinação de técnicas que observem o comportamento cerebral. No estudo de conectividade três opções podem ser utilizadas: conectividade anatômica, conectividade funcional e conectividade efetiva. Os experimentos realizados neste trabalho são discutidos

abaixo de acordo com o objetivo de cada experimento. Outros seis trabalhos, publicados previamente em revistas indexadas e apresentados na sessão de metodologia, têm a discussão apresentada no corpo do artigo e não são reproduzidos nesta sessão.

### **SEM aplicado à plasticidade etária e codificação verbal**

O protocolo desenvolvido neste experimento objetivou a detecção da conectividade efetiva entre amígdala e hipocampo ipsilaterais e em ambos os sentidos durante a codificação de palavras com conteúdo emocional. Os indivíduos que participaram deste estudo foram apenas sujeitos sadios cuja distinção foi marcada apenas pela faixa etária em que se encontravam, formando dois grupos, o de jovens e o de adultos mais velhos. A técnica empregada para se estimar a ecMRI foi a SEM que, como descrita anteriormente, pode apenas estabelecer relações estáticas de um modelo anatômico. A combinação de SEM com indivíduos pertencente à mesma classe (controles), cuja única variação é a diferença etária, revela o comportamento plástico existente entre estes grupos durante a realização da mesma tarefa. A interpretação dos resultados deste estudo deve ser fixada nas relações intrínsecas entre as estruturas cerebrais presentes no modelo anatômico. Buscou-se aqui não o entendimento de um comportamento neural dinâmico, que varia com uma determinada tarefa, mas sim, como essa tarefa, no caso a de codificação verbal de palavras abstratas e concretas e com conteúdo emocional, varia com a idade dos indivíduos separados em dois grupos.

Em ambos os grupos, a influência das amígdalas sobre os hipocampos foi maior do que na direção oposta, sugerindo que a tarefa efetivamente apresentava conteúdo emocional. No grupo de adultos mais velhos, os parâmetros de conectividade efetiva estavam mais intensos no lado direito que no lado esquerdo. Este padrão não foi encontrado no grupo de jovens. Ao se correlacionar este achado com o desempenho dos grupos, pode-se suportar a hipótese de que os adultos mais velhos realizem processos distintos dos jovens e que tal performance

pode estar associado às diferentes estratégias escolhidas por cada grupo.

Além disso, a influência da amígdala sobre o hipocampo é maior do lado esquerdo nos jovens, enquanto que para os adultos mais velhos, esta influência é maior do lado direito. Esta diferença sugere haver mudanças na conectividade efetiva em função da idade, dado que a tarefa verbal se encontra majoritariamente lateralizada à esquerda. Pode-se supor portanto uma mudança de estratégia para se realizar a codificação como obtenção de estratégias não-verbais para realizar uma atividade eminentemente verbal.

Por fim, a influência de ambos hipocampos nas amídalas ipsilaterais são equivalentes para os jovens, enquanto que nos adultos mais velhos há uma predominância da influência exercida à direita. Considerando os achados anteriores, este dado fortalece a hipótese de que os hipocampos nos mais velhos exercem menor influência sobre as amídalas do que nos jovens durante a realização da tarefa de codificação verbal.

### **SEM aplicado a ELTM esquerdo com codificação verbal**

Objetivou-se neste experimento estimar os parâmetros de conectividade efetiva entre regiões frontais e mediais temporais durante a codificação de palavras abstratas e neutras. Diferentemente do experimento anterior, os indivíduos que participaram deste estudo foram sujeitos controles e indivíduos portadores de ELTM esquerda contudo, a técnica empregada para se estimar a ecMRI foi a mesma, a SEM. Buscou-se aqui compreender a plasticidade cerebral, em forma de conectividade efetiva, durante a realização de uma determinada tarefa, não em função da idade dos sujeitos mas em detrimento de uma condição neurológica, no caso, ELTM esquerda. A interpretação dos resultados dá-se em termos das relações intrínsecas entre as estruturas cerebrais do modelo anatômico desse experimento.

A influência do hipocampo esquerdo sobre o parahipocampo ipsilateral mostrou-se significativamente maior para os controles que para os pacientes. O achado sugere que,

durante a codificação, há uma maior sincronia dessas estruturas mediais nos controles que nos pacientes. Essa hipótese é reforçada pelos dados de conectividade funcional. Semelhantemente, observou-se a redução da influência entre as porções triangular e opercular do giro frontal inferior para o giro frontal médio, quando comparados controles e pacientes. Por fim, a influência da região medial temporal sobre a região frontal também se apresentou reduzida nos pacientes.

A generalizada redução da intensidade dos parâmetros de conectividade efetiva, entre as regiões frontais e mediais temporais, nos pacientes com ELTM esquerda, sugere que a plasticidade neural, causada pela condição neurológica nestes indivíduos, deve tornar distinta a função de codificação verbal, entretanto, com este modelo e técnica não se pode avaliar se a extensão do dano funcional estende-se ao lobo frontal, uma vez que o fluxo da informação já está comprometido em sua origem, ou seja, entre hipocampo e parahipocampo.

### **DCM aplicado a ELTM unilateral com codificação verbal**

O experimento desenhado com DCM buscou estimar os parâmetros de conectividade efetiva de regiões cerebrais envolvidas no processamento de memória verbal, durante a codificação de palavras abstratas e neutras. Semelhantemente ao experimento anterior, foram selecionadas regiões mediais temporais (hipocampo) e frontais (região dorsolateral do córtex pré-frontal) contudo, outras áreas foram acrescentadas no modelo anatômico, como visual primária e a porção caudal do giro temporal superior para simular o fluxo da informação verbal. A importante vantagem do DCM consiste no fato de que os parâmetros de conectividade efetiva, associados ao caráter modulatório da tarefa realizada, podem ser estimados a partir das séries temporais, para isso, utilizou-se fMRI de sujeitos controles e indivíduos portadores de ELTM unilateral (esquerda e direita) durante a codificação de palavras abstratas.

A interpretação dos resultados dá-se nos termos das relações intrínsecas entre as estruturas cerebrais do modelo anatômico sugerido. Deve-se ressaltar, entretanto, que a tarefa de codificação verbal foi capaz de modular a interação entre o córtex occipital primário e hipocampo esquerdo para os controles mas não para os pacientes, sejam estes com atrofia hipocampal à esquerda ou à direita. Semelhante modulação também foi observada na influência que o hipocampo esquerdo exerce sobre a área de Wernick. Os indivíduos controles apresentaram valores significativamente distintos quando comparado com os pacientes. Além dos parâmetros modulatórios que diferenciam controles de pacientes, os parâmetros intrínsecos também apresentam significativa diferenciação. Ressalta-se que as influências do córtex occipital primário sobre o hipocampo esquerdo e do hipocampo esquerdo sobre a área de Wernick e sobre a porção dorsolateral do córtex pré-frontal são bem mais evidentes nos controles que nos pacientes.

O conjunto de achados sugere que, não obstante ao fato de que os pacientes com ELTM direita não apresentarem lesão estrutural no hipocampo esquerdo (perceptível pela MRI), deve haver comprometimento funcional ou rearranjo plástico na realização da tarefa. Em contra posição, os indivíduos com ELTM esquerda, dado o comprometimento estrutural locado no hipocampo esquerdo, devem apresentar comprometimento funcional e, conseqüentemente, menores parâmetros de conectividade efetiva durante a codificação verbal.

Enquanto o desempenho verbal de indivíduos com ELTM esquerda tem se mostrado inferior à dos controles, desempenho de pacientes com ELTM direita apresenta índices semelhantes aos indivíduos controles. Pode-se supor que a plasticidade ocorrida nos pacientes com ELTM direita foi eficiente enquanto o mesmo não ocorreu com os indivíduos com ELTM esquerda. Tal fato sugere que as estruturas mediais temporais do hemisfério dominante para linguagem possam estar envolvidas diretamente no processo de plasticidade para realização da tarefa de codificação verbal.

## **CONSIDERAÇÕES FINAIS**



O estudo do conectoma humano por imageamento de ressonância magnética nuclear mostrou-se sensível para detectar diferenças na organização entre regiões cerebrais, tanto em sujeitos saudáveis como em pacientes com condições neuropsiquiátricas diversas. No presente trabalho, buscou-se observar plasticidade cérebro-mental em pacientes com mutações gênicas (SPG11), depressão, epilepsia, obesidade mórbida, doença de Alzheimer, déficit cognitivo leve, envelhecimento saudável.

Indivíduos com mutação no gene SPG11 apresentaram diferença significativa nos níveis de acMRI, em especial RD e FA. Com esse estudo, concluiu-se que pacientes com mutação em SPG11 apresentaram dano neuronal muito mais difuso e extenso do que se previa. Em oposição a esses achados, idosos com diagnóstico de depressivos quando comparados a sujeitos controles não mostraram diferenças significativas em FA. Hipotetiza-se que tal índice não seja robusto para detectar alterações neuro-estruturais mais sutis indicando a necessidade de se evoluir no desenvolvimento de novos índices de anisotropia que possam detectar tais alterações, como geometrias toroidais e superquadráticas.

Em idosos saudáveis observou-se significativa alteração dos níveis de ecMRI (comparados a jovens saudáveis) durante a codificação de palavras com conteúdo emocional indicando que a plasticidade funcional está presente no envelhecimento. Pacientes com epilepsia também apresentaram significativas diferenças nas comparações dos grupos de pacientes com ELTM-esquerda, ELTM-direita e sujeitos controles seja durante a codificação de memória verbal, visual e em estado de repouso. Tais indicadores são potenciais biomarcadores da ELTM unilateral.

Pacientes com doença de Alzheimer apresentaram a rede de modo padrão distinta dos sujeitos controles além de terem elevada correlação da rede saliente com parâmetros neuropsicológicos de agitação. Essa observação, obtida com fcMRI, indica a potencialidade de uso clínicos e de diagnóstico. O mesmo se observou com pacientes portadores de obesidade mórbida e a parcial reversibilidade de quadro inflamatório acompanhado de

alterações nas redes neurais desses paciente após intervenção de cirurgia bariátrica.

Diante das diversas condições neurológicas que foram exploradas pela técnicas de conectividade, pode-se concluir que a estimativa do conectoma humano representa uma potente ferramenta no entendimento da dinâmica cerebral normal e patológica sendo que, no presente trabalhos, pretendeu-se demonstrar a integração dessa metodologia com estudos que vão desde a genética até a neuropsicologia. A característica multimodal e multiescalar de estudos do conectoma revela as potencialidades da técnica no campo das neurociências.

## **REFERÊNCIA BIBLIOGRÁFICA**



- ABBOTT, D. F., WAITES, A. B., LILLYWHITE, L. M. & JACKSON, G. D. 2010. fMRI assessment of language lateralization: an objective approach. *Neuroimage*, 50, 1446-55.
- AERTSEN, A., VAADIA, E., ABELES, M., AHISSAR, E., BERGMAN, H., KARMON, B., LAVNER, Y., MARGALIT, E., NELKEN, I. & ROTTER, S. 1991. Neural interactions in the frontal cortex of a behaving monkey: signs of dependence on stimulus context and behavioral state. *J Hirnforsch*, 32, 735-43.
- ALESSIO, A., PEREIRA, F. R., SERCHELI, M. S., RONDINA, J. M., OZELO, H. B., BILEVICIUS, E., PEDRO, T., COVOLAN, R. J., DAMASCENO, B. P. & CENDES, F. 2011. Brain plasticity for verbal and visual memories in patients with mesial temporal lobe epilepsy and hippocampal sclerosis: An fMRI study. *Hum Brain Mapp.***
- ASTOLFI, L., CINCOTTI, F., MATTIA, D., SALINARI, S., BABILONI, C., BASILISCO, A., ROSSINI, P. M., DING, L., NI, Y., HE, B., MARCIANI, M. G. & BABILONI, F. 2004. Estimation of the effective and functional human cortical connectivity with structural equation modeling and directed transfer function applied to high-resolution EEG. *Magn Reson Imaging*, 22, 1457-70.
- BALTHAZAR, M. L., PEREIRA, F. R., LOPES, T. M., DA SILVA, E. L., COAN, A. C., CAMPOS, B. M., DUNCAN, N. W., STELLA, F., NORTHOFF, G., DAMASCENO, B. P. & CENDES, F. 2013. Neuropsychiatric symptoms in Alzheimer's disease are related to functional connectivity alterations in the salience network. *Hum Brain Mapp.***
- BASSER, P. J., MATTIELLO, J. & LEBIHAN, D. 1994. MR diffusion tensor spectroscopy and imaging. *Biophys J*, 66, 259-67.
- BECK, A. T. 1979. *Cognitive therapy of depression*, New York, Guilford Press.

- BEZERRA, D. M., PEREIRA, F. R., CENDES, F., JACKOWSKI, M. P., NAKANO, E. Y., MOSCOSO, M. A., RIBEIZ, S. R., AVILA, R., CASTRO, C. C. & BOTTINO, C. M. 2012. DTI voxelwise analysis did not differentiate older depressed patients from older subjects without depression. *J Psychiatr Res*, 46, 1643-9.**
- BONILHA, L., RORDEN, C., CASTELLANO, G., PEREIRA, F., RIO, P. A., CENDES, F. & LI, L. M. 2004. Voxel-based morphometry reveals gray matter network atrophy in refractory medial temporal lobe epilepsy. *Arch Neurol*, 61, 1379-84.**
- BRADLEY, M. M. & LANG, P. J. 1999. Affective norms for English words (ANEW): Instruction manual and affective rating, Gainesville, FL, Center for Research in Psychophysiology.
- BUCHEL, C. & FRISTON, K. J. 1997. Modulation of connectivity in visual pathways by attention: cortical interactions evaluated with structural equation modelling and fMRI. *Cereb Cortex*, 7, 768-78.
- BUCHEL, C. & FRISTON, K. J. 1998. Dynamic changes in effective connectivity characterized by variable parameter regression and Kalman filtering. *Hum Brain Mapp*, 6, 403-8.
- CARMACK, P. S., SPENCE, J., GUNST, R. F., SCHUCANY, W. R., WOODWARD, W. A. & HALEY, R. W. 2004. Improved agreement between Talairach and MNI coordinate spaces in deep brain regions. *Neuroimage*, 22, 367-71.
- CHAIGNEAU, E., TIRET, P., LECOQ, J., DUCROS, M., KNOPFEL, T. & CHARPAK, S. 2007. The relationship between blood flow and neuronal activity in the rodent olfactory bulb. *Journal of Neuroscience*, 27, 6452-6460.
- CHEN, B. & HSU, E. W. 2005. Noise removal in magnetic resonance diffusion tensor imaging. *Magn Reson Med*, 54, 393-401.

- CORDES, D., HAUGHTON, V. M., ARFANAKIS, K., CAREW, J. D., TURSKI, P. A., MORITZ, C. H., QUIGLEY, M. A. & MEYERAND, M. E. 2001. Frequencies contributing to functional connectivity in the cerebral cortex in "resting-state" data. *AJNR Am J Neuroradiol*, 22, 1326-33.
- CORKIN, S. 1998. Functional MRI for studying episodic memory in aging and Alzheimer's disease. *Geriatrics*, 53 Suppl 1, S13-5.
- DAS, A. & GILBERT, C. D. 1995. Long-range horizontal connections and their role in cortical reorganization revealed by optical recording of cat primary visual cortex. *Nature*, 375, 780-4.
- DELLA-JUSTINA, H. M., PASTORELLO, B. F., SANTOS-PONTELLI, T. E., PONTES-NETO, O. M., SANTOS, A. C., BAFFA, O., COLAFEMINA, J. F., LEITE, J. P. & DE ARAUJO, D. B. 2008. Human variability of fMRI brain activation in response to oculomotor stimuli. *Brain Topogr*, 20, 113-21.
- DESKAN, R. S., SEGONNE, F., FISCHL, B., QUINN, B. T., DICKERSON, B. C., BLACKER, D., BUCKNER, R. L., DALE, A. M., MAGUIRE, R. P., HYMAN, B. T., ALBERT, M. S. & KILLIANY, R. J. 2006. An automated labeling system for subdividing the human cerebral cortex on MRI scans into gyral based regions of interest. *Neuroimage*, 31, 968-980.
- DUPONT, S., VAN DE MOORTELE, P. F., SAMSON, S., HASBOUN, D., POLINE, J. B., ADAM, C., LEHERICY, S., LE BIHAN, D., SAMSON, Y. & BAULAC, M. 2000. Episodic memory in left temporal lobe epilepsy: a functional MRI study. *Brain*, 123 (Pt 8), 1722-32.
- ENGEL, S. A., RUMELHART, D. E., WANDELL, B. A., LEE, A. T., GLOVER, G. H., CHICHILNISKY, E. J. & SHADLEN, M. N. 1994. fMRI of human visual cortex. *Nature*, 369, 525.

- FELDMAN, R. P. & GOODRICH, J. T. 1999. The Edwin Smith Surgical Papyrus. *Childs Nerv Syst*, 15, 281-4.
- FINGELKURTS, A. A. & KAHKONEN, S. 2005. Functional connectivity in the brain--is it an elusive concept? *Neurosci Biobehav Rev*, 28, 827-36.
- FISCHL, B., RAJENDRAN, N., BUSA, E., AUGUSTINACK, J., HINDS, O., YEO, B. T., MOHLBERG, H., AMUNTS, K. & ZILLES, K. 2008. Cortical folding patterns and predicting cytoarchitecture. *Cereb Cortex*, 18, 1973-80.
- FISCHL, B., SALAT, D. H., BUSA, E., ALBERT, M., DIETERICH, M., HASELGROVE, C., VAN DER KOUWE, A., KILLIANY, R., KENNEDY, D., KLAVENESS, S., MONTILLO, A., MAKRIS, N., ROSEN, B. & DALE, A. M. 2002. Whole brain segmentation: automated labeling of neuroanatomical structures in the human brain. *Neuron*, 33, 341-55.
- FISCHL, B., VAN DER KOUWE, A., DESTRIEUX, C., HALGREN, E., SEGONNE, F., SALAT, D. H., BUSA, E., SEIDMAN, L. J., GOLDSTEIN, J., KENNEDY, D., CAVINESS, V., MAKRIS, N., ROSEN, B. & DALE, A. M. 2004. Automatically parcellating the human cerebral cortex. *Cereb Cortex*, 14, 11-22.
- FRANCA, M. C., JR., YASUDA, C. L., PEREIRA, F. R., D'ABREU, A., LOPES-RAMOS, C. M., ROSA, M. V., CENDES, F. & LOPES-CENDES, I. 2012. White and grey matter abnormalities in patients with SPG11 mutations. *J Neurol Neurosurg Psychiatry*.**
- FRISTON, K. 1994. Functional and effective connectivity in neuroimaging: A synthesis. *Human Brain Mapping*, 2, 56-78.
- FRISTON, K. J. 2007. *Statistical parametric mapping : the analysis of funtional brain images*, Amsterdam ; Boston, Elsevier/Academic Press.

- FRISTON, K. J. & BUCHEL, C. 2000. Attentional modulation of effective connectivity from V2 to V5/MT in humans. *Proc Natl Acad Sci U S A*, 97, 7591-6.
- FRISTON, K. J., FRITH, C. D. & FRACKOWIAK, R. S. J. 1993a. Time-dependent changes in effective connectivity measured with PET. *Human Brain Mapping*, 1, 69-79.
- FRISTON, K. J., FRITH, C. D., LIDDLE, P. F. & FRACKOWIAK, R. S. 1993b. Functional connectivity: the principal-component analysis of large (PET) data sets. *J Cereb Blood Flow Metab*, 13, 5-14.
- FRISTON, K. J., HARRISON, L. & PENNY, W. 2003. Dynamic causal modelling. *Neuroimage*, 19, 1273-302.
- FROST, J. J. 2003. Molecular imaging of the brain: a historical perspective. *Neuroimaging Clin N Am*, 13, 653-8.
- GALLAGHER, M. & CHIBA, A. A. 1996. The amygdala and emotion. *Curr Opin Neurobiol*, 6, 221-7.
- GARBADE, K. 1977. Two Methods for Examining the Stability of Regression Coefficients. *Journal of the American Statistical Association*, 72, 54-63.
- GAZZANIGA, M. S., IVRY, R. B. & MANGUN, G. R. 2009. *Cognitive neuroscience : the biology of the mind*, New York, Norton.
- GLIELMI, C. B., SCHUCHARD, R. A. & HU, X. P. 2009. Estimating Cerebral Blood Volume With Expanded Vascular Space Occupancy Slice Coverage. *Magnetic Resonance in Medicine*, 61, 1193-1200.
- GOELMAN, G. 2004. Radial correlation contrast--a functional connectivity MRI contrast to map changes in local neuronal communication. *Neuroimage*, 23, 1432-9.

- GREENE, J. D., SOMMERVILLE, R. B., NYSTROM, L. E., DARLEY, J. M. & COHEN, J. D. 2001. An fMRI investigation of emotional engagement in moral judgment. *Science*, 293, 2105-8.
- HEINZEN, E. L., YOON, W., WEALE, M. E., SEN, A., WOOD, N. W., BURKE, J. R., WELSH-BOHMER, K. A., HULETTE, C. M., SISODIYA, S. M. & GOLDSTEIN, D. B. 2007. Alternative ion channel splicing in mesial temporal lobe epilepsy and Alzheimer's disease. *Genome Biol*, 8, R32.
- HERMAN, P., SANGANAHALLI, B. G., BLUMENFELD, H. & HYDER, F. 2009. Cerebral oxygen demand for short-lived and steady-state events. *J Neurochem*, 109 Suppl 1, 73-9.
- HORWITZ, B. 2003. The elusive concept of brain connectivity. *Neuroimage*, 19, 466-70.
- HYDE, P. S. & KNUDSEN, E. I. 2002. The optic tectum controls visually guided adaptive plasticity in the owl's auditory space map. *Nature*, 415, 73-6.
- ILAE 1989. Proposal for revised classification of epilepsies and epileptic syndromes. Commission on Classification and Terminology of the International League Against Epilepsy. *Epilepsia*, 30, 389-99.
- KALMAN, R. E. 1960. A New Approach to Linear Filtering and Prediction Problems. *Transactions of the ASME , Journal of Basic Engineering*, 35-45.
- KELLER, S. S., WIESHMANN, U. C., MACKAY, C. E., DENBY, C. E., WEBB, J. & ROBERTS, N. 2002. Voxel based morphometry of grey matter abnormalities in patients with medically intractable temporal lobe epilepsy: effects of side of seizure onset and epilepsy duration. *J Neurol Neurosurg Psychiatry*, 73, 648-55.
- KENDALL, M. G. & GIBBONS, J. D. 1990. Rank correlation methods, London New York, NY, E. Arnold ;

Oxford University Press.

KENSINGER, E. A., KRENDL, A. C. & CORKIN, S. 2006. Memories of an emotional and a nonemotional event: effects of aging and delay interval. *Exp Aging Res*, 32, 23-45.

KOBAYASHI, E., FACCHIN, D., STEINER, C. E., LEONE, A. A., CAMPOS, N. L., CENDES, F. & LOPES-CENDES, I. 2002. Mesial temporal lobe abnormalities in a family with 15q26qter trisomy. *Arch Neurol*, 59, 1476-9.

KRUGER, G. & GLOVER, G. H. 2001. Physiological noise in oxygenation-sensitive magnetic resonance imaging. *Magn Reson Med*, 46, 631-7.

LE BIHAN, D., BRETON, E., LALLEMAND, D., GRENIER, P., CABANIS, E. & LAVAL-JEANTET, M. 1986. MR imaging of intravoxel incoherent motions: application to diffusion and perfusion in neurologic disorders. *Radiology*, 161, 401-7.

LOGOTHETIS, N. K., PAULS, J., AUGATH, M., TRINATH, T. & OELTERMANN, A. 2001. Neurophysiological investigation of the basis of the fMRI signal. *Nature*, 412, 150-7.

LURIA, A. R. 1973. *The working brain; an introduction to neuropsychology*. Translated by Basil Haigh, London,, Allen Lane.

LURIA, A. R. 1980. *Higher cortical functions in man*, New York, Basic Books.

MCCOLL, R. M., CLARKE, G. D. & PESHOCK, R. M. 1992. Echo-Planar Imaging - Image-Reconstruction from K-Space Trajectories. *Radiology*, 185, 253-253.

MCINTOSH, A. R. & GONZALEZ-LIMA, F. 1994. Structural equation modeling and its application to network analysis in functional brain imaging. *Human Brain Mapping*, 2, 2-22.

MCMILLAN, A. B., HERMANN, B. P., JOHNSON, S. C., HANSEN, R. R., SEIDENBERG, M. & MEYERAND, M. E. 2004. Voxel-based morphometry of

- unilateral temporal lobe epilepsy reveals abnormalities in cerebral white matter.  
*Neuroimage*, 23, 167-74.
- MINAGAR, A., RAGHEB, J. & KELLEY, R. E. 2003. The Edwin Smith surgical papyrus:  
description and analysis of the earliest case of aphasia. *J Med Biogr*, 11, 114-7.
- OGAWA, S., LEE, T. M., KAY, A. R. & TANK, D. W. 1990. Brain magnetic resonance  
imaging with contrast dependent on blood oxygenation. *Proc Natl Acad Sci U S A*,  
87, 9868-72.
- OLDFIELD, R. C. 1971. The assessment and analysis of handedness: the Edinburgh  
inventory. *Neuropsychologia*, 9, 97-113.
- PASCUAL, J. M., CAMPISTOL, J. & GIL-NAGEL, A. 2008. Epilepsy in inherited  
metabolic disorders. *Neurologist*, 14, S2-S14.
- PAULING, L. 1977. Magnetic properties and structure of oxyhemoglobin. *Proc Natl Acad  
Sci U S A*, 74, 2612-3.
- PAULING, L. & CORYELL, C. D. 1936. The Magnetic Properties and Structure of  
Hemoglobin, Oxyhemoglobin and Carbonmonoxyhemoglobin. *Proc Natl Acad Sci U  
S A*, 22, 210-6.
- PAULSON, O. B., HASSELBALCH, S. G., ROSTRUP, E., KNUDSEN, G. M. &  
PELLIGRINO, D. 2010. Cerebral blood flow response to functional activation. *J  
Cereb Blood Flow Metab*, 30, 2-14.
- PEREIRA, F. R., ALESSIO, A., SERCHELI, M. S., PEDRO, T., BILEVICIUS, E.,  
RONDINA, J. M., OZELO, H. F., CASTELLANO, G., COVOLAN, R. J.,  
DAMASCENO, B. P. & CENDES, F. 2010. Asymmetrical hippocampal  
connectivity in mesial temporal lobe epilepsy: evidence from resting state fMRI.  
*BMC Neurosci*, 11, 66.**

- PEREIRA, F. R. S. 2011. Conectividade funcional por imageamento de ressonância magnética (MRI) em pacientes com epilepsia de lobo temporal mesial. Mestre em Ciências Médicas - Ciências Biomédicas, Universidade Estadual de Campinas.**
- RADANOVIC, M., PEREIRA, F. R., STELLA, F., APRAHAMIAN, I., FERREIRA, L. K., FORLENZA, O. V. & BUSATTO, G. F. 2013. White matter abnormalities associated with Alzheimer's disease and mild cognitive impairment: a critical review of MRI studies. Expert Rev Neurother, 13, 483-93.**
- RAYENS, W. S. & ANDERSEN, A. H. 2006. Multivariate analysis of fMRI data by oriented partial least squares. Magn Reson Imaging, 24, 953-8.
- RIDGE, R. M. & BETZ, W. J. 1984. The effect of selective, chronic stimulation on motor unit size in developing rat muscle. J Neurosci, 4, 2614-20.
- RODER, B., STOCK, O., BIEN, S., NEVILLE, H. & ROSLER, F. 2002. Speech processing activates visual cortex in congenitally blind humans. Eur J Neurosci, 16, 930-6.
- SALAT, D. H., TUCH, D. S., GREVE, D. N., VAN DER KOUWE, A. J., HEVELONE, N. D., ZALETA, A. K., ROSEN, B. R., FISCHL, B., CORKIN, S., ROSAS, H. D. & DALE, A. M. 2005. Age-related alterations in white matter microstructure measured by diffusion tensor imaging. Neurobiol Aging, 26, 1215-27.
- SAVICKI, J. P., LANG, G. & IKEDA-SAITO, M. 1984. Magnetic susceptibility of oxy- and carbonmonoxyhemoglobins. Proc Natl Acad Sci U S A, 81, 5417-9.
- SHEIKH, J. I., YESAVAGE, J. A., BROOKS, J. O., 3RD, FRIEDMAN, L., GRATZINGER, P., HILL, R. D., ZADEIK, A. & CROOK, T. 1991. Proposed factor structure of the Geriatric Depression Scale. Int Psychogeriatr, 3, 23-8.
- SINGH, M., AL-DAYEH, L., PATEL, P., KIM, T., GUCLU, C. & NALCIOGLU, O. 1998. Correction for head movements in multi-slice EPI functional MRI. Ieee Transactions on Nuclear Science, 45, 2162-2167.

- SPORNS, O., TONONI, G. & KOTTER, R. 2005. The human connectome: A structural description of the human brain. *PLoS Comput Biol*, 1, e42.
- TZOURIO-MAZOYER, N., LANDEAU, B., PAPATHANASSIOU, D., CRIVELLO, F., ETARD, O., DELCROIX, N., MAZOYER, B. & JOLIOT, M. 2002. Automated anatomical labeling of activations in SPM using a macroscopic anatomical parcellation of the MNI MRI single-subject brain. *Neuroimage*, 15, 273-89.
- VAN DE SANDE-LEE, S., PEREIRA, F. R., CINTRA, D. E., FERNANDES, P. T., CARDOSO, A. R., GARLIPP, C. R., CHAIM, E. A., PAREJA, J. C., GELONEZE, B., LI, L. M., CENDES, F. & VELLOSO, L. A. 2011. Partial reversibility of hypothalamic dysfunction and changes in brain activity after body mass reduction in obese subjects. *Diabetes*, 60, 1699-704.**
- VAN ESSEN, D. C. & UGURBIL, K. 2012. The future of the human connectome. *Neuroimage*, 62, 1299-310.
- VAN OUYEN, A. 2001. Competition in the development of nerve connections: a review of models. *Network*, 12, R1-47.
- WALDVOGEL, D., VAN GELDEREN, P., IMMISCH, I., PFEIFFER, C. & HALLETT, M. 2000. The variability of serial fMRI data: correlation between a visual and a motor task. *Neuroreport*, 11, 3843-7.
- WANG, Z., WANG, J., CALHOUN, V., RAO, H., DETRE, J. A. & CHILDRESS, A. R. 2006. Strategies for reducing large fMRI data sets for independent component analysis. *Magn Reson Imaging*, 24, 591-6.
- WEBSTER, M. J., UNGERLEIDER, L. G. & BACHEVALIER, J. 1995. Development and plasticity of the neural circuitry underlying visual recognition memory. *Can J Physiol Pharmacol*, 73, 1364-71.

- WIESER, H. G. 2004. ILAE Commission Report. Mesial temporal lobe epilepsy with hippocampal sclerosis. *Epilepsia*, 45, 695-714.
- YESAVAGE, J. A., BRINK, T. L., ROSE, T. L., LUM, O., HUANG, V., ADEY, M. & LEIRER, V. O. 1983. Development and Validation of a Geriatric Depression Screening Scale - a Preliminary-Report. *Journal of Psychiatric Research*, 17, 37-49.
- ZBOROWSKI, M., OSTERA, G. R., MOORE, L. R., MILLIRON, S., CHALMERS, J. J. & SCHECHTER, A. N. 2003. Red blood cell magnetophoresis. *Biophys J*, 84, 2638-45.
- ZHAO, X., GLAHN, D., TAN, L. H., LI, N., XIONG, J. & GAO, J. H. 2004. Comparison of TCA and ICA techniques in fMRI data processing. *J Magn Reson Imaging*, 19, 397-402.